

Prepared in cooperation with the Miami-Dade Water and Sewer Department

# Hydrologic Conditions in Urban Miami-Dade County, Florida, and the Effect of Groundwater Pumpage and Increased Sea Level on Canal Leakage and Regional Groundwater Flow

Scientific Investigations Report 2014–5162  
Version 1.2, July 2016

U.S. Department of the Interior  
U.S. Geological Survey

**Cover.** Miami River downstream of structure S26 looking northwest toward Miami International Airport.  
Photograph provided by the South Florida Water Management District.

# **Hydrologic Conditions in Urban Miami-Dade County, Florida, and the Effect of Groundwater Pumpage and Increased Sea Level on Canal Leakage and Regional Groundwater Flow**

By Joseph D. Hughes and Jeremy T. White

Prepared in cooperation with the Miami-Dade Water and Sewer Department

Scientific Investigations Report 2014–5162

Version 1.2, July 2016

**U.S. Department of the Interior  
U.S. Geological Survey**

**U.S. Department of the Interior**  
SALLY JEWELL, Secretary

**U.S. Geological Survey**  
Suzette M. Kimball, Director

**U.S. Geological Survey, Reston, Virginia**

First release: 2014

Revised: July 2016 (ver. 1.2)

For more information on the USGS—the Federal source for science about the Earth, its natural and living resources, natural hazards, and the environment, visit <http://www.usgs.gov> or call 1–888–ASK–USGS.

For an overview of USGS information products, including maps, imagery, and publications, visit <http://www.usgs.gov/pubprod>

To order this and other USGS information products, visit <http://store.usgs.gov>

Any use of trade, firm, or product names is for descriptive purposes only and does not imply endorsement by the U.S. Government.

Although this information product, for the most part, is in the public domain, it also may contain copyrighted materials as noted in the text. Permission to reproduce copyrighted items must be secured from the copyright owner.

Suggested citation:

Hughes, J.D., and White, J.T., 2016, Hydrologic conditions in urban Miami-Dade County, Florida, and the effect of groundwater pumpage and increased sea level on canal leakage and regional groundwater flow (ver. 1.2, July 2016): U.S. Geological Survey Scientific Investigations Report 2014–5162, 175 p., <http://dx.doi.org/10.3133/sir20145162>.

ISSN: 2328-0328 (Online)

## Acknowledgments

The authors would like to extend special thanks to Virginia Walsh, Idia MacFarlane, and Sonia Villamil of the Miami-Dade Water and Sewer Department for their guidance and assistance in obtaining data for the study. John E. Doherty of Watermark Numerical Computing also provided assistance refining the model calibration process applied in this study.

The authors would like to extend appreciation to U.S. Geological Survey (USGS) scientists Kevin Cunningham and Christian D. Langevin, whose assistance was invaluable to the development of the model used in this study. The authors would like to acknowledge other USGS scientists, including Linzy Brakefield, Joann Dixon, Melinda Lohmann, and Scott Prinos for their contributions to this report. The authors are also grateful to the technical reviewers of this report, including Brian Clark and Jon Traum of the U.S. Geological Survey.



# Contents

Abstract .....	1
Introduction .....	2
Purpose and Scope .....	4
Location of the Study Area.....	4
Approach.....	5
Previous Investigations.....	5
Hydrologic Conditions in Urban Miami-Dade County .....	6
Climate .....	6
Surface-Water Hydrology .....	7
Topography .....	7
Land Use.....	9
Evapotranspiration .....	9
Surface Runoff .....	9
Surface-Water Discharge .....	14
Groundwater Hydrology.....	15
Hydrostratigraphy .....	22
Aquifer Properties .....	22
Water Supply and Use .....	27
Municipal Groundwater Water Use.....	27
Agricultural Water Use .....	28
Recreational Irrigation.....	29
Septic System Return to the Water Table.....	29
Estimates of Groundwater Recharge and Surface-Water/Groundwater Interactions .....	30
Groundwater Recharge .....	30
Surface-Water/Groundwater Interaction.....	31
Freshwater-Seawater Interface.....	31
Model Development .....	33
Spatial and Temporal Discretization.....	33
Calibration Approach .....	41
Model Parameterization .....	41
Observation Processing and Weighting .....	49
Calibration and Error-Based Calibration Criteria.....	54
Boundary Conditions .....	55
Specified Flux Boundaries .....	56
Rainfall.....	56
Net Agricultural Water Use and Irrigation System Losses.....	56
Recreational Irrigation Water Use.....	57
Septic System Return Flow to the Water Table .....	57
Surface-Water Runoff.....	59
Municipal Groundwater Use.....	59
Head-Dependent Boundaries .....	62
Evapotranspiration .....	62

Internal Surface-Water Structure Flows .....	62
Coastal Surface-Water Boundaries .....	67
Coastal and Marine Groundwater Boundaries.....	67
Water Conservation Area 3, Everglades National Park, and Southern Glades Groundwater Boundaries .....	71
Initial Conditions.....	71
Hydraulic Parameters .....	72
Canal Roughness and Bed Conductance Coefficients.....	72
Hydraulic Conductivity .....	72
Storage Coefficients and Porosity .....	73
Model Calibration and Fit, and Simulation of Hydrologic System from 1996 to 2010.....	73
Surface-Water Stage .....	75
Surface-Water Discharge .....	75
Net Surface-Water Subbasin Discharge.....	75
Groundwater Levels .....	75
Groundwater Boundary Fluxes.....	81
Water Budgets .....	81
Urban Area.....	81
Selected Surface-Water Basins .....	90
Freshwater-Seawater Interface.....	91
Response of the System to Increased Groundwater Pumpage and Sea Level .....	92
Increased Groundwater Pumpage (Scenario 1).....	95
Increased Sea Level (Scenario 2).....	97
Increased Groundwater Pumpage and Sea Level (Scenario 3) .....	101
Model Reliability.....	101
Model Sensitivity.....	101
Model Limitations.....	105
Summary.....	108
References Cited .....	110
Appendix 1. Documentation for the General Flux Boundary Package for MODFLOW .....	118
Appendix 2. Observed and Simulated Canal Stages .....	137
Appendix 3. Observed and Simulated Canal Discharge .....	151
Appendix 4. Observed and Simulated Net Canal Discharge.....	158
Appendix 5. Observed and Simulated Groundwater Levels.....	162

## Figures

1. Map showing the study area in southeastern Florida .....	3
2. Graph showing monthly rainfall rates in the onshore part of the study area, 1996–2010 .....	7
3. Map showing topography and bathymetry in the study area .....	8
4. Maps showing land use in the study area in 1995, 2000, 2004, and 2008 .....	12
5. Graph showing monthly reference and maximum evapotranspiration rates in the onshore part of the study area, 1996–2010 .....	15
6. Maps showing land-use-based estimated fraction of directly connected impervious area in the study area in 1995, 2000, 2004, and 2008 .....	16

7. Graph showing estimated monthly surface runoff rate from directly connected impervious areas in the onshore part of the study area .....	18
8. Conceptual block diagram showing the components of the surface-water management in Miami-Dade County.....	18
9. Maps showing location of primary and secondary surface-water control structures and average surface-water discharge for the period from 1996 through 2010.....	19
10. Photographs showing typical primary surface-water system control structures at a gated culvert, gated spillway, and pump station.....	21
11. Photographs showing typical gated culverts in the secondary surface-water system at Northwest 12th street, Northwest 25th street, and Minton Dam .....	21
12. Hydrogeologic section showing relations of geologic formations, aquifers, and semiconfining units of the surficial aquifer system across central Miami-Dade County.....	23
13. Map showing the areal extent of the Biscayne aquifer in southeastern Florida and the line of hydrogeologic section across central Miami-Dade County .....	24
14. Conceptual hydrogeologic column for the western part of the study area that includes ages, geologic units, groundwater flow types, Q-units of Perkins, high-frequency sequence stratigraphic cycles, hydrogeologic units, and associated model layers.....	25
15. Map showing the thickness of the Biscayne aquifer in the study area and the location of wells used to determine the thickness.....	26
16. Map showing the transmissivity of the Biscayne aquifer interpolated from aquifer performance tests conducted in the study area .....	26
17. Graph showing the monthly production well field withdrawals, estimated agricultural demand, and estimated agricultural water use in the onshore part of the study area, 1996–2010 .....	28
18. Map showing the average municipal water use in the study area for the period from 1996 through 2010.....	29
19. Graph showing the estimated monthly septic return rates, recreational demand, and recreational irrigation in the onshore part of the study area, 1996–2010 .....	30
20. Maps showing estimated septic return rates in the onshore part of the study area for 1990, 2000, and 2010.....	32
21. Graph showing estimated monthly net groundwater recharge in the onshore part of the study area, 1996–2010 .....	34
22. Graph showing estimated monthly net surface-water flow in urban areas upstream of the salinity control structures in the study area, 1996–2010.....	34
23. Map showing the position of the freshwater-seawater interface at the base of the Biscayne aquifer in 1984, 1995, and 2011 .....	35
24. Map showing the horizontal model discretization.....	36
25. Map showing the lines of hydrogeologic sections and topographic/bathymetric elevations in the model domain .....	37
26. Hydrogeologic sections A–A' through I–I' in the model domain.....	38
27. Map showing surface-water gages used to evaluate model fit .....	42
28. Map showing groundwater monitoring well locations and well identification numbers.....	43
29. Map showing distribution of pilot points used to condition select groundwater properties adjusted during model calibration .....	54

30. Maps showing the spatial distribution of average annual NEXRAD rainfall for the period from 1996 through 2010, the driest year of the simulation period, and the wettest year of the simulation period .....	58
31. Maps showing the spatial distribution of estimated average annual agricultural demand and, net agricultural water use and irrigation system losses for the period from 1996 through 2010.....	60
32. Maps showing the spatial distribution of estimated average annual recreational demand and recreational irrigation for the period from 1996 through 2010 .....	61
33. Maps showing average annual reference and maximum evapotranspiration for the period from 1996 through 2010.....	63
34. Diagram showing segmented evapotranspiration approach used to represent water-table-dependent evapotranspiration in nonagricultural parts of the study area .....	64
35. Maps showing maximum depth of dense roots and evapotranspiration extinction depth below land surface in nonagricultural onshore model cells.....	65
36. Map showing internal and external surface-water boundary conditions.....	66
37. Graph showing average daily stage fluctuations in Biscayne Bay, Florida, at Virginia Key.....	67
38. Map showing basic sediment types used to calculate coastal and wetland area head-dependent groundwater boundary condition conductance values .....	72
39. Maps showing calibrated canal roughness and bed leakance coefficients.....	74
40. Maps showing calibrated horizontal hydraulic conductivity of permeable model layers 1 and 3.....	76
41. Maps showing calibrated specific storage coefficient for model layers 1, 2, and 3, and calibrated specific yield of the Biscayne aquifer .....	78
42. Maps showing mean surface-water stage differences and normalized average surface-water discharge differences between measured and model-simulated values, 1997–2004.....	80
43. Hydrographs showing net surface-water subbasin discharge differences between measured and model-simulated values for select surface-water basins in the urban area of the model domain, 1997–2004 .....	84
44. Map showing normalized average net surface-water subbasin discharge differences between measured and model-simulated values results for select surface-water subbasins, 1997–2004 .....	85
45. Map showing mean differences between measured and model-simulated groundwater levels, 1997–2004.....	85
46. Maps showing simulated water-table elevation for October 1996 and May 1997 .....	86
47. Maps showing simulated water-table elevation for October 2005 and May 2006 .....	87
48. Maps showing simulated net groundwater recharge for the calibration and verification periods.....	88
49. Maps showing simulated net groundwater general head boundary and drain fluxes for the calibration and verification periods .....	89
50. Map showing urban surface-water and groundwater water budget area .....	90
51. Diagram showing simulated canal water budgets for urban area of the model domain .....	91

52. Diagram showing simulated groundwater budgets for the urban area of the model domain .....	91
53. Maps showing simulated position of the freshwater-seawater interface in May 1997 and May 2006.....	93
54. Graph showing calculated daily and annual-average Virginia Key tidal stage used in the 30-year base-case future and increased sea-level scenarios .....	95
55. Maps showing areas with land-surface elevations at or below the average and maximum stage at Virginia Key between 1996 and 2010, and areas with land-surface elevations at or below the average and maximum stage under current and high rates of sea-level rise after 30-years .....	96
56. Maps showing percentage of time water-table elevations are less than 0.5 ft below land surface in the 30th year of the scenario simulation period for base-case future, increased groundwater pumpage, increased sea level, and increased sea-level and groundwater pumpage conditions.....	98
57. Maps showing simulated change in water-table elevations from the base-case future scenario for the increased groundwater pumpage, increased sea level, and increased sea-level and groundwater pumpage scenarios at the end of May in the 30th year of the scenario simulation period.....	102
58. Maps showing simulated change in the position of the freshwater-seawater interface from the base-case future scenario for the increased groundwater pumpage, increased sea level, and increased sea-level and groundwater pumpage scenarios at the end of May in the 30th year of the scenario simulation period.....	104
59. Graphs showing composite parameter sensitivity of simulated surface-water stages, groundwater levels, and net surface-water subbasin discharge at calibration points to parameter changes .....	106

## Tables

1. Relation of basic land-use categories and the Florida Land Use and Cover Classification System .....	10
2. Percentage of the onshore part of the study area in each basic land-use category.....	11
3. Land-use based crop coefficients.....	14
4. Estimated range of total impervious area in each basic land-use category, 1996–2010.....	15
5. Theoretical semivariogram models and parameters for Holocene and Pleistocene sediment sequences and Biscayne aquifer hydraulic conductivity .....	27
6. Surface-water stage observation locations, data source, number of weekly observations, and model-fit statistics.....	44
7. Monthly net surface-water subbasin canal discharge locations, data source, number of daily observations, and model-fit statistics .....	48
8. Groundwater monitoring well locations, data source, number of daily observations, and model-fit statistics.....	50
9. Calibration criteria applied to surface-water stage and groundwater level observations. ....	57

10.	Calibration criteria applied to surface-water discharge and net surface-water subbasin canal discharge observations. ....	57
11.	Calibrated crop coefficients for urban land-use types. ....	62
12.	Surface-water control structure dimensions and hydraulic characteristics .....	68
13.	Sediment types and hydraulic properties used to calculate leakance coefficients used to calculate coastal and wetland area head-dependent groundwater boundary condition conductance values .....	73
14.	Surface-water discharge observation locations, data source, number of daily observations, and model-fit statistics.....	82
15.	Simulated groundwater budget for selected basins during the calibration period .....	92
16.	Simulated groundwater budget for selected basins during the verification period .....	92
17.	Base and increased Miami-Dade Water and Sewer Department future groundwater pumpage rates .....	94
18.	Simulated base-case future scenario groundwater budget for select basins.....	100
19.	Simulated groundwater budget change from the base-case future scenario for select basins with increased groundwater pumpage.....	100
20.	Simulated groundwater budget change for select basins with increased sea level .....	101
21.	Simulated groundwater budget change for select basins with increased sea level and increased groundwater pumpage.....	106

## Conversion Factors

### Inch/Pound to SI

<b>Multiply</b>	<b>By</b>	<b>To obtain</b>
Length		
inch (in.)	2.54	centimeter (cm)
foot (ft)	0.3048	meter (m)
mile (mi)	1.609	kilometer (km)
Area		
square foot (ft <sup>2</sup> )	0.09290	square meter (m <sup>2</sup> )
square mile (mi <sup>2</sup> )	2.590	square kilometer (km <sup>2</sup> )
Flow rate		
cubic foot per second (ft <sup>3</sup> /s)	0.02832	cubic meter per second (m <sup>3</sup> /s)
gallon per day (gal/d)	0.003785	cubic meter per day (m <sup>3</sup> /d)
million gallons per day (Mgal/d)	0.04381	cubic meter per second (m <sup>3</sup> /s)
inch per year (in/yr)	25.4	millimeter per year (mm/yr)
mile per hour (mi/h)	1.609	kilometer per hour (km/h)
Withdrawal		
inch per month (in/mo)	2.54	centimeter per month (cm/mo)
Sea-level rise		
foot per year (ft/yr)	0.3048	meter per year (m/yr)
Density		
pound per cubic foot (lb/ft <sup>3</sup> )	16.02	kilogram per cubic meter (kg/m <sup>3</sup> )
Hydraulic conductivity		
foot per day (ft/d)	0.3048	meter per day (m/d)
Transmissivity*		
foot squared per day (ft <sup>2</sup> /d)	0.09290	meter squared per day (m <sup>2</sup> /d)
Leakance		
foot per day per foot [(ft/d)/ft]	1	meter per day per meter

### SI to Inch/Pound

<b>Multiply</b>	<b>By</b>	<b>To obtain</b>
Length		
centimeter (cm)	0.3937	inch (in.)
meter (m)	3.281	foot (ft)
Roughness coefficient (Manning's <i>n</i> )		
second meter <sup>1/3</sup> (sec•m <sup>1/3</sup> )	1.4859	second foot <sup>-1/3</sup> (sec•ft <sup>-1/3</sup> )

Temperature in degrees Fahrenheit (°F) may be converted to degrees Celsius (°C) as follows:  
 $^{\circ}\text{C}=(^{\circ}\text{F}-32)/1.8$

Temperature in degrees Celsius (°C) may be converted to degrees Fahrenheit (°F) as follows:  
 $^{\circ}\text{F}=(1.8\times^{\circ}\text{C})+32$

Vertical coordinate information is referenced to the North American Vertical Datum of 1988 (NAVD 88).

Horizontal coordinate information is referenced to the North American Datum of 1983 (NAD 83).

Elevation, as used in this report, is the distance above the vertical datum.

Concentrations of chemical constituents in water are given in milligrams per liter (mg/L).

\*Transmissivity: The standard unit for transmissivity is cubic foot per day per square foot times foot of aquifer thickness  $[(\text{ft}^3/\text{d})/\text{ft}^2]\text{ft}$ . In this report, the mathematically reduced form, foot squared per day ( $\text{ft}^2/\text{d}$ ), is used for convenience.

## Abbreviations

APT	aquifer performance test
BLU	basic land use
DCIA	directly connected impervious area
DCPA	directly connected pervious areas
DRN	drain (boundary)
E1	modified Nash-Sutcliffe model efficiency coefficient
EDEN	Everglades Depth Estimation Network
ENP	Everglades National Park
ETS	Evapotranspiration Segments (Package)
FLUCCS	Florida Land Use and Cover Classification System
GOES	Geostationary Operational Environmental Satellite
GFB	General Flux Boundary (Package)
GHB	general head boundary
lidar	light detection and ranging
ME	mean error
MDWASD	Miami-Dade County Water and Sewer Department
NEXRAD	Next Generation Radar
NGDC	National Geophysical Data Center
NME	normalized mean error
NOAA	National Oceanic and Atmospheric Administration
NRMSE	normalized root mean square error
NWS	National Weather Service
NWWF	Northwest well field
PEST	parameter estimation software
RCH	Recharge (Package)
RMSE	root mean square error
SFWMD	South Florida Water Management District
SFWMM	South Florida Water Management Model

SWI2	Seawater Intrusion (Package)
SWR1	Surface-Water Routing (Process)
TIA	total impervious surface area
USGS	U.S. Geological Survey
UTM	Universal Transverse Mercator
WCA	water conservation area
WEL	Well (Package)
WSI	Weather Services Incorporated



# Hydrologic Conditions in Urban Miami-Dade County, Florida, and the Effect of Groundwater Pumpage and Increased Sea Level on Canal Leakage and Regional Groundwater Flow

By Joseph D. Hughes and Jeremy T. White

## Abstract

The extensive and highly managed surface-water system in southeastern Florida constructed during the 20th Century has allowed for the westward expansion of urban and agricultural activities in Miami-Dade County. In urban areas of the county, the surface-water system is used to (1) control urban flooding, (2) supply recharge to production well fields, and (3) control seawater intrusion. Previous studies in Miami-Dade County have determined that on a local scale, leakage from canals adjacent to well fields can supply a large percentage (46 to 78 percent) of the total groundwater pumpage from production well fields. Canals in the urban areas also receive seepage from the Biscayne aquifer that is derived from a combination of local rainfall and groundwater flow from Water Conservation Area 3 and Everglades National Park, which are west of urban areas of Miami-Dade County.

To evaluate the effects of groundwater pumpage on canal leakage and regional groundwater flow, the U.S. Geological Survey (USGS) developed and calibrated a coupled surface-water/groundwater model of the urban areas of Miami-Dade County, Florida. The model was calibrated by using observation data collected from January 1997 through December 2004. The model calibration was verified using observation data collected from January 2005 through December 2010. A 1-year warmup period (January 1996 through December 1996) was added prior to the start of the calibration period to reduce the effects of inaccurate initial conditions on model calibration. The model is designed to simulate surface-water stage and discharge in the managed canal system and dynamic canal leakage to the Biscayne aquifer as well as seepage to the canal from the aquifer. The model was developed using USGS MODFLOW–NWT with the Surface-Water Routing (SWR1) Process to simulate surface-water stage, surface-water discharge, and surface-water/groundwater interaction and the Seawater Intrusion (SWI2) Package to simulate seawater intrusion, respectively.

Automated parameter estimation software (PEST) and highly parameterized inversion techniques were used to calibrate the model to observed surface-water stage, surface-water discharge, net surface-water subbasin discharge, and groundwater level data from 1997 through 2004 by modifying hydraulic conductivity, specific storage coefficients, specific yield, evapotranspiration parameters, canal roughness coefficients (Manning's  $n$  values), and canal leakance coefficients. Tikhonov regularization was used to produce parameter distributions that provide an acceptable fit between model outputs and observation data, while simultaneously minimizing deviations from preferred values based on field measurements and expert knowledge.

Analytical and simulated water budgets for the period from 1996 through 2010 indicate that most of the water discharging through the salinity control structures is derived from within the urban parts of the study area and that, on average, the canals are draining the Biscayne aquifer. Simulated groundwater discharge from the urban areas to the coast is approximately 7 percent of the total surface-water inflow to Biscayne Bay and is consistent with previous estimates of fresh groundwater discharge to Biscayne Bay. Simulated groundwater budgets indicate that groundwater pumpage in some surface-water basins ranges from 13 to 27 percent of the sum of local sources of groundwater inflow. The largest percentage of groundwater pumpage to local sources of groundwater inflow occurs in the basins that have the highest pumping rates (C–2 and C–100 Basins). The ratio of groundwater pumpage to simulated local sources of groundwater inflow is less than values calculated in previous local-scale studies.

The position of the freshwater-seawater interface at the base of the Biscayne aquifer did not change notably during the simulation period (1996–2010), consistent with the similar positions of the interface in 1984, 1995, and 2011 under similar hydrologic and groundwater pumping conditions. Landward movement of the freshwater-seawater interface above the base of the aquifer is more prone to occur during relatively dry years.

## 2 Hydrologic Conditions and Effect of Pumpage and Sea Level on Canal Leakage and Regional Groundwater Flow

The model was used to evaluate the effect of increased groundwater pumpage and (or) increased sea level on canal leakage, regional groundwater flow, and the position of the freshwater-seawater interface. Permitted groundwater pumping rates, which generally exceed historical groundwater pumping rates, were used for Miami-Dade County Water and Sewer Department groundwater pumping wells in the base-case future scenario. Base-case future and increased pumping scenario results suggest seawater intrusion may occur at the Miami-Springs well field if the Miami Springs, Hialeah, and Preston well fields are operated using current permitted groundwater pumping rates. Scenario simulations also show that, in general, the canal system limits the adverse effects of proposed groundwater pumpage increases on water-level changes and saltwater intrusion. Proposed increases (up to a 7 percent increase) in groundwater pumpage do not have a notable effect on movement of the freshwater-seawater interface. Increased groundwater pumpage increased lateral groundwater inflow into basins subject to additional groundwater pumpage; however, most (55 percent) of the additional groundwater extracted from pumping wells was supplied by changes in canal seepage and leakage in urban areas of the model. Increased sea level caused increased water-table elevations in urban areas and decreased hydraulic gradients across the system; the largest increases in water-table elevations occurred seaward of the salinity control structures. The extent of flood-prone areas and the percentage of time water-table elevations in flood-prone areas were less than 0.5 foot below land surface increased with increased sea level. Increased sea level also resulted in landward migration of the freshwater-seawater interface; the largest changes in the position of the interface occurred seaward of the salinity control structures except in parts of the model area that were inundated by increased sea level. Decreased water-table gradients reduced groundwater inflow, groundwater outflow, canal exchanges, surface-water inflow, and surface-water outflow through salinity control structures. Results for the scenario that evaluated the combination of increased groundwater pumpage and increased sea level did not differ substantially from the scenario that evaluated increased sea level alone. Groundwater inflow, groundwater outflow, and canal exchanges were reduced in urban areas of the study area as a result of decreased water-table gradients across the system, although reductions were less than those in the increased sea-level scenario. The decline in groundwater levels caused by increased groundwater pumpage was less under the increased sea-level scenario than under the increased groundwater-pumpage scenario. The largest reductions in surface-water outflow from the salinity control structures occurred with increased sea level and increased groundwater pumpage.

The model was designed specifically to evaluate the effect of groundwater pumpage on canal leakage at the surface-water-basin scale and thus may not be appropriate for (1) predictions that are dependent on data not included in the calibration process (for example, subdaily simulation of high-intensity events and travel times) and (or) (2) hydrologic

conditions that are substantially different from those during the calibration and verification periods. The reliability of the model is limited by the conceptual model of the surface-water and groundwater system, the spatial distribution of physical properties, the scale and discretization of the system, and specified boundary conditions. Some of the model limitations are manifested in model errors. Despite these limitations, however, the model represents the complexities of the interconnected surface-water and groundwater systems that affect how the systems respond to groundwater pumpage, sea-level rise, and other hydrologic stresses. The model also quantifies the relative effects of groundwater pumpage and sea-level rise on the surface-water and groundwater systems.

## Introduction

The natural hydrologic setting of southeastern Florida has been altered substantially by anthropogenic activities since the early 20th Century, making evaluations and management of the water supply increasingly complex. Urban and agricultural areas of southeastern Florida generally lie between the Everglades (Everglades National Park and water-conservation areas) to the west and Biscayne Bay and the Atlantic Ocean to the east (fig. 1). An extensive and highly managed surface-water system constructed in southeastern Florida during the 20th Century to provide drained land has allowed urban and agricultural activities to expand westward (Renken and others, 2005a). Surface water is impounded in water-conservation areas that lie west of a protective levee system. The water-conservation areas are managed and used to (1) provide water to the Everglades, (2) prevent overland sheetflow from moving eastward and flooding urban and agricultural areas, and (3) supply water for agricultural and municipal uses. The surface-water system east of the water-conservation areas is used to (1) control urban flooding, (2) supply recharge to production well fields, and (3) control seawater intrusion. Miami-Dade County is underlain by the shallow, unconfined to semiconfined, highly permeable Biscayne aquifer, which is the primary municipal water supply for the county. The surface-water system in Miami-Dade County is hydraulically connected to the groundwater system; thus, the management of the surface-water system can affect groundwater resources, and vice versa.

In 2007, the South Florida Water Management District (SFWMD) approved a rule that prevents water users from relying on the Everglades for new or additional supplies of water; instead, users are required to seek alternative sources of water that are not dependent on the Everglades for recharge (South Florida Water Management District, 2008). Alternative sources may include recycled water, using treated wastewater to recharge the Biscayne aquifer, water pumped from the Floridan aquifer system, and (or) water conservation. An additional source of water that may potentially be used in the absence of additional water released from the



## 4 Hydrologic Conditions and Effect of Pumpage and Sea Level on Canal Leakage and Regional Groundwater Flow

water conservation areas is local groundwater recharge that is currently captured by the surface-water system, discharged to Biscayne Bay or Florida Bay at the coast from salinity control structures, and not needed to support coastal wetland and estuarine habitats. To ensure that the county is not reliant on the Everglades for additional water supply, it is important that Miami-Dade County be able to evaluate components of the hydrologic budget.

Previous attempts have been made to quantify the amount of water released from the Everglades and subsequently withdrawn by groundwater pumping from the Biscayne aquifer for water supply. Because the canal system is used to convey water from the Everglades, these attempts have focused on how groundwater pumping from the Biscayne aquifer affects canal leakage. The canal system in the urban areas also receives seepage from the Biscayne aquifer that is derived from a combination of local rainfall and groundwater flow from Water Conservation Area 3 and Everglades National Park. To quantify current surface-water/groundwater interactions in the C-2 Canal (Snapper Creek) near the Snapper Creek production well field (fig. 1), Sunderland and Krupa (2007) used a combination of canal stage, groundwater level, and acoustic Doppler current profiler (ADCP) streamgage data. Sunderland and Krupa (2007) indicate that (1) groundwater elevation is influenced by changes in surface-water stage along the C-2 Canal, (2) groundwater elevations near the Snapper Creek well field are always lower than C-2 Canal stage and indicate the canal is a source of recharge to the Biscayne aquifer, (3) as much as 20 cubic feet per second ( $\text{ft}^3/\text{s}$ ) was lost between two C-2 Canal streamgage locations when the Snapper Creek well field was in operation, and (4) the loss of flow in the C-2 Canal was equivalent to approximately 60 percent of the pumpage ( $33.1 \pm 9.9 \text{ ft}^3/\text{s}$ ) from the well field. Surface-water losses in the C-6 Canal (Miami Canal) and adjacent tributaries near the Miami Springs-Hialeah-Preston well fields (fig. 1) contributed about 78 percent ( $100 \times 53.7 \text{ ft}^3/\text{s} \div 69 \text{ ft}^3/\text{s}$ ) of the total pumpage on March 28, 1946 (Parker and others, 1955), 52 percent ( $100 \times 71.9 \text{ ft}^3/\text{s} \div 1.7 \text{ ft}^3/\text{s}$ ), 55 percent ( $100 \times 78.4 \text{ ft}^3/\text{s} \div 142.4 \text{ ft}^3/\text{s}$ ) of the total pumpage in 1970 and 1971, respectively (Meyer, 1972), and 46 percent ( $100 \times 75.2 \text{ ft}^3/\text{s} \div 162.5 \text{ ft}^3/\text{s}$ ) of the total pumpage in 1973 (Miller, 1978). Although these studies have quantified the effect of groundwater pumpage on canal leakage in Miami-Dade County, these analyses were limited to brief periods for the Miami Springs-Hialeah-Preston well fields and the Snapper Creek and Alexander Orr well fields, and no determination was made of how increased groundwater withdrawals would affect groundwater inflow from the Everglades or reductions in freshwater discharge to tide at the coast from salinity control structures.

In 2008, the U.S. Geological Survey (USGS), in cooperation with the Miami-Dade County Water and Sewer Department, initiated a hydrologic analysis to improve the understanding of the contribution of various hydrologic components to the water supply at the county scale. One of the objectives of this study was to create a tool that would allow various components of the complex hydrologic system to be

quantified, and to evaluate effects of historical and potential system stresses on the coupled surface-water/groundwater system and hydrologic budget. The tool created is a coupled surface-water/groundwater flow model of the urban areas of Miami-Dade County that can quantify canal leakage and groundwater inflow from the Everglades, as well as simulate changes in surface-water stage and discharge, groundwater levels, and the position of the freshwater-seawater interface (Hughes and White, 2016).

### Purpose and Scope

The purpose of this report is to (1) quantify hydrologic conditions in urban areas of Miami-Dade County between 1996 and 2010, (2) quantify the effect of groundwater pumpage from the Biscayne aquifer on canal leakage throughout the urban areas of the county for all of the well fields operated by the Miami-Dade County Water and Sewer Department (MDWASD), (3) determine how canal leakage may change in response to increased groundwater pumpage and increases in sea level, and (4) determine how increased groundwater pumpage may change groundwater seepage from the Everglades. This report also describes the development and calibration of a coupled surface-water/groundwater model of the urban areas of Miami-Dade County, Florida, used to evaluate these effects in the hydrologic system. The report includes discussions of (1) the surface-water and groundwater hydrology of Miami-Dade County, (2) the hydraulic characteristics of the surface-water system, (3) the hydrogeologic framework of the Biscayne aquifer in Miami-Dade County, (4) the numerical model used to simulate the surface-water and groundwater systems, (5) the surface-water stage and discharge and groundwater levels used to calibrate the model, (6) hydraulic characteristics of the calibrated model, (7) current and future surface-water stage and discharge, groundwater levels, and the position of the freshwater-seawater interface simulated with the model, (8) sensitivity of model results at surface-water gages and groundwater monitoring wells to model parameters, and (9) potential errors and limitations of the model to guide the interpretation of simulation results and future applications of the model.

The model presented herein was used to estimate changes in surface-water stage and discharge, groundwater levels, canal leakage, and the position of the freshwater-seawater interface resulting from projections of future groundwater pumpage rates and (or) sea level. The sensitivity of model results at surface-water gages and groundwater monitoring wells to model parameters were calculated. Limitations of the model are presented to guide the interpretation of simulation results and future model applications.

### Location of the Study Area

The study area is in southeastern Florida along the Atlantic Ocean to east of the Everglades (fig. 1). The study

area includes the urban area of Miami-Dade County and the part of the C-9 surface-water basin in Broward County that contributes surface water and groundwater to the C-9 Canal. A total of 17 surface-water basins covering the urban part of Miami-Dade County are included in this study. Parts of Water-Conservation Area 3 and Everglades National Park (ENP) are included in the study area so that surface-water deliveries and groundwater seepage from the water-conservation area and Everglades can be simulated in the model. The study area also includes Biscayne Bay, Card Sound, Barnes Sound, and part of Florida Bay and the Atlantic Ocean to allow the model to simulate the effects of offshore saline groundwater on groundwater discharge to the coast and the position of the freshwater-seawater interface.

## Approach

To quantify effects of changes in groundwater pumpage and sea level on canal leakage and groundwater inflow from the Everglades, a numerical model was developed that simulates surface-water stage and flow in the managed canal system in urban areas of Miami-Dade County, groundwater flow within the Biscayne aquifer, exchange between the canals and the aquifer, groundwater seepage from the Everglades, as well as the position of the freshwater-seawater interface. The model was constructed by using existing hydraulic and hydrogeologic data and the estimated position of the freshwater-seawater interface. The model is based on a number of previous groundwater-flow and solute-transport models designed to (1) investigate groundwater flux into Biscayne Bay (Langevin, 2001), (2) evaluate the factors contributing to hypersalinity events in Biscayne Bay (Lohmann and others, 2012), and (3) estimate time-based capture zones and drawdown contours for two well fields in Miami-Dade County (Brakefield and others, 2013). This study extends these previous studies by specifically simulating surface-water stage and discharge in the managed canal system, and dynamic canal leakage to the Biscayne aquifer and discharge from the Biscayne aquifer to the canal system. This study also expands on these previous studies by including estimates of agricultural water use, recreational (lawn) irrigation, and septic tank return flows.

Observation data collected from January 1997 through December 2010 were used to calibrate and verify the model and include periods of below-average, average, and above-average rainfall. The model was calibrated by using highly parameterized inversion methods with surface-water stage and discharge observations, net surface-water subbasin discharge, and groundwater level observations. Simulations of changes in surface-water stage and discharge, groundwater levels, and the position of the freshwater-seawater interface were made using projections of future groundwater pumpage rates and sea level.

The model was developed by using the MODFLOW-NWT code, developed by the USGS (Niswonger and others, 2011), with the Surface-Water Routing (SWR1) Process (Hughes and others, 2012) and the Seawater Intrusion (SWI2) Package (Bakker and others, 2013). MODFLOW-NWT is

based on MODFLOW-2005 (Harbaugh, 2005) and is designed to solve problems involving drying and rewetting nonlinearities of the unconfined groundwater-flow equation (Niswonger and others, 2011). The SWR1 Process was developed to simulate surface-water stage, surface-water discharge, and surface-water/groundwater interaction in areas where surface-water gradients are small and (or) control structures are used to manage surface water. The SWI2 Package was developed to simulate variable-density flow in regional-scale models by using a rigorous but simplified approach that requires fewer layers than required by variable-density groundwater flow models, such as SEAWAT (Langevin and others, 2007), which solve the advective-dispersive transport equation.

Model design and input were modified from existing models that simulated groundwater discharge from the Biscayne aquifer into Biscayne Bay and capture zones and drawdown for two well fields in Miami-Dade County (Langevin, 2001; Lohmann and others, 2012; Brakefield and others, 2013). Additional data were used to define rainfall rates, potential evapotranspiration rates, crop coefficients, canal geometry, canal leakage, and canal roughness coefficients. The model was calibrated to measured canal stage, canal discharge, groundwater levels in the Biscayne aquifer, estimated net surface-water subbasin discharge, and qualitatively to the general location of the freshwater-seawater interface in the Biscayne aquifer. Scenarios representing the effects of increased groundwater pumpage and (or) increased sea level on canal leakage were simulated.

## Previous Investigations

Numerous studies of the surface-water system, the Biscayne aquifer, and the interaction between the surface-water system and the Biscayne aquifer in Miami-Dade County have been completed since the 1940s. Representative publications describing the evolution and flow characteristics of the surface-water system in Miami-Dade County include Sherwood and Leach (1962), Leach and Sherwood (1963), Kohout and Leach (1964), Leach and Grantham (1966), Leach and others (1972), Meyer (1972), and Cooper and Lane (1987). Representative publications describing the Biscayne aquifer in Miami-Dade County, many of which focus on aquifer response to groundwater pumpage and its effect on seawater intrusion, include Brown and Parker (1945), Parker (1945), Parker (1951), Parker and others (1955), Klein (1957), Schroeder and others (1958), Cooper (1959), Kohout (1960a, b; 1961a, b), Kohout and Hoy (1963), Kohout (1964), Kohout and Klein (1967), Kohout and Kolipinski (1967), Hull and Meyer (1973), Klein and Waller (1985), Klein and Ratzlaff (1989), Fish and Stewart (1991), Sonenshein and Koszalka (1996), and Sonenshein (1997). Recently, cyclostratigraphic and (or) geophysical methods have been used to develop a more detailed, stratigraphic understanding of Biscayne aquifer heterogeneity and are summarized in Cunningham and others (2001, 2004, 2006, 2009), Hickey and others (2010), and Cunningham and Sukop (2011). The publications of Leach

and Sherwood (1963), Kohout and Leach (1964), Leach and Grantham (1966), Leach and others (1972), and Meyer (1972) also evaluated the effect of surface-water system management on seawater intrusion in the Biscayne aquifer. The study of Meyer (1972) is notable because it specifically evaluated canal leakage induced by groundwater pumpage in the Miami Springs-Hialeah area. Other representative publications that have evaluated interaction of the surface-water system and the Biscayne aquifer include Chin (1990), Nemeth and others (2000), Sonenshein (2001), Nemeth and Solo-Gabriele (2003), and Sunderland and Krupa (2007).

Numerous models have been constructed of the surface-water system and Biscayne aquifer in Miami-Dade County. The first model was that of Henry (1964), which was based on the Cutler and Silver Bluff areas of Miami-Dade County and simulated seawater intrusion in the Biscayne aquifer. Appel (1973) developed an electric-analog model of Miami-Dade County that simulated surface-water discharge, surface-water structure operations, groundwater flow in the Biscayne aquifer, and surface-water/groundwater interactions. Other numerical models of Miami-Dade County include (1) surface-water flow models, (2) groundwater flow models, and (3) coupled surface-water and groundwater flow models. Published groundwater flow models include those by Merritt (1996b, 1997), Langevin (2001), Giddings and others (2006), Guha (2008), Guha and Panday (2012), and Brakefield and others (2013). Numerous surface-water flow models have been developed to evaluate how the surface-water system might respond during storm events. Representative published surface-water flow models include those by the Miami-Dade Department of Environmental Resources Management (2000), CDM (2003, 2005), CH2MHILL (2003, 2006), Earth Tech (2003, 2006), URS (2003, 2005), Keith and Schnars (2004), PBS&J (2004, 2006), and Chin and Patterson (2005). The SFWMD has developed the South Florida Water Management Model (SFWMM) (MacVicar and others, 1984; South Florida Water Management District, 2005) to simulate the regional response of the surface-water and groundwater system to canal structure operations and groundwater use. The SFWMM area extends from just north of Lake Okeechobee to the southern coastline of ENP. Additional published coupled surface-water and groundwater flow models include those by Swain and others (1996), Lin and others (2000), Langevin and others (2005), Wang and others (2007a), Cook (2012), and Lohmann and others (2012).

## Hydrologic Conditions in Urban Miami-Dade County

Climate, surface-water hydrology, groundwater hydrology, water supply and use, groundwater recharge, surface-water/groundwater interaction, and the position of the freshwater-seawater interface in urban Miami Dade County and portions of Water Conservation Area 3 (WCA3) and ENP were

evaluated for the period from 1996 through 2010. The assessment includes land-use-based estimates of evapotranspiration, surface runoff, agricultural water use, and recreational irrigation, which are used to estimate groundwater recharge in the study area. Observed surface-water discharge is used to estimate surface-water/groundwater interaction in urban parts of the study area. The assessment of recent hydrologic conditions is also used to provide the framework for the coupled surface-water/groundwater model discussed in subsequent sections and qualitatively assess the reasonableness of model results.

## Climate

The climate of southeastern Florida is characterized as tropical monsoon with mean, monthly temperatures above 64 °F (Peel and others, 2007). The average temperature at Miami International Airport during the period from 1981 through 2010 was 76.9 °F and ranged from a low of 59.8 °F in January to a high of 90.7 °F in August (National Oceanic and Atmospheric Administration, 2013). From 1991 through 2011, the percentage of time it was sunny at this location averaged 70 percent and ranged from a low of 63 percent in December to 76 percent in April (National Oceanic and Atmospheric Administration, 2014).

The monthly average wind speed at a 30-foot (ft) height for the period from 1949 through 2012 (63 years) averaged 9.2 miles per hour (mi/hr) and ranged from 7.9 mi/hr in July and August to 10.5 mi/hr in April (National Oceanic and Atmospheric Administration, 2014). Maximum wind speeds ranged from 37 to 86 mi/hr and generally emanated from 17° east of true north from 1957 through 2012 (55 years).

Tropical monsoon climates also are characterized by notable seasonal variation in precipitation, with the driest month during or just after the winter solstice. Rainfall in Florida generally is the result of seasonal convective, tropical, or frontal storms (Skinner and others, 2009). Peninsular Florida experiences distinct wet and dry seasons that are related to the predominant storm types during those periods. Convective and tropical storms are common during the wet season, which typically begins in June and ends in October. Frontal storms are common from December through April during the dry season. May and November are generally transitional months that can include storms characteristic of both the wet and the dry seasons.

Daily rainfall data calculated from Next Generation Radar (NEXRAD) return-intensity data are available on a 1.24×1.24-mile (mi) grid in the study area from the SFWMD. NEXRAD return-intensity data collected in the study area by the National Weather Service (NWS) are corrected to account for blockage caused by obstructions (clutter suppression) and then converted to precipitation by Weather Services Incorporated (WSI) using an empirical lookup table. The WSI NEXRAD rainfall data are further refined by the One Rain Company through a gage-correction procedure to produce the final rainfall dataset available from the SFWMD. More detail on the methods used to convert raw NWS NEXRAD

return-intensity data to gage-corrected rainfall data in the study area are provided in Skinner and others (2009).

A select number of rain gages maintained by the SFWMD are used in the gage-correction procedure; as a result, there may be discrepancies between NEXRAD rainfall data and rain gages not included in the gage-correction procedure. Systematic and temporal biases between the two sources of rainfall data have been observed elsewhere (for example, see Neary and others, 2004; Wang and others, 2007b; and Watkins and others, 2007). Skinner and others (2009) determined that NEXRAD rainfall data were a factor of 0.95 less than gage data north of Lake Okeechobee (fig. 1). Furthermore, Skinner and other (2009) determined that the NEXRAD rainfall data tended to overestimate rainfall events less than 0.5 inch (in.) and underestimate rainfall events greater than 1.0 in. Following the work of Skinner and others (2009), a constant NEXRAD bias-correction factor of 1.05 was used to scale the daily NEXRAD data to be more comparable to rain gage data in southern Florida.

The average annual NEXRAD-based rainfall for onshore parts of the study area (about 1,100 square miles [mi<sup>2</sup>]) was 55.70 in. for the period from 1996 through 2010, and ranged from 36.36 in. for 1996 to 68.16 in. for 2005 (fig. 2). Rainfall was more than 1 standard deviation ( $\sigma$ ; 7.72 in.) below the annual mean in 1996 and 2004, and more than 1 $\sigma$  above the annual mean in 1999 and 2005.

The average relative humidity in the morning for the period from 1964 through 2011 (47 years) ranged from 77 percent in April to 85 percent in September, and in the afternoon it ranged from 54 percent in April to 66 percent in September (National Oceanic and Atmospheric Administration, 2014). The average morning and afternoon relative humidity was 82 and 61 percent, respectively, at Miami International Airport.

## Surface-Water Hydrology

Southeastern Florida is characterized by distinct wet and dry seasons, high rainfall and evapotranspiration rates, relatively low topographic relief, and high water-table conditions. The concurrence of low topographic relief and a high water table requires an extensive surface-water management system to drain excess water in the study area.

## Topography

A composite topographic dataset was developed by using elevation data from the SFWMD (South Florida Water Management District, 2009a, b), the Everglades Depth Estimation Network (EDEN) database (U.S. Geological Survey, 2012), and the National Oceanic and Atmospheric Administration (NOAA) National Geophysical Data Center (NGDC) Coastal Relief Model database (National Oceanic and Atmospheric Administration, 2006). The SFWMD dataset was upscaled from high-resolution light detection and ranging (lidar) data to a 50-ft grid and was used to define land-surface elevations in urban parts of the study area. The EDEN dataset was developed from a combination of 1-ft contours and point elevation data and was used to define land-surface elevations in the water-conservation areas and ENP. The NOAA dataset was used to define offshore bathymetric elevations. The EDEN and NOAA datasets were interpolated to a common 50-ft grid and merged with the SFWMD dataset to develop the final composite land surface and bathymetric data for the study area (fig. 3).

The highest natural elevation in Miami is 22.75 ft NAVD 88 along the Miami Rock Ridge in Coconut Grove, and the average elevation is 4.86 ft NAVD 88. The average tidal stage at Virginia Key, Florida (National Oceanic and Atmospheric Administration, 2013a) for the period from 1996 through 2010 was -0.808 ft NAVD 88; the coastline shown in figure 3 corresponds to elevations equal to the average tidal stage at Virginia Key. The relatively high area of the Atlantic Coastal Ridge in the study area, with elevations as high as 24.89 ft NAVD 88, is prominent immediately west of Biscayne Bay (fig. 3). The Atlantic Coastal Ridge ranges from 4 to 10 mi wide in the study area and is breached by shallow sloughs or transverse glades (McPherson and Halley, 1996). The most prominent transverse glade in the study area is Miami River (Canal) flood plain, which is about 1 mi wide through the lower 2 or 3 mi of the Miami River and widens to the west toward the Everglades (White, 1970). Several primary canals are aligned with transverse glades through the Atlantic Coastal Ridge. Prior to development of southeastern Florida in the 20th Century, surface-water discharge from the Everglades to Biscayne Bay occurred only during wet periods, when surface-water stages in the Everglades exceeded land-surface elevations in the transverse glades.

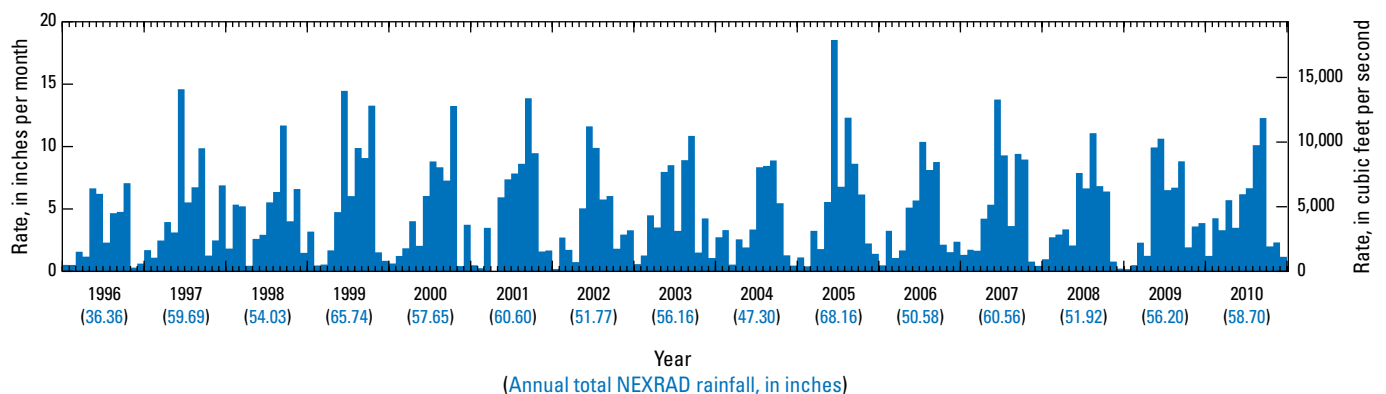
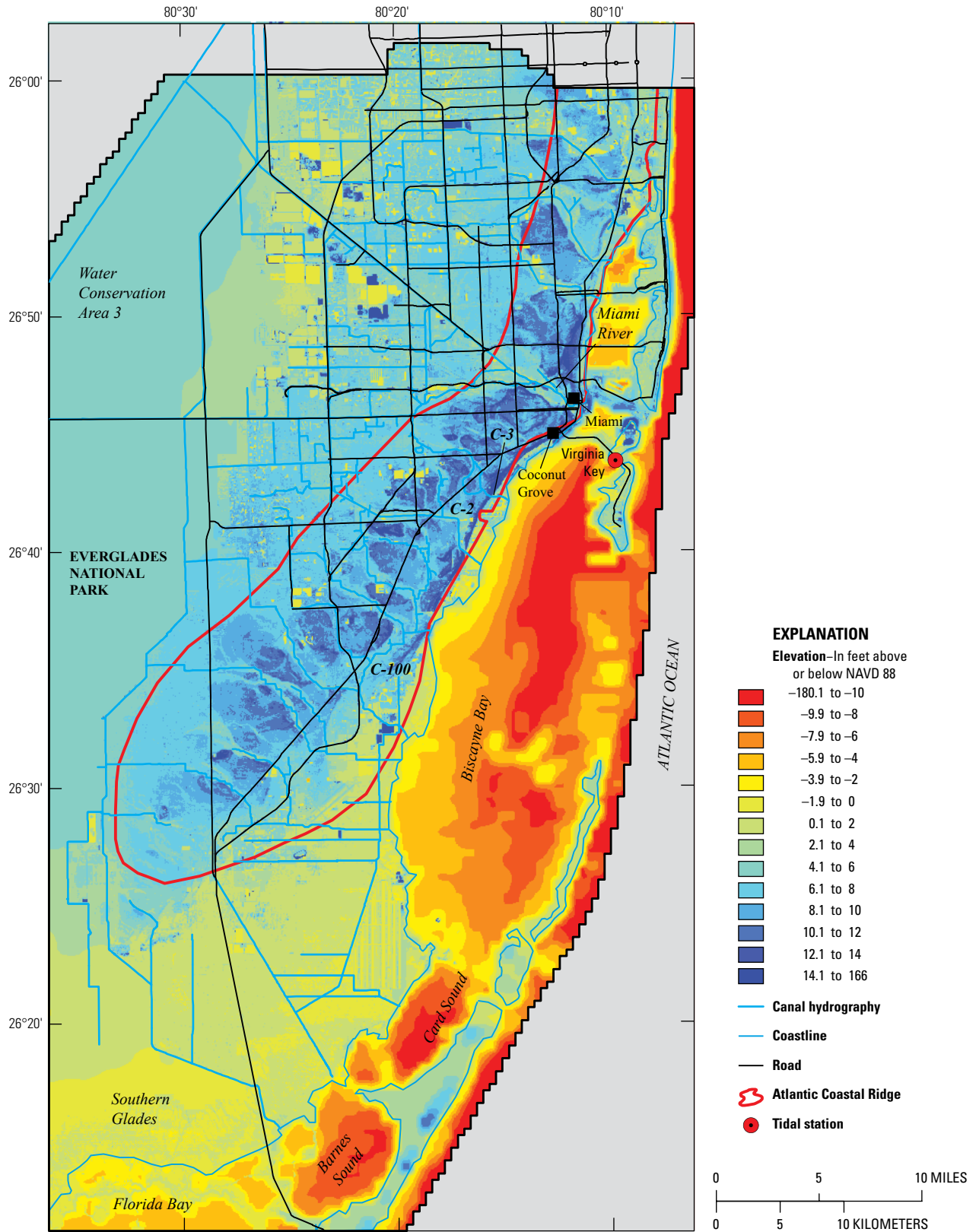


**Figure 2.** Monthly rainfall rates in the onshore part of the study area, 1996–2010.

8 Hydrologic Conditions and Effect of Pumpage and Sea Level on Canal Leakage and Regional Groundwater Flow



Base modified from U.S. Geological Survey  
 1:2,000,000-scale digital data

Figure 3. Topography and bathymetry in the study area.

## Land Use

In urban and agricultural areas, potential evapotranspiration, infiltration, and irrigation can be related to land-use classification data. Furthermore, surface runoff to surface-water features can be related to a combination of land-use classification and surface-slope data. Land-use data developed by the SFWMD for 1995, 2000, 2004, and 2008 (South Florida Water Management District, 1995; 2002a; 2011a, b) were evaluated. The Florida Land Use and Cover Classification System (FLUCCS) attributes in the land-use datasets were reduced to 20 basic land use (BLU) categories, which are used in the SFWMM (South Florida Water Management District, 2005). FLUCCS is a land use, vegetation cover and land form classification system that facilitates development of spatially distributed land use and land cover data from aerial photography of various types (panchromatic, natural color, or false color infrared) and scales (large, medium, and small) and from airborne and satellite multispectral imaging systems (Florida Department of Transportation, 1999).

Land use FLUCCS attributes were converted to BLU categories by using the relation developed for the SFWMM (Jennifer Barnes, South Florida Water Management District, written commun., 2012). The relations between FLUCCS codes and BLU categories are presented in table 1.

BLU categories in the study area for 1995, 2000, 2004, and 2008 are shown in figure 4. Urban land use was relatively constant between 1995 and 2008 and ranged from 32.99 to 36.6 percent of the onshore area of the model domain; the percentage of low-, medium-, and high-density urban land use remained relatively constant, increased, and decreased, respectively, between 1995 and 2008 (table 2). Agricultural land use decreased from a maximum of approximately 13.86 percent in 1995 to a minimum of 8.84 percent in 2008. Natural land uses (BLU categories 4–6, 12–16, and 18–19) increased from 43.90 to 49.12 percent between 1995 and 2008.

## Evapotranspiration

Evapotranspiration, defined as the loss of water to the atmosphere from evaporation and plant transpiration, is considerable in southeastern Florida and can exceed rainfall in lakes and in areas with ponded water. Evapotranspiration estimates typically require net radiation or incoming solar radiation instrumentation (Jacobs and others, 2008). Ground-based evapotranspiration networks in Florida are sparse and were nonexistent prior to 1990. Examples of ground-based evapotranspiration studies include Bidlake and others (1996), German (2000), Shoemaker and others (2011), Sumner (1997, 2001), and Swancar and others (2000).

To overcome the sparsity of evapotranspiration data in Florida, Jacobs and others (2008) developed a spatially distributed potential and reference evapotranspiration dataset on the basis of solar radiation data obtained from the Geostationary Operational Environmental Satellites (GOES). The spatially distributed dataset is developed for the same 1.24×1.24-mi

grid used to develop the NEXRAD rainfall data in the study area and has been extended as new GOES data become available. Additional information about the methods used to estimate potential and reference evapotranspiration data from GOES data, as well as the error inherent in the methods, are provided in Jacobs and others (2008) and Mecikalski and others (2011).

The satellite-based reference evapotranspiration data were evaluated in the study area because they represent the evaporation that would occur from a reference crop (4.7 in grass) having adequate soil moisture (Allen and others, 1998). Because of its extensive use in southeastern Florida investigations (for example, Giddings and others, 2006), reference evapotranspiration was selected instead of potential evapotranspiration.

Reference evapotranspiration is converted to a crop (vegetation)-specific maximum evapotranspiration using

$$ET_c = Kc \times ET_o, \quad (1)$$

where

- $ET_c$  is the maximum evapotranspiration rate for a specific crop [ $LT^{-1}$ ],
- $Kc$  is a crop-specific coefficient [unitless], and
- $ET_o$  is the reference evapotranspiration rate [ $LT^{-1}$ ] (Allen and others, 1998).

Typically, crop coefficients vary throughout the year to account for planting, plant growth, and die-off.  $ET_c$  does not account for soil moisture deficit under conditions in which rainfall and irrigation are insufficient to satisfy crop demands. Land-use-based crop coefficients were developed for the BLU classifications shown in figure 4 and were based on values used in the SFWMM (South Florida Water Management District, 2005) (table 3).

The average annual reference evapotranspiration for onshore parts of the study area (about 1,100 mi<sup>2</sup>) was 56.83 in. for the period from 1996 through 2010, and ranged from 53.77 in. for 1999 to 61.64 in. for 2007 (fig. 5). Application of the land-use-based crop coefficients (table 3) results in an average annual maximum evapotranspiration rate of 33.52 in. and rates that range from 31.66 in. for 2001 to 35.52 in. for 2005, within the onshore part of the study area. Average annual maximum evapotranspiration rates ranged from 49 to 94 percent of rainfall in 2005 and 1996, respectively, and are comparable in magnitude to average annual rainfall.

## Surface Runoff

Surface runoff occurs when the infiltration capacity of the soil and detention storage on the land surface is exceeded. Factors that affect and control surface runoff include (1) rainfall intensity, (2) the spatial distribution of rainfall, (3) the duration of rainfall events, (4) the size and shape of the drainage area, (5) detention storage in the drainage area, (6) the size and spatial density of connected surface-water features, (7) the slope of the land surface, and (8) the surface-water stage slope

## 10 Hydrologic Conditions and Effect of Pumpage and Sea Level on Canal Leakage and Regional Groundwater Flow

**Table 1.** Relation of basic land-use categories and the Florida Land Use and Cover Classification System (FLUCCS).

Basic land use code	Description	FLUCCS codes
1	Low density urban	1000, 1100, 1110, 1120, 1130, 1180, 1190, 1480, 1640, 1800, 1820, 1850, 1860, 1890, 2300, 2310, 2320, 2330, 2500, 2510, 2520, 2530, 2540, 2590, 8115, 8170, 8200, 8210, 8320
3	Medium density urban	1009, 1200, 1210, 1220, 1230, 1290, 1530, 1550, 1700, 1710, 1720, 1723, 1730, 1760, 1830, 1840, 1843, 1870, 1880, 8113, 8120, 8300, 8310
11	High density urban	1300, 1310, 1320, 1330, 1340, 1350, 1390, 1400, 1410, 1411, 1420, 1423, 1430, 1440, 1450, 1450, 1460, 1470, 1490, 1500, 1510, 1520, 1540, 1560, 1590, 1740, 1750, 1770, 1780, 1790, 8000, 8100, 8110, 8110, 8130, 8140, 8150, 8180, 8190, 8220, 8290, 8330, 8335, 8340, 8350, 8390
2	Citrus	2200, 2210, 2220, 2230, 2400, 2410, 2430, 2460
7	Row crops	2140, 2150, 2160, 2420, 2440, 2450
8	Sugar cane	2156, 2156
9	Irrigated pasture	2000, 2100, 2110, 2120, 2120
6	Shrubland	1650, 1670, 1810, 1900, 1910, 1920, 1930, 1940, 2600, 2610, 3000, 3100, 3200, 3200, 3210, 3220, 3230, 3290, 3291, 3292, 3300, 4350, 6500, 6520, 7000, 7100, 7110, 7200, 7300, 7310, 7400, 7410, 7420, 7430, 7430, 7431, 7440, 7450, 8146, 9130
18	Marl prairie	6150, 6160, 6410, 6410
4	Sawgrass plains	6411, 6411a, 6411b, 6411c, 6411d, 6411i
15	Cattail	6412, 6412a, 6412b, 6412c, 6412d
19	Mix cattail/sawgrass	6411e, 6411f, 6411g, 6411h
5	Wet prairie	6413, 6414, 6415, 6416, 6417, 6418, 6419, 6420, 6421, 6422, 6423, 6424, 6425, 6426, 6430, 6431, 6439, 6440, 6446, 6447, 6448, 6448, 9100, 9120
12	Forested wetland	6000, 6100, 6110, 6111, 6125, 6130, 6140, 6170, 6171, 6172, 6172b, 6173, 6173a, 6173b, 6173c, 6173d, 6173e, 6173f, 6173g, 6174, 6174a, 6174b, 6180, 6190, 6192, 6193, 6194, 6195, 6200, 6210, 6211, 6212, 6215, 6216, 6217, 6219, 6220, 6230, 6240, 6250, 6260, 6280, 6300, 6300
16	Forested uplands	2130, 4000, 4100, 4110, 4110, 4120, 4130, 4140, 4190, 4191, 4192, 4193, 4194, 4195, 4200, 4210, 4220, 4230, 4250, 4260, 4261, 4270, 4271, 4280, 4280, 4287, 4288, 4290, 4300, 4310, 4320, 4330, 4340, 4370, 4380, 4390, 4400, 4410, 4420, 4430, 4440, 4450, 9140, 9150, 9160, 9170
13	Mangroves	6120, 6120, 6121, 6122, 6123, 6124
14	Melaleuca	4119, 4240, 4289, 6191, 6218
20	Water	1660, 5000, 5100, 5110, 5120, 5200, 5210, 5220, 5230, 5240, 5250, 5300, 5310, 5320, 5330, 5340, 5430, 5500, 5600, 6450, 6510, 6530, 6540, 8160, 9110,
30	Offshore	5400, 5410, 5420, 5710, 5720
31	Rock quarries	1600, 1610, 1620, 1630

or bed slope of connected surface-water features (Bedient and Huber, 1988). When antecedent soil moisture content is low and (or) detention storage is available, surface runoff will not occur until the infiltration capacity is exceeded or the soil becomes saturated and detention storage is filled. Conversely, when antecedent soil moisture content is high and detention storage is filled, surface runoff occurs immediately or shortly after the beginning of a rainfall event and runoff rates increase as rainfall intensity increases.

Approximately 33 (1995) to 37 (2004) percent of the study area is composed of urban land having predominantly impervious surface area, which typically results in high

surface runoff rates when rainfall in such areas is routed directly to nearby drains, ditches, streams, or canals rather than to detention storage. In Miami-Dade County, all developed land is required to have stormwater management systems capable of accepting runoff from impervious and pervious surfaces resulting from 5-year storms of any duration (Chin, 2004). Stormwater management systems typically include some combination of retention areas, detention devices, and filtering devices.

Although stormwater management currently is required in Miami-Dade County, many areas of the county were developed prior to implementation of current stormwater

**Table 2.** Percentage of the onshore part of the study area in each basic land-use category.

Basic land use code	Description	Year			
		1995	2000	2004	2008
1	Low density urban	4.73	4.68	5.43	4.24
3	Medium density urban	14.19	15.93	19.02	19.51
11	High density urban	14.07	14.59	12.15	11.18
2	Citrus	2.83	4.35	4.77	4.58
7	Row crops	8.81	6.66	5.59	4.07
8	Sugar Ccne	0.00	0.00	0.00	0.00
9	Irrigated pasture	2.22	0.59	0.47	0.19
6	Shrubland	2.61	4.79	3.97	3.14
18	Marl prairie	21.14	5.07	3.39	4.43
4	Sawgrass plains	7.83	21.20	25.47	29.16
15	Cattail	0.01	0.20	0.00	0.00
19	Mix cattail/sawgrass	0.00	0.00	0.00	0.00
5	Wet prairie	0.56	2.75	2.05	2.04
12	Forested wetland	2.59	2.20	3.45	3.66
16	Forested uplands	2.71	2.06	0.89	0.63
13	Mangroves	2.17	3.81	3.42	3.55
14	Melaleuca	4.28	3.41	2.04	2.51
20	Water	7.10	6.42	6.88	6.48
30	Offshore	0.40	0.38	0.40	0.37
31	Rock quarries	1.73	0.92	0.57	0.27
Total area, in square miles		1,094			

management requirements, and in these areas, flooding and uncontrolled surface runoff can occur during high-intensity rainfall events. Furthermore, it is also possible for drainage structures designed to meet current stormwater management requirements to discharge excess surface runoff during storms with intensities exceeding those of 5-year design storms (Chin, 2004) and (or) as a result of successive storms without enough intervening time for infiltration to occur in available retention areas and detention devices. Surface runoff in urban catchments, such as those in Miami-Dade County, can be considered to be the sum of the runoff from directly connected impervious areas (DCIAs) and directly connected pervious areas (DCPAs). Surface runoff from DCPAs occurs only when rainfall rates exceed the infiltration capacity of the soil, and these rates are typically high throughout much of the study area. As a result, surface runoff is controlled primarily by DCIA. Chin and Patterson (2005) found that the ratio of runoff

to rainfall was in relatively close agreement with the percentage of DCIA in the catchments evaluated in the C-103 Basin, in the Homestead area south of Miami (fig. 1).

Although the processes affecting and controlling surface runoff in Miami-Dade County are understood, quantitative assessments of total impervious surface area (TIA), DCIA, and DCPA are limited. As a result, land-use-based average TIA data contained in Keith and Schnars (2004) for southern Miami-Dade County (C-1, C-2, C-3, C-100, C-102, and C-103 Basins) were used to estimate surface runoff in the study area. The range of average TIA in urban BLU categories is summarized in table 4. Non-urban BLU categories were assumed to be 100 percent pervious.

DCIA without detention storage was assumed to compose 25 percent of the total estimated impervious area (Keith and Schnars, 2004; ADA Engineering, 2012). An assumed DCIA

12 Hydrologic Conditions and Effect of Pumpage and Sea Level on Canal Leakage and Regional Groundwater Flow

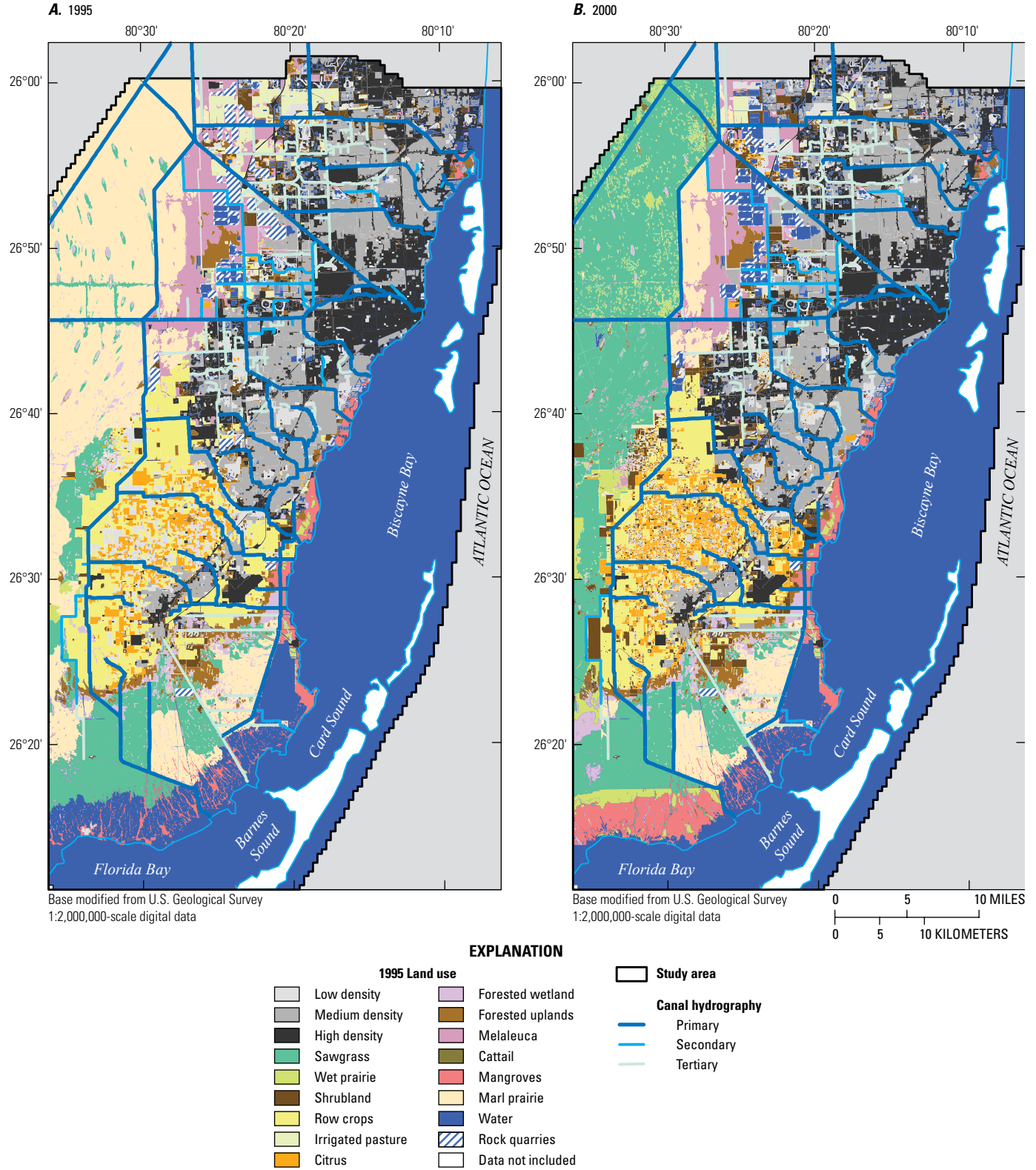


Figure 4. Land use in the study area in A, 1995, B, 2000, C, 2004, and D, 2008.

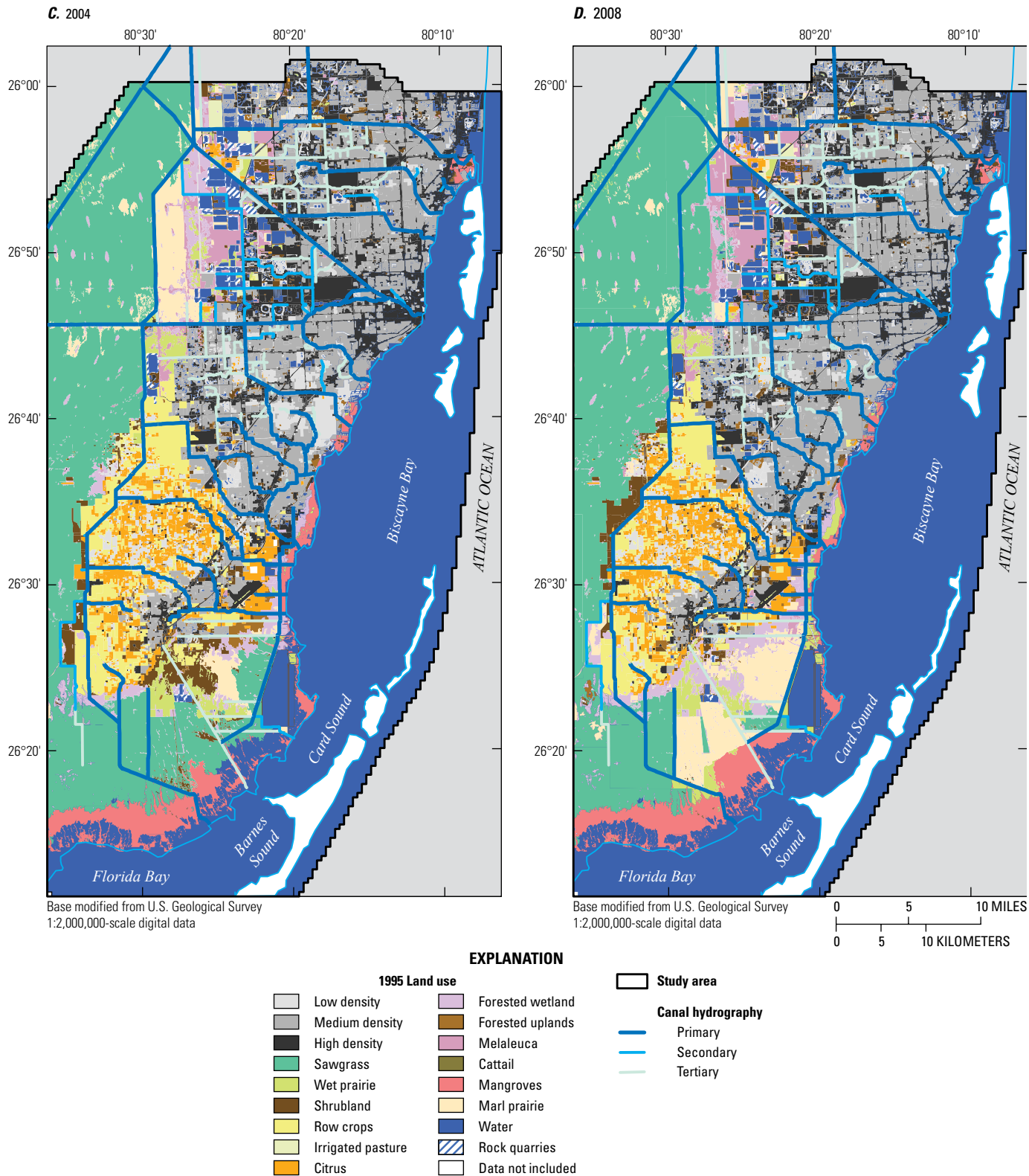


Figure 4. Land use in the study area in A, 1995, B, 2000, C, 2004, and D, 2008.—Continued

**Table 3.** Land-use based crop coefficients.

Basic land use code	Description	Month											
		1	2	3	4	5	6	7	8	9	10	11	12
1	Low density urban	0.28	0.25	0.27	0.27	0.28	0.28	0.31	0.35	0.35	0.34	0.30	0.28
3	Medium density urban	0.23	0.21	0.22	0.23	0.23	0.23	0.26	0.29	0.28	0.29	0.25	0.23
11	High density urban	0.18	0.16	0.18	0.18	0.19	0.19	0.20	0.22	0.21	0.23	0.20	0.18
2	Citrus	0.70	0.69	0.61	0.54	0.66	0.71	0.74	0.81	0.82	0.70	0.72	0.70
7	Row crops	0.64	0.69	0.87	0.95	0.86	0.66	0.61	0.66	0.71	0.87	0.93	0.88
8	Sugar cane	0.80	0.60	0.55	0.80	0.95	1.00	1.05	1.05	1.05	1.00	0.95	0.90
9	Irrigated pasture	0.65	0.70	0.75	0.95	0.95	0.98	0.98	0.98	0.94	0.80	0.87	0.65
6	Shrubland	0.86	0.80	0.85	0.88	0.88	0.87	0.88	0.90	0.90	0.88	0.82	0.81
18	Marl prairie	0.89	0.86	0.91	0.93	0.93	0.92	0.96	0.98	0.97	0.92	0.94	0.89
4	Sawgrass plains	0.82	0.79	0.83	0.84	0.85	0.87	0.88	0.91	0.91	0.84	0.80	0.79
15	Cattail	0.80	0.77	0.80	0.81	0.82	0.84	0.85	0.89	0.89	0.83	0.80	0.79
19	Mix cattail/sawgrass	0.80	0.79	0.81	0.82	0.83	0.85	0.86	0.90	0.90	0.84	0.80	0.79
5	Wet prairie	0.74	0.73	0.76	0.76	0.77	0.78	0.79	0.82	0.82	0.77	0.76	0.74
12	Forested wetland	0.72	0.70	0.75	0.75	0.77	0.76	0.77	0.79	0.79	0.74	0.77	0.74
16	Forested uplands	0.74	0.72	0.77	0.77	0.78	0.78	0.81	0.82	0.82	0.76	0.77	0.75
13	Mangroves	0.79	0.76	0.83	0.86	0.88	0.88	0.88	0.90	0.90	0.82	0.80	0.75
14	Melaleuca	0.80	0.77	0.85	0.88	0.91	0.90	0.91	0.97	0.97	0.86	0.88	0.80
20	Water	1.00	1.00	1.00	1.00	1.00	1.00	1.00	1.00	1.00	1.00	1.00	1.00
30	Offshore	1.00	1.00	1.00	1.00	1.00	1.00	1.00	1.00	1.00	1.00	1.00	1.00
31	Rock quarries	1.00	1.00	1.00	1.00	1.00	1.00	1.00	1.00	1.00	1.00	1.00	1.00

to TIA ratio of 25 percent is comparable to values calculated by Chin and Patterson (2005) for two catchment areas in the C-103 Basin (28.6 and 23.5 percent). Estimated DCIA for 1995, 2000, 2004, and 2008, shown in figure 6, ranges from 5.41 (1995) to 6.22 (2008) percent of the onshore part of the study area. Estimated monthly surface runoff rates are shown in figure 7. Average annual surface runoff rates range from 2.11 in. (170 ft<sup>3</sup>/s) to 4.31 in. (347 ft<sup>3</sup>/s).

## Surface-Water Discharge

Surface-water canals in Miami-Dade County were originally constructed for drainage and are located in low areas that historically routed overland flow of freshwater from the Everglades to Biscayne Bay. Additional details on the development of the surface-water system are provided in Renken and others (2005a).

Currently, the primary surface-water system in Miami-Dade County is managed to control urban flooding, supply recharge to production well fields, and control seawater intrusion (fig. 8). The SFWMD uses surface-water control structures at 58 locations in the study area to manage the surface-water system (fig. 9). Surface-water inflow to urban areas of Miami-Dade County is controlled through a series of surface-water control structures that separate WCA3 from urban areas

in eastern Miami-Dade County (for example, S31, S334, and S196). Surface-water discharge to Biscayne Bay and seawater intrusion are controlled through a series of salinity control structures located close to the coast (for example, S29, S22, and S20F). All of the primary surface-water control structures are used to control urban flooding except those used to deliver surface water from WCA3 (S30, S31, S337, S335, S334) or to ENP (S174, S332, S332B, S332C, and S332D). Primary surface-water control structure types include gated culverts, gated spillways, and pump stations (fig. 10).

The average primary surface-water structure flows for the period from 1996 through 2010 are shown in figure 9B; average structure flow was calculated by using data available through the SFWMD DBHYDRO database (South Florida Water Management District, 2011c). Total average inflow to the urban area through S30, S31, G119, S338, S194, S196, and S176 was 354.5 ft<sup>3</sup>/s. Average inflow from WCA3 through S337 and S334 was 139.6 ft<sup>3</sup>/s. Total average discharge to ENP through S332B, S332C, S174, and S332D was 517.8 ft<sup>3</sup>/s; discharge through S332 was not considered because it is located downstream of S174 and S332D. Average discharge to the southern Glades and Florida Bay through S18C was 259.9 ft<sup>3</sup>/s. Average discharge to the coast through S29, S28, S27, S26, S25, S25B, G93, S22, S123, S21, S21A, S20G, S20F, and S20 was 1,869.5 ft<sup>3</sup>/s. Differences between total average inflows from WCA3 and total average discharges

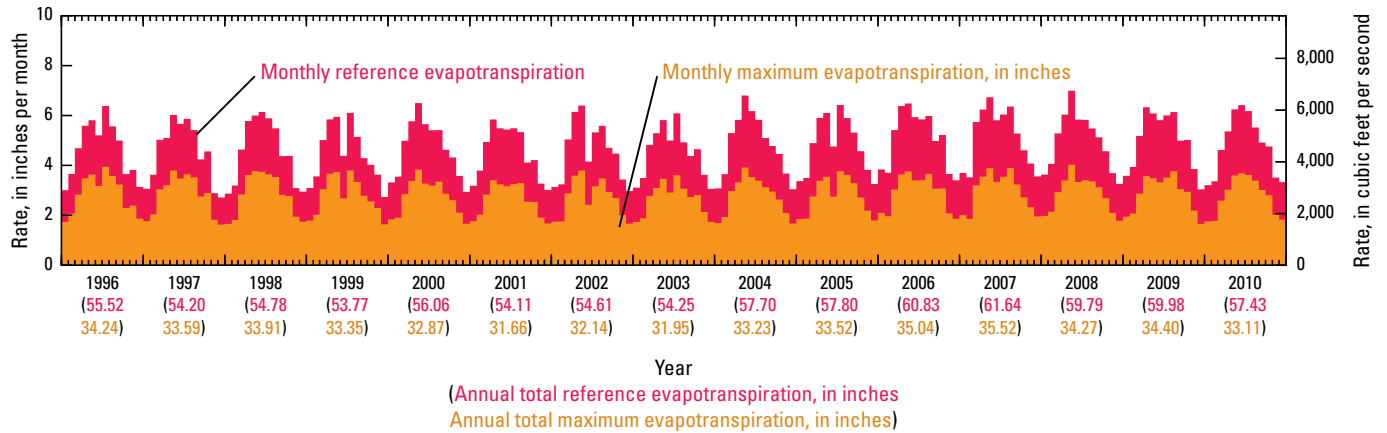


Figure 5. Monthly reference and maximum evapotranspiration rates in the onshore part of the study area, 1996–2010.

Table 4. Estimated range of total impervious area in each basic land-use category, 1996–2010.

Basic land use code	Description	Total impervious area, in percent
1	Low density urban	0 to 70.5
3	Medium density urban	0 to 79.7
11	High density urban	27.0 to 86.2

to ENP, the southern Glades, and the coast are the result of (1) additional groundwater seepage to the L–33, L–30, and L–31N Canals adjacent to WCA3 and ENP; (2) surface-water evaporation; and (3) local sources of water that include surface runoff and groundwater seepage to canals in urban areas of Miami-Dade County. Groundwater seepage to the L–33, L–30, and L–31N Canals averaged 404.7 ft<sup>3</sup>/s, calculated as the difference between the total average inflow from WCA3 through S337 and S334 (139.6 ft<sup>3</sup>/s) and the sum of total average inflow to the urban areas of Miami-Dade County through G119, S338, S194, S196, and S176 (286.4 ft<sup>3</sup>/s) and average discharge to ENP (257.9 ft<sup>3</sup>/s); the calculated groundwater seepage rate ignores surface-water evaporation in the canals. Local sources of water in urban areas of Miami-Dade County averaged 1,774.9 ft<sup>3</sup>/s, calculated as the difference between the total average inflow to the urban area (354.5 ft<sup>3</sup>/s) and the sum of total average outflows to the coast (1,869.5 ft<sup>3</sup>/s) and the southern Glades (259.9 ft<sup>3</sup>/s).

Miami-Dade County operates eight secondary-canal surface-water control structures in the study area (fig. 9A), all of which are gated culverts (fig. 11). Milton Dam also includes a weir to allow increased structure discharge when canal stages exceed 1.2 ft above NAVD88. The majority of the Miami-Dade County surface-water control structures (DBL1, DBL2, NW58, NW25, and NW12) are operated to maintain elevated groundwater levels in the Northwest well field (NWWF) and Snapper Creek Extension Canals, and to protect

the NWWF from contaminated groundwater present north and east of these canals. Control structure BCN1 is used to maintain elevated groundwater levels in the 25th Street Canal and to protect the NWWF from industrial activities south of the well field. The Ludlam Glades and Minton Dam structures are used to maintain elevated groundwater levels and to protect these areas from seawater intrusion and industrial contamination, respectively.

Rock-mining activities have created large quarry lakes in many parts of the study area (fig. 9). These lakes are estimated to extend to depths of 50 to 80 ft into the Biscayne aquifer. The quarry lakes are not directly connected to primary or secondary canals but can represent a large volume of stored water in some areas.

### Groundwater Hydrology

The groundwater flow system in Miami-Dade County is composed of a shallow surficial aquifer system, which includes the Biscayne aquifer and gray limestone aquifer, and the underlying, confined Floridan aquifer system. The surficial and Floridan aquifer systems are separated by alternating beds of sand, silt, and clay that collectively restrict the movement of groundwater between the two aquifer systems. A hydrogeologic section through central Miami-Dade County shows the lithostratigraphic units and structure of the surficial aquifer

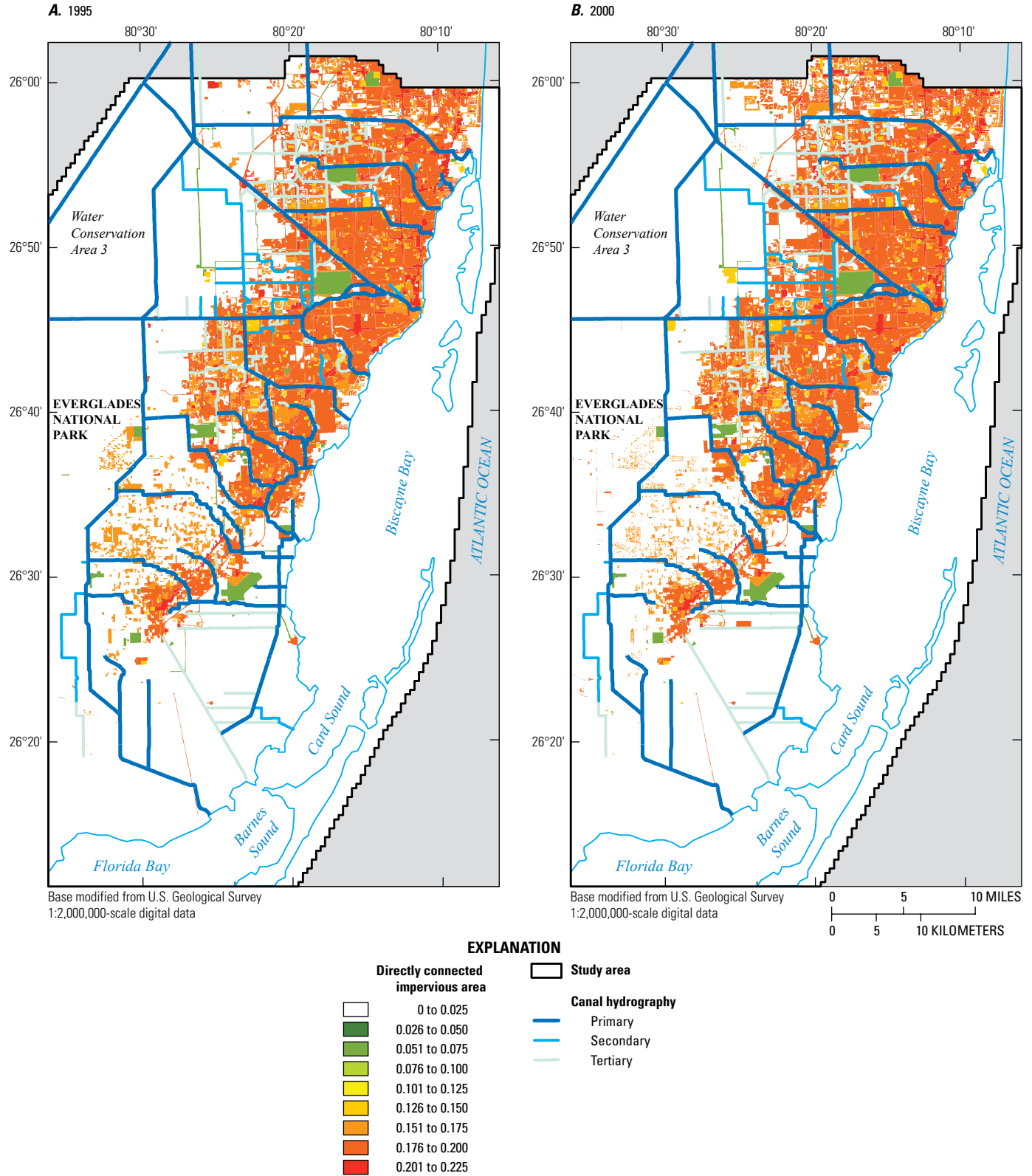


**Figure 6.** Land-use-based estimated fraction of directly connected impervious area in the study area in A, 1995, B, 2000, C, 2004, and D, 2008.

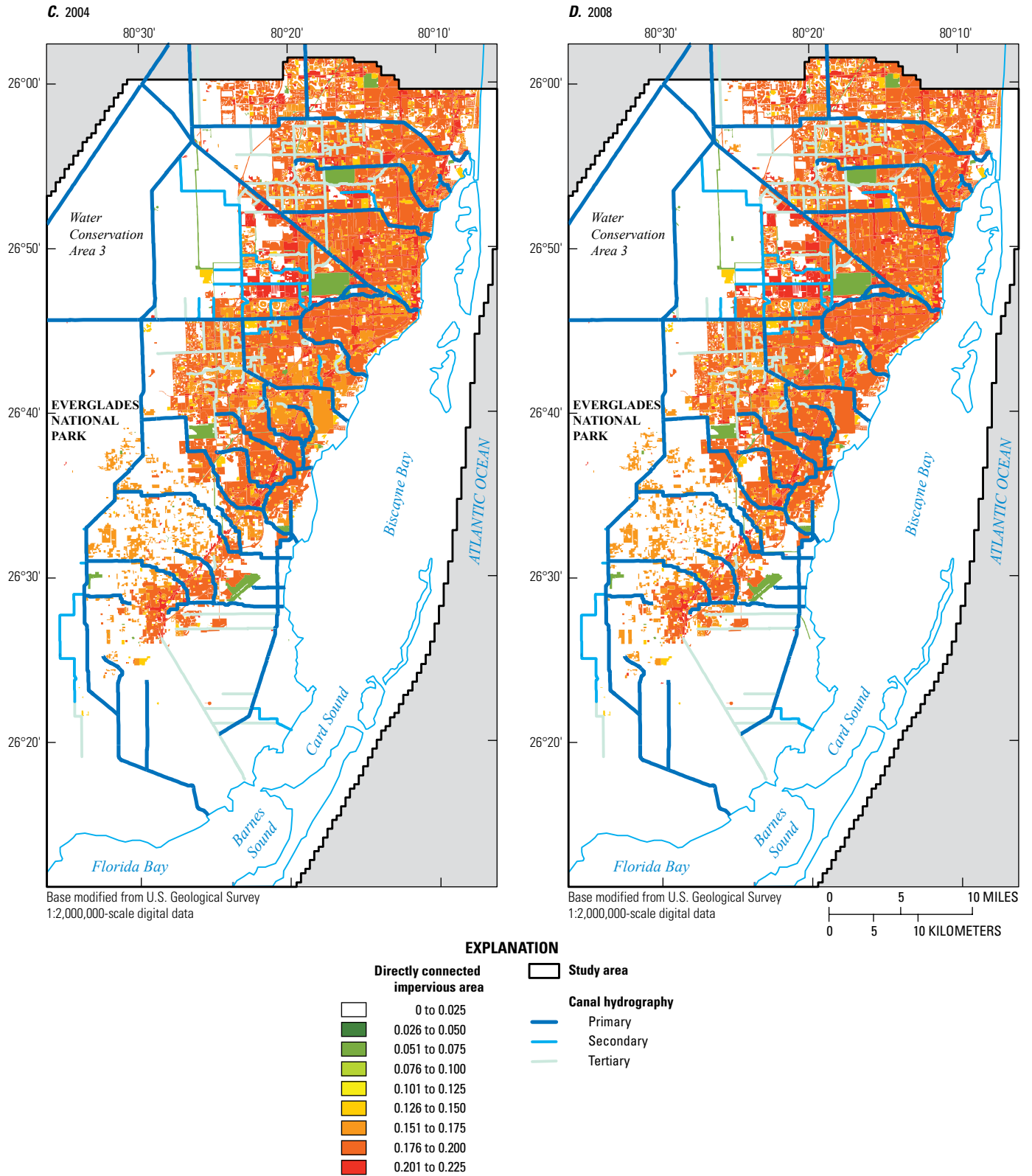


**Figure 6.** Land-use-based estimated fraction of directly connected impervious area in the study area in A, 1995, B, 2000, C, 2004, and D, 2008.—Continued

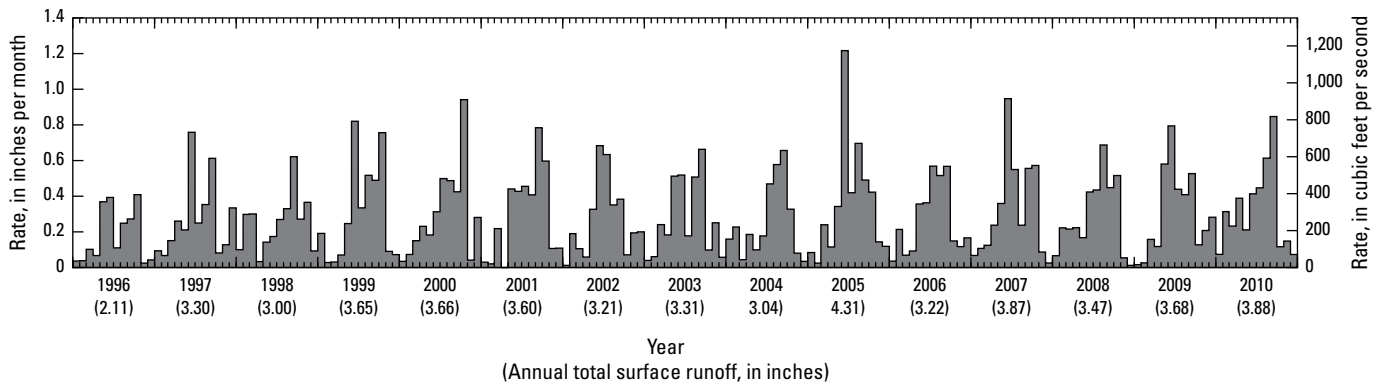


**Figure 7.** Estimated monthly surface runoff rate from directly connected impervious areas in the onshore part of the study area.

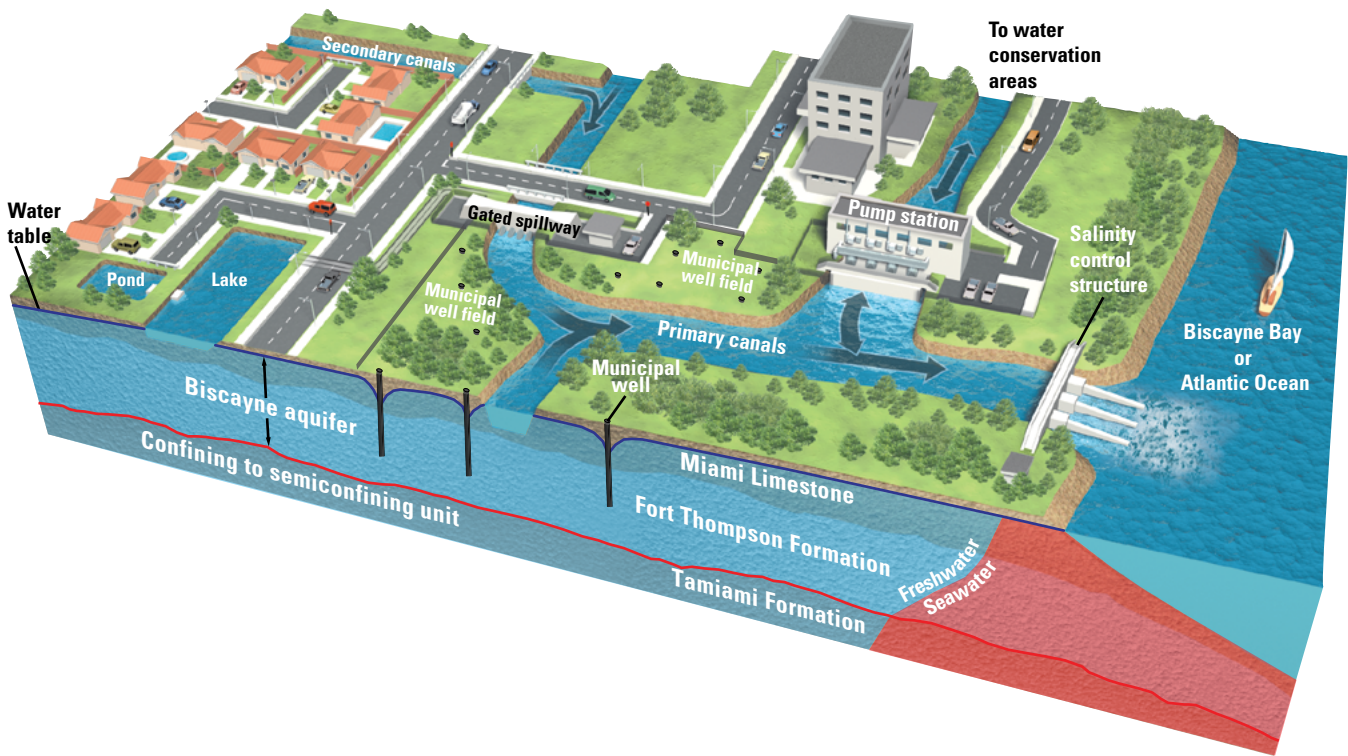


**Figure 8.** Conceptual block diagram showing the components of the surface-water management in Miami-Dade County (modified from South Florida Water Management District, 2010).

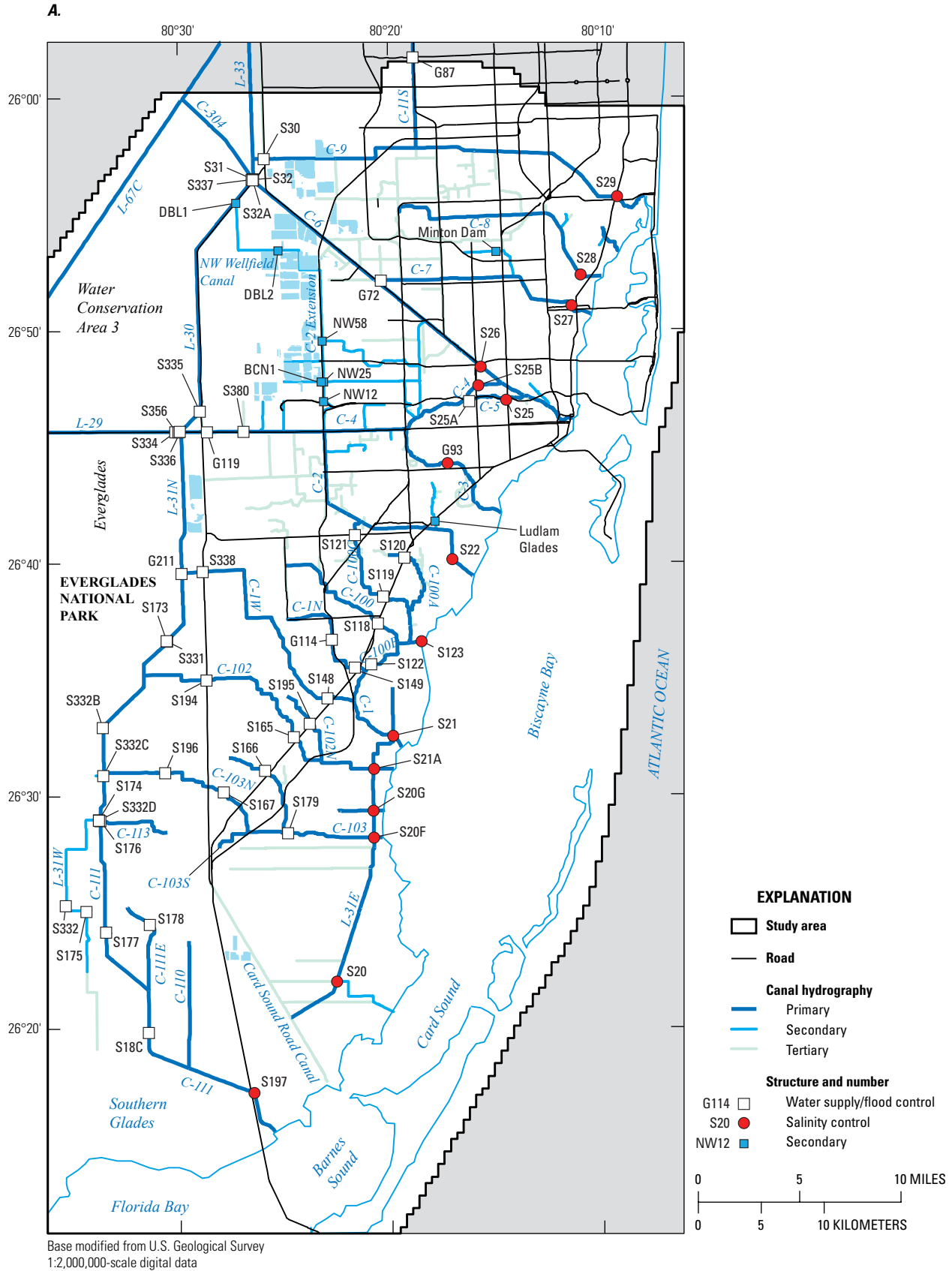


**Figure 9.** Location of, *A*, primary and secondary surface-water control structures and, *B*, average surface-water discharge for the period from 1996 through 2010.

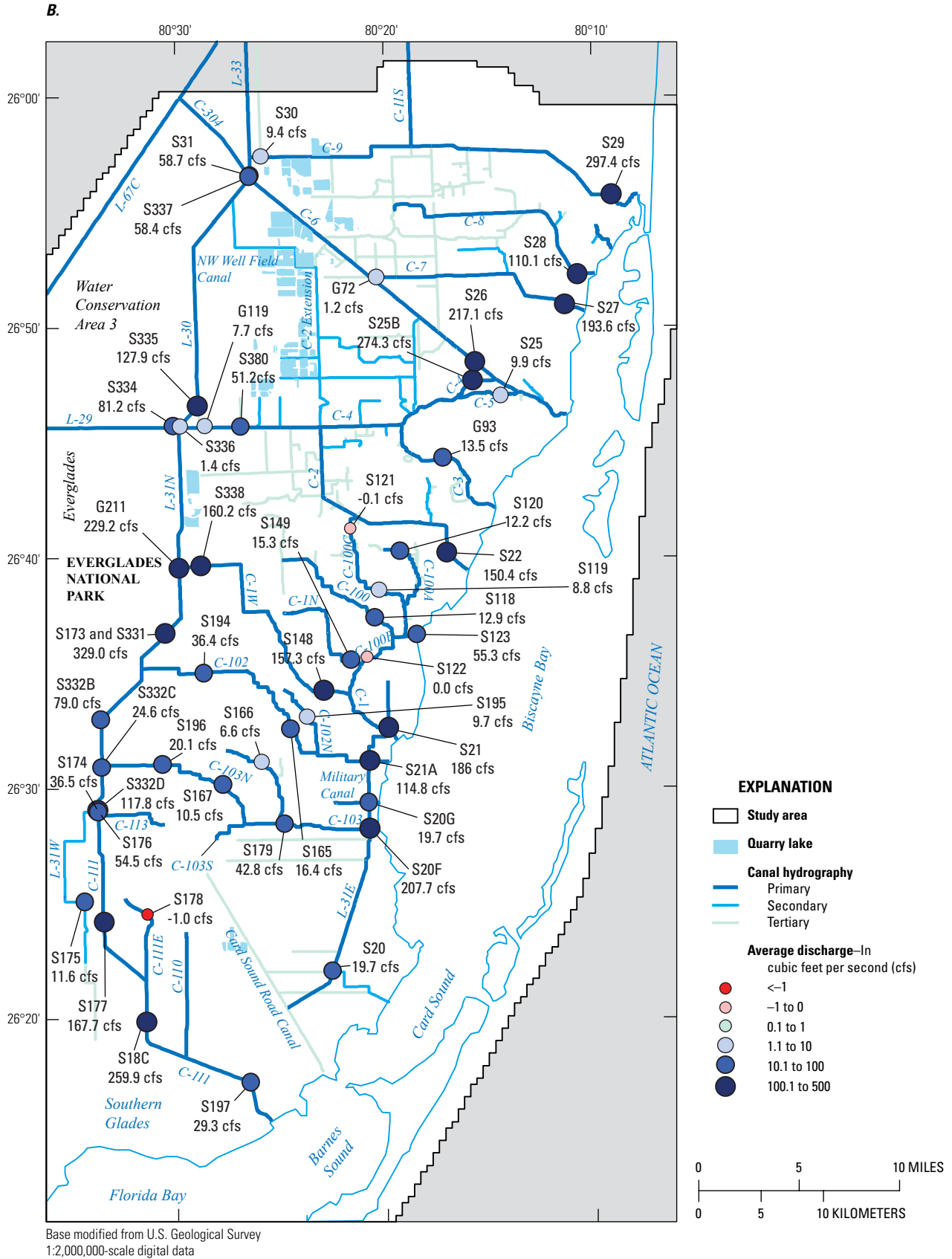


**Figure 9.** Location of, *A*, primary and secondary surface-water control structures and, *B*, average surface-water discharge for the period from 1996 through 2010.—Continued

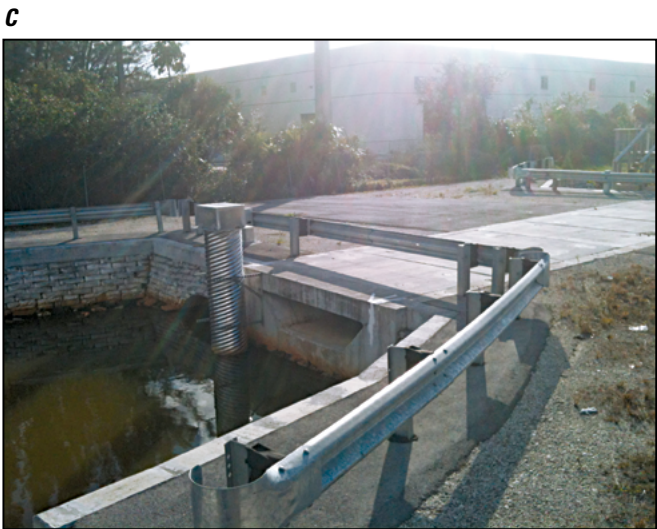


**Figure 10.** Typical primary surface-water system control structures: *A*, gated culvert (S121), *B*, gated spillway (S22), and *C*, pump station (S331).

**Figure 11.** Typical gated culverts in the secondary surface-water system: *A*, Northwest 12th street, *B*, Northwest 25th street, and *C*, Minton Dam.

in the study area (fig. 12). The line of the hydrogeologic section is shown in figure 13. In general, the Biscayne aquifer thickens from approximately 10 ft at the western end of the hydrogeologic section to more than 100 ft at the eastern end. Conversely, the gray limestone aquifer decreases in thickness from approximately 75 ft at the west end of the hydrogeologic section to less than 10 ft in the east. The Biscayne aquifer is the primary source of groundwater for municipal, agricultural, and recreational water use within the study area (Marella, 1999, 2004, and 2009) and the groundwater discharging to Biscayne Bay (Langevin, 2001), and is a designated sole source of drinking water (Federal Register Notice, 1979).

## Hydrostratigraphy

The highly transmissive Biscayne aquifer does not directly correlate with lithostratigraphic boundaries (fig. 12). Instead, the aquifer includes several mappable geologic units extending from land surface down to the base of contiguous, highly permeable beds within the Tamiami Formation that are at least 10 ft thick and have a horizontal hydraulic conductivity of at least 1,000 feet per day (ft/d; Fish, 1988). The Biscayne aquifer includes the Pamlico Sand, Miami Limestone, Anastasia Formation, Key Largo Limestone, and Fort Thompson Formation, as well as the Pinecrest Sand Member of the Tamiami Formation, where permeable. Fish (1988), Fish and Stewart (1991), and Reese and Cunningham (2000) provide detailed descriptions of the hydrogeology and hydraulic properties of the Biscayne aquifer and surficial aquifer system and their constituent formations. The Biscayne aquifer extends from southern Palm Beach County to southeastern Monroe County and southern Miami-Dade County and underlies the entire study area (fig. 13). Geologic units composing the Biscayne aquifer extend beneath Biscayne Bay and the Atlantic Ocean, but the offshore lateral extent of these units has not been fully delineated.

Highly transmissive Pleistocene-age limestones of the Biscayne aquifer were divided into five Quaternary marine sequences, Q1-Q5, defined by Perkins (1977), which have been correlated to previously identified high-frequency sequence stratigraphic depositional cycles (Cunningham and others, 2006). These sequences compose multiple vertical lithofacies successions bounded by unconformities characterized by soil and solution features correlated to sea-level fluctuations associated with Pleistocene glacial-interglacial cycles (Cunningham and others, 2006; Hickey and others, 2010). Vertical lithofacies successions record the prevailing water depth during a single cycle of relative rise and fall in sea level (Kerans and Tinker, 1997). The porosity and permeability of the Biscayne aquifer in the study area are typically linked to the vertical arrangement of lithofacies within each succession that composes a high-frequency cycle (Cunningham and others, 2006; Hickey and others, 2010). A conceptual hydrogeologic column for the western part of the study area adapted from Cunningham and others (2004 and 2006) is shown in figure 14.

The thickness of the Biscayne aquifer portrayed in figure 15 is based on data from Perkins (1977), Causaras (1985, 1987), Giddings (1999), Harvey and others (2002), and Reese and Cunningham (2000) and summarized in Giddings and others (2006). Thickness data from 133 wells and ordinary kriging (Deutsch and Journel, 1998) were used to estimate Q-unit thicknesses at the center of each 1,640.41×1,640.41-ft cell in a mesh encompassing the study area. Kriging requires specifying the correlation structure for interpolation, which is described using a function called a semivariogram that relates variance to the distance and spatial orientation between data points. An experimental semivariogram was calculated from the 133 wells by calculating the average variance of the thickness data between pairs of well locations having similar separation distances. A theoretical semivariogram, namely a mathematical function that models the behavior of the experimental semivariogram, is usually necessary because the experimental semivariogram contains a finite number of data pairs that cannot fully describe the correlation relation at all separation distances and directions evaluated during the interpolation (Isaaks and Srivastava, 1989). The SGEMS software suite (Remy and others, 2009) was used to develop the experimental semivariogram and corresponding theoretical semivariogram for each marine sequence within the Biscayne aquifer. The parameters that define the theoretical semivariograms were manually adjusted to improve their agreement with experimental semivariograms and are summarized in table 5. Experimental semivariograms for Holocene sediments and the Q-units showed anisotropic correlation structure with principal direction oriented 10° east of true north, which approximately coincides with the orientation of the shoreline of southern Florida.

The interpolated thickness of the Biscayne aquifer ranges from 36 to 125 ft in the study area (fig. 15). Highly porous groundwater flow zones have been characterized and mapped throughout much of the study area and identified in other parts of the limestone of the Biscayne aquifer in Miami-Dade County (Cunningham and others, 2004, 2006; Renken and others, 2005b, 2008; Shapiro and others, 2008; Cunningham and Sukop, 2011). The cumulative thickness of the flow zones across the entire thickness of the aquifer at the NWWF is estimated to be about 29.5 ft (Renken and others, 2008), which is approximately 47 percent of the total thickness of the Biscayne aquifer in the area.

## Aquifer Properties

Transmissivity values for the Biscayne aquifer that were derived from aquifer performance tests (APTs) vary widely throughout Miami-Dade County. Fish and Stewart (1991) reported transmissivity estimates ranging from 49 to more than  $1.0 \times 10^6$  feet squared per day (ft<sup>2</sup>/d) for APTs conducted in 23 wells completed in the Biscayne aquifer in Miami-Dade County. Results of an APT at the NWWF (Renken and others, 2008) yielded transmissivity estimates ranging from  $1.67 \times 10^6$  to  $3.07 \times 10^6$  ft<sup>2</sup>/d.

Horizontal hydraulic conductivity data were interpolated to a grid encompassing the study area and having cells 1,640.41 ft on each side using ordinary kriging. Horizontal hydraulic conductivity was calculated by dividing the estimated transmissivity of each APT by the full thickness of the Biscayne aquifer at that location. A theoretical semivariogram was calculated by using the parameters summarized in table 5. The estimated Biscayne aquifer transmissivity was calculated as the product of the interpolated aquifer thickness and interpolated horizontal hydraulic conductivity. Transmissivity interpolated from APTs in Miami-Dade County (Fish and Stewart, 1991; Renken and others, 2008) averaged

$4.3 \times 10^5$  ft<sup>2</sup>/d in the study area and ranged from approximately  $3.2 \times 10^4$  to  $1.9 \times 10^6$  ft<sup>2</sup>/d (fig. 16).

Vertical hydraulic conductivity data for the Biscayne aquifer are limited. Cunningham and others (2006) measured the air permeability data of 267 whole-core samples from 13 wells. The permeameter methods used to determine air permeability are not accurate for permeabilities greater than  $3.2 \times 10^{-10}$  square feet (ft<sup>2</sup>; 85 ft/d for freshwater at 20 °C), however, and underestimate the hydraulic conductivity of flow zone samples from the Biscayne aquifer by 3 to 6 orders of magnitude (Sukop and others, 2013). The ratio of horizontal to vertical hydraulic conductivity of flow zone samples,

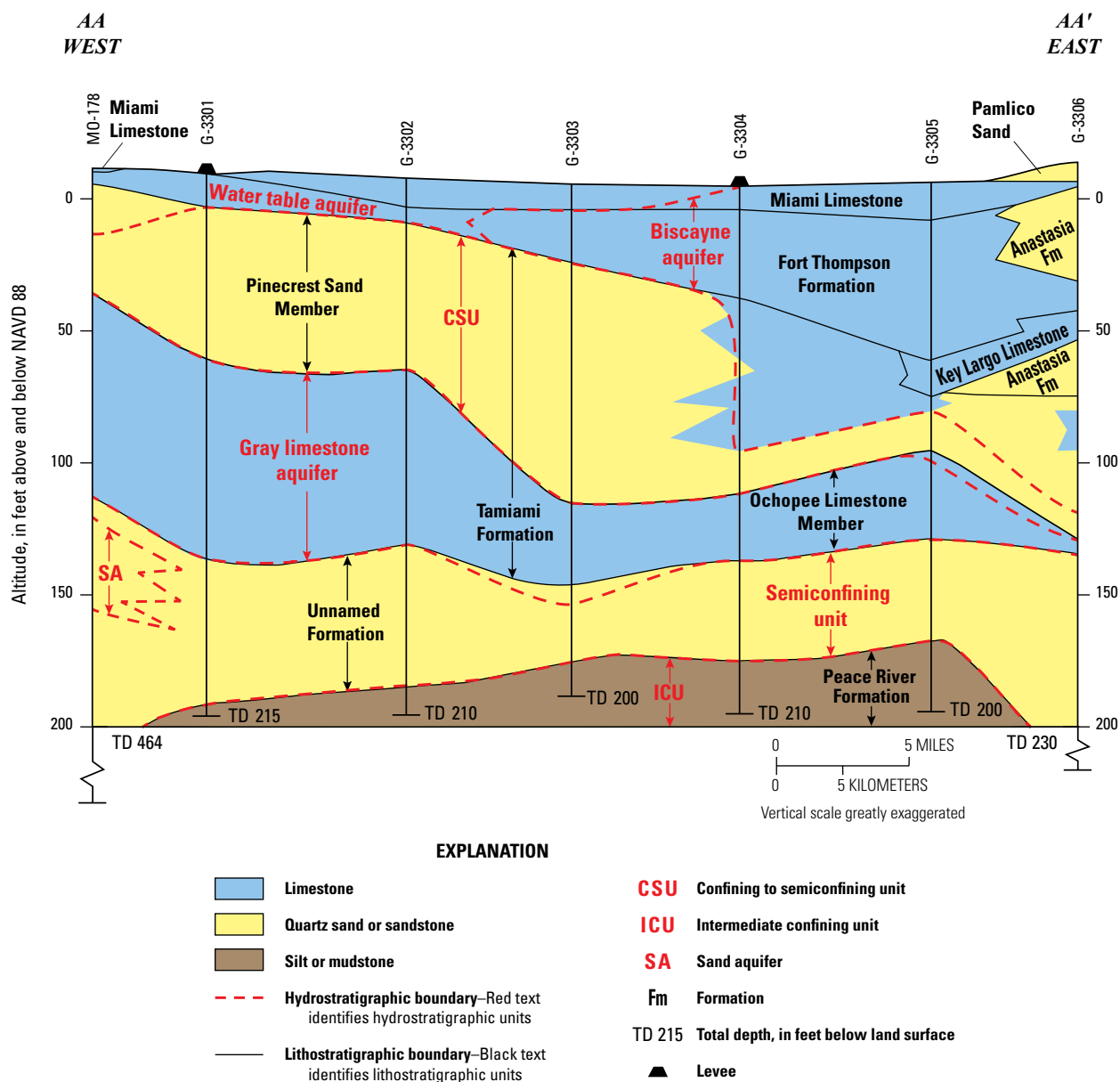
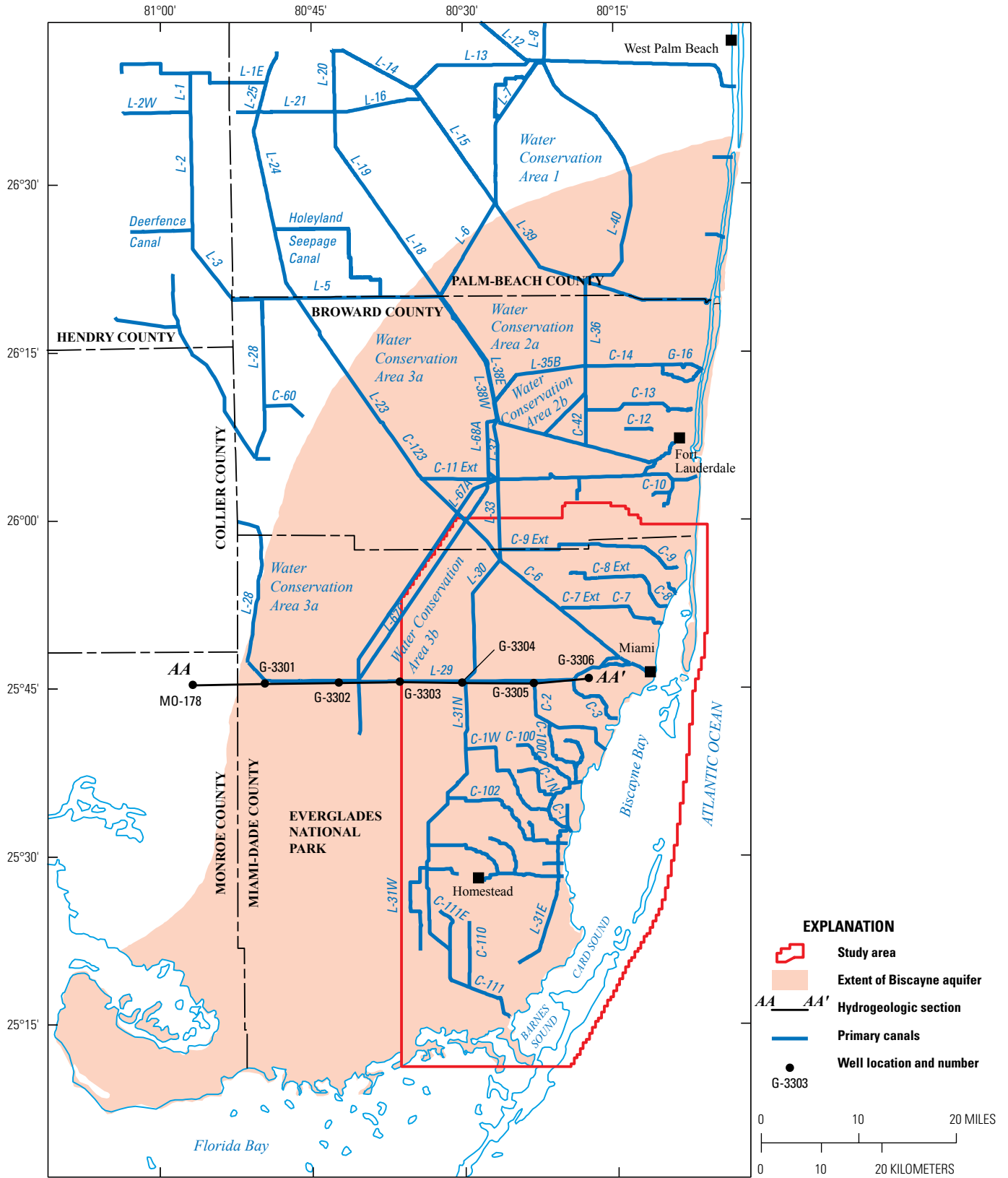


**Figure 12.** Hydrogeologic section showing relations of geologic formations, aquifers, and semiconfining units of the surficial aquifer system across central Miami-Dade County (modified from Reese and Cunningham, 2000). Location of section line shown in figure 13.



Base modified from U.S. Geological Survey  
1:2,000,000-scale digital data

**Figure 13.** Areal extent of the Biscayne aquifer in southeastern Florida (from Klein and others, 1975) and the line of hydrogeologic section (in fig. 12) across central Miami-Dade County.

determined by the Lattice Boltzman method, ranged from 0.58 to 1.3 (Sukop and others, 2013), which indicates that within flow zones, differences between horizontal and vertical hydraulic conductivity are small. Furthermore, the presence of cross-cutting vertical solution features connecting Biscayne aquifer flow zones (Cunningham and others, 2009) may reduce the importance of local differences between horizontal and vertical hydraulic conductivities in units separating flow zones.

Although few data are available, measured water-level differences with depth are generally small and support the assessment that vertical hydraulic conductivity differences are of limited importance, except at a very local scale. Fish and Stewart (1991) noted that in most of the area (except near well fields or margins of water-conservation areas), water levels at depth are almost identical to local water-table elevations. They also noted that variations in the vertical distribution of water-level responses may exhibit semiconfined behavior during the

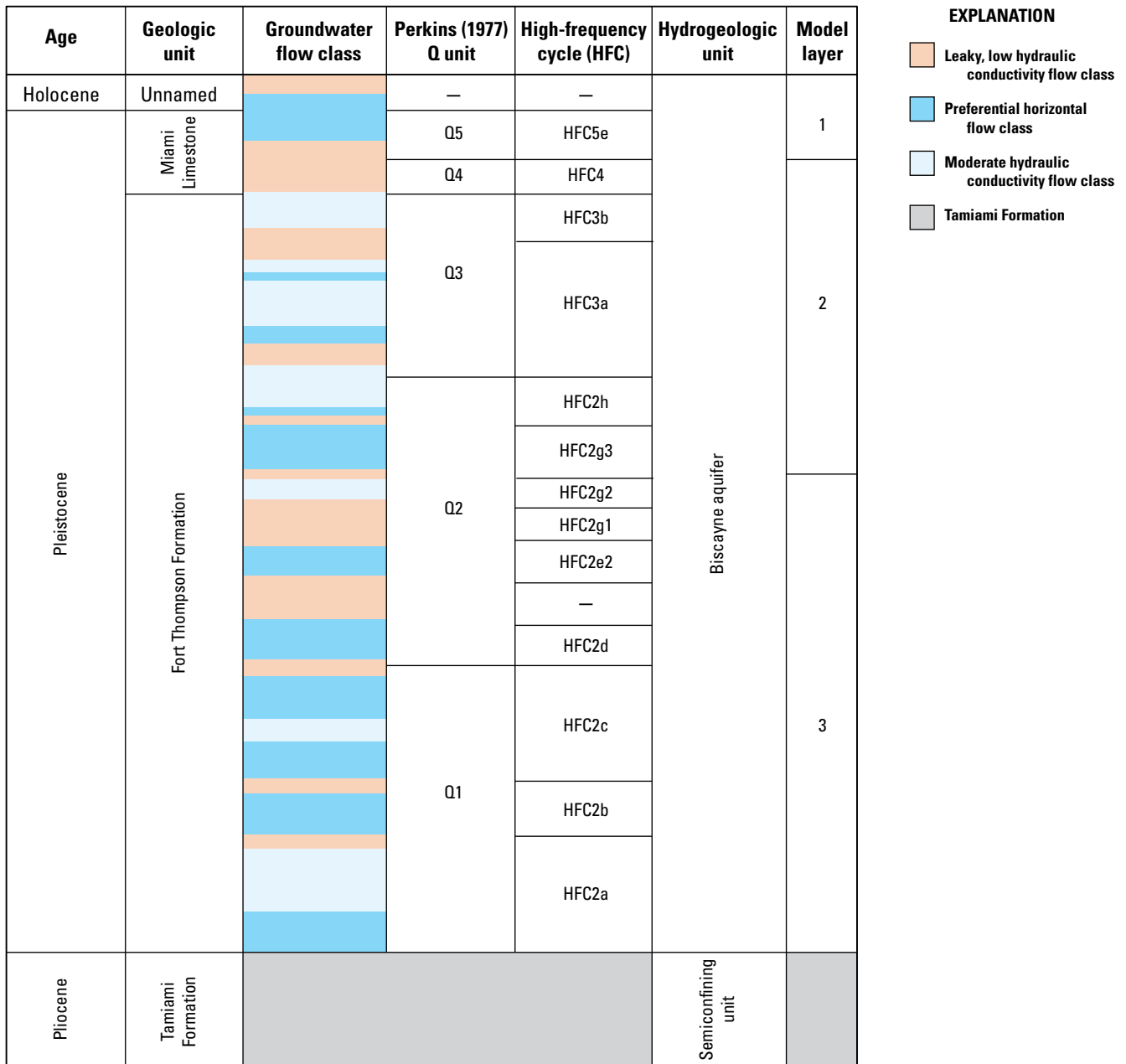
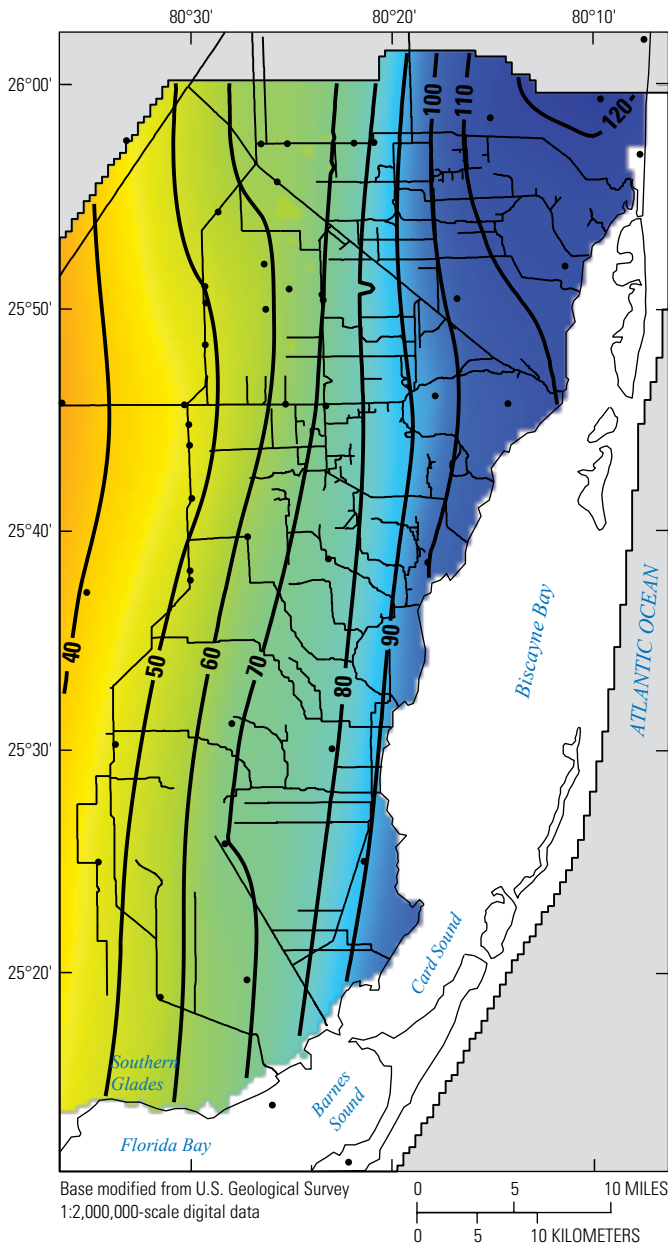


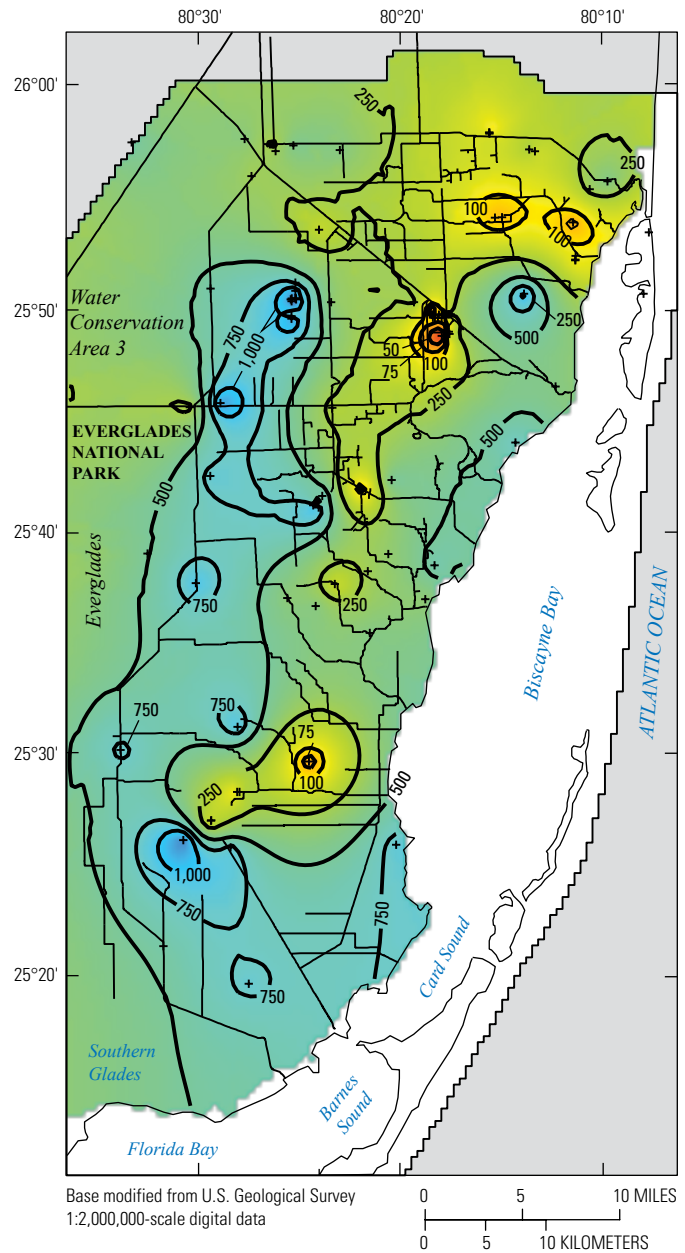
**Figure 14.** Conceptual hydrogeologic column for the western part of the study area that includes ages, geologic units, groundwater flow types, Q-units of Perkins (1977), high-frequency sequence stratigraphic cycles, hydrogeologic units, and associated model layers (adapted from Cunningham and others 2004 and 2006).



**EXPLANATION**

- |  |  |
|--|--|
| <p><b>Aquifer thickness, in feet</b></p> | <p>□ Study area</p> <p>—90— Line of equal thickness of the Biscayne aquifer—In feet. Interval 10 feet</p> <p>— Canal hydrography</p> <p>• Hydrogeologic control location</p> |
|--|--|

**Figure 15.** Thickness of the Biscayne aquifer in the study area and the location of wells used to determine the thickness.



**EXPLANATION**

- |  |  |
|--|--|
| <p><b>Transmissivity—In thousands of square feet per day</b></p> | <p>□ Study area</p> <p>—750— Line of equal transmissivity of the Biscayne aquifer—In thousands of square feet per day. Interval is variable</p> <p>— Canal hydrography</p> <p>+ APT location</p> |
|--|--|

**Figure 16.** Transmissivity of the Biscayne aquifer interpolated from aquifer performance tests (APTs) conducted in the study area. The locations of aquifer performance test data are also shown.

**Table 5.** Theoretical semivariogram models and parameters for Holocene and Pleistocene sediment sequences and Biscayne aquifer hydraulic conductivity.

Data item	Variogram model	Nugget contribution to sill	Variogram contribution to sill	Practical range/range, in miles	Anisotropy	Principal direction of anisotropy, in degrees <sup>1</sup>
Holocene	Exponential	5	10	128 / 43	1.78	10
Q5	Exponential	5	40	252 / 84	6.3	10
Q4	Exponential	10	75	233 / 78	4.65	10
Q3	Spherical	50	300	314 / 392	5.16	10
Q2	Exponential	20	350	180 / 60	3	10
Q1	Exponential	30	250	328 / 109	2.34	10
Hydraulic conductivity <sup>2</sup>	Exponential	0	3.3	3.11 / 9.32	1	0

<sup>1</sup>Degrees clockwise from north.

<sup>2</sup>Log-transformed.

early stages of pumping in wells open to highly permeable zones overlain by less permeable sands. Fish and Stewart (1991) further noted that water levels measured at depth may differ from those observed for the water table in areas where surface water is ponded and strong vertical gradients might exist. Sonenshein (2001) measured vertical water-level differences on the order of 0.1 ft or less in WCA3. Merritt (1996a) noted vertical water-level differences ranging from 0.1 to 0.5 ft at two wells near the Hallandale well field in southern Broward County.

The Biscayne aquifer generally acts as an unconfined aquifer in response to rainfall, evapotranspiration, pumping, and other hydrologic and hydraulic stresses. In unconfined aquifers, the specific yield is equivalent to the storage coefficient, which controls storage changes. Specific yield estimates for the Biscayne aquifer range from 0.20 to 0.25 and have been obtained by using (1) aquifer responses during large rainfall events and (2) calibrated models (Merritt, 1996a, b; Langevin, 2001; Lohmann and others, 2012).

Transport rates for dissolved constituents in aquifers (for example, contaminants and conservative constituents such as chloride) are influenced by effective porosity. Although aquifer bulk porosity is defined as the ratio of the volume of voids to the total aquifer volume in a representative volume, effective porosity is usually smaller because it only includes interconnected voids. Cunningham and others (2009) describe the Biscayne aquifer as a dual-porosity system consisting of (1) matrix porosity and (2) macroporosity in defined flow zones and vertical solution features. Reported bulk helium porosities for Biscayne aquifer samples collected in the study area range from 5.5 to 81 percent (Cunningham and others, 2006, 2009; Sukop and others, 2013). Estimates of effective

porosity based on results of a tracer test in the NWWF range from 4 to 41 percent (Renken and others, 2008). Calibrated numerical models of the Biscayne aquifer in Miami-Dade County have used effective porosity values of 0.20 (Merritt, 1996b, 1997; Langevin, 2001; Chin and others, 2010; Lohmann and others, 2012; Brakefield and others, 2013).

## Water Supply and Use

The Biscayne aquifer is the primary source of water used in Miami-Dade County (Marella, 1999, 2004, 2009). Water use types in the county include domestic, commercial, industrial, agricultural, and municipal water use.

## Municipal Groundwater Water Use

Municipal groundwater use data from January 1, 1996, through December 31, 2010, were acquired from the MDWASD and the SFWMD. Data were provided for all municipal Biscayne aquifer wells permitted in the study area. The withdrawals from 12 MDWASD well fields and 8 other well fields in the onshore parts of the study area (about 1,100 mi<sup>2</sup>) were relatively consistent from January 1996 through December 2010, and ranged from 0.52 to 0.68 inches per month (in/mo; 504 to 652 ft<sup>3</sup>/s; 326 to 423 million gallons per day [Mgal/d]) (fig. 17). Average groundwater pumpage at production well fields ranged from 0.01 Mgal/d (Redavo well field) to 85 Mgal/d (Southwest well field) from 1996 through 2010 (fig. 18).

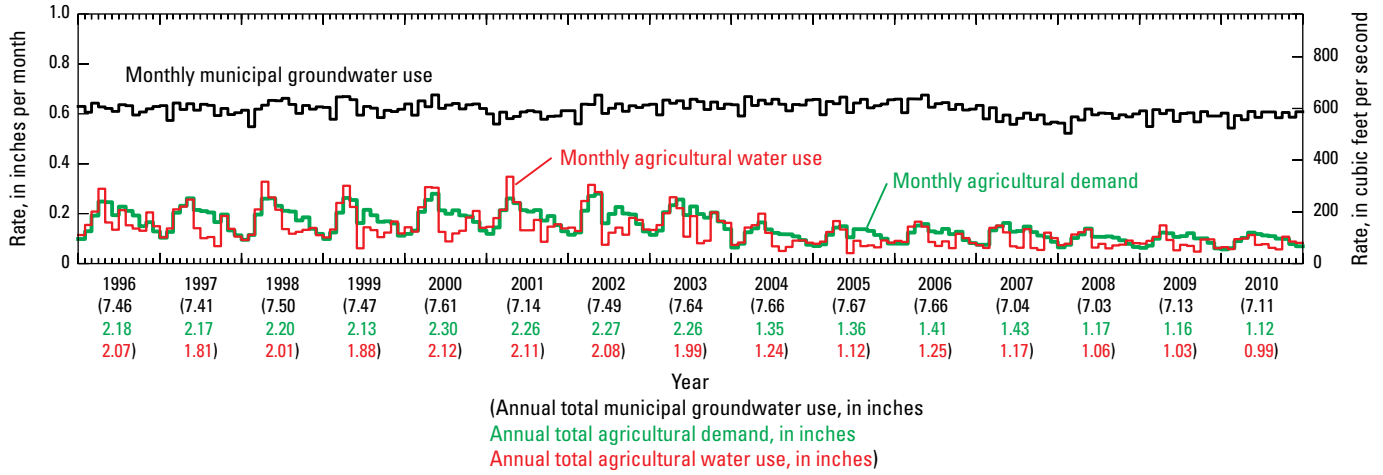


**Figure 17.** Monthly production well field withdrawals, estimated agricultural demand, and estimated agricultural water use in the onshore part of the study area, 1996–2010.

### Agricultural Water Use

Estimated total annual agricultural water use in Miami-Dade County ranges from 1.12 to 2.12 in. (89.83 to 170.74 ft<sup>3</sup>/s; 58.06 to 110.35 Mgal/d) (Marella, 1999, 2004, 2009). Most agricultural water use occurs in the southern part of Miami-Dade County and is withdrawn from shallow, uncased wells and conveyed through truck-mounted pump and spray irrigation systems (Renken and others, 2005a). Agricultural water use can be estimated using

$$Q_{AG} = \left( \frac{1}{E_{AG}} \right) \times \max(f_a \times KcET_o - q_{RAI}, 0.0) \times A, \tag{2}$$

where

- $Q_{AG}$  is the estimated agricultural water use [L<sup>3</sup>T<sup>-1</sup>];
- $E_{AG}$  is irrigation system efficiency [unitless];
- $f_a$  is a scaling factor used to scale calculated irrigation water use to the estimated annual agricultural self-supplied water withdrawal rate for Miami-Dade County in 1995, 2000, and 2005 (Marella, 1999, 2004, 2009) [unitless];
- $q_{RAI}$  is the rainfall rate per unit area [LT<sup>-1</sup>]; and
- $A$  is the irrigated area [L<sup>2</sup>].

The max operator is used in equation 2 to ensure that estimated agricultural water use is zero on days when rainfall rates exceed  $f_a \times Kc \times q_{RET}$ .

The irrigation system efficiency is determined on the basis of a combined efficiency factor that incorporates the efficiency of the system delivering the water to the point of diversion into an irrigation system and the efficiency of the irrigation system itself. An irrigation system efficiency of 0.75 was used to estimate agricultural water use in the study area

and assumes that solid set overhead sprinklers are used (Renken and others, 2005a). Irrigation system efficiencies less than 1 indicate that there are losses in the irrigation system and that irrigation water use exceeds the quantity of water required to satisfy crop demand. Surface runoff resulting from use of solid set overhead sprinklers was assumed to be negligible and agricultural water demand in excess of precipitation was satisfied.

Agricultural water demand ( $f_a \times Kc \times ET_o$  in eq. 2) in the study area was estimated by using land-use data for 1995, 2000, 2004, and 2008 (South Florida Water Management District, 1995; 2002a; 2011a, b) (fig. 4), daily satellite-based reference evapotranspiration rates, and land-use-based crop coefficients (table 3). The land-use data for a given year were used until the beginning of the year for the next land-use dataset; for example, the 1995 land-use dataset was used until January 1, 2000, after which the dataset for 2000 was used. Estimated annual agricultural demand from 1996 through 2010, shown in figure 17, ranged from a low of 1.12 in. (90.10 ft<sup>3</sup>/s; 58.23 Mgal/d) in 2010 to a high of 2.30 in. (185.03 ft<sup>3</sup>/s; 119.59 Mgal/d) in 2000. The reduction in estimated agricultural demand between 1996 and 2010 reflects the concurrent decline in agricultural land use from 13.87 to 8.84 percent of the study area. Estimated monthly agricultural demand in the study area ranged from 0.06 to 0.28 in. (54.79 to 270.35 ft<sup>3</sup>/s; 35.41 to 174.73 Mgal/d) during the same period.

Estimated annual agricultural water use in the study area from 1996 through 2010 is shown in figure 17 and ranged from a low of 0.99 in. (79.64 ft<sup>3</sup>/s; 58.06 Mgal/d) in 2010 to a high of 2.12 in. (170.55 ft<sup>3</sup>/s; 110.23 Mgal/d) in 2000. Estimated monthly agricultural water use in the study area ranged from 0.042 to 0.35 in. (40.42 to 335.95 ft<sup>3</sup>/s; 26.12 to 217.13 Mgal/d) during the same period. Estimated agricultural water use can exceed agricultural demand, when demand is greater than rainfall, as a result of a specified irrigation system efficiency,  $E_{AG}$ , less than 1.

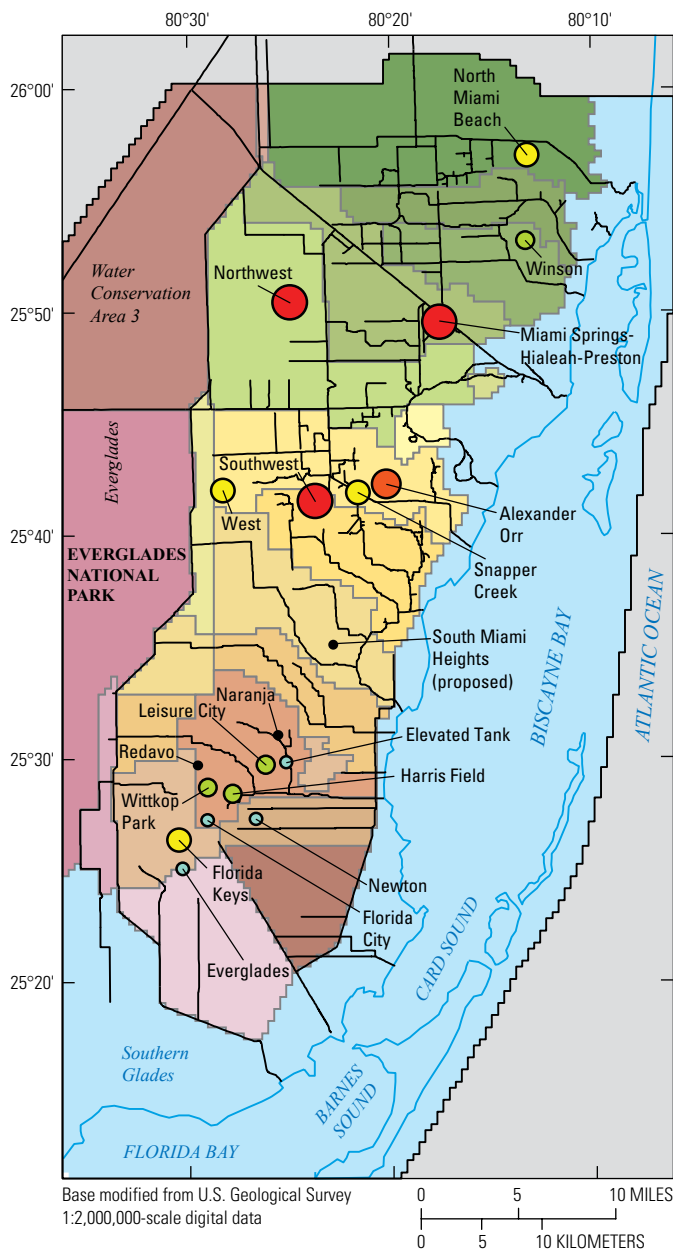


Figure 18. Average municipal water use in the study area for the period from 1996 through 2010.

### Recreational Irrigation

Recreational irrigation is a water use category that represents application of water to satisfy landscape vegetation water demands for primarily nonresidential urban land-use types (for example, athletic fields, cemeteries, golf courses, common public areas, parks, and playgrounds). Water used for recreational irrigation is obtained from a municipal water supplier, reclaimed wastewater, or is self-supplied. Most recreational irrigation in Miami-Dade County is supplied by groundwater (Marella, 1999, 2004, 2009). As a result, recreational irrigation is considered to be groundwater use. Total annual recreational irrigation in Miami-Dade County is estimated to range from 0.26 to 0.32 in. (20.72 to 25.98 ft<sup>3</sup>/s; 13.39 to 16.79 Mgal/d) (Marella, 1999, 2004, 2009).

Recreational irrigation demand in the study area was estimated by using land-use data for 1995, 2000, 2004, and 2008 (South Florida Water Management District, 1995; 2002a; 2011a, b) (fig. 4), daily satellite-based reference evapotranspiration rates, land-use-based crop coefficients (table 3), and a scaling factor used to scale calculated recreational water use to the annual recreational irrigation water withdrawal rate estimated for Miami-Dade County in 1995, 2000, and 2005 (Marella, 1999, 2004, 2009). Recreational irrigation was assumed to occur in the low- and medium-density urban BLU categories (table 1). Estimated annual recreational irrigation demand from 1996 through 2010 ranged from 0.37 in. (29.77 ft<sup>3</sup>/s; 19.24 Mgal/d) in 2004 and 2005 to 0.41 in. (32.98 ft<sup>3</sup>/s; 21.32 Mgal/d) in 1996 and 2000 (fig. 19). Estimated monthly recreational demand in the study area ranged from 0.018 to 0.049 in. (17.47 to 46.85 ft<sup>3</sup>/s; 11.29 to 30.28 Mgal/d) during the same period.

Estimated annual recreational irrigation in the study area from 1996 through 2010 ranged from a low of 0.18 in. (14.48 ft<sup>3</sup>/s; 9.36 Mgal/d) in 2010 to a high of 0.24 in. (19.31 ft<sup>3</sup>/s; 12.48 Mgal/d) in 2000 (fig. 19). Estimated monthly recreational water use in the study area ranged from 0.0046 to 0.039 in. (4.42 to 37.54 ft<sup>3</sup>/s; 2.85 to 24.26 Mgal/d) during the same period.

### Septic System Return to the Water Table

Discharge to the Biscayne aquifer from septic systems was calculated from a dataset compiled by the Florida Department of Health (Hall and Clancy, 2009). Septic tank locations were estimated using tax records to identify improved parcels of land and the probability that a given parcel has an active septic tank. Probabilities were calculated using tax record data in areas where septic tank locations are known. Parcels having a probability greater than or equal to 0.5 were considered to have an actively discharging septic tank. These parcel data were intersected with 1990, 2000, and 2010 census data to estimate domestic wastewater discharge to each active septic tank based on population density. The septic system database included data from 112,280 septic tanks in the onshore part of the study area and the mean population per household in each

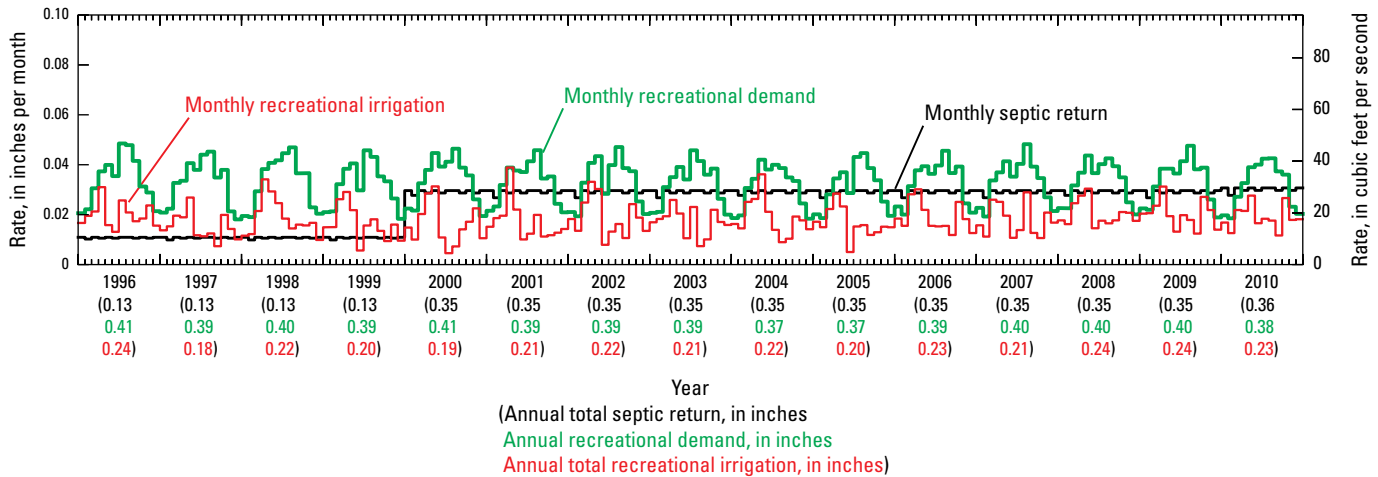


**Figure 19.** Estimated monthly septic return rates, recreational demand, and recreational irrigation in the onshore part of the study area, 1996–2010.

census block with septic tanks ranged from 0.96 to 145.50, 0.06 to 989.00, and 0.12 to 57.50 in 1990, 2000, and 2010, respectively. Large values for mean population per household correspond to census blocks that have a large number of people but a relatively small number of houses, such as those found in census blocks with institutions listed as single residences but having a large number of inhabitants (for example, correctional facilities and nursing homes). Using an average discharge of 55 gallons per day (gal/d) per person (Marella, 2004), total discharge to septic tanks in the study area was 7.89, 20.3, and 18.9 Mgal/d in 1990, 2000, and 2010, respectively. The assumption is that all water used in homes with a septic system ultimately recharges the water table.

Estimated annual septic return in the study area was 0.13 in. (10.46 ft<sup>3</sup>/s; 6.76 Mgal/d) from 1996 through 1999, 0.35 in. (28.16 ft<sup>3</sup>/s; 18.20 Mgal/d) from 2000 through 2009, and 0.36 in. (28.96 ft<sup>3</sup>/s; 18.72 Mgal/d) in 2010 (fig. 19). Estimated monthly septic return in the study area ranged from 0.01 to 0.031 in. (9.53 to 29.65 ft<sup>3</sup>/s; 6.16 to 19.16 Mgal/d). The spatial distribution of septic return rates for 1990, 2000, and 2010 are shown in figure 20.

### Estimates of Groundwater Recharge and Surface-Water/Groundwater Interactions

Climate data in combination with data for a number of surface-water, groundwater, and water-use components can be used to estimate groundwater recharge and surface-water/groundwater interactions in the study area.

#### Groundwater Recharge

Net groundwater recharge to the water table is typically defined as the difference between the sum of rainfall and additional water sources infiltrating at land surface and

entering the underlying aquifer, and the sum of evapotranspiration, surface-water runoff, and storage of water above the water table. Thus in the study area, estimated net groundwater recharge can be calculated as

$$Q_{GWRCH} = Q_{RAI} + Q_{SEP} + Q_{REC} - Q_{AET} - Q_{SRO} - Q_{AG} - Q_{NAG} - Q_{STO}, \quad (3)$$

where

- $Q_{GWRCH}$  is net groundwater recharge [L<sup>3</sup>T<sup>-1</sup>],
- $Q_{RAI}$  is rainfall [L<sup>3</sup>T<sup>-1</sup>],
- $Q_{SEP}$  is estimated septic return [L<sup>3</sup>T<sup>-1</sup>],
- $Q_{REC}$  is estimated recreational irrigation [L<sup>3</sup>T<sup>-1</sup>],
- $Q_{AET}$  is the product of  $Kc$  and reference evapotranspiration ( $Q_{RET}$ ) [L<sup>3</sup>T<sup>-1</sup>],
- $Q_{SRO}$  is estimated surface water runoff [L<sup>3</sup>T<sup>-1</sup>],
- $Q_{AG}$  is the product of  $Kc$  and reference evapotranspiration ( $Q_{RET}$ ) [L<sup>3</sup>T<sup>-1</sup>],
- $Q_{NAG}$  is estimated evapotranspiration in nonagricultural areas [L<sup>3</sup>T<sup>-1</sup>], and
- $Q_{STO}$  is the estimated change in water stored above the water table [L<sup>3</sup>T<sup>-1</sup>].

Net groundwater recharge in the study area for the period from 1996 through 2010 was calculated using daily NEXRAD rainfall, census-based septic return estimates, land-use data for 1995, 2000, 2004, and 2008 (fig. 4), daily satellite-based reference evapotranspiration rates, land-use-based crop coefficients (table 3), land-use-based DCIA values calculated from TIA values (table 4), agricultural and recreational water use in Miami-Dade County (Marella, 1999, 2004, 2009), and the assumption that the change in water stored above the water table is negligible.

Estimated annual net groundwater recharge in the study area from 1996 through 2010 ranged from a low of 4.02 in. (323.40 ft<sup>3</sup>/s; 209.02 Mgal/d) in 1996 to a high of 34.16 in. (2,748.09 ft<sup>3</sup>/s; 1,776.14 Mgal/d) in 2005 to (fig. 21).

Estimated monthly net groundwater recharge in the study area ranged from -3.06 to 14.86 in. (-2,951.39 to 14,349.02 ft<sup>3</sup>/s; -1,907.53 to 9,274.01 Mgal/d). Average annual estimated net groundwater recharge ranged from 11.06 to 50.12 percent of rainfall in 1996 and 2005, respectively.

### Surface-Water/Groundwater Interaction

Groundwater in the Biscayne aquifer is closely coupled to the surface-water system because of the high transmissivity of the aquifer and its direct hydraulic connection to the canals. Canals can act as both a source of water to the aquifer (mostly in the dry season) and sink for the aquifer (mostly in the wet season and adjacent to ENP and WCA3). Actual volumes or rates of inflow to the aquifer (canal leakage) and outflow to the canals (canal seepage) in the study area are difficult to quantify and are currently not well understood, but are a large component of the water budget. Estimates of net flow in a surface-water basin are better understood because calculated structure discharge can be used to compute a net gain or loss from the surface-water system and it is a surrogate for canal leakage and seepage. Net flow in a surface-water basin can be calculated as

$$Q_{SWNET} = Q_{INFLOW} + Q_{SRO} + Q_{SWRAI} - Q_{SWEVAP} - Q_{OUTFLOW}, \quad (4)$$

where

- $Q_{SWNET}$  is the net flow for a surface-water basin [L<sup>3</sup>T<sup>-1</sup>],
- $Q_{INFLOW}$  is the sum of all inflows to a surface-water basin [L<sup>3</sup>T<sup>-1</sup>],
- $Q_{SWRAI}$  is direct rainfall on surface-water features [L<sup>3</sup>T<sup>-1</sup>],
- $Q_{SWEVAP}$  is evaporation from surface-water features [L<sup>3</sup>T<sup>-1</sup>], and
- $Q_{OUTFLOW}$  is the sum of all outflows from a surface-water basin [L<sup>3</sup>T<sup>-1</sup>].

$Q_{SWNET}$  includes canal leakage, canal seepage, and canal storage changes; for long evaluation periods (months and years), canal storage changes should be negligible.  $Q_{INFLOW}$  and  $Q_{OUTFLOW}$  can include uncontrolled surface-water flow from adjacent surface-water basins not separated by surface-water control structures. Uncontrolled surface-water flow between surface-water basins is unengaged and assumed to be zero. Monthly and annual net surface-water flow rates were calculated, in inches, by using the total onshore area (1,187.15 mi<sup>2</sup>) of the study area.

Estimated average annual rainfall and evaporation from surface-water features in urban parts of the study area for the period from 1996 through 2010 were 0.23 in. (19.63 ft<sup>3</sup>/s; 12.69 Mgal/d) and 0.23 in. (20.41 ft<sup>3</sup>/s; 13.19 Mgal/d), respectively. Average annual surface-water inflow to, and surface-water outflow from, the urban areas of the study area were estimated to be 3.96 in. (346.46 ft<sup>3</sup>/s; 223.92 Mgal/d) and

23.06 in. (2,015.23 ft<sup>3</sup>/s; 1,302.48 Mgal/d), respectively. Average annual surface runoff from urban areas upstream of the salinity control structures in the study area were estimated to be 2.44 in. (212.89 ft<sup>3</sup>/s; 137.597 Mgal/d) for the period from 1996 through 2010. The average annual net surface-water flow from urban areas of the study area was estimated to be 19.10 in. (1,668.77 ft<sup>3</sup>/s; 1,078.55 Mgal/d) for the period from 1996 through 2010. The urban area between the water-supply/flood-control structures and the salinity control structures is 545.26 mi<sup>2</sup> (fig. 9A). Net surface-water flow rates in inches were calculated by using the total onshore area (1,187.15 mi<sup>2</sup>) of the study area.

Estimated annual net surface-water flow from urban areas of the study area from 1996 through 2010 ranged from a minimum of 12.05 in. (483.68 ft<sup>3</sup>/s; 312.63 Mgal/d) in 2004 to a maximum of 20.30 in. (806.03 ft<sup>3</sup>/s; 520.95 Mgal/d) in 2002 to (fig. 22). Estimated monthly net surface-water flow ranged from -0.26 to 5.68 in. (-246.74 to 5,454.11 ft<sup>3</sup>/s; -159.47 to 3,523.14 Mgal/d) during the same period. Annual and monthly net surface-water flow data from urban areas of the study area indicate that, in general, canal seepage predominates and the surface-water system in the urban area is draining the Biscayne aquifer.

### Freshwater-Seawater Interface

The density of seawater is 2.5 percent greater than that of freshwater, which can affect groundwater flow in coastal settings. As fresh groundwater flows towards the coast, it meets saline water that originated from the ocean or other coastal features, such as Biscayne Bay. Mixing of freshwater and seawater occurs in a transition zone, the size and location of which is controlled by aquifer properties and freshwater discharge to the coast. The freshwater-seawater interface is usually defined as the approximate location, within the transition zone, of a specific chloride concentration at the base of the aquifer. The position of the freshwater-seawater interface at the base of the Biscayne aquifer was delineated using a chloride concentration of 100 milligrams per liter (mg/L) in 1984 (Klein and Waller, 1985), 1995 (Sonenshein, 1997), and 2011 (Prinos and others, 2014) and is shown in figure 23.

Changes in the position of the freshwater-seawater interface between 1984 and 1995 and between 1995 and 2011 were small throughout much of the study area, with the largest differences attributed to the availability of more information than to actual movement of the interface (Sonenshein, 1997; Prinos and others, 2014). The surface-water system and groundwater pumpage from MDWASD well fields influence the movement of the freshwater-seawater interface. The position of the interface in 1995 was a substantial distance inland from salinity control structures in the northern (S29, S28, and S27) and southern (S21, S21A, S20G, S20F, S20, and S197) parts of the study area (fig. 23).

In the north-central part of the study area, near the Hialeah-Miami Springs-Preston well fields, the

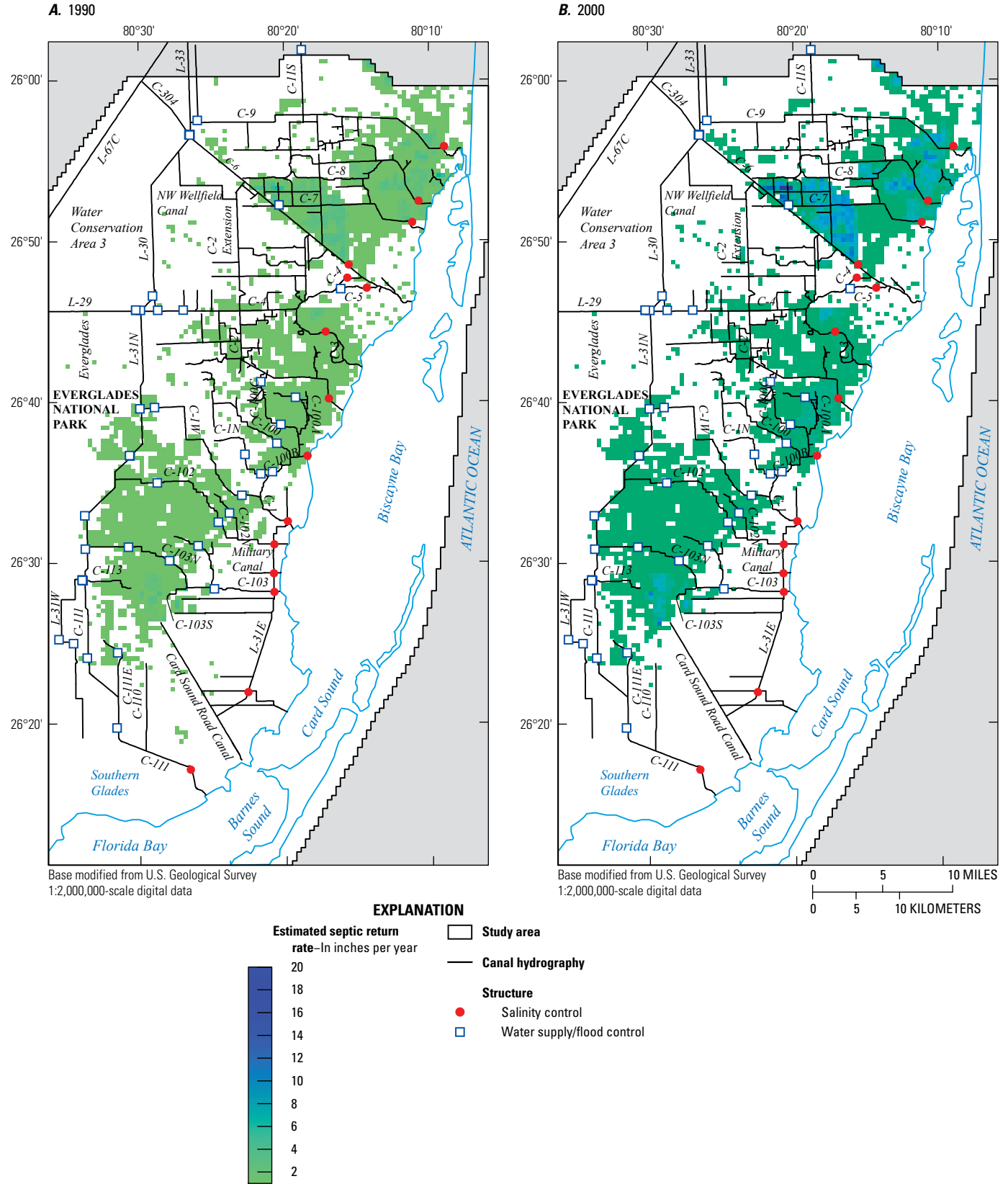
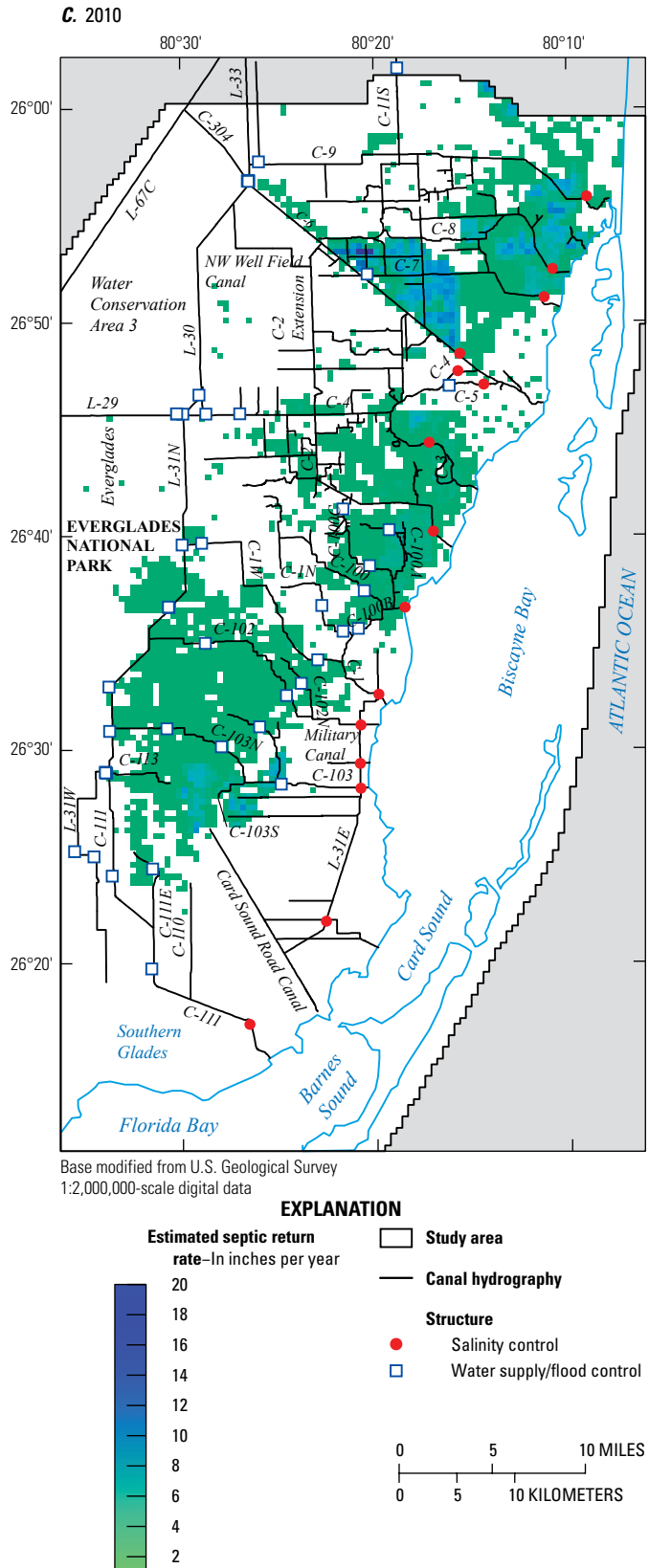


Figure 20. Estimated septic return rates in the onshore part of the study area for A, 1990, B, 2000, and C, 2010.



**Figure 20.** Estimated septic return rates in the onshore part of the study area for *A*, 1990, *B*, 2000, and *C*, 2010.—Continued

freshwater-seawater interface also moved seaward, possibly in response to decreased pumpage at the well fields from 1984 to 1992 (Sonenshein, 1997). In the south-central part of the study area, the freshwater-seawater interface moved inland north of the C-2 Canal between 1984 and 1995, due either to increased pumping from the Alexander Orr well field, a lowering of water levels in the C-3 Canal, or both. South of the C-2 Canal, the freshwater-seawater interface was not as far inland in 1995 as was previously estimated in 1984. In the southeastern part of the study area, the freshwater-seawater interface moved inland between the C-1W and C-103 Canals between 1984 and 1995.

The freshwater-seawater interface in 2011 was interpreted to be landward of its position in 1995 in several locations as a result of interface movement or improved information (Prinos and others, 2014). Between 1995 and 2011, the freshwater-seawater interface moved a small distance landward in northern parts of the study area (north of S28), between S26 and S27, and between S22 and S123. Larger landward movement of the freshwater-seawater interface occurred between S25A and G93 (approximately 600 ft) and near S20F (approximately 1 mile). The availability of more information in 2011 resulted in a more seaward position of the freshwater-seawater interface between G93 and S22 (approximately 1,300 ft), west of the area between S21A and S20G (as much as 3,000 ft), and in the southern Glades (as much as 3,000 ft). Elsewhere, the position of freshwater-seawater interface in 2011 was comparable to 1995.

## Model Development

A MODFLOW–NWT model (Niswonger and others, 2011) was developed to quantify the effect of groundwater withdrawals on canal leakage and regional groundwater flow in the study area (Hughes and White, 2016). The numerical model also includes (1) the Surface-Water Routing (SWR1) Process (Hughes and others, 2012) to represent surface-water discharge; and (2) the Seawater Intrusion (SWI2) Package (Bakker and others, 2013) to simulate effect of fluid density on groundwater flow and the position of the freshwater-seawater interface. The combination of MODFLOW–NWT and selected additional MODFLOW processes and packages allows simulation of coupled surface-water and groundwater flow in a coastal area.

## Spatial and Temporal Discretization

The groundwater part of the model was horizontally discretized into 101 columns and 189 rows of uniformly sized model cells (1,640.405 ft). In the Universal Transverse Mercator (UTM) Zone 17 North coordinate system using the horizontal North American Datum of 1983 (NAD 83), the southwestern corner of the model grid is located at  $x = 1,770,828$  and  $y = 9,139,572$  ft. There is no rotation of the model grid

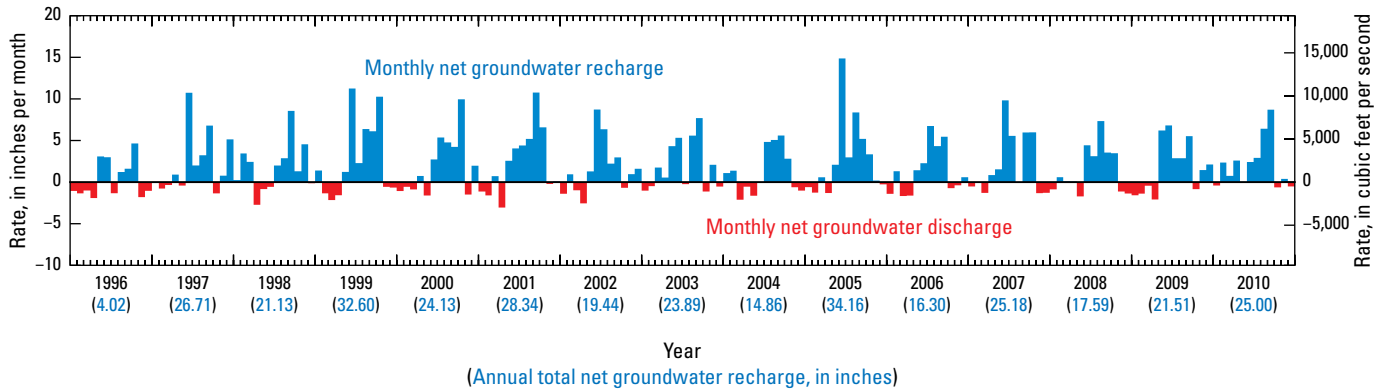


Figure 21. Estimated monthly net groundwater recharge in the onshore part of the study area, 1996–2010.

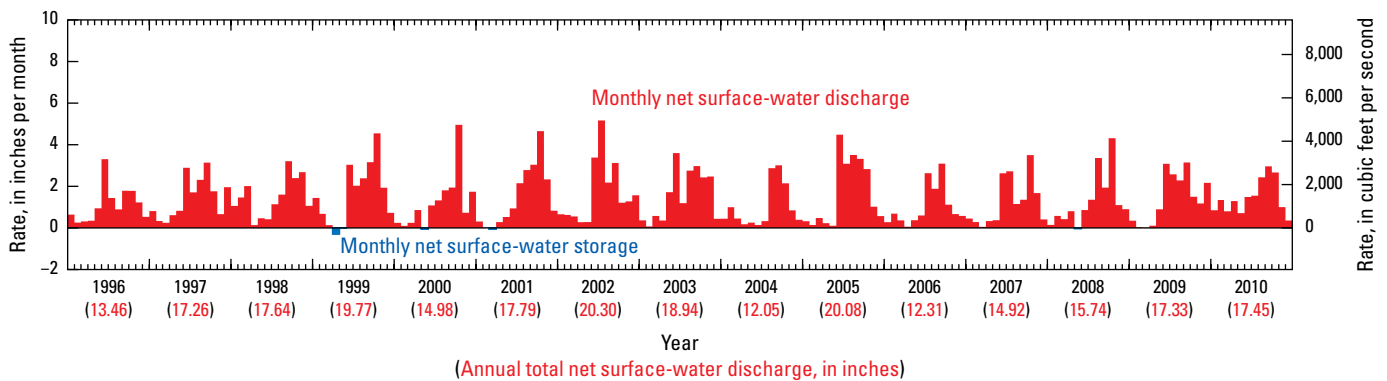


Figure 22. Estimated monthly net surface-water flow in urban areas upstream of the salinity control structures in the study area, 1996–2010. The estimated monthly net surface-water flow surface-water storage represents the combination of canal storage changes, canal seepage, and canal leakage. Monthly and annual net surface-water flow rates in inches were calculated using the total onshore area (1,187.15 square miles) of the study area.

from the UTM coordinate system. The horizontal model domain contains a total of 19,089 cells, of which 15,853 cells, covering an area of 1,530.191 mi<sup>2</sup>, are in the active model domain (fig. 24). In the active model domain, 11,335 cells (1,094.099 mi<sup>2</sup>) are considered onshore cells and 4,518 cells (436.034 mi<sup>2</sup>) are considered offshore cells. All islands (Miami Beach) and keys (Virginia Key, Key Biscayne, Elliott Key, and Key Largo) are considered offshore cells.

The groundwater model is discretized into three layers within the Biscayne aquifer. Model layering was developed on the basis of (1) topographic/bathymetric data; (2) Q-unit thickness data interpolated to the model grid using the geostatistical parameters summarized in table 5; and (3) a conceptual hydrostratigraphic model. The conceptual model assumes that the Biscayne aquifer is composed of upper and lower permeable units (each a composite of multiple flow zones) separated by a unit approximately two orders of magnitude less permeable than the overlying and underlying composite units. The elevation of the top and bottom of each Q-unit was determined using the average topographic/bathymetric elevation within each cell (fig. 25) and the cumulative thickness for all Q-units younger than the Q-unit of interest. For example, the top of

the Q3 unit in a cell would be calculated by subtracting the sum of the thickness of the Q5 and Q4 units in the cell from the average topographic/bathymetric elevation for the cell. The Q-units were converted to model layers (fig. 14) using the relation between defined high-frequency marine cycles and the presence or absence of flow zones (K. Cunningham, U.S. Geological Survey, written commun., 2012). Model layer 1 includes the Q5 unit. Model layer 2 includes the Q4 and Q3 units, and the upper third of the Q2 unit. Model layer 3 includes the lower two-thirds of the Q2 unit and the Q1 unit. All three model layers were simulated as convertible layers to allow the model to transition between confined and unconfined conditions in response to changing hydrologic conditions and groundwater pumping rates. Specific storage and specific yield data are specified for convertible layers.

Nine hydrogeologic sections show interpolated Q-unit elevations and the top and bottom elevations of each layer in the model domain (fig. 26). Sections A–A' through F–F' extend west to east in onshore parts of the model domain (fig. 26A–F). Sections G–G', H–H', and I–I' extend south to north in onshore parts of the model domain (fig. 26G–I). The west to east cross sections show the general thickening of the

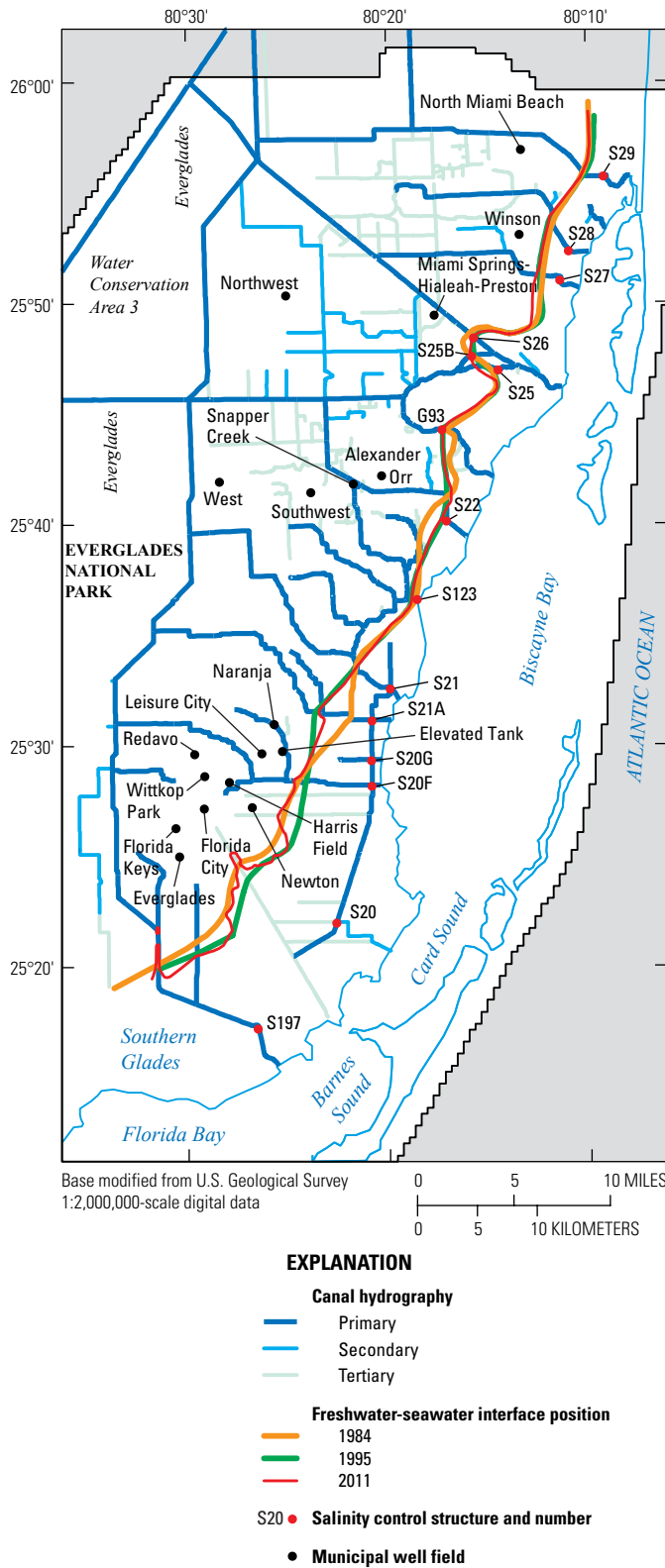


**Figure 23.** Position of the freshwater-seawater interface at the base of the Biscayne aquifer in 1984, 1995, and 2011.

Biscayne aquifer toward the coast. The increased thickness of the aquifer in northern parts of the model domain is shown on the south-north cross sections. Model topography and average water-table elevations are also shown on the cross sections.

The surface-water hydrography for the primary, secondary, and selected tertiary canals (fig. 1) was intersected with the groundwater model grid (fig. 24), which resulted in a total of 2,352 discretized SWR1 reaches having lengths ranging from 0.67 to 2,868.28 ft. The discretized SWR1 reaches were combined into 637 SWR1 reach groups to reduce the problem size and model run times; a number of different groupings were evaluated to confirm that grouping of reaches did not limit the ability of the model to simulate surface-water stages and discharge. As many as 14 individual SWR1 reaches were combined into individual SWR1 reach groups having lengths ranging from 4.04 to 16,415.47 ft. More information about combining SWR1 reaches into SWR1 reach groups is provided in Hughes and others (2012).

SWR1 reach geometry was specified for each reach by using 1,009 unique trapezoidal cross sections developed on the basis of a spatial dataset of canal geometry provided by the SFWMD (Giddings and others, 2006). The SFWMD canal dataset included canal bottom widths, top widths, and bottom elevations. The side slope of each unique reach cross section was calculated by using estimated canal top elevations along with the canal top width, bottom width, and bottom elevation data from the SFWMD canal geometry dataset (Giddings and others, 2006). The calculated canal top elevation was assumed to correspond to the average headwater or tailwater stage, for the period from 1996 through 2010, at the closest primary SFWMD surface-water control structure or the target control elevation for the closest primary SFWMD or secondary Miami-Dade surface-water control structure (fig. 9). Each reach group includes at least one unique trapezoidal cross section. Details about the SWR1 Process are provided in Hughes and others (2012).

Aerial photographs from 1999 were used to define the spatial extent of quarry lakes in the study area. Model cells in which most of the cell was covered by quarry lakes were defined to be quarry lake cells (fig. 24). Quarry lakes were not simulated using the SWR1 Process because they are assumed to be disconnected from the primary and secondary canals. Instead, quarry lakes were represented as high hydraulic conductivity cells, which is an accepted approach for simulating the interaction of a deep lake with an aquifer (Brakefield and others, 2013). Quarry lakes are estimated to reach depths of 50 to 80 ft into the Biscayne aquifer, which in some cases is as deep as or deeper than the level of the production zone. As a result, quarry lakes are assumed to penetrate the full thickness of the Biscayne aquifer (model layers 1 to 3).

The simulation period for the model is January 1996 through December 2010. A total of 5,479 transient 1-day stress periods were used. A 1-day time step length was used in the surface-water and groundwater domains.

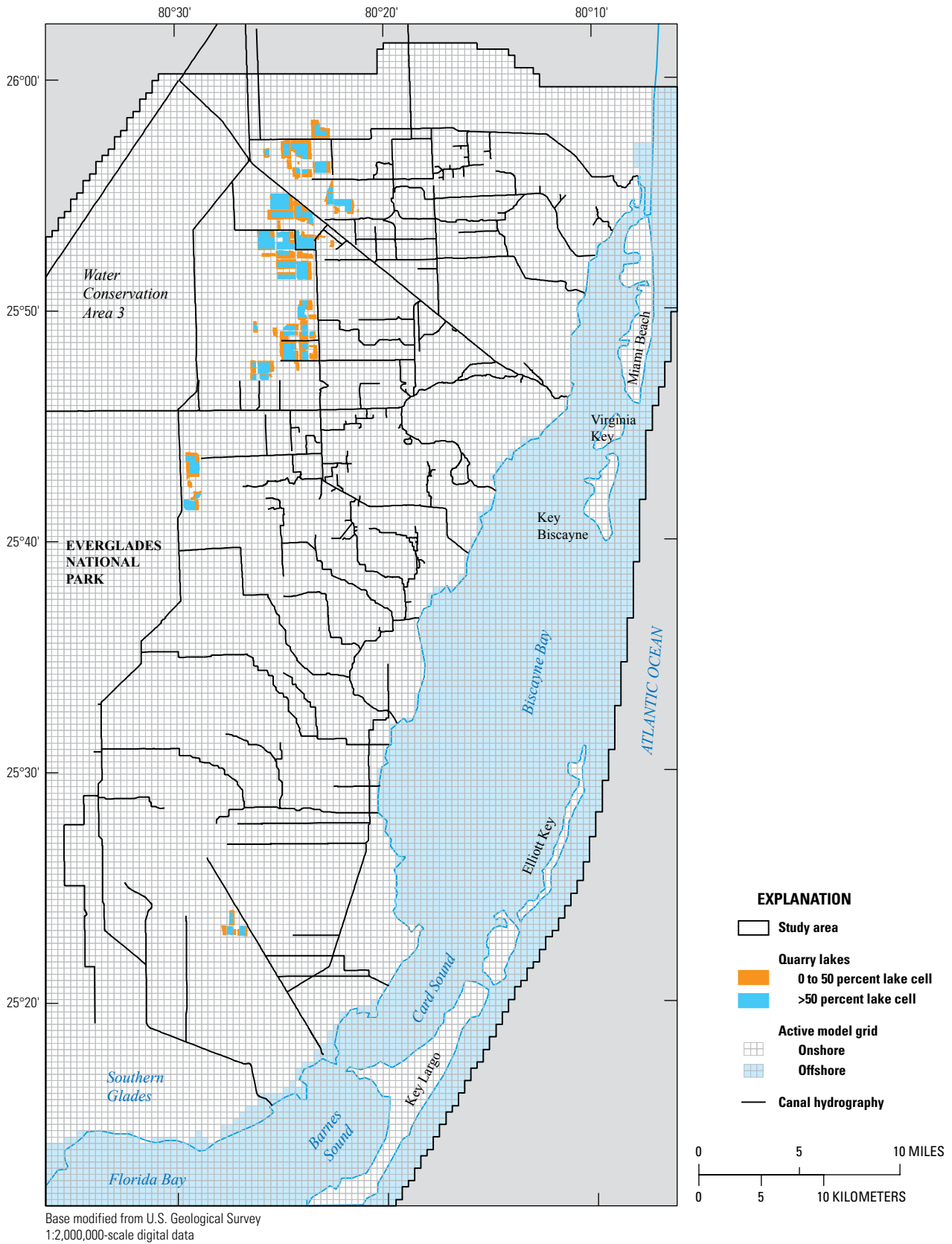


**Figure 24.** Horizontal model discretization.

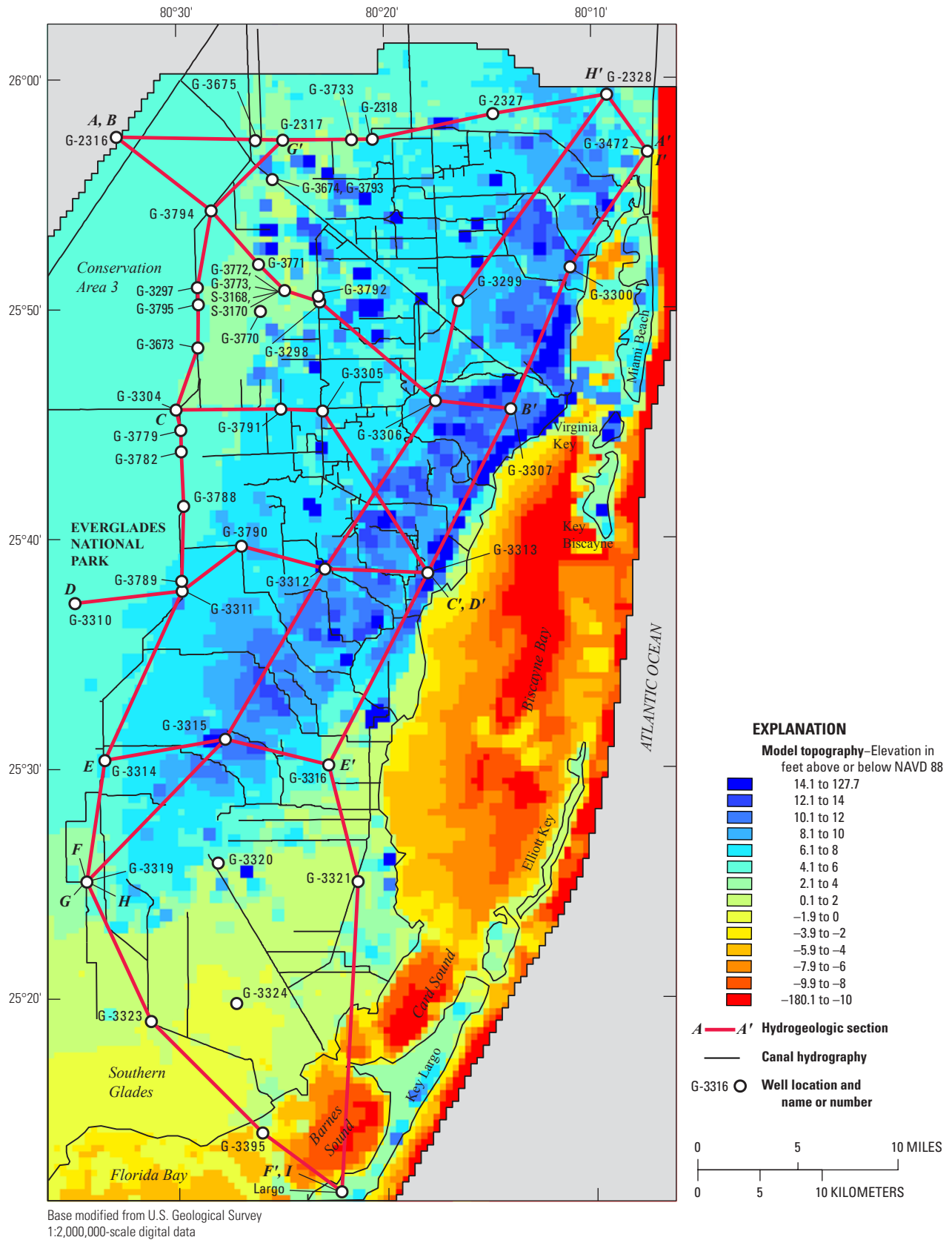


Figure 25. Lines of hydrogeologic sections and topographic/bathymetric elevations in the model domain.

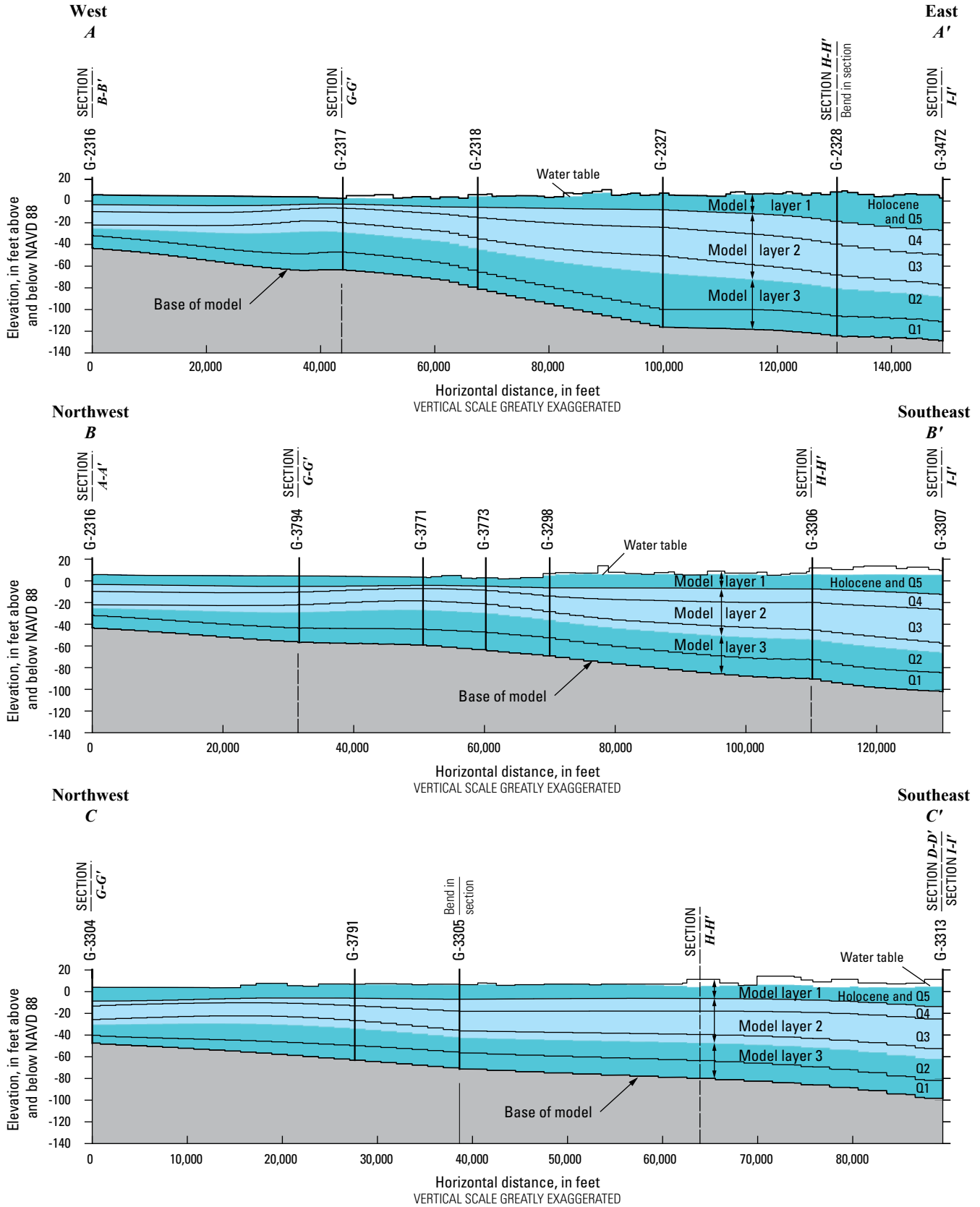


Figure 26. Hydrogeologic sections A–A’ through I–I’ in the model domain. Location of section lines shown in figure 25.

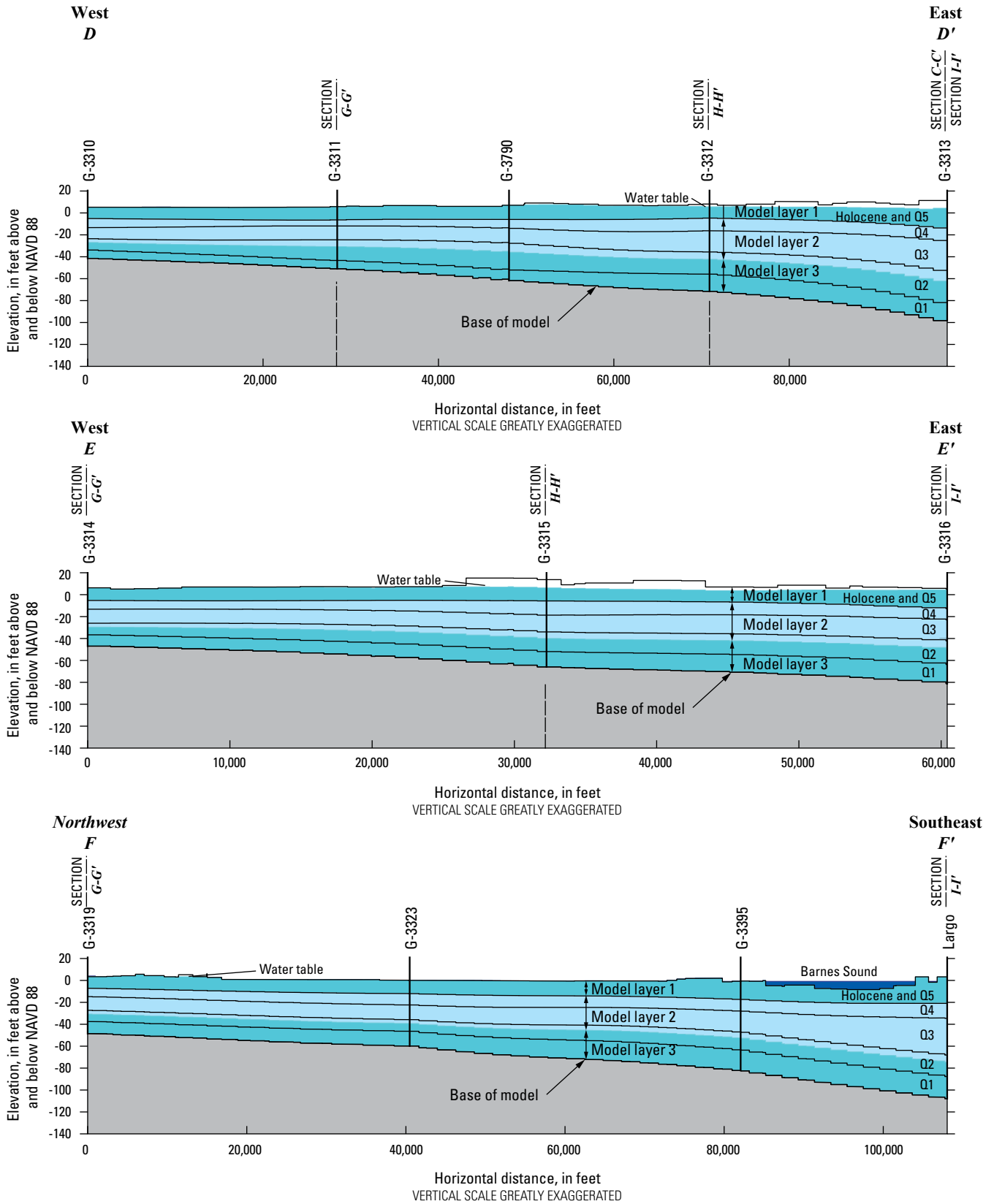


Figure 26. Hydrogeologic sections A–A' through I–I' in the model domain. Location of section lines shown in figure 25.—Continued

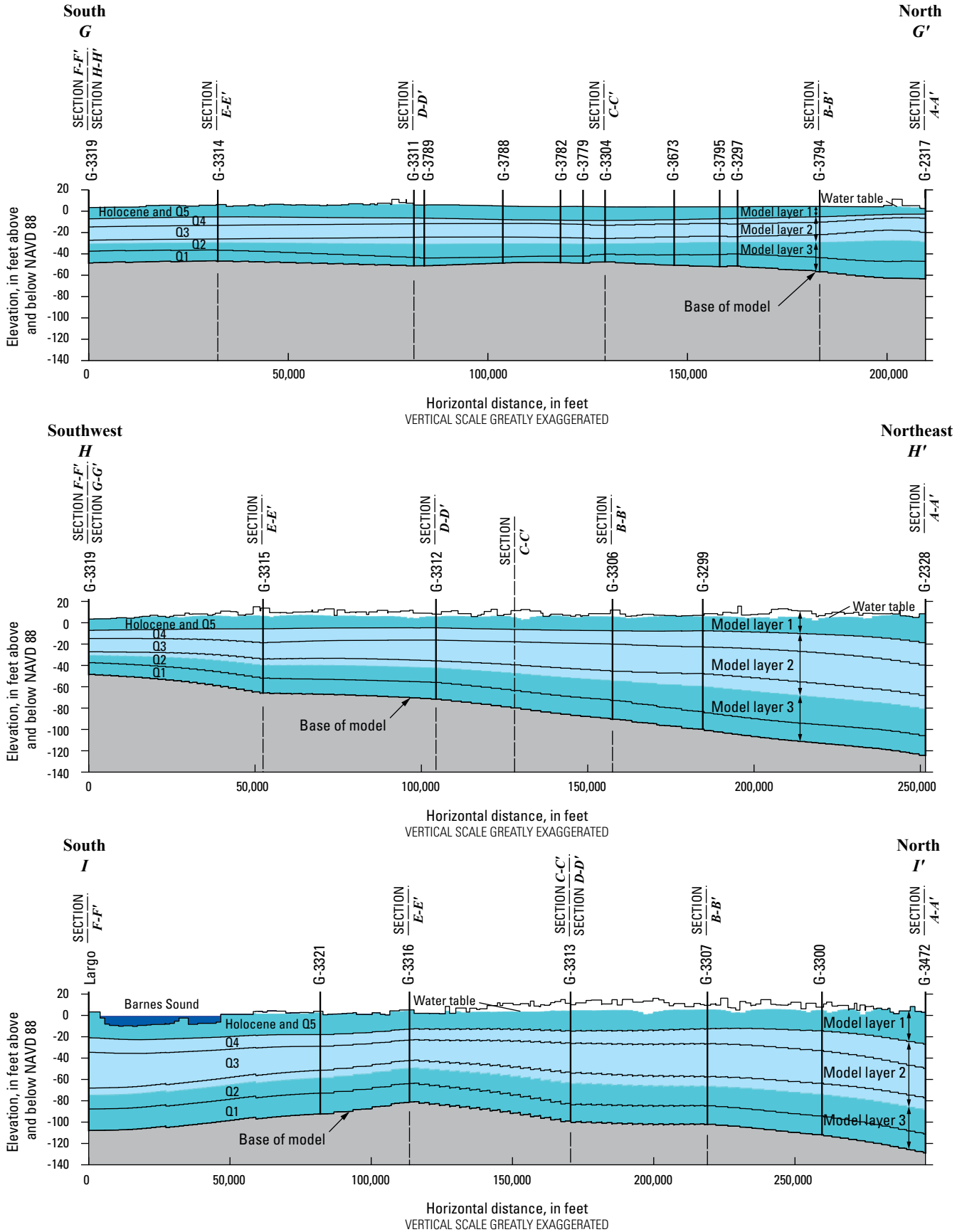


Figure 26. Hydrogeologic sections A–A’ through I–I’ in the model domain. Location of section lines shown in figure 25.—Continued

## Calibration Approach

The model was calibrated with the automated parameter estimation software (PEST) (Doherty, 2010) using highly parameterized inversion techniques (Doherty and Hunt, 2010). The calibration process was constrained using surface-water stage data collected at 58 surface-water control structures and surface-water stage data collected at 12 additional stage gages locations (fig. 27). The calibration process was also constrained using surface-water discharge data collected at the upstream and downstream ends of each surface-water basin in urban parts of the study area (fig. 1) and compiled as net surface-water canal discharge. Surface-water discharge data were summed on a monthly basis and differenced to determine the net surface-water canal discharge for each subbasin. The monthly net surface-water canal discharge for the subbasin was compared to the monthly sum of surface runoff, direct rainfall, evaporation, and reach-aquifer exchange for each SWR1 Process reach in the surface-water subbasin. Model calibration was also constrained by water-level data from 112 groundwater monitoring wells (fig. 28). Model parameters were calibrated by using data for an 8-year period, from January 1997 through December 2004, and model calibration was verified by using observed data from January 2005 through December 2010. A 1-year warmup period prior to the start of the calibration period was included to reduce the effect of inaccurate initial conditions on model results.

The observation sites used for calibration, data sources, and the number of weekly observations available during the calibration and verification periods for surface-water stage are summarized in table 6. For surface-water subbasins in which net canal discharge was evaluated, data sources, and the number of monthly observations available during the calibration and verification periods are summarized in table 7. Monitoring well locations, data sources, and the number of weekly groundwater level observations available during the calibration and verification periods are summarized in table 8.

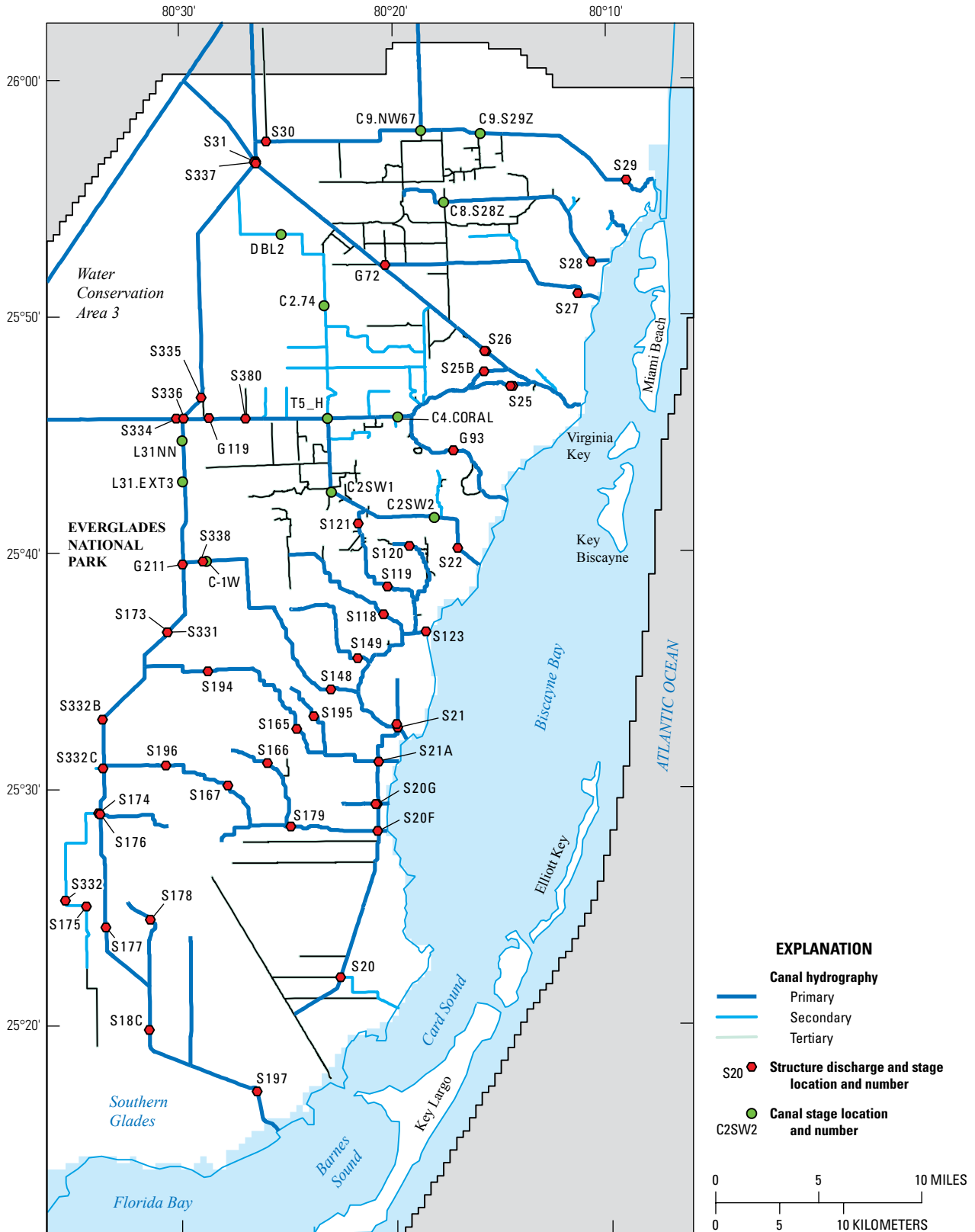
## Model Parameterization

Model calibration involves modification of model properties, or input parameters (for example, crop coefficients, canal roughness coefficients, or hydraulic conductivity) to estimate unknown physical properties and (or) state conditions. During model calibration, selected model input parameters are modified until differences between simulation results and observations (model error) are reduced to an acceptable level. The combination of the inherent variability of physical systems and limited observation data in most settings make it possible to achieve similar, and acceptable, levels of model error with different (non-unique) model parameter datasets.

Mathematically, the process of model calibration is the solution of an inverse problem in which model error is minimized by modifying selected model input parameters, whereby

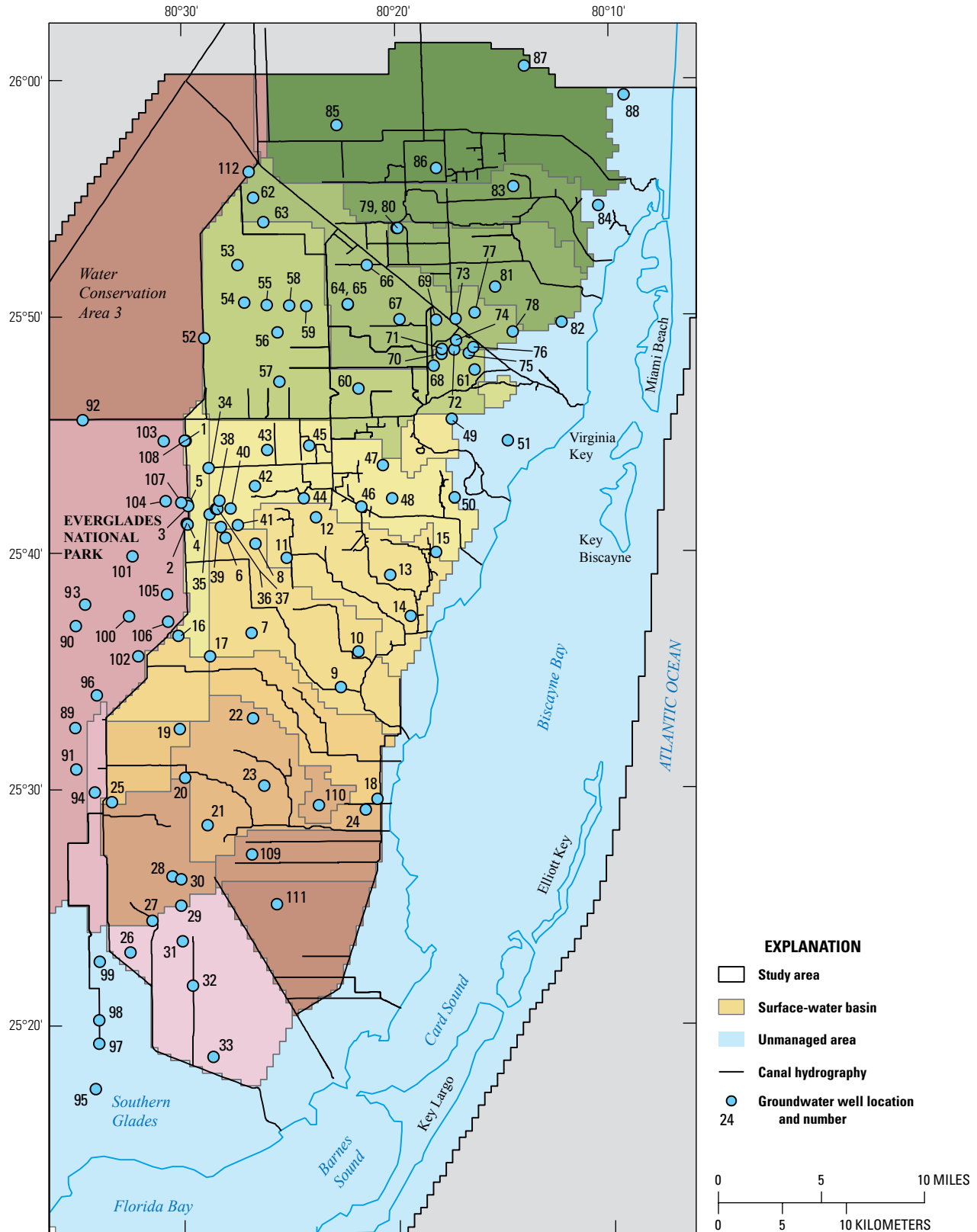
parameter modifications are determined on the basis of the response of the model at observation locations to parameter changes (sensitivities). Because the solution of the inverse problem for physical systems having limited observation data is typically non-unique, there will be an infinite number of parameter combinations that will result in models that meet acceptable calibration criteria (Moore and Doherty 2005). Additionally, if the number of parameters is greater than the number of observations, the inverse problem will be difficult to solve and is said to be ill-posed. The process of reducing the number of parameters to form a well-posed inverse problem having a unique solution is known as regularization (Vogel, 2002). Traditional, over-determined inverse problem formulation, commonly achieved by using zone-based parameterization, reduces the number of parameters prior to calibration to find a unique solution, while under-determined (highly parameterized) problem formulations rely on mathematical regularization (Tikhonov and Arsenin, 1977) to find a unique solution and enforce expert knowledge (Aster and others, 2005). Given the heterogeneity of Biscayne aquifer hydraulic properties, highly parameterized approaches (Doherty and Hunt, 2010; Doherty and others, 2010a, b) were used to calibrate the model. Highly parameterized inversion allows greater flexibility in the inverse problem so that more information in the observation data can be used to condition model parameters while also removing the need to discretize model properties in piecewise constant zones before the calibration process.

A regular distribution of 182 pilot points (Doherty, 2010) was used to parameterize the hydraulic conductivity for each model layer, specific yield ( $S_y$ ) for model layer 1, and specific storage ( $S_s$ ) for model layers 1, 2, and 3 (fig. 29). The horizontal and vertical hydraulic conductivity of each layer were assumed to be equal. Estimated  $S_y$  values for model layer 1 were applied in model layers 2 and 3. Biscayne aquifer porosity was assumed to be equal to the estimated  $S_y$  of model layer 1; porosity is required to simulate movement of the freshwater-seawater interface using the SWI2 Package. The  $S_y$  of layer 1 was estimated because unconfined conditions occur throughout most of the study area. The  $S_y$  was not estimated for layer 2 because unconfined conditions only occur in isolated areas of the study area (near the Miami Springs, Hialeah, and Preston well fields).  $S_y$  was not estimated for layer 3 because unconfined conditions do not currently occur in this layer;  $S_y$  was specified for model layer 3 so that the model can be used to simulate hydrologic conditions that cause this layer to become unconfined. The  $S_s$  of layer 1 was estimated because the Biscayne aquifer in WCA2, ENP, and the southern Glades is frequently inundated by surface water. Pilot points were used as multiplier parameters and assigned an initial value of 1.0 for all properties. During each forward model run, pilot point values were interpolated from pilot point locations to the center of each model grid cell using ordinary kriging. The interpolated multiplier value for each cell was then multiplied by the base property value for each cell. The model



Base modified from U.S. Geological Survey  
1:2,000,000-scale digital data

**Figure 27.** Surface-water gages used to evaluate model fit. Surface-water headwater and tailwater stage data and calculated discharge data are available at surface-water gages located at surface-water control structures. Surface-water stage data are available at canal stage locations.



Base modified from U.S. Geological Survey  
1:2,000,000-scale digital data

**Figure 28.** Groundwater monitoring well locations and well identification numbers. The correspondence between well identification numbers and well names are given in table 8.

**44 Hydrologic Conditions and Effect of Pumpage and Sea Level on Canal Leakage and Regional Groundwater Flow**

**Table 6.** Surface-water stage observation locations, data source, number of weekly observations, and model-fit statistics.

[All data are from the South Florida Water Management District DBHYDRO database. SWR, surface-water routing; --, data not available; %, percent]

Station	SWR Process reach	Calibration period (1997–2004)			Verification period (2005–10)		
		Number of weekly observations	Mean error, in feet	Root mean square error, in feet	Number of weekly observations	Mean error, in feet	Root mean square error, in feet
S30 headwater	1964	366	-0.04	0.48	274	-0.04	0.52
S30 tailwater	1963	366	0.45	0.56	271	0.66	0.68
S29 headwater	2080	366	0.14	0.24	274	0.22	0.29
S29 tailwater	2081	366	0.05	0.19	274	0.03	0.16
S28 headwater	2150	366	0.13	0.29	274	0.41	0.49
S28 tailwater	2151	366	-0.13	0.14	274	-0.14	0.15
G72 headwater	260	364	0.33	0.54	274	0.76	0.83
G72 tailwater	261	363	0.34	0.46	274	0.67	0.71
S27 headwater	2179	366	0.18	0.39	274	0.44	0.54
S27 tailwater	2180	366	-0.18	0.19	274	-0.20	0.20
S151 tailwater	1	366	-0.79	0.86	274	-0.65	0.69
S31 headwater	24	366	-0.77	0.83	274	-0.62	0.66
S31 tailwater	25	366	0.18	0.69	274	0.93	0.97
S26 headwater	395	366	0.28	0.55	274	0.53	0.72
S26 tailwater	396	366	0.01	0.17	274	0.01	0.20
S25 headwater	1735	366	0.44	0.52	274	0.47	0.53
S25 tailwater	1736	366	0.01	0.17	274	-0.03	0.17
S336 headwater	1177	366	0.00	0.23	274	0.31	0.41
S336 tailwater	1201	366	-0.12	0.28	274	0.16	0.29
G119 headwater	1206	357	-0.18	0.31	267	0.07	0.26
G119 tailwater	1213	357	0.40	0.61	255	0.79	0.91
S380 headwater	1219	24	0.98	1.03	274	0.76	0.90
S380 tailwater	1220	24	0.93	0.97	274	1.14	1.17
S25B headwater	409	366	0.18	0.36	274	0.25	0.36
S25B tailwater	408	366	0.00	0.15	274	0.00	0.18
G93 headwater	466	366	0.28	0.46	274	0.36	0.49
G93 tailwater	467	366	-0.22	0.29	274	-0.21	0.27
S22 headwater	1685	363	0.38	0.52	274	0.52	0.58

**Table 6.** Surface-water stage observation locations, data source, number of weekly observations, and model-fit statistics.—Continued

[All data are from the South Florida Water Management District DBHYDRO database. SWR, surface-water routing; --, data not available; %, percent]

Station	SWR Process reach	Calibration period (1997–2004)			Verification period (2005–10)		
		Number of weekly observations	Mean error, in feet	Root mean square error, in feet	Number of weekly observations	Mean error, in feet	Root mean square error, in feet
S22 tailwater	1686	366	-0.05	0.10	274	-0.08	0.11
S337 tailwater	29	366	-0.13	0.40	274	-0.01	0.28
S335 headwater	1136	366	-0.17	0.37	274	-0.07	0.26
S335 tailwater	1135	366	0.08	0.25	274	0.31	0.40
G618B	1200	359	-0.40	0.47	274	-0.39	0.45
S334 headwater	1180	366	-0.47	0.58	274	-0.53	0.61
S334 tailwater	1179	366	0.08	0.24	274	0.23	0.36
S338 headwater	1061	366	0.06	0.33	274	0.33	0.46
S338 tailwater	1062	366	0.30	0.54	274	0.83	0.91
S148 headwater	1104	366	0.03	0.39	274	0.50	0.61
S148 tailwater	795	366	0.29	0.39	274	0.47	0.54
S149 headwater	759	363	0.23	0.44	226	0.45	0.58
S149 tailwater	758	--	--	--	103	0.51	0.56
S21 headwater	1545	366	0.16	0.28	274	0.37	0.44
S21 tailwater	1546	364	-0.22	0.28	274	-0.10	0.14
S121 headwater	675	366	0.30	0.48	274	0.62	0.67
S121 tailwater	676	366	0.25	0.52	274	0.75	0.80
S120 headwater	724	366	0.18	0.45	274	0.49	0.59
S120 tailwater	723	366	0.30	0.46	274	0.54	0.60
S119 headwater	695	366	0.33	0.53	274	0.66	0.72
S119 tailwater	696	366	0.31	0.47	274	0.55	0.62
S118 headwater	1566	366	0.27	0.44	274	0.68	0.74
S118 tailwater	1565	366	0.30	0.44	272	0.54	0.60
S122 headwater	752	366	0.31	0.48	274	0.52	0.59
S122 tailwater	753	366	0.49	0.57	274	0.53	0.62
S123 headwater	1627	366	0.28	0.43	274	0.54	0.60
S123 tailwater	1628	366	-0.14	0.16	274	-0.18	0.19
S194 headwater	964	366	0.11	0.44	273	0.84	1.16

**Table 6.** Surface-water stage observation locations, data source, number of weekly observations, and model-fit statistics.—Continued

[All data are from the South Florida Water Management District DBHYDRO database. SWR, surface-water routing; --, data not available; %, percent]

Station	SWR Process reach	Calibration period (1997–2004)			Verification period (2005–10)		
		Number of weekly observations	Mean error, in feet	Root mean square error, in feet	Number of weekly observations	Mean error, in feet	Root mean square error, in feet
S194 tailwater	965	366	0.03	0.40	274	0.65	0.81
S195 headwater	1024	366	0.42	0.54	274	0.78	0.84
S195 tailwater	1023	360	-0.02	0.33	274	0.28	0.39
S165 headwater	990	366	0.32	0.50	274	0.51	0.66
S165 tailwater	991	366	-0.00	0.26	274	0.24	0.31
S21A headwater	1010	366	0.13	0.23	274	0.25	0.31
S21A tailwater	1011	366	-0.04	0.12	274	-0.07	0.13
S20G headwater	1541	366	0.10	0.26	274	0.24	0.35
S20G tailwater	1542	366	-0.10	0.15	274	-0.09	0.15
S196 headwater	916	366	0.06	0.52	274	0.74	1.15
S196 tailwater	915	366	0.01	0.37	274	0.51	0.69
S166 headwater	863	366	0.22	0.36	274	0.51	0.63
S166 tailwater	862	366	0.09	0.27	274	0.28	0.39
S167 headwater	901	366	0.11	0.36	274	0.53	0.70
S167 tailwater	900	366	0.06	0.28	274	0.27	0.39
S179 headwater	846	366	0.07	0.26	274	0.25	0.37
S179 tailwater	845	366	0.17	0.27	274	0.28	0.34
S20F headwater	1531	366	0.21	0.30	274	0.31	0.37
S20F tailwater	1532	366	-0.09	0.15	274	-0.06	0.13
S20 headwater	2324	356	-0.36	0.44	253	-0.21	0.33
S20 tailwater	2323	312	-0.34	0.42	218	-0.33	0.41
S174 headwater	1418	366	0.18	0.62	267	0.88	1.33
S174 tailwater	1419	366	-0.14	0.51	267	-0.05	0.39
S332D headwater	1418	185	0.34	0.75	274	0.89	1.35
S332 headwater	1440	366	0.04	0.74	274	0.02	0.44
S175 headwater	1444	366	0.05	0.72	274	0.12	0.45
S175 tailwater	1445	366	-0.01	0.25	274	0.02	0.17
G211 headwater	1057	366	-0.01	0.28	274	0.27	0.39

**Table 6.** Surface-water stage observation locations, data source, number of weekly observations, and model-fit statistics.—Continued

[All data are from the South Florida Water Management District DBHYDRO database. SWR, surface-water routing; --, data not available; %, percent]

Station	SWR Process reach	Calibration period (1997–2004)			Verification period (2005–10)		
		Number of weekly observations	Mean error, in feet	Root mean square error, in feet	Number of weekly observations	Mean error, in feet	Root mean square error, in feet
G211 tailwater	1056	366	0.20	0.59	274	0.67	0.98
S331 headwater	1043	366	0.22	0.63	274	0.63	0.96
S331 tailwater	1042	366	0.13	0.51	274	0.82	1.16
S332B headwater	937	152	0.42	0.76	274	0.95	1.35
S332C headwater	1266	--	--	--	172	1.11	1.50
S176 headwater	1276	366	0.19	0.63	274	0.89	1.34
S176 tailwater	1277	366	0.03	0.34	274	0.31	0.56
S177 headwater	1311	366	0.03	0.35	274	0.32	0.56
S177 tailwater	1312	366	0.18	0.34	274	0.30	0.45
S178 headwater	1342	366	0.06	0.36	274	0.24	0.49
S178 tailwater	1341	366	0.14	0.33	274	0.31	0.45
S18C headwater	1357	366	0.17	0.34	274	0.33	0.47
S18C tailwater	1358	366	0.11	0.28	274	0.21	0.35
S197 headwater	1405	366	0.09	0.27	274	0.17	0.33
S197 tailwater	1406	366	-0.28	0.30	274	-0.29	0.31
DBL2 headwater	54	366	0.09	0.66	274	0.42	0.83
DBL2 tailwater	55	85	0.55	0.75	256	1.11	1.17
C2.74	75	351	0.22	0.64	119	1.22	1.27
T5_H	533	366	0.08	0.43	272	0.49	0.55
C2SW1	654	97	0.27	0.43	274	0.49	0.54
C2SW2	1660	97	0.34	0.52	274	0.53	0.60
C4.CORAL	508	366	0.09	0.34	274	0.25	0.35
C8.S28Z	2094	366	0.05	0.31	274	0.44	0.52
C9.NW67	1935	362	0.27	0.37	274	0.31	0.49
C9.S29Z	2041	366	0.28	0.36	274	0.45	0.51
L31NN	1124	27	-0.45	0.75	274	-0.54	0.74
L31.EXT3	1118	366	-0.08	0.24	272	0.15	0.31
Global average			0.10	0.42		0.34	0.57
Percentage of observations satisfying calibration criteria			95%	99%		59%	90%

**Table 7.** Monthly net surface-water subbasin canal discharge locations, data source, number of daily observations, and model-fit statistics.

[All data are from the South Florida Water Management District DBHYDRO database. --, data not available; %, percent]

Station	Calibration period (1997–2004)				Verification period (2005–10)			
	Number of monthly observations	Normalized mean error	Normalized root mean square error	Nash-Sutcliffe model efficiency	Number of monthly observations	Normalized mean error	Normalized root mean square error	Nash-Sutcliffe model efficiency
C-9 at S29	96	-0.02	0.07	0.83	69	-0.02	0.04	0.89
C-8 at S28	96	0.01	0.06	0.81	71	0.07	0.11	0.64
C-7 at S27	95	0.03	0.09	0.54	66	0.21	0.24	-0.52
C-6 at S26	95	-0.03	0.11	0.59	70	-0.06	0.10	0.64
L-30 at S335	95	0.02	0.11	0.63	71	-0.05	0.10	0.44
DBL-2	89	0.16	0.24	0.10	72	0.13	0.26	0.33
C-5 at S25A, C-4 at S25B, C-3 at G93, and C-2 at S22	92	0.01	0.05	0.84	62	0.03	0.05	0.85
C-5 at S25	96	0.01	0.06	0.78	71	-0.00	0.09	0.77
L-30 at S335	95	0.02	0.11	0.63	71	-0.05	0.10	0.44
C-100A at S120	96	-0.04	0.13	0.64	72	-0.05	0.12	0.57
C-100C at S119	96	0.01	0.04	0.75	67	0.02	0.10	0.62
C-100 at S118	96	-0.01	0.04	0.85	68	0.02	0.11	0.76
C-100 at S123	96	0.01	0.08	0.51	72	0.04	0.11	0.38
C-1N at S149	--	--	--	--	23	-0.07	0.20	0.60
C-1W at S148	96	0.01	0.08	0.68	63	0.06	0.09	0.57
L-31N at G211	96	-0.03	0.15	0.27	72	-0.02	0.18	0.07
L-31N at S331	96	0.00	0.07	0.49	67	0.10	0.35	-0.23
L-31N at S176	96	-0.12	0.19	0.24	72	-0.30	0.47	-0.29
C-102N at S195	93	-0.05	0.12	0.68	72	-0.03	0.10	0.75
C-102 at S165	96	-0.06	0.13	0.43	66	-0.03	0.08	0.65
C-102 at S21A	96	0.06	0.15	0.44	72	0.16	0.30	-0.20
Military Canal at S20G	96	-0.13	0.19	0.12	72	-0.12	0.19	-0.06
C-103N at S166	96	0.04	0.10	0.62	72	-0.01	0.10	0.67
C-103 at S167	96	-0.16	0.27	-0.40	72	-0.09	0.25	-0.03
C-103 at S179	96	-0.00	0.13	0.65	72	-0.01	0.07	0.71
C-103 at S20F	96	0.02	0.12	0.57	72	0.03	0.12	0.48
L-31E at S20	77	0.03	0.11	0.30	52	0.07	0.21	0.19
C-111 at S177	96	-0.01	0.05	0.84	71	0.00	0.05	0.87
C-111E at S178	96	0.12	0.36	-1.19	72	0.35	0.65	-1.89
C-111 at S18C	96	0.01	0.09	0.60	72	0.22	0.35	-0.51
C-111 at S197	96	0.00	0.12	0.69	72	-0.18	0.29	0.34
Global average		-0.00	0.12	0.48		0.01	0.18	0.31
Percentage of observations satisfying calibration criteria		83%	90%	67%		74%	68%	48%

property distributions resulting from this operation were used as model inputs. Model parameters for a given cell,  $P_{ij}$ , were calculated from pilot point multipliers and base property values by using

$$P_{ij} = M_{ij} \times P_{ij}^0, \quad (5)$$

where

$M_{ij}$  is the interpolated multiplier for cell  $ij$ , and  
 $P_{ij}^0$  is the base property value for cell  $ij$ .

APT data and theoretical semivariogram parameters summarized in table 5 were used to determine the base transmissivity of the Biscayne aquifer (fig. 16). The base transmissivity, model layer thicknesses, and the conceptual hydrostratigraphic model were used to develop the base hydraulic conductivity distribution for model layers 1, 2, and 3.  $S_y$  storage is poorly defined in the study area. As a result, the interpolated  $S_y$  multipliers were multiplied by a base  $S_y$  value of 0.2 for all cells. Similar to  $S_y$ ,  $S_s$  is also poorly defined in the study area and the interpolated  $S_s$  multipliers were multiplied by a base  $S_s$  value of  $3.28 \times 10^{-5} \text{ ft}^{-1}$  for all cells. Estimated  $S_s$  values for model layer 3 were used in model layer 1.

In addition to hydraulic conductivity, the extinction depth and the depth of dense roots, properties used in the Evapotranspiration Segments (ETS) Package, were parameterized by using pilot points (fig. 29). The leakance coefficient and roughness coefficient for each of 1,009 unique trapezoidal cross sections was adjusted during calibration, as were monthly crop coefficients for urban land-use types.

A total of 3,668 parameters were allowed to be adjusted during calibration. Truncated singular value decomposition was used to reduce the number of parameters estimated during each model forward run by combining nonorthogonal parameters into linear combinations of parameters (Aster and others, 2005). Tikhonov regularization (Tikhonov and Arsenin, 1977) was also used to penalize deviations of parameters from initial values. This formulation produces parameter distributions that provide an acceptable fit between model output and observation data, while simultaneously minimizing deviations from preferred values based on field measurements and expert knowledge.

## Observation Processing and Weighting

Because all models of physical systems are a simplification of reality, it is unreasonable to expect that the model will exactly reproduce observations made in the natural system. This is especially true of observation time series, inasmuch as these data are the result of a convolution of many signals, each having a unique amplitude and frequency (Chatfield, 1999). Observations should instead be processed and filtered into a form that the model is capable of reproducing while preserving the important aspects of the system behavior as it relates to the purpose of the model (Doherty and Welter,

2010). Because the model is designed to predict weekly to monthly canal leakage and regional groundwater flow, daily observations of groundwater level and surface-water stage were processed to remove unwanted high-frequency components (noise). Observation processing is expected to improve the predictive ability of the model because the potential for estimated parameters to be adversely affected by noise is reduced. An additional goal of the observation processing for this study was to reduce the number of observations used to calibrate model parameters and reduce the size of the matrix being inverted at the end of each forward run. The total number of daily surface-water stages, daily groundwater heads, and monthly net surface-water subbasin discharge observations in the period from January 1997 through December 2004 exceeds 540,000 unique values.

Each observed surface-water and groundwater time series was processed by using a recursive low-pass filter (Nathan and McMahon, 1990) and then sampled at a 14-day frequency. Low-pass filtering removes high-frequency signal components that contain information related to subdaily temporal processes, which the model will be unable to reproduce. Because the model uses daily forcing effects (rainfall, evapotranspiration, and groundwater pumpage for MDWASD well fields) the Nyquist principle indicates that it is unreasonable to expect that the model can reproduce processes having less than a 2-day period (Chatfield, 1999). Sampling at a 14-day frequency effectively reduces the number of observations to a more manageable number while maintaining the information content of the observation dataset. Sampling at a 14-day frequency involved binning the time series data into 2-week wide bins and calculating the arithmetic average for each bin containing data. Use of a low-pass filter with sampling at a 14-day frequency is equivalent to a simple 14-day average. The model equivalent of each observed series was processed using the same steps during each forward run. All time-series processing was completed by using the software TSPROC (Westenbroek and others, 2012). No additional processing was performed on the data for monthly net surface-water subbasin discharge nor that for the monthly sum of surface runoff, direct rainfall, evaporation, and reach-aquifer exchange for each SWRI Process reach in the surface-water basin.

A total of 83,006 observations were used for the calibration. A weight value of 100.0 was assigned to the processed surface-water stage and groundwater level observations included in the objective function that was minimized as a part of the parameter estimation process. Several groundwater level observation locations are spatially clustered, and data within each cluster were down-weighted by dividing the weight by the number of locations having a 152.4-ft cluster radius. The weights assigned to the monthly net surface-water subbasin discharge were adjusted so that they accounted for 25 percent of the total precalibration objective function. The net surface-water subbasin discharge observations were assigned a relatively large weight so that they could contribute substantially to the composite objective function. Without such weighting, the large number of surface-water stage and groundwater level

**Table 8.** Groundwater monitoring well locations, data source, number of daily observations, and model-fit statistics.

[UTM, Universal Transverse Mercator; NAD 83, North American Datum of 1983; --, data not available; %, percent]

Well name	Well number	Basin	x-coordinate		y-coordinate	Model layer	Model row	Model column	Calibration period (1997–2004)			Verification period (2005–10)		
			UTM 17N NAD 83 meters	UTM 17N NAD 83 meters					Number of weekly observations	Mean error, in feet	Root mean square error, in feet	Number of weekly observations	Mean error, in feet	Root mean square error, in feet
G-3559	1	C-1	550444.317	2847685.455	2841133.632	2	66	22	366	-0.07	0.22	274	0.17	0.27
G-1487	2	C-1	550519.990	2841210.932	2842582.673	1	79	22	366	-0.03	0.28	274	0.31	0.43
G-3575	3	C-1	550546.575	2842791.586	2840111.66	1	75	22	364	-0.41	0.53	274	-0.04	0.35
G-3557	4	C-1	550577.983	2841133.632	2832669.511	2	79	22	361	0.04	0.26	274	0.40	0.48
G-3551	5	C-1	550617.048	2842582.673	2839647.598	2	76	22	366	0.01	0.28	274	0.34	0.44
G-855	6	C-1	553542.298	2840111.66	2828425.116	1	81	28	358	0.33	0.43	274	0.68	0.72
G-1362	7	C-1	555590.808	2832669.511	2831218.059	1	96	32	356	0.21	0.40	257	0.75	0.84
G-3561	8	C-1	555888.625	2839647.598	2838524.13	1	82	33	356	0.31	0.44	270	0.70	0.75
G-3899	9	C-1	562560.840	2828425.116	2841677.074	1	104	46	--	--	--	82	0.41	0.45
S-182A	10	C-1	563929.934	2831218.059	2837210.462	1	99	49	350	0.13	0.36	258	0.43	0.51
G-3897	11	C-100	558313.017	2838524.13	2833985.237	2	84	38	--	--	--	79	0.58	0.63
G-551	12	C-100	560601.751	2841677.074	2839002.026	2	78	42	337	0.57	1.15	267	1.70	1.99
G-553	13	C-100	566413.373	2837210.462	2819692.546	2	87	54	358	0.18	0.45	274	0.55	0.61
G-860	14	C-100	567982.942	2833985.237	2825172.253	1	93	57	364	0.31	0.46	263	0.57	0.63
G-580A	15	C-100	569994.416	2839002.026	2817668.606	1	83	61	366	0.41	0.55	267	0.64	0.69
G-3627	16	C-102	549877.516	2832443.846	2826000.833	1	96	21	366	0.48	0.62	274	1.05	1.19
G-757A	17	C-102	552352.239	2830844.512	2820756.563	1	99	26	361	0.25	0.45	274	0.86	1.01
G-3549	18	C-102	565420.217	2819692.546	2818866.732	1	122	52	337	-0.01	0.20	269	0.07	0.25
G-1363	19	C-103	549991.245	2825172.253	2819425.718	1	111	21	364	0.36	0.53	269	0.94	1.14
S-196A	20	C-103	550389.710	2821337.2	2807704.621	1	118	22	366	0.06	0.39	274	0.47	0.71
F-358	21	C-103	552152.613	2817668.606	2810168.431	1	126	25	343	0.22	0.41	262	0.44	0.60
G-614	22	C-103	555705.978	2826000.833	2813662.411	1	109	32	353	0.38	0.52	246	0.83	0.95
G-1486	23	C-103	556576.516	2820756.563	281384.329	1	119	34	347	0.21	0.35	264	0.51	0.61
G-3550	24	C-103	564499.507	2818866.732	2813418.855	1	123	50	331	0.25	0.33	251	0.36	0.42
G-789	25	C-111	544680.226	2819425.718	2813418.855	1	122	10	366	0.48	0.62	271	0.94	1.14
G-3620	26	C-111	546124.837	2807704.621	281384.329	1	146	13	366	0.09	0.31	274	0.24	0.41
G-613	27	C-111	547851.344	2810168.431	2813418.855	2	141	17	362	-0.01	0.29	267	0.14	0.35
G-864A	28	C-111	549425.370	2813662.411	2813418.855	1	134	20	359	0.20	0.44	274	0.40	0.56
G-3901	29	C-111	550107.295	2811384.329	2813418.855	2	138	21	--	--	--	80	0.67	0.73
G-864	30	C-111	550107.798	2813418.855	2813418.855	1	134	21	363	0.04	0.39	266	0.46	0.64

**Table 8.** Groundwater monitoring well locations, data source, number of daily observations, and model-fit statistics.—Continued

[UTM, Universal Transverse Mercator; NAD 83, North American Datum of 1983; --, data not available; %, percent]

Well name	Well number	Basin	x-coordinate		y-coordinate		Model layer	Model row	Model column	Calibration period (1997–2004)			Verification period (2005–10)		
			UTM 17N NAD 83 meters	UTM 17N NAD 83 meters	Number of weekly observations	Mean error, in feet				Root mean square error, in feet	Number of weekly observations	Mean error, in feet	Root mean square error, in feet		
G-3355	31	C-111	550201.255	2808592.83	1	144	21	366	-0.26	0.45	266	-0.42	0.63		
G-3621	32	C-111	551002.333	2805132.189	1	151	23	366	-0.01	0.37	264	0.08	0.41		
G-3354	33	C-111	552619.921	2799573.819	1	162	26	340	0.04	0.40	152	0.03	0.42		
G-3558	34	C-2	552220.963	2845562.369	2	70	25	363	-0.10	0.36	260	0.18	0.32		
G-3552	35	C-2	552308.581	2841930.931	2	77	26	357	0.13	0.34	272	0.49	0.55		
G-3898	36	C-2	552795.249	2842345.688	2	76	27	--	--	--	81	0.49	0.55		
G-3553	37	C-2	552908.902	2842360.907	2	76	27	366	0.09	0.32	274	0.42	0.49		
G-3556	38	C-2	553073.614	2842989.114	2	75	27	360	0.18	0.37	272	0.49	0.54		
G-3560	39	C-2	553179.386	2840937.701	2	79	27	356	0.28	0.41	255	0.63	0.67		
G-3554	40	C-2	553940.096	2842371.215	2	76	29	339	-0.21	0.36	269	0.16	0.25		
G-3555	41	C-2	554516.696	2841096.941	2	79	30	349	0.34	0.44	266	0.71	0.74		
G-3473	42	C-2	555833.552	2844139.742	1	73	33	347	0.21	0.41	87	0.46	0.50		
G-3439	43	C-2	556805.182	2846939.101	1	67	35	329	0.05	0.45	210	0.45	0.51		
G-3565	44	C-2	559672.442	2843167.918	1	75	40	357	-0.01	0.41	269	0.41	0.46		
G-3572	45	C-2	560085.694	2847295.057	2	66	41	355	0.13	0.42	274	0.48	0.52		
G-3074	46	C-2	564149.568	2842516.667	3	76	49	358	0.26	0.76	271	1.15	1.39		
G-3563	47	C-2	565846.728	2845756.636	1	69	53	342	0.01	0.56	264	0.34	0.57		
G-1074B	48	C-2	566559.103	2843176.106	3	75	54	359	0.27	1.11	220	0.55	1.24		
G-3570	49	C-3	571219.112	2849377.615	1	62	63	360	0.12	0.58	268	0.29	0.44		
F-319	50	C-3	571445.226	2843260.999	1	74	64	354	0.50	0.58	269	0.60	0.64		
F-179	51	C-3	575581.565	2847732.288	1	66	72	359	0.67	0.76	263	0.66	0.71		
G-1488	52	C-4	551886.652	2855689.276	1	50	25	356	-0.22	0.34	274	-0.06	0.27		
G-975	53	C-4	554461.913	2861399.405	2	38	30	364	0.02	0.44	272	0.29	0.49		
G-3818	54	C-4	554996.248	2858473.611	2	44	31	--	--	--	265	0.34	0.54		
G-3761	55	C-4	556767.562	2858275.014	2	44	35	145	0.26	0.66	272	0.70	0.96		
G-976	56	C-4	557592.796	2856143.824	1	49	36	355	0.09	0.71	--	--	--		
G-3676	57	C-4	557762.517	2852292.877	2	56	37	277	0.13	0.54	268	0.56	0.70		
G-3253	58	C-4	558501.982	2858248.764	3	45	38	319	0.31	1.58	263	1.54	2.22		
G-3259A	59	C-4	559860.731	2858193.342	2	45	41	352	-0.04	1.01	274	0.78	1.21		
G-3568	60	C-4	563925.704	2851755.236	1	57	49	357	0.61	0.70	219	0.63	0.69		

**Table 8.** Groundwater monitoring well locations, data source, number of daily observations, and model-fit statistics.—Continued

[UTM, Universal Transverse Mercator; NAD 83, North American Datum of 1983; --, data not available; %, percent]

Well name	Well number	Basin	x-coordinate		y-coordinate		Model layer	Model row	Model column	Calibration period (1997–2004)			Verification period (2005–10)		
			UTM 17N NAD 83 meters	UTM 17N NAD 83 meters	Number of weekly observations	Mean error, in feet				Root mean square error, in feet	Number of weekly observations	Mean error, in feet	Root mean square error, in feet		
G-3328	61	C-4	572978.965	2853236.037	1	55	67	246	0.46	0.57	--	--	--		
G-972	62	C-6	555682.823	2866655.8	2	28	32	--	--	--	--	--	--		
G-3567	63	C-6	556508.743	2864737.225	2	32	34	350	-0.00	0.56	267	0.65	0.78		
G-3264A	64	C-6	563067.814	2858291.351	2	44	47	308	0.52	0.71	--	--	--		
G-3264AR	65	C-6	563080.905	2858343.728	2	44	47	--	--	--	193	1.14	1.18		
G-973	66	C-6	564577.494	2861405.793	1	38	50	358	-0.13	0.66	250	0.35	0.58		
G-3566	67	C-6	567142.995	2857154.8	2	47	55	337	0.49	0.66	225	0.95	1.01		
G-3329	68	C-6	569802.261	2853557.253	1	54	61	361	0.35	0.51	274	0.49	0.59		
G-3	69	C-6	569966.173	2857135.647	1	47	61	334	0.46	0.75	274	0.93	1.04		
G-3465	70	C-6	570417.575	2854458.534	1	52	62	364	0.41	0.69	272	0.78	0.98		
S-19	71	C-6	570454.604	2854824.819	3	51	62	362	-1.00	1.35	268	-0.15	0.84		
G-3466	72	C-6	571401.393	2854820.681	1	51	64	330	0.20	0.53	256	0.58	0.76		
G-1368A	73	C-6	571524.833	2857217.847	1	47	64	366	0.21	1.05	225	1.13	1.32		
S-68	74	C-6	571547.919	2855529.041	2	50	64	361	0.14	0.52	274	0.60	0.75		
G-3327	75	C-6	572526.269	2854525.53	1	52	66	350	0.12	0.42	274	0.50	0.66		
G-3467	76	C-6	572895.700	2855007.284	1	51	67	364	0.26	0.47	274	0.63	0.73		
F-239	77	C-6	572996.383	2857693.836	1	46	67	355	0.87	0.97	255	1.21	1.27		
G-3564	78	C-6	575963.040	2856196.704	1	49	73	350	0.71	0.83	233	1.01	1.10		
G-1166R	79	C-7	566900.591	2864309.193	1	32	55	91	0.27	0.43	272	0.38	0.49		
G-1166	80	C-7	566962.635	2864309.029	1	32	55	198	0.03	0.38	--	--	--		
G-3562	81	C-7	574598.225	2859723.7	1	42	70	356	-0.85	0.97	268	-0.33	0.51		
F-45	82	C-7	579762.920	2856970.413	3	47	81	363	0.62	0.71	268	0.76	0.81		
S-18	83	C-8	575987.819	2867557.346	1	26	73	321	0.26	0.40	237	0.57	0.62		
G-852	84	C-8	582618.591	2866089.997	1	29	86	366	0.68	0.74	272	0.73	0.77		
G-1636	85	C-9	562223.949	2872343.218	1	16	45	360	0.02	0.31	274	0.09	0.27		
G-3571	86	C-9	570000.557	2868973.793	2	23	61	352	0.09	0.33	271	0.32	0.40		
G-1225	87	C-9	576850.702	2876975.704	1	7	75	354	0.32	0.37	272	0.33	0.36		
G-1473	88	C-9	584621.78	2874747.155	3	12	90	364	0.61	0.67	15	0.43	0.44		
MRSHOPB1	89	ENP	541831.129	2825218.015	1	111	5	--	--	--	206	0.15	0.48		
G-1502	90	ENP	541865.786	2833193.88	2	95	5	353	-0.41	0.50	274	-0.09	0.42		

**Table 8.** Groundwater monitoring well locations, data source, number of daily observations, and model-fit statistics.—Continued

[UTM, Universal Transverse Mercator; NAD 83, North American Datum of 1983; --, data not available; %, percent]

Well name	Well number	Basin	x-coordinate		y-coordinate		Model layer	Model row	Model column	Calibration period (1997–2004)			Verification period (2005–10)		
			UTM 17N NAD 83 meters	UTM 17N NAD 83 meters	Number of weekly observations	Mean error, in feet				Root mean square error, in feet	Number of weekly observations	Mean error, in feet	Root mean square error, in feet		
MRSOPC1	91	ENP	541905.435	2821991.423	1	117	5	--	--	202	0.22	0.49			
G-618	92	ENP	542401.712	2849272.232	2	62	6	356	-0.29	0.36	272	-0.28	0.34		
G-3273	93	ENP	542597.746	2834862.879	1	91	6	--	--	58	1.50	1.50			
G-3622	94	ENP	543368.355	2820190.423	1	121	8	363	0.20	0.42	256	0.54	0.67		
G-3353	95	ENP	543408.036	2797040.258	1	167	8	353	0.02	0.14	172	-0.01	0.11		
G-3437	96	ENP	543483.145	2827804.153	1	105	8	366	-0.24	0.44	260	0.10	0.48		
G-1251	97	ENP	543705.744	2800572.455	1	160	8	310	0.20	0.28	274	0.20	0.24		
G-3336	98	ENP	543710.921	2802424.235	1	156	8	69	0.27	0.34	255	0.27	0.32		
G-3619	99	ENP	543724.064	2806982.957	1	147	8	366	0.04	0.34	274	0.06	0.26		
ANGEL	100	ENP	546014.846	2833958.778	1	93	13	--	--	58	0.40	0.44			
G-3272	101	ENP	546272.901	2838658.819	1	84	14	366	-0.34	0.39	274	-0.13	0.29		
G-3628	102	ENP	546730.334	2830818.37	1	99	14	366	0.28	0.48	274	0.83	0.99		
G-3576	103	ENP	548717.224	2847626.686	1	66	18	364	-0.12	0.17	270	-0.08	0.16		
G-3578	104	ENP	548870.736	2842943.415	1	75	19	364	-0.34	0.37	274	-0.19	0.28		
G-596	105	ENP	548989.770	2835685.904	2	90	19	366	-0.06	0.32	274	0.40	0.55		
G-3626	106	ENP	549067.970	2833536.874	1	94	19	366	0.25	0.45	274	0.80	0.95		
G-3577	107	ENP	550108.810	2842845.296	1	75	21	366	-0.42	0.53	242	-0.09	0.42		
G-3574	108	ENP	550357.929	2847691.279	1	66	22	366	-0.36	0.43	274	-0.07	0.26		
G-3900	109	FLORIDA CITY	555609.857	2815356.656	2	130	32	--	--	81	0.23	0.31			
G-1183	110	HOME- STEAD	560850.612	2819214.17	1	123	43	354	0.37	0.46	274	0.59	0.64		
G-3356	111	MODEL LAND	557551.625	2811464.629	1	138	36	364	0.06	0.43	274	0.17	0.39		
G-968	112	WCA-3B	555362.520	2868663.884	1	24	32	363	-0.30	0.60	265	-0.13	0.50		
Global average								0.14	0.51	0.46	0.65				
Percentage of observations satisfying calibration criteria					89%			94%	58%	85%					

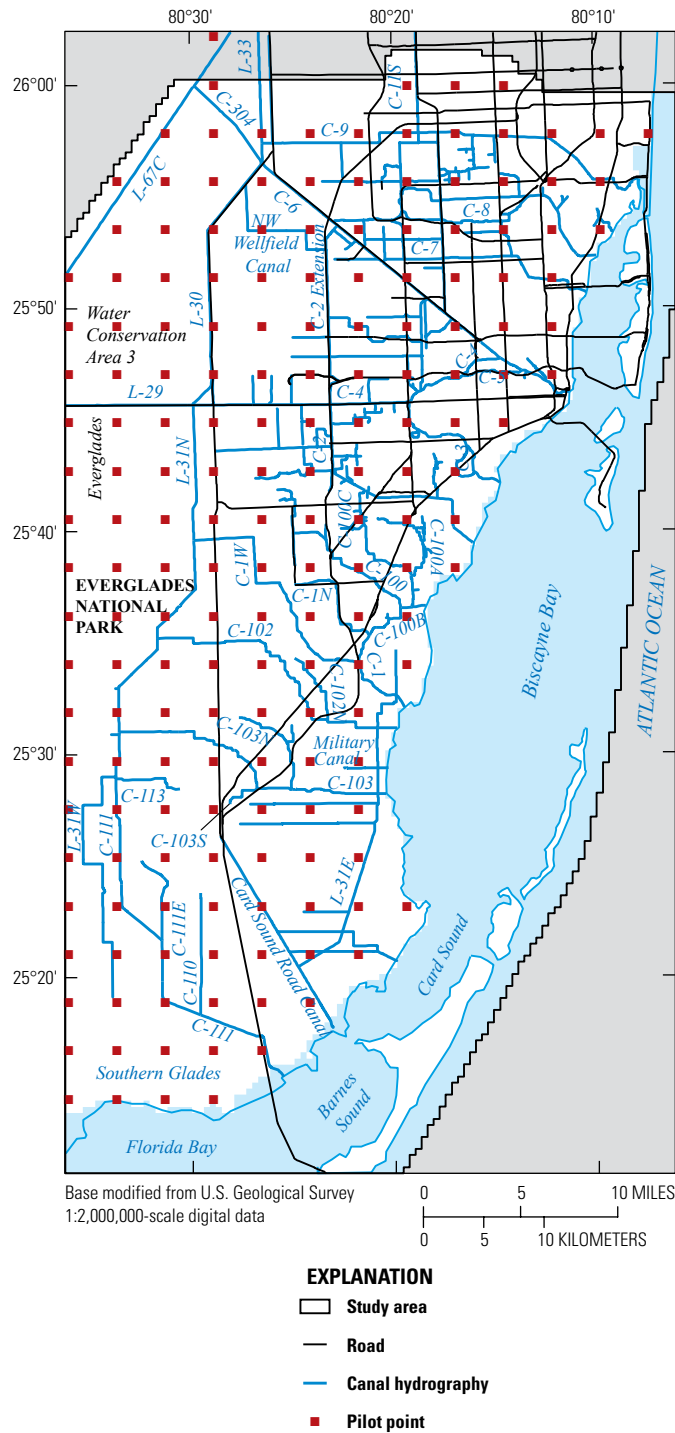


**Figure 29.** Distribution of pilot points used to condition select groundwater properties adjusted during model calibration.

observations would reduce the contribution of the monthly net surface-water subbasin discharge observations to the overall composite objective function and minimize their influence on parameter upgrades during the inversion process.

### Calibration and Error-Based Calibration Criteria

The model was calibrated by using PEST, version 12.1 (Doherty, 2010). PEST uses a variant of the Gauss-Newton algorithm with the Marquardt-Levenburg trust region (Marquardt, 1963). The PEST algorithm seeks the minimum of a weighted L-2 norm objective function by applying a multi-dimensional form of Newton’s method by using first-order approximation to the Hessian matrix (Oliver and others, 2008). A form of the weighted L-2 norm objective function minimized by PEST during the calibration process using the Gauss-Newton algorithm with the Marquardt-Levenburg trust region algorithm is

$$\Phi = \sum_{i=1}^n (w_i r_i)^2 = \sum_{i=1}^n (w_i [s_i - o_i])^2, \tag{6}$$

where

- $\Phi$  is the weighted L-2 norm objective function,
- $n$  is the number of observations,
- $w_i$  is the weight of observation  $i$ ,
- $r_i$  is the residual of observation  $i$ ,
- $s_i$  is the simulated value of observation  $i$ ,
- $o_i$  is the measured value of observation  $i$ .

Minimization of the objective function using the Gauss-Newton algorithm with the Marquardt-Levenburg trust region algorithm can be time consuming because it requires repeated formulation of a Jacobian matrix, calculated using finite-difference first derivatives. The subspace dimensionality-reduction approach, known as SVD-Assist (Tonkin and Doherty, 2005), was used to further reduce the computational burden related to formulating the Jacobian matrix and subsequent solution of the linear system of equations.

The model fit was further evaluated by comparing the simulated data to the measured daily time-series data at individual surface-water stage and groundwater monitoring locations and calculating error statistics for both individual stations and the entire model domain. Two error statistics that are commonly used to quantify model calibration error include (1) the mean error (ME), or the average of the differences between the simulated and observed values; and (2) the root mean square error (RMSE), which is equivalent to the uncorrected sample standard deviation and is the square root of the average of the squared differences between simulated and observed values (Anderson and Woessner, 1992). ME is calculated as

$$ME = \frac{\sum_{i=1}^n (s_i - o_i)}{n}. \tag{7}$$

RMSE is calculated as

$$RMSE = \left[ \frac{\sum_{i=1}^n (s_i - o_i)^2}{n} \right]^{1/2} \quad (8)$$

Because surface-water discharge and net canal discharge for surface-water subbasins are typically log-normally distributed, normalized mean error (NME) and normalized root mean square error (NRMSE) statistics are used to evaluate simulated surface-water discharge results. NME and NRMSE allow simulated surface-water discharge for surface-water control structures or surface-water basins having notably different flow rates/volumes to be directly compared. NME is calculated as

$$NME = \frac{ME}{|o_{max} - o_{min}|} \quad (9)$$

where

$o_{max}$  is the maximum observed data value, and  
 $o_{min}$  is the minimum observed data value.

The NME is equivalent to the normalized cumulative flow error and represents the difference between observed and simulated cumulative flow over the period evaluated. NRMSE is calculated as

$$NRMSE = \frac{RMSE}{|o_{max} - o_{min}|} \quad (10)$$

Another commonly used error statistic applied in surface-water models is the modified Nash-Sutcliffe model efficiency coefficient (E1), which is a measure of the percentage of the data variance explained by the model (Nash and Sutcliffe, 1970). The E1 statistic is calculated as

$$E1 = 1 - \frac{\sum_{i=1}^n (s_i - o_i)^2}{\sum_{i=1}^n (o_i - \bar{o})^2} \quad (11)$$

where

$\bar{o}$  is the mean of the observation data.

Model accuracy increases as the E1 statistic approaches 1, with E1 = 1 indicating perfect model predictions. A zero or negative E1 statistic indicates model predictions are as accurate as, or less accurate than, the mean of the observed data, respectively. The modified E1 statistic reduces the effect of squared differences (sum of squares of residuals and the total sum of squares) on the calculated statistic (Legates and McCabe, 1999). In an evaluation of alternative forms of the E statistic, Krause and others (2005) found that the E1 statistic provided a better global statistic of model efficiency.

Combined use of the ME and RMSE statistics for surface-water stage and groundwater level and the NME, NRMSE, and E1 statistics for surface-water discharge and net surface-water subbasin discharge facilitate the assessment of model bias, the average differences between simulated and observed data, and the predictive efficiency of simulated flows.

The surface-water stage gages and surface-water structure gate elevations have an accuracy of ±0.02 ft (South Florida Water Management District, 2011c.). Propagating land-surface elevation and stage-gage measurement errors through the spillway structure equation (eqns. 37 and 43 in Hughes and others, 2012) results in an average accuracy of approximately ±6.32 ft<sup>3</sup>/s for structure discharge. The land-surface elevations at groundwater monitoring locations have an accuracy of ±0.05 ft (B. Irvin, U.S. Geological Survey, oral commun., 2013). On the basis of the accuracy of the observed data used to calibrate the model, it might be expected that the model can be calibrated to a similar level. Model-to-measurement misfits, however, are typically far greater, and far less random, than would be expected on the basis of the accuracy of the observation data used to calibrate the model (Doherty and Welter, 2010). Typically, a large part of model-to-measurement misfit is a result of structural defects in a model. Structural defects are a consequence of the model design and include, but are not limited to (1) spatial and temporal discretization, (2) mathematical simplifications in the numerical code, and (3) simplified representation of hydraulic property heterogeneity.

Recognizing that structural defects limit the ability to calibrate a model to the level of measurement accuracy, previous models of the study area (for example, South Florida Water Management District, 2005; Giddings and others, 2006; Lohmann and others, 2012) have used calibration criteria that exceed measurement accuracy. ME and RMSE calibration criteria used to evaluate surface-water stage and groundwater level model fit at each observation location in this study are summarized in table 9; these criteria are less than 10 percent of the observed data range. NME, NRMSE, and E1 calibration criteria used to evaluate surface-water discharge model fit at each observation location in this study are summarized in table 10. Model fit was considered acceptable if the defined criteria were met at 75 percent of the observation locations.

## Boundary Conditions

Boundary conditions for the model include specified fluxes and head-dependent fluxes. Specified fluxes include rainfall, surface-water runoff, municipal groundwater pumpage, net agricultural water use and irrigation system losses, recreational irrigation, and septic-system return flow. Head-dependent fluxes include evapotranspiration, internal surface-water structure flows, coastal surface-water boundaries, groundwater discharge to the coast, and groundwater recharge and discharge in WCA3 and ENP. The base of the Biscayne aquifer (model layer 3) is defined as a no-flow boundary.

## Specified Flux Boundaries

Rainfall, net agricultural water use, recreational water use, and septic system return flow to the water table were combined into a single daily specified-flux value, which was simulated using the MODFLOW General Flux Boundary (GFB) Package and applied to the uppermost model layer. The GFB Package is described further in appendix 1. Surface-water runoff was simulated using the direct surface-water runoff option in the SWR1 Process. Municipal groundwater use was simulated using the MODFLOW Well (WEL) Package. The methodology used to develop individual specified flux boundary components is described next in detail.

### Rainfall

Area-weighted daily NEXRAD rainfall depths were calculated for each pervious and unconnected impervious model grid cell and bias-corrected to reduce discrepancies between NEXRAD rainfall depths and rainfall gage data. Bias-corrected daily rainfall data applied to the model were calculated using

$$\hat{R}_{i,j,t} = (1 - DCIA_{i,j,t}) \times f_{NEXRAD} \times RAIN_{i,j,t}, \quad (12)$$

where

- $\hat{R}_{i,j,t}$  is the daily bias-corrected rainfall applied for each model cell [ $LT^{-1}$ ],
- $DCIA_{i,j,t}$  is the fraction of directly connected impervious area in each model cell [unitless],
- $f_{NEXRAD}$  is the NEXRAD bias-correction factor [unitless], and
- $RAIN_{i,j,t}$  is the area-weighted daily NEXRAD rainfall rate [ $LT^{-1}$ ].

A  $f_{NEXRAD}$  value of 1.05 was applied in the model (Skinner and others, 2009).  $\hat{R}_{i,j,t}$  was specified to be zero in offshore areas of the model.  $\hat{R}_{i,j,t}$  is defined as a daily specified flux in the GFB Package.

The mean annual  $\hat{R}$  for the period from 1996 through 2010, as well as rainfall during the driest and the wettest years in the simulation period, are shown in figure 30. Spatially, average annual  $\hat{R}$  ranged from 41.21 to 69.18 in.; the highest mean annual rainfall occurred west of Miami International Airport.

Daily bias-corrected rainfall for each model cell ( $\hat{R}_{i,j,t}$ ) was also applied to SWR1 reaches to simulate direct rainfall input to the surface-water system. The maximum surface area of each SWR1 reach was used to calculate daily volumetric rainfall rates.

### Net Agricultural Water Use and Irrigation System Losses

The net agricultural water use and irrigation systems losses were calculated and applied in model grid cells

classified as agricultural land-use types (fig. 4). The number and location of model grid cells classified as agricultural land-use types varied throughout the simulation period to reflect temporal changes in land use. The land use for a given year was used until the beginning of the year for the next land-use dataset; for example, the 1995 land-use dataset was used until January 1, 2000, after which the 2000 land-use dataset was used. Additionally, it has been assumed that all surface-water sources used to satisfy agricultural demand ultimately withdraw water locally from surface-water features connected to the Biscayne aquifer, rather than from regional (external) surface-water sources; this assumption can therefore be represented in the form of withdrawals from the Biscayne aquifer.

The daily actual evapotranspiration ( $AET$ ) for each model cell [ $LT^{-1}$ ] in which the majority of land-use types represented are agricultural was calculated using

$$AET_{i,j,t} = f_{a,t} \times Kc_{i,j,t} \times RET_{i,j,t}, \quad (13)$$

where

- $f_{a,t}$  is a coefficient [unitless] used to scale calculated irrigation water-use rates to the estimated annual agricultural self-supplied water withdrawal rate for Miami-Dade County in 1995, 2000, and 2005 (Marella, 1999, 2004, 2009), and
- $RET_{i,j,t}$  is the reference evapotranspiration rate for the cell [ $LT^{-1}$ ].

The daily net irrigation requirement ( $NIR$ ) for each agricultural model cell [ $LT^{-1}$ ] was calculated using

$$NIR_{i,j,t} = AET_{i,j,t} - \hat{R}_{i,j,t}, \quad (14)$$

The supplemental irrigation ( $SIR$ ) that is applied to the landscape and represents agricultural groundwater use [ $LT^{-1}$ ] was calculated using

$$SIR_{i,j,t} = \frac{NIR_{i,j,t}}{E_{AG}}. \quad (15)$$

The net water use in agricultural cells is defined as a daily specified flux in the GFB Package. As a result, the ETS Package is not used in agricultural cells and the net agricultural water use ( $AWU$ ) is specified to be

$$AWU_{i,j,t} = SIR_{i,j,t} + RAIN_{i,j,t}. \quad (16)$$

The net agricultural use specified in the model represents the combination of agricultural water demand satisfied by daily rainfall and the supplemental groundwater required to satisfy the remaining agricultural use and overcome irrigation system

**Table 9.** Calibration criteria applied to surface-water stage and groundwater level observations.

Observation data type	Mean error, in feet	Root mean square error, in feet	Observed data range, in feet	Minimum observed value, in feet	Maximum observed value, in feet
Surface-water stage	±0.5	≤ 1.0	10.81	-2.56	8.25
Groundwater level	±0.5	≤ 1.0	21.33	-11.59	9.74

**Table 10.** Calibration criteria applied to surface-water discharge and net surface-water subbasin canal discharge observations.

Observation data type	Normalized mean error	Normalized root mean square error	Nash-Sutcliffe model efficiency
Surface-water discharge	≤ ±0.10	≤ 0.20	≥ 0.5
Net surface-water discharge	≤ ±0.10	≤ 0.20	≥ 0.5

inefficiencies. Agricultural irrigation water in the study area is withdrawn from shallow uncased wells and conveyed using truck-mounted pump and spray irrigation systems (Renken and others, 2005a). As a result, the location of irrigation withdrawal wells is unknown and all supplemental groundwater is assumed to be extracted from the same model cell with a calculated net irrigation requirement.

The spatial distribution of estimated average annual agricultural demand in the study area from 1996 through 2010 ranged from 1.65 to 15.5 in. within areas having agricultural land-use types (fig. 31A). The estimated average sum of annual net agricultural water use and irrigation system losses in the study area from 1996 through 2010 ranged from 2.01 to 19.1 in. within areas having agricultural land-use types (fig. 31B).

### Recreational Irrigation Water Use

Recreational irrigation water use was applied to model cells classified as low- and medium-density land-use types (fig. 4). Recreational irrigation water use was not applied to model cells classified as high-density land use because it was assumed that green space is minimal in these cells and irrigation is negligible. The model grid cells classified as low- and medium-density land-use types were varied throughout the simulation period to reflect temporal changes in land use. The land use for a given year was used until the beginning of the year for the next land-use dataset; for example, the 1995 land-use dataset was used until January 1, 2000, after which the dataset for 2000 was used.

The AET for each model cell [LT<sup>-1</sup>] in which the majority of land-use types represented are low- or medium-density urban area was calculated using

$$AET_{i,j,t} = f_{REC,t} \times Kc_{i,j,t} \times RET_{i,j,t}, \tag{17}$$

where  $f_{REC,t}$  is a coefficient [unitless] used to scale calculated recreational irrigation water use rates to the annual recreational irrigation water withdrawal rates for Miami-Dade County in 1995, 2000, and 2005 (Marella, 1999, 2004, 2009). The daily recreational NIR for each low- and medium-density model cell [LT<sup>-1</sup>] was calculated using equation 14 and was assumed to be delivered from an external source, namely a municipal water supply. Irrigation efficiencies were not considered because the source for recreational irrigation water was assumed to be external. Daily recreational water use ( $RWU$ ) was specified to be equal to the daily net recreational irrigation requirement and is defined as a daily specified flux in the GFB Package. The recreational water use specified in the model represents the supplemental, externally sourced water not satisfied by rainfall and required to satisfy the net recreational irrigation water demand.

The estimated average annual recreational demand for the period from 1996 through 2010 ranged from 0.63 to 2.14 in. within areas having agricultural land-use types figure 32A. The average annual recreational irrigation water use in the study area for the period from 1996 through 2010 ranged from 0.20 to 1.22 in. within areas having agricultural land use types (fig. 32B).

### Septic System Return Flow to the Water Table

Estimated septic system return rates for 1990, 2000, and 2010 (fig. 20) were applied to the model as a daily specified flux in the GFB Package. Septic return flow to the water table supplements rainfall and recreational irrigation. The estimated septic return rates for a given year were used until the beginning of the year for the next estimated septic return rate dataset; for example, 1990 estimated septic return rates were used until January 1, 2000, after which estimated septic return rates for 2000 was used.

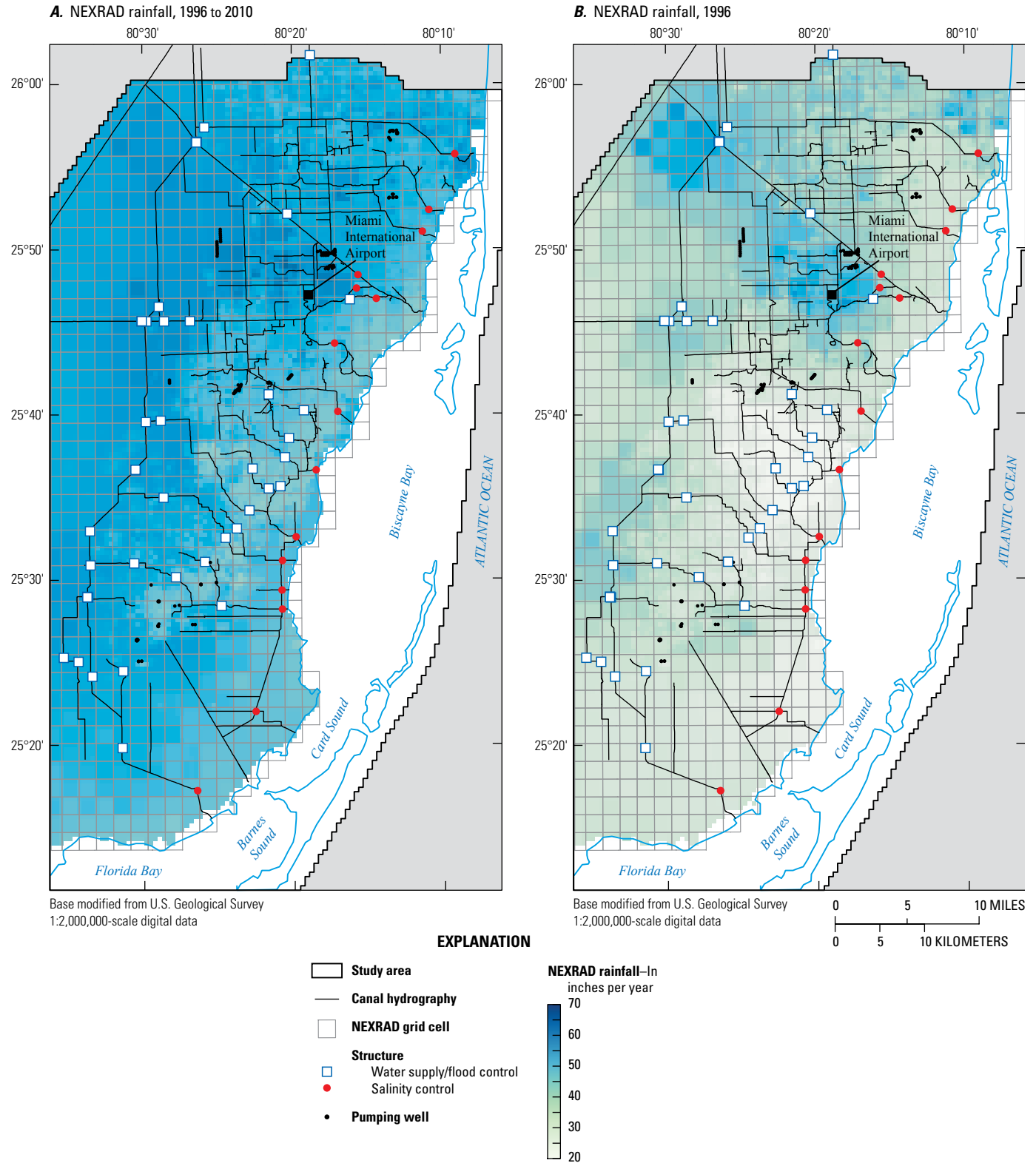


**Figure 30.** Spatial distribution of average annual NEXRAD rainfall for, *A*, the period from 1996 through 2010, *B*, the driest year of the simulation period (1996), and *C*, the wettest year of the simulation period (2005). The 1.24×1.24-mile grid used to calculate NEXRAD rainfall data is also shown.

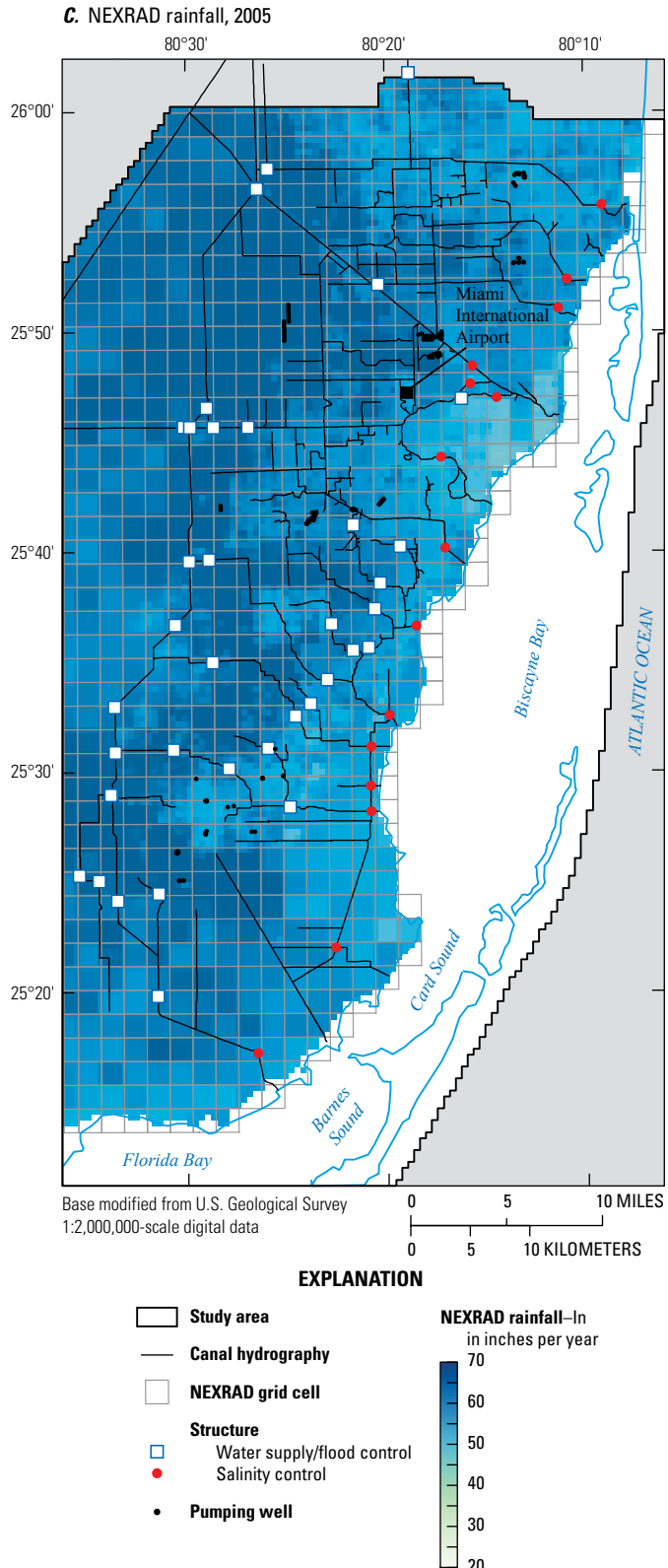


**Figure 30.** Spatial distribution of average annual NEXRAD rainfall for, *A*, the period from 1996 through 2010, *B*, the driest year of the simulation period (1996), and *C*, the wettest year of the simulation period (2005). The 1.24×1.24-mile grid used to calculate NEXRAD rainfall data is also shown.—Continued

### Surface-Water Runoff

Surface-water runoff from each grid cell,  $Ro_{i,j,t}$ , was calculated using the land-use-based DCIA for 1995, 2000, 2004, and 2008 (fig. 6) and the bias-corrected daily NEXRAD rainfall.  $Ro_{i,j,t}$  for each model cell was calculated using

$$Ro_{i,j,t} = DCIA_{i,j,t} \times f_{NEXRAD} \times RAIN_{i,j,t}. \quad (18)$$

The DCIA for model grid cells were varied throughout the simulation period to reflect temporal changes in land-use-based DCIA values. The DCIA for a given year was used until the beginning of the year for the next land-use-based DCIA dataset; for example, the 1995 land-use dataset was used until January 1, 2000, after which the dataset for 2000 was used. The calculated daily surface-water runoff for each cell having DCIA values greater than zero was applied to the closest SWR1 Process reach in the same surface-water basin. Surface-water runoff was applied to the closest SWR1 Process reach because maps of stormwater collection systems were not readily available, and it is reasonable to assume that stormwater collection systems would be connected to the closest primary or secondary surface-water feature.  $Ro_{i,j,t}$  was not calculated for offshore cells.

### Municipal Groundwater Use

Municipal pumping rates for the period from January 1, 1996, through December 31, 2010, were acquired from MDWASD and the SFWMD. Data were obtained for a large number of public-supply wells but were only used in the analysis if a given well had an average pumping rate of at least 0.5 Mgal/d or was part of a group of wells within a larger well field with an average pumping rate greater than 0.5 Mgal/d. Excluded wells account for less than 0.14 percent (1.1 Mgal/d) of the total maximum municipal groundwater use in the study area. A total of 139 wells in 20 well fields are included in the model using the MODFLOW WEL Package. All municipal groundwater pumpage is withdrawn from model layer 3, which represents the primary Biscayne aquifer production zone in the study area.

Pumping rates were obtained as daily or monthly values for either individual wells or as monthly well-field totals for combined well fields. Daily values for individual wells were directly applied in the model. Monthly well-field totals were divided by the number of days per month to obtain average daily pumping rates for combined well fields. Pumping rates for individual wells in combined well fields were divided by the total number of active wells in the well field. The calculation of total monthly well-field pumping rates averages out daily pumping variability that probably occurred, except when pumping rates were relatively constant during a specific month.

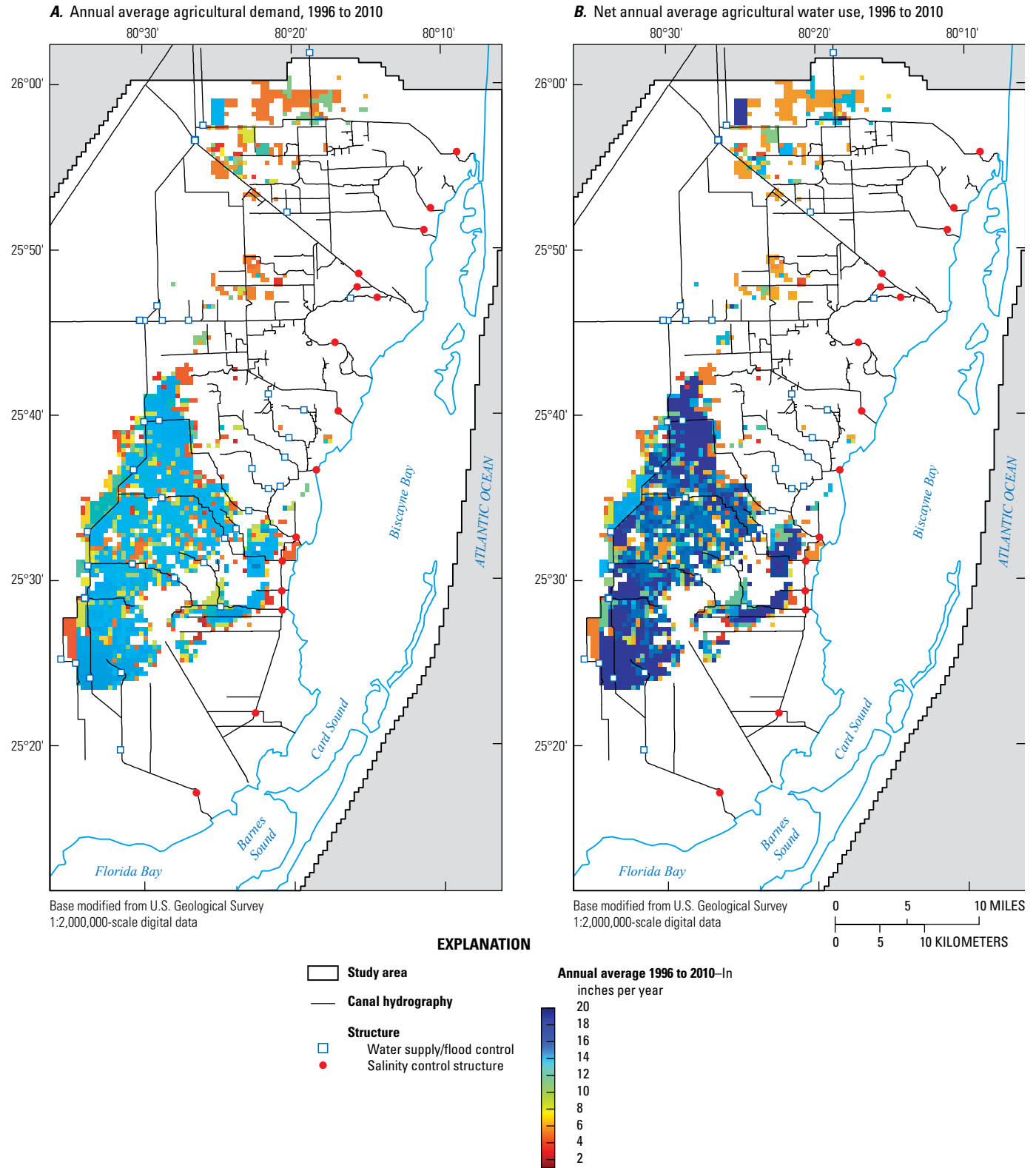


**Figure 31.** Spatial distribution of estimated average annual, *A*, agricultural demand and, *B*, net agricultural water use and irrigation system losses for the period from 1996 through 2010.

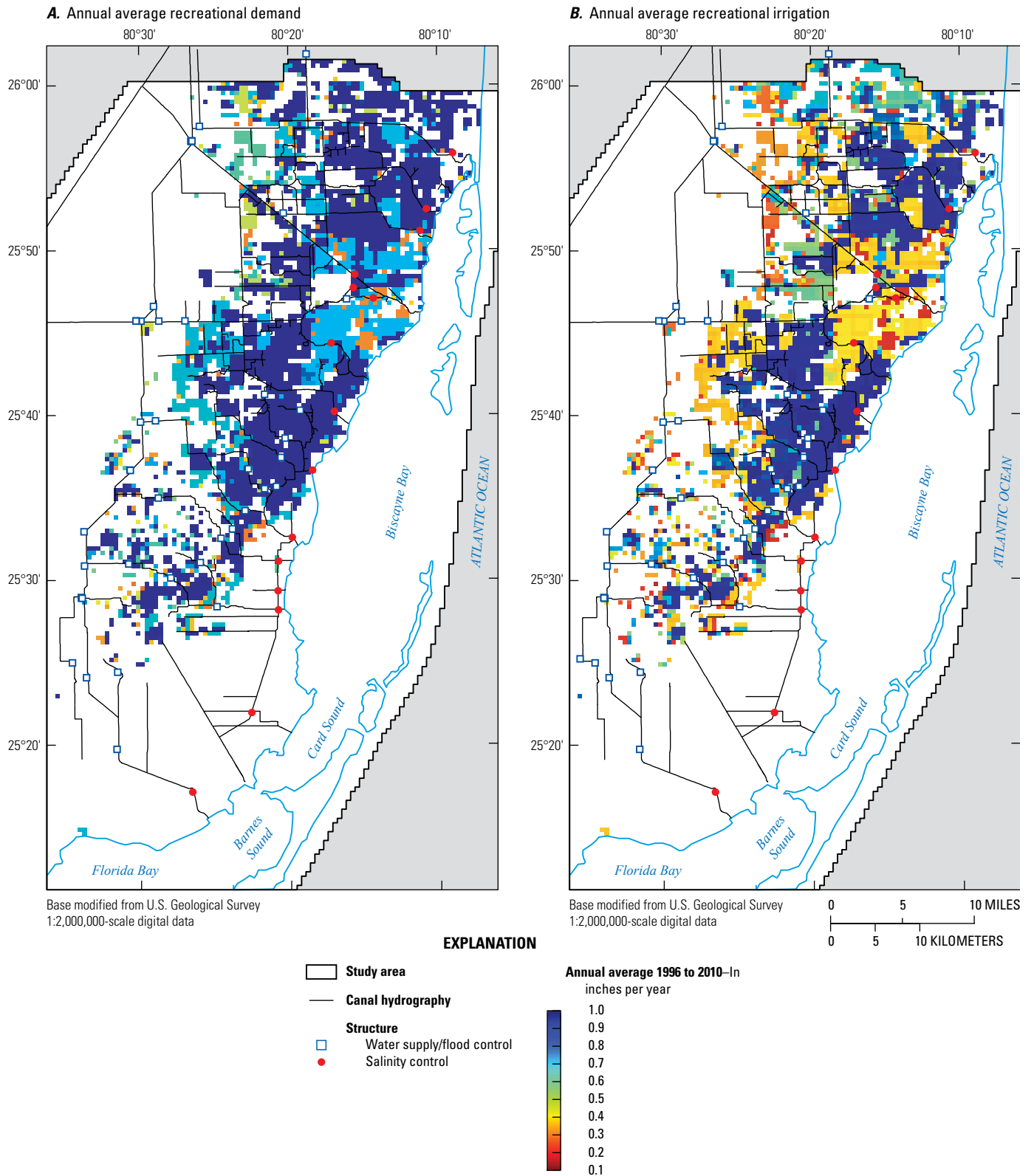


**Figure 32.** Spatial distribution of estimated average annual, *A*, recreational demand and, *B*, recreational irrigation for the period from 1996 through 2010.

## Head-Dependent Boundaries

### Evapotranspiration

Area-weighted daily GOES-based reference evapotranspiration rates were calculated for each onshore, nonagricultural model cell. The spatial distribution of average annual reference and maximum evapotranspiration rates for all onshore model cells, including agricultural cells, for the period from 1996 through 2010 are shown in figure 33. Maximum evapotranspiration rates for dry soil conditions, when the water table is below the maximum depth of soil evaporation, were calculated using the product of area-weighted reference evapotranspiration rates and land-use-based crop coefficients (table 3). The crop coefficients for urban land-use types were further refined during model calibration from those shown in table 3; calibrated monthly crop coefficients for urban land-use types ranged from a low of 0.15 in January during the dry season to a high of 2.05 at the end of the wet season in September and October (table 11). The crop coefficients represent effective parameters and values greater than one at the end of the wet season compensate for processes not explicitly included in the model (for example, ponding, collection, and evapotranspiration of water in areas not directly connected to the surface-water system). Spatially, average annual maximum evapotranspiration rates in the study area range from 9.95 to 58.10 inches per year (in/yr; fig. 33B).

The ETS Package was used to represent evapotranspiration in nonagricultural areas of the model. The approach used to calculate evapotranspiration as a function of the depth to the water table is shown in figure 34. Where the elevation of the water table is greater than or equal to land surface, open-water evaporation occurs; the rate of such evaporation is equal to 1.05 times the daily reference evapotranspiration rate (Allen and others, 1998). Where the depth to the water table is less than the maximum depth of soil evaporation (assumed to be the average capillary potential for coarse sand), evapotranspiration varies linearly from open-water evaporation at land surface to  $Kc \times RET$  at approximately 3.5 in. (9 cm) below land surface. Evapotranspiration varies linearly from  $Kc \times RET$  when the depth to the water table exceeds the

maximum depth of soil evaporation to  $0.9 \times Kc \times RET$  at the maximum depth of dense roots in the soil. Between the base of dense roots in the soil to the maximum root depth, evapotranspiration varies from  $0.9 \times Kc \times RET$  to 0.0, respectively. No evapotranspiration occurs when the water table is below the maximum root depth.

For soil in which (1) the capillary potential is 0.3 ft (3.5 in.), (2) the dense root zone extends to a depth of 1.0 ft, and (3) the extinction depth is 3.0 ft, the calculated evapotranspiration rate would be 95.7 percent of  $Kc \times RET$  if the water table (hydraulic head) were 0.6 ft below land surface. Similarly, for the same soil and cases in which the water table is 0.15, 0.75, 1.0, 1.5, or 2.0 ft below land surface, the calculated evapotranspiration rate would be 102.5, 93.6, 90.0, 67.5, or 45.0 percent of  $Kc \times RET$ , respectively.

The maximum depth of soil evaporation was specified to be 0.3 ft (3.5 in.). The initial maximum depth of the dense root zone and the extinction depth were set to be 1 and 3 ft below land surface, respectively, in nonagricultural onshore model cells. The final calibrated maximum depth of the dense roots and evapotranspiration extinction depth below land surface in nonagricultural onshore model cells are shown in figure 35.

Daily surface-water evaporation rates were calculated as the product of  $RET$  and the 1.05 reference evapotranspiration to open-water evaporation scaling factor. Daily surface-water evaporation rates for each cell were applied to SWR1 reaches to simulate direct evaporation from the surface-water system. The simulated surface area of each SWR1 reach was used to calculate daily volumetric evaporation rates.

### Internal Surface-Water Structure Flows

A total of 61 primary and 12 secondary canal surface-water control structures were represented in the surface-water component of the model and include fixed-crest weirs, operable gates, and pumps. These structures represent internal stage-dependent boundary conditions for the surface-water component of the model that control surface-water flow between reach groups separated by one or more surface-water control structures (fig. 36). The physical dimensions and hydraulic characteristics of the surface-water control structures are summarized in table 12.

**Table 11.** Calibrated crop coefficients for urban land-use types.

Basic land use code	Description	Month											
		1	2	3	4	5	6	7	8	9	10	11	12
1	Low density urban	0.15	0.17	0.40	0.31	0.31	0.52	0.79	0.66	1.55	2.05	0.40	0.35
3	Medium density urban	0.15	0.17	0.40	0.31	0.31	0.52	0.79	0.66	1.55	2.05	0.40	0.35
11	High density urban	0.15	0.17	0.40	0.31	0.31	0.52	0.79	0.66	1.55	2.05	0.40	0.35

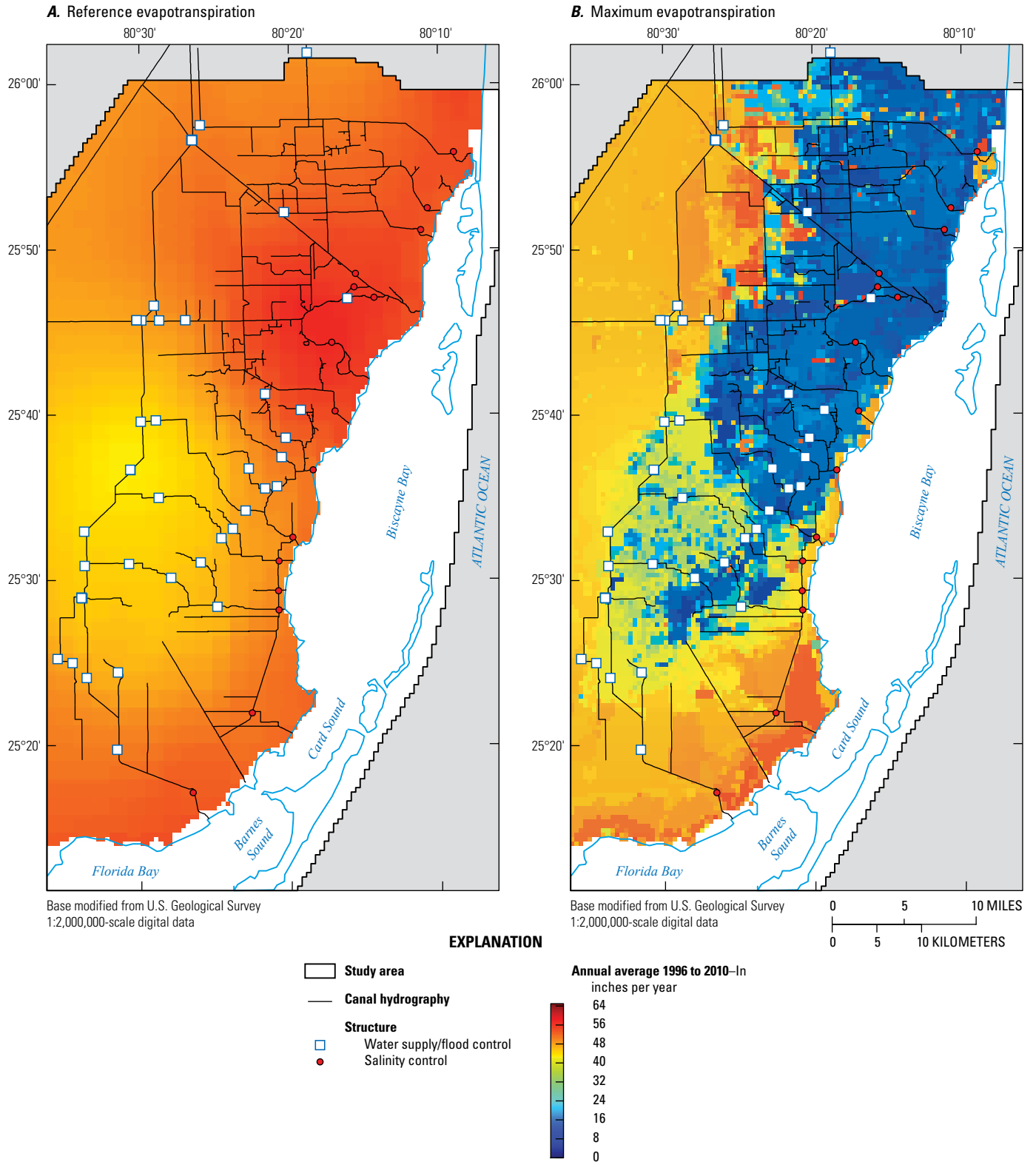


**Figure 33.** Average annual, *A*, reference and, *B*, maximum evapotranspiration for the period from 1996 through 2010. The 1.24×1.24-mile geostationary operational environmental satellite (GOES)-based reference evapotranspiration grid is shown in figure 30.

To maximize the SWR1 Process time-step length, primary canal gated spillways and flashboard weirs (table 12) were operated using effective gate opening data. These data were calculated using the following rearranged form of the fixed-gate spillway equation in Hughes and others (2012):

$$G_{eff} = \frac{|Q_s|}{C_o C_f W_s (2gd_{max})^{1/2}}, \tag{19}$$

where

- $G_{eff}$  is the calculated daily effective gate opening [L],
- $Q_s$  is the calculated average daily structure discharge [ $L^3T^{-1}$ ],
- $C_o$  is the discharge coefficient [unitless],
- $C_f$  is a submergence factor [unitless],
- $W_s$  is the width of the structure [L],
- $g$  is gravitational acceleration [ $LT^{-2}$ ], and
- $d_{max}$  is the maximum height of water above the structure invert elevation [L].

The term  $d_{max}$  is defined as

$$d_{max} = \max(h_{max} - h_s, 0), \tag{20}$$

where

- $h_{max}$  is the maximum observed average daily stage on either the headwater or tailwater side of the structure [L], and
- $h_s$  is the structure invert elevation [L].

The submergence factor is defined as

$$C_f = \left(1 - \frac{d_{min}}{d_{max}}\right)^{1/2}, \tag{21}$$

where

$d_{min}$  is the minimum height of water above the structure invert elevation [L].

The term  $d_{min}$  is defined as

$$d_{min} = \max(h_{min} - h_s, 0), \tag{22}$$

where

$h_{min}$  is the minimum observed average daily stage on either the headwater or tailwater side of the structure [L].

$G_{eff}$  and  $C_f$  are only calculated for days when  $Q_s$  is nonzero; otherwise,  $G_{eff}$  is equal to zero.

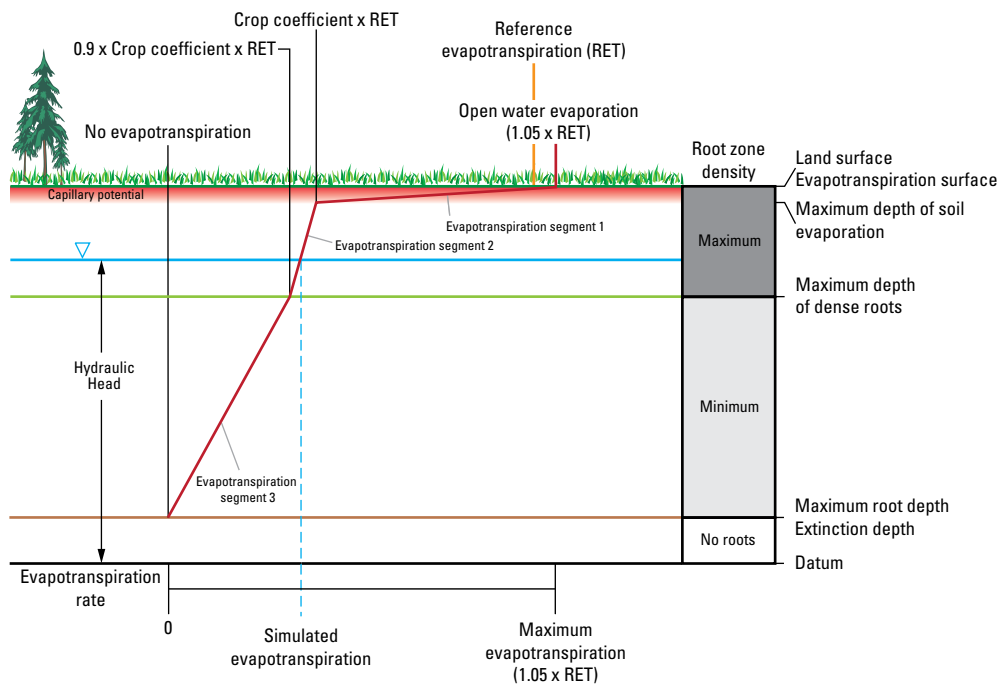


**Figure 34.** Segmented evapotranspiration approach used to represent water-table-dependent evapotranspiration in nonagricultural parts of the study area.

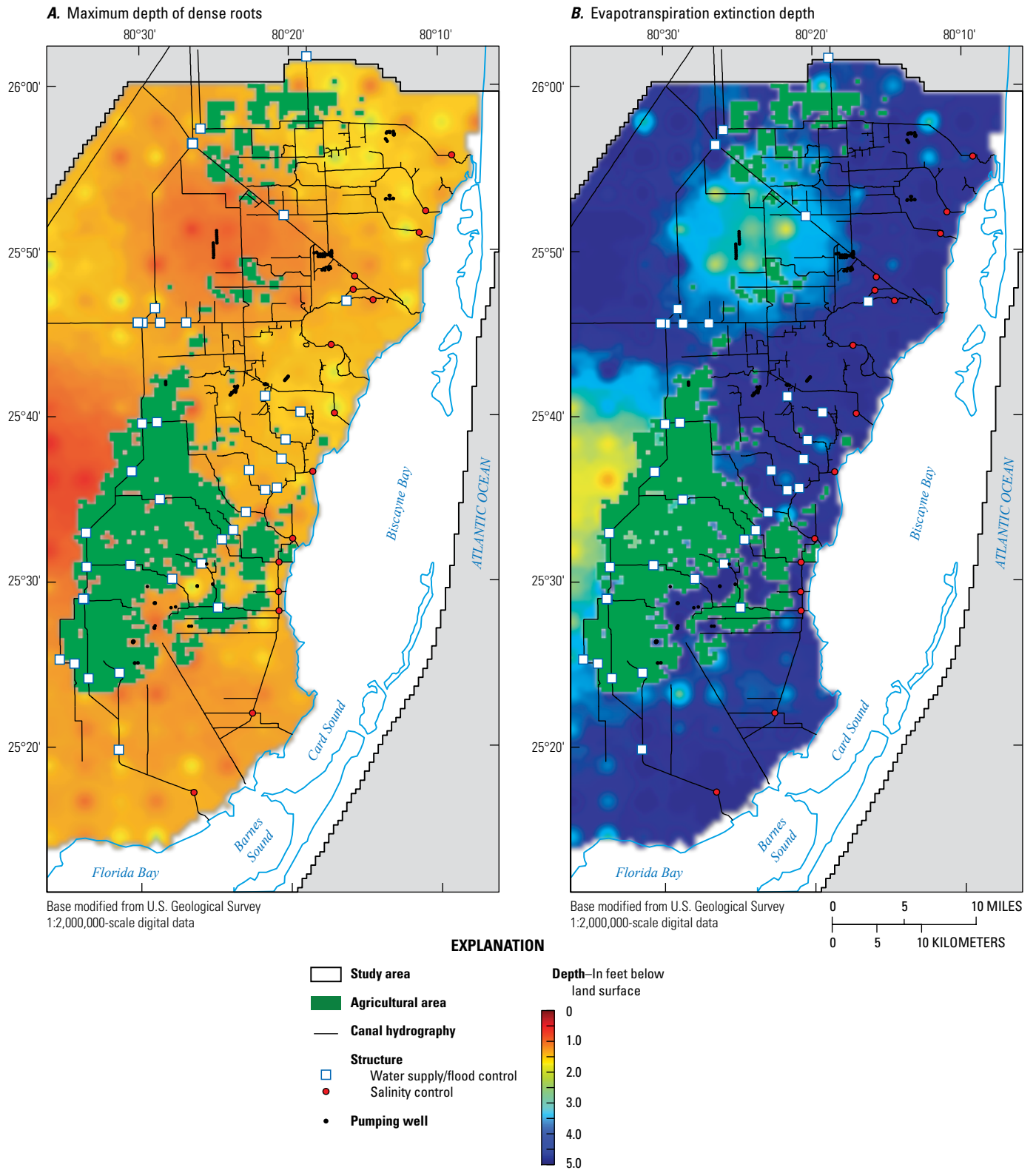


**Figure 35.** Maximum depth of dense roots, *A*, and evapotranspiration extinction depth, *B*, below land surface in nonagricultural onshore model cells.

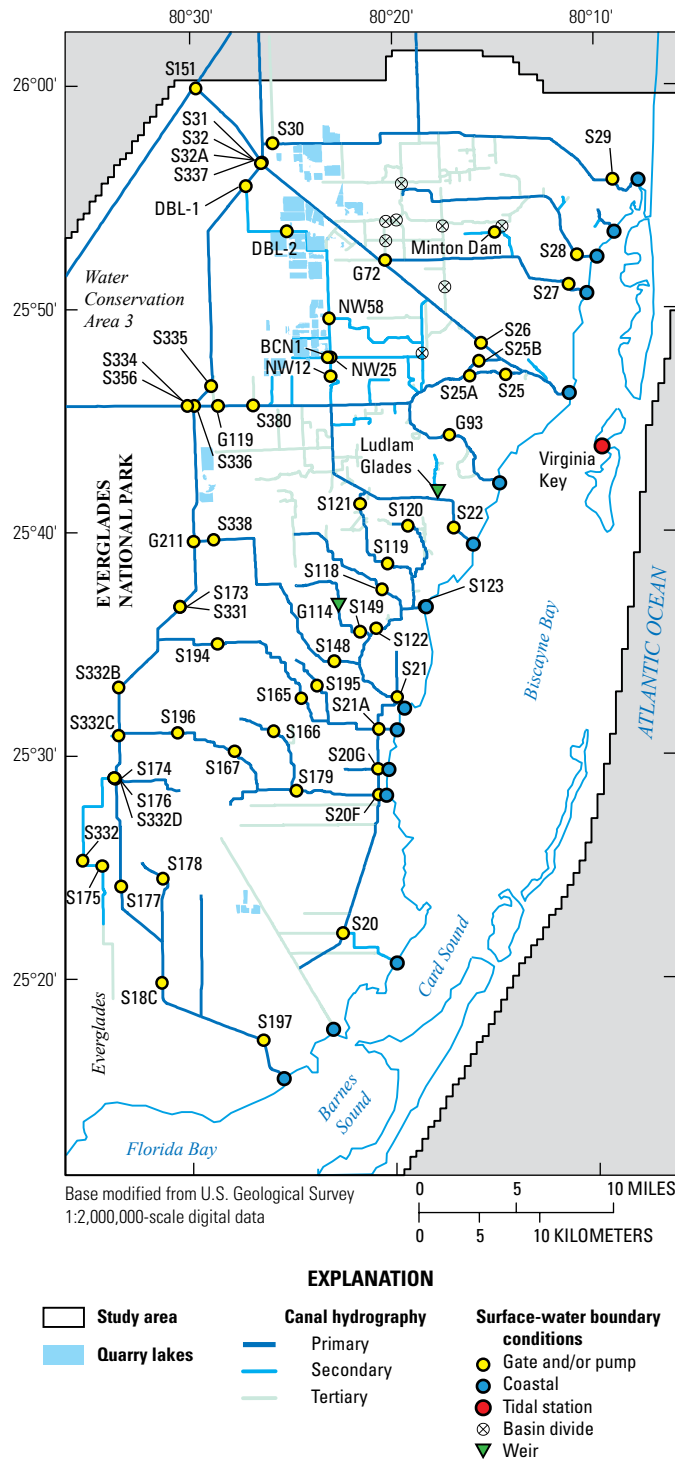


**Figure 36.** Internal and external surface-water boundary conditions.

For gated culverts represented as operable gates, the effective structure width of the composite operable structure was calculated as

$$W_s = \frac{N_s \times 2\pi \left[ \frac{D_s}{2} \right]^2}{D_s}, \quad (23)$$

where

- $N_s$  is the number of gated culverts at a specific reach connection [integer], and
- $D_s$  is the diameter of the circular culvert [L].

Effective gate opening data were used at secondary canal surface-water control structure DBL2. Secondary canal structures in the Snapper Creek Extension Canal (NW58, NW25, NW12, and BCN1) were operated using data provided by the Miami-Dade Department of Environmental Resources Management or operational criteria and historical stage data.

Operable control structures constructed during the simulation period were represented as uncontrolled connections prior to construction. Structures constructed during the simulation period include S380, DBL2, and the Beacon 1 operable control structures (fig. 36).

A total of 10 surface-water pumps were simulated in the surface-water component of the model. The simulated pumps represent supplemental pumps at primary canal locations with gated spillways (S26, S25B, S173/S331, and S174/S332D) or one or more pumps at pump stations delivering water to ENP (S332B, S332C, and S332). Calculated pump discharge rates were specified for each simulated pump. Inflow to WCA3 from S151 was simulated as a specified inflow using a pump that used the calculated structure discharge.

Two physical weirs (G114 and Minton Dam) and two conceptual weirs (S149 and Ludlam Glades) were represented in the model. S149 was represented as a weir set at the structure control elevation of 4.0 ft NAVD 88 prior to October 2008, when tailwater stage data were first collected at this surface-water control structure. Ludlam Glades was specified as a weir set at the structure control elevation of 3 ft NAVD 88 because observed data are not available for this structure. The three culverts at the secondary canal NW12 structure and the one culvert at Minton Dam were included in the model because they control high- and low-flow discharge at these structure locations, respectively.

Although the C-4, C-6, C-7, C-8, and C-9 Basins are defined as separate features (Cooper and Lane, 1987), operable structures are not used to control inter-basin water transfers between adjacent basins. Instead, small diameter culverts separating adjacent basins restrict inter-basin water transfers (PBS&J, 2004, 2006; CDM, 2005; Earth Tech, 2006). Although notable inter-basin water transfers may occur during localized convective storms, SWR1 Process reaches connecting the C-4, C-6, C-7, C-8, and C-9 Basins have been separated using no-flow structures representing basin divides (fig. 36).

### Coastal Surface-Water Boundaries

A stage-dependent boundary, or general head boundary (GHB), was specified at the downstream end of each SWR1 Process reach that discharges surface water to Biscayne Bay, Card Sound, or Barnes Sound (fig. 36). Coastal surface-water boundary flows were calculated internally by the SWR1 Process using

$$Q_{swghb} = \frac{h_{coast} - h_i}{|h_{coast} - h_i|} \frac{1.486}{n_i} A_i \left( \frac{A_i}{w_{Pi}} \right)^{2/3} \left( \frac{|h_{coast} - h_i|}{d_{swghb}} \right)^{1/2}, \quad (24)$$

where

- $Q_{swghb}$  is the calculated coastal boundary discharge [ $L^3T^{-1}$ ],
- $h_{coast}$  is the specified coastal boundary stage [L],
- $h_i$  is the simulated stage of reach  $i$  [L],
- $n_i$  is the Manning's roughness coefficient of reach  $i$  [ $TL^{-1/3}$ ],
- $A_i$  is the cross-sectional area of reach  $i$  at stage  $h_i$  [ $L^2$ ],
- $w_{Pi}$  is the wetted perimeter of reach  $i$  at stage  $h_i$  [L], and
- $d_{swghb}$  is the distance from the center of reach  $i$  to the coastal boundary [L].

Average daily tide data from the Virginia Key tidal station (fig. 37) were used at each coastal surface-water boundary ( $h_{coast}$ ) (fig. 36). All other data used to calculate  $Q_{swghb}$  at each coastal boundary were determined from reach geometry and roughness data.

### Coastal and Marine Groundwater Boundaries

Model cells representing the Atlantic Ocean, Biscayne Bay, Card Sound, Barnes Sound, or Florida Bay were simulated using either GHB or drain (DRN) boundaries in model layer 1 (Harbaugh, 2005). The offshore bathymetry (fig. 3) and the average daily stage data collected at Virginia Key were used to define the equivalent freshwater head at the top of the model in every coastal GHB cell. The equivalent freshwater head at the top of the model was calculated using

$$h_f = \frac{\rho_s}{\rho_f} h_{coast} - \frac{\rho_s - \rho_f}{\rho_f} z, \quad (25)$$

where

- $h_f$  is the equivalent freshwater head [L],
- $\rho_s$  is the density of seawater [ $ML^{-3}$ ],
- $\rho_f$  is the density of freshwater [ $ML^{-3}$ ], and
- $z$  is the bathymetric elevation [L].

A freshwater and seawater density of 62.42 and 63.98 pounds per cubic foot ( $lb/ft^3$ ; 1,000 and 1,025 kilograms per cubic meter [ $kg/m^3$ ]), respectively, were used for all equivalent freshwater head calculations.

Coastal boundaries (GHB or DRN) were specified in model layer 1 cells underlying the Atlantic Ocean, Biscayne Bay, Card Sound, Barnes Sound, or Florida Bay that have land-surface elevations less than or equal to the average stage at Virginia Key between 1996 and 2010 (-0.808 ft NAVD 88). Coastal cells were defined to be coastal GHB or DRN cells on a daily basis using the average daily stage at Virginia Key. GHBs were specified for all coastal boundary cells having a surface elevation less than the stage at Virginia Key to allow for bidirectional water exchange based on the difference between the Biscayne aquifer and overlying coastal water bodies. Conversely, DRNs were specified for all coastal boundary cells having a surface elevation greater than or equal to the surface-water stage at Virginia Key to allow groundwater discharge at the surface in coastal areas.

The cooling canal system at the Turkey Point power plant (fig. 38) was represented in the model using GHB boundaries. Stages in the Turkey Point cooling canal system were derived from the average daily stage at Virginia Key. GHB boundary heads on the western and eastern sides of the cooling canal system were increased by 0.623 ft and decreased by 0.361 ft to reflect elevated stage on the discharge side of the cooling canal system and reduced stage on the return side of the cooling canal system (Hughes and others, 2010).

GHB and DRN conductance values were calculated using cell areas and assumed leakance values for a number of basic sediment types. Assumed leakance values were derived from Langevin and others (2005) and Hughes and others (2010), and are summarized in table 13. The distribution of coastal

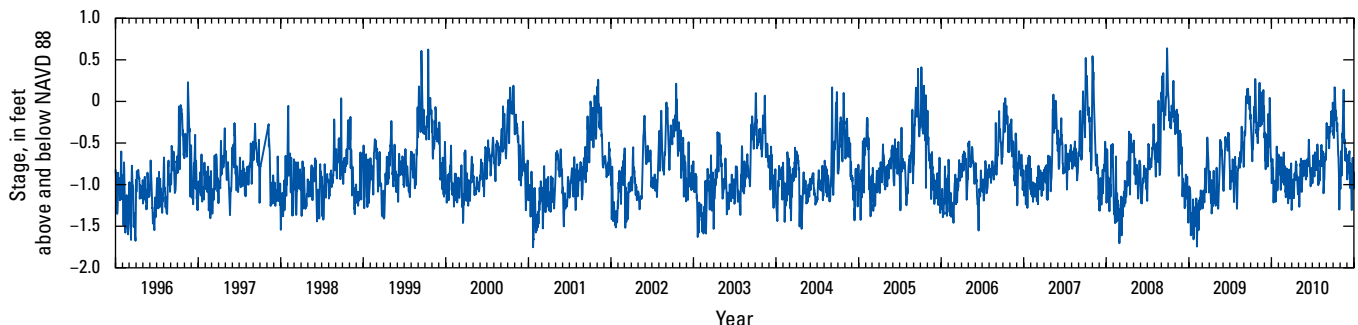


**Figure 37.** Average daily stage fluctuations in Biscayne Bay, Florida, at Virginia Key. Stage data at Virginia Key are collected by the National Oceanic and Atmospheric Administration.

**Table 12.** Surface-water control structure dimensions and hydraulic characteristics.

[NAVD 88, North American Vertical Datum of 1988; --, data not available; %, percent]

Structure name	Type	Number of gates, pumps, or barrels	Head-water reach	Tail-water reach	Structure number	Weir discharge coefficient	Orifice discharge coefficient	Submergence factor exponent	Structure invert elevation, in feet NAVD 88	Downstream			Notes	
										structure invert elevation, in feet NAVD 88	structure width, in feet	Gate height, in feet		Culvert length, in feet
Primary structures														
S30	Gate	3	1964	1963	1	0.61	0.61	0.5	-6.5	--	21	7	--	--
S29	Gate	4	2080	2081	1	0.61	0.61	0.5	-12.5	--	88	15	--	--
S28	Gate	2	2150	2151	1	0.61	0.61	0.5	-15	--	54	17.5	--	--
G72	Flashboard weir	4	260	261	1	0.61	0.61	0.5	-3.9	--	24	--	--	--
S27	Gate	2	2179	2180	1	0.61	0.61	0.5	-12.5	--	54	15	--	--
S151	Gate	6	1	0	1	0.65	0.65	0.5	-3	--	42	7	--	Simulated as specified inflow from external boundary
S31	Gate	3	24	25	1	0.61	0.61	0.5	-4.5	--	21	7	--	--
S26	Gate	2	395	396	1	0.61	0.61	0.5	-11.6	--	52	14.1	--	--
S26	Pump	1	395	396	2	--	--	--	--	--	--	--	--	--
S336	Gate	3	1177	1201	1	0.61	0.61	0.5	-3.3	--	13.5	4.5	--	--
G119	Gate	2	1206	1213	1	0.61	0.61	0.5	-5	--	12	6	--	--
S380	Gate	5	1219	1220	1	0.61	0.61	0.5	-4.5	--	30	6	--	Constructed and operational in 6/2004
S25	Gate	1	1735	1736	1	0.61	0.61	0.5	-5.5	--	8	8	--	--
S25A	Gate	1	1728	1729	1	0.61	0.61	0.5	-3.2	--	4.5	4.5	--	--
S25B	Gate	2	409	408	1	0.61	0.61	0.5	-9.4	--	44	11.9	--	--
S25B	Pump	1	409	408	2	--	--	--	--	--	--	--	--	--
G93	Gate	2	466	467	1	0.61	0.61	0.5	-3.3	--	20	5	--	--
S22	Gate	2	1685	1686	1	0.61	0.61	0.5	-12.5	--	34	15	--	--
S121	Gate	1	675	676	1	0.61	0.61	0.5	-6	--	8	8	--	--
S120	Gate	1	724	723	1	0.61	0.61	0.5	-2.5	--	6	6	--	--
S119	Gate	1	695	696	1	0.61	0.61	0.5	-3.9	--	12	7.3	--	--
S118	Gate	1	1566	1565	1	0.61	0.61	0.5	-6.5	--	20	10	--	--
S122	Gate	2	752	753	1	0.61	0.61	0.5	-4.5	--	12	6	--	--

**Table 12.** Surface-water control structure dimensions and hydraulic characteristics.—Continued

[NAVD 88, North American Vertical Datum of 1988; --, data not available; %, percent]

Structure name	Type	Number of gates, pumps, or barrels	Head-water reach	Tail-water reach	Structure number	Weir discharge coefficient	Orifice discharge coefficient	Submergence factor exponent	Structure invert elevation, in feet NAVD 88	Downstream structure invert elevation, in feet NAVD 88	Cumulative structure width, in feet	Gate height, in feet	Culvert length, in feet	Culvert Manning's roughness coefficient	Notes
S123	Gate	2	1627	1628	1	0.61	0.61	0.5	-8.8	--	50	12.7	--	--	
S337	Gate	6	30	29	1	0.61	0.61	0.5	-4.5	--	42	7	--	--	
S335	Gate	1	1136	1135	1	0.61	0.61	0.5	-5.7	--	20	12.2	--	--	
S334	Gate	1	1180	1179	1	0.61	0.61	0.5	-8.4	--	29	17	--	--	
S338	Gate	2	1061	1062	1	0.61	0.61	0.5	-6	--	14	7	--	--	
S148	Gate	2	1104	795	1	0.61	0.61	0.5	-8.5	--	40	12	--	--	
G114	Weir	1	768	767	1	0.65	--	0.5	2	--	39.75	--	--	--	
S149	Gate	2	759	758	1	0.61	0.61	0.5	-4.5	--	14	7	--	--	Tailwater data not available before 2008 - prior to 10/2008 represented as a fixed weir at 4 feet NAVD 88
S21	Gate	3	1545	1546	1	0.61	0.61	0.5	-8	--	81	10.7	--	--	
S194	Gate	2	964	965	1	0.61	0.61	0.5	-4	--	14	7	--	--	
S195	Gate	1	1024	1023	1	0.61	0.61	0.5	-3.3	--	6	6	--	--	
S165	Gate	1	990	991	1	0.61	0.61	0.5	-2	--	12	7	--	--	
S21A	Gate	2	1010	1011	1	0.61	0.61	0.5	-9.3	--	40	11.8	--	--	
S20G	Gate	1	1541	1542	1	0.61	0.61	0.5	-9.8	--	25	12.3	--	--	
S196	Gate	1	916	915	1	0.61	0.61	0.5	-4	--	7	7	--	--	
S166	Gate	1	863	862	1	0.61	0.61	0.5	-3.5	--	12	8.5	--	--	
S167	Gate	1	901	900	1	0.61	0.61	0.5	-2	--	12	7	--	--	
S179	Gate	2	846	845	1	0.61	0.61	0.5	-9	--	50	12	--	--	
S20F	Gate	3	1531	1532	1	0.61	0.61	0.5	-10.5	--	75	13	--	--	
S20	Gate	1	2324	2323	1	0.61	0.61	0.5	-8.9	--	16	11.4	--	--	
S174	Gate	1	1418	1419	1	0.61	0.61	0.5	-3	--	16	8	--	--	Discharge to external boundary
S332D	Pump	1	1418	0	2	--	--	--	--	--	--	--	--	--	Discharge to external boundary
S332D	Pump	1	1418	0	3	--	--	--	--	--	--	--	--	--	Discharge to external boundary

**Table 12.** Surface-water control structure dimensions and hydraulic characteristics.—Continued

[NAVD 88, North American Vertical Datum of 1988; --, data not available; %, percent]

Structure name	Type	Number of gates, pumps, or barrels	Headwater reach	Tailwater reach	Structure number	Weir discharge coefficient	Orifice discharge coefficient	Submergence factor exponent	Structure invert elevation, in feet NAVD 88	Downstream			Culvert Manning's roughness coefficient	Notes	
										Structure invert elevation, in feet NAVD 88	Structure invert elevation, in feet NAVD 88	Cumulative structure width, in feet			Gate height, in feet
S175	Gate	3	1444	1445	1	0.61	0.61	0.5	-6.5	--	21	7	--	--	
G211	Gate	6	1057	1056	1	0.61	0.61	0.5	-4	--	36	6	--	--	
S173	Gate	1	1043	1042	1	0.61	0.61	0.5	-4	--	6	6	--	--	
S331	Pump	1	1043	1042	2	--	--	--	--	--	--	--	--	--	
S331	Siphon	1	1043	1042	3	--	--	--	--	--	--	--	--	Discharge to external boundary	
S332B	Pump	1	937	0	1	--	--	--	--	--	--	--	--	Discharge to external boundary	
S332B	Pump	1	937	0	2	--	--	--	--	--	--	--	--	Discharge to external boundary	
S332C	Pump	1	1266	0	1	--	--	--	--	--	--	--	--	Discharge to external boundary	
S176	Gate	1	1276	1277	1	0.61	0.61	0.5	-2.5	--	20	8	--	--	
S332	Pump	1	1440	0	1	--	--	--	--	--	--	--	--	Discharge to external boundary	
S177	Gate	1	1311	1312	1	0.61	0.61	0.5	-8.6	--	22	12.6	--	--	
S178	Gate	2	1342	1341	1	0.61	0.61	0.5	-4.5	--	16	8	--	--	
S18C	Gate	2	1357	1358	1	0.61	0.61	0.5	-8.5	--	44	11	--	--	
S197	Gate	3	1405	1406	1	0.61	0.61	0.5	-9.5	--	21	7	--	--	
S197	Gate	20	1405	1406	2	0.61	0.61	0.5	-9.5	--	70	12	--	--	
Secondary canal structures															
DBL1	Gate	1	39	40	1	0.61	0.61	0.5	-10.47	--	11.4	14.5	--	Closed	
DBL2	Gate	2	54	55	1	0.61	0.61	0.5	-4.5	--	14	9	--	Constructed August 2002 - Operated after 2/25/2003	
NW58	Gate	2	149	148	1	0.61	0.61	0.5	-3.95	--	11	7	--	Open	
NW25	Gate	2	95	96	1	0.61	0.61	0.5	-3.99	--	11	7	--	--	
NW12	Gate	1	546	545	1	0.61	0.61	0.5	-8.22	--	7	9	--	Closed	
NW12	Culvert	1	546	545	2	0.61	0.8	--	2.47	2.53	3.35	--	113.7	0.03	Circular culvert
NW12	Culvert	1	546	545	3	0.61	0.8	--	2.48	2.62	3.35	--	118.4	0.03	Circular culvert
NW12	Culvert	1	546	545	4	0.61	0.8	--	2.53	2.79	3.35	--	123.1	0.03	Circular culvert

**Table 12.** Surface-water control structure dimensions and hydraulic characteristics.—Continued

[NAVD 88, North American Vertical Datum of 1988; --, data not available; %, percent]

Structure name	Type	Number of gates, pumps, or barrels	Head-water reach	Tail-water reach	Structure number	Weir discharge coefficient	Orifice discharge coefficient	Submergence factor exponent	Structure invert elevation, in feet NAVD 88	Downstream structure invert elevation, in feet NAVD 88	Cumulative structure width, in feet	Gate height, in feet	Culvert length, in feet	Culvert Manning's roughness coefficient	Notes
Ludlam Glades	Gate	1	1665	1664	1	0.61	0.61	0.5	-10.1	--	9.4	12	--	--	Simulated as a weir set at control elevation (3 feet NAVD 88)
Minton Dam	Weir	1	1795	1794	1	0.65	--	0.5	1.2	--	15	--	--	--	Estimated from design drawings for new structure installed after 1/2012
Minton Dam	Culvert	1	1795	1794	2	0.61	0.8	--	-4.18	-4.17	5.5	--	24	0.03	
BCNI	Gate	1	551	550	1	0.61	0.61	0.5	-4.59	--	5.1	6.5	--	--	Constructed September 2004 - closed

boundary sediment types used to define leakance values are based on data from Prager and Halley (1997) and Lirman and others (2003) (fig. 38).

### Water Conservation Area 3, Everglades National Park, and Southern Glades Groundwater Boundaries

Wetland areas within WCA3, ENP, and the southern Glades (west and south of the C-111 Canal) were simulated using either GHB or DRN boundaries in model layer 1 based on surface sediment type (fig. 38). Daily stage data from the Everglades Depth Estimation Network (EDEN) were used to define boundary stages in wetland areas. Daily EDEN stage data are interpolated to a 400×400-m grid covering all of the water conservation areas, most of ENP, and parts of the southern Glades (Pearlstine and others, 2007; Telis, 2006). Daily EDEN stage data were interpolated to the model grid using bilinear interpolation (Press and others, 1990). Delaunay triangulation (de Berg and others, 2008) was used to fill gaps in the southern Glades between the EDEN stage dataset and coastal boundaries.

Model cells were defined to be wetland GHB or DRN cells on a daily basis using the interpolated average daily EDEN stage. Consistent with the approach used to specify GHBs and DRNs for coastal boundaries, GHBs were specified in model layer 1 for each wetland cell having a surface elevation less than the interpolated EDEN stage for the cell. DRNs were specified in model layer 1 for each wetland cell having a surface elevation greater than or equal to the interpolated EDEN stage for the cell. Wetland stages that exceeded the stage at Virginia Key were assumed to be freshwater (fluid density = 62.47 lb/ft<sup>3</sup>); otherwise, it was assumed the water is seawater (fluid density = 63.98 lb/ft<sup>3</sup>).

GHB and DRN conductance values in wetland cells were calculated using cell areas and assumed leakance values calculated using head difference and seepage data for WCA3 from Sonenshein (2001). The calculated wetland soil leakance value (table 13) is consistent with mean hydraulic conductivity data for peat in WCA-2A (Harvey and others, 2004).

### Initial Conditions

Initial water levels for the three model layers were specified by interpolating water levels from a water-table map for November 1993 (Sonenshein and Koszalka, 1996) to cell centers for every model grid cell. Initial surface-water stages were developed for each SWR1 reach using observed headwater stage data for primary structures in the study area on January 1, 1996. Headwater stage values were applied to all reaches between a given structure and the next structure upstream. Hydrographs of observed headwater stages at the primary structures are included in appendix 2. The initial position of the freshwater-seawater interface at the base of the Biscayne aquifer (model layer 3)

was specified using the interpreted position of the interface in 1995 (fig. 23) determined by Sonenshein (1997). In model layers 1 and 2, initial water-table elevations and the Ghyben-Herzberg relation (Ghyben, 1889; Herzberg, 1901) were used to specify the initial position of the freshwater-seawater interface seaward of the interpreted position of the interface in 1995.

### Hydraulic Parameters

The hydraulic properties of the interconnected surface-water system and the underlying Biscayne aquifer control the effects of groundwater pumping on canal leakage and regional groundwater flow. For the model to successfully predict those effects, the values of the hydraulic properties were adjusted within reasonable limits during model calibration to improve the model simulations and fit to observed data.

### Canal Roughness and Bed Conductance Coefficients

To account for the effect of the canal sediment and vegetation on flow in the canals, Manning’s roughness coefficients, which represent frictional resistance to horizontal surface-water discharge, were estimated during the calibration process. Calibrated Manning’s roughness coefficients range from 0.01 to 0.5 second per meter<sup>1/3</sup> (s/m<sup>1/3</sup>) (fig. 39A).

Canal conductance was dynamically calculated by the SWR1 Process using the leakance option. Canal conductance is calculated from leakance using

$$C_{i,k} = L_i \chi_{i,k} l_i, \tag{26}$$

where

- $C_{i,k}$  is the canal conductance of reach  $i$  in layer  $k$  [ $L^2T^{-1}$ ],
- $L_i$  is the defined leakance coefficient for reach  $i$  [ $T^{-1}$ ],
- $\chi_{i,k}$  is the maximum exchange perimeter of reach  $i$  in layer  $k$  [ $L$ ], and
- $l_i$  is the length of reach  $i$  [ $L$ ].

Additional details on canal conductance are provided in Hughes and other (2012). Canal leakance coefficients also were estimated during the calibration process. Calibrated canal leakance coefficients range from 1 to 5,000 days<sup>-1</sup> (fig. 39B).

### Hydraulic Conductivity

The hydraulic conductivities of model layers 1, 2, and 3 were estimated during the calibration process. Initially, the hydraulic conductivity of model layer 2 was assumed to be two orders of magnitude less than the hydraulic conductivity of model layers 1 and 3, but was allowed to deviate from this initial ratio if observation data used to constrain model

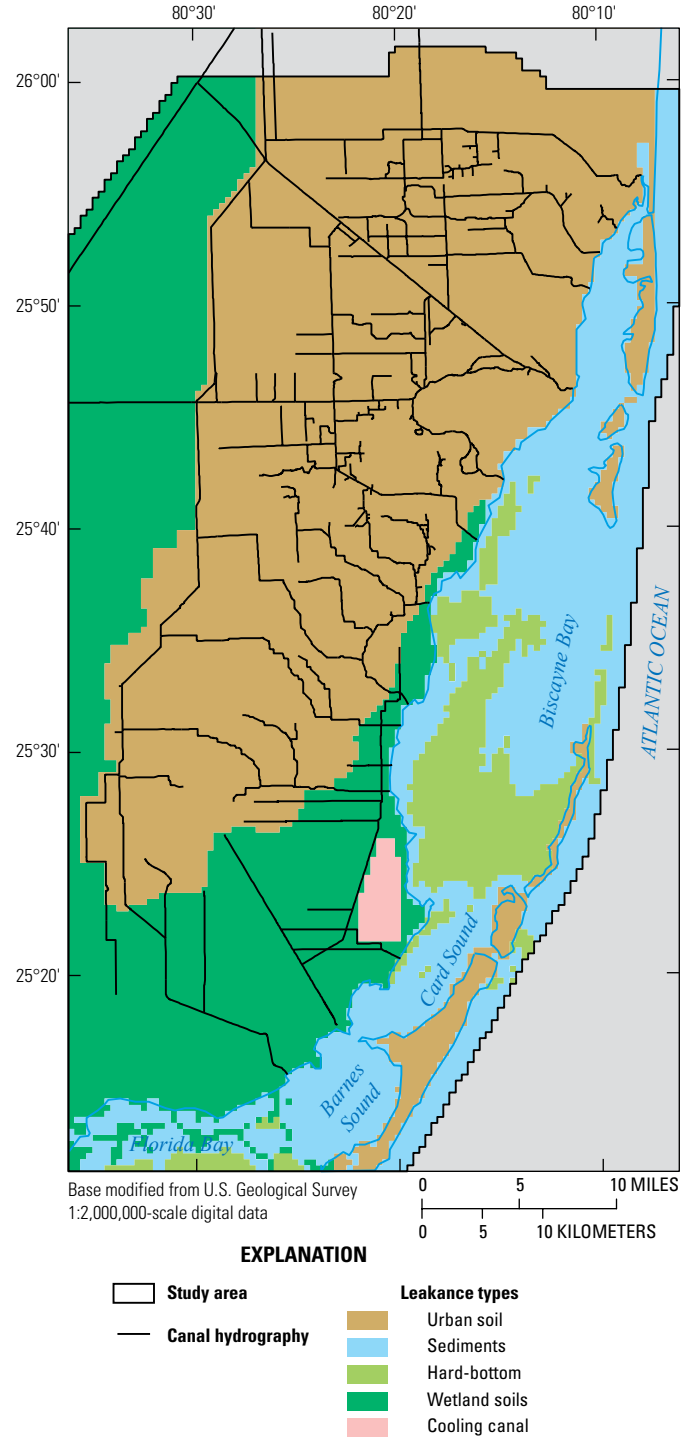


**Figure 38.** Basic sediment types used to calculate coastal and wetland area head-dependent groundwater boundary condition conductance values.

calibration supported such variation. Decreased or increased hydraulic conductivity ratios between model layers 1 and 2, or 2 and 3, effectively reduce or increase the head difference between the upper and lower permeable units of the Biscayne aquifer, respectively. A horizontal hydraulic conductivity of

**Table 13.** Sediment types and hydraulic properties used to calculate leakance coefficients used to calculate coastal and wetland area head-dependent groundwater boundary condition conductance values.

Sediment type	Hydraulic conductivity, in feet per day	Sediment thickness, in feet	Leakance, in feet per day per foot
Urban soil	0.328	3.28	0.1
Sediments <sup>1</sup>	0.328	3.28	0.1
Hard-bottom <sup>1</sup>	2.46	3.28	0.75
Wetland soils <sup>2</sup>	1.20	5.0	0.24
Cooling canal <sup>3</sup>	9.84	3.28	3.0

<sup>1</sup>Langevin and others (2005).

<sup>2</sup>Sonenshein (2001).

<sup>3</sup>Hughes and others (2010).

$3.3 \times 10^5$  ft/d was applied in grid cells containing quarry lakes (fig. 24) in cases where this value was less than the hydraulic conductivity estimated as part of the calibration process; the minimum horizontal hydraulic conductivity used in quarry lakes is based on the value used by Brakefield and others (2013) to represent quarry lakes. The horizontal and vertical hydraulic conductivity for each layer were assumed to be equal.

The calibrated hydraulic conductivity of more permeable model layers 1 and 3 ranged from approximately  $6.0 \times 10^2$  to  $8.7 \times 10^5$  ft/d and  $2.8 \times 10^2$  to  $1.2 \times 10^7$  ft/d, respectively (fig. 40A–B). The calibrated hydraulic conductivity of less permeable model layer 2 ranged from approximately  $3.0 \times 10^0$  to  $3.3 \times 10^5$  ft/d (fig. 40C). The calibrated transmissivity of the Biscayne aquifer ranged from approximately  $2.0 \times 10^5$  to  $8.7 \times 10^8$  ft<sup>2</sup>/d (fig. 40D).

### Storage Coefficients and Porosity

The specific storage coefficient and specific yield of the model layers were estimated during the calibration process. All model layers were defined as being convertible, and specific storage coefficients and specific yield values were specified for each model cell. Convertible layers allow the model to transition between confined and unconfined conditions in response to changing hydrologic conditions and groundwater pumping rates. The specific storage was estimated for model layers 2 and 3, and the specific yield was estimated for model layer 1. The specific yield for model layer 1 was applied in model layers 2 and 3. Data were not available to constrain specific storage and yield at specific points. Specific storage was constrained to be between  $1.0 \times 10^{-8}$  and  $0.8$  ft<sup>-1</sup>, and specific yield was constrained to be between 0.01 and 0.9. A specific storage value of  $1$  ft<sup>-1</sup> and specific yield value of 1 were used to calculate the average specific storage and specific yield in grid cells containing quarry lakes (fig. 24).

Calibrated specific storage values for model layers 1, 2, and 3 in non-quarry lakes grid cells ranged from  $3.5 \times 10^{-6}$  to  $4.3 \times 10^{-5}$  ft<sup>-1</sup> (fig. 41A–C). Calibrated specific yield values for model layer 1 in non-quarry lakes grid cells ranged from 0.08 to 0.9 (fig. 41D). The 25th percentile, median, and 75th percentile of calibrated specific yield values for model layer 1 were 0.29, 0.33, and 0.38, respectively. The highest specific yield values were generally located in wetland areas or near quarry lakes and represent effective parameters that are a combination of aquifer and surface-water storage.

The porosity of the Biscayne aquifer was assumed to be equal to the specific yield of model layer 1 (fig. 41D). The porosity value is used by the SWI2 Package to simulate movement of the freshwater-seawater interface.

## Model Calibration and Fit, and Simulation of Hydrologic System from 1996 to 2010

The model was calibrated by adjusting selected input parameters to reduce the differences between the observed data and simulation results. Differences between the observed data and simulation results for the period from January 1997 through December 2004 were evaluated using an L–2 norm objective function. The automated parameter estimation software (PEST) (Doherty, 2010) was used to reduce the L–2 norm objective function to an acceptable value. The automated parameter estimation process refined a total of 9 times to improve observation processing, the number and type of parameters estimated, and the final weighting strategy. The 9th and final PEST run was manually terminated after the 6th parameter estimation iteration when the reduction in the weighted L–2 norm objective function (eq. 6) between successive iterations was less than 1 percent. A pareto front analysis (Doherty, 2010) was performed after the automated process was completed to reduce local-scale heterogeneity introduced during the parameter estimation process. Local-scale heterogeneity that could not be supported by field data or expert knowledge was reduced if the model fit from a pareto front iteration was comparable to that of the final parameter estimation iteration. During each pareto front iteration, the regularization weight was increased and up to three inversion iterations were performed to achieve comparable model fit to the final automated parameter estimation iteration or to previous pareto iterations. A combination of the L–2 norm and calibration criteria at individual observation locations were used to terminate the pareto iterations, which occurred after 11 iterations were completed. A weighted L–2 norm of  $2.165 \times 10^7$  was obtained during the final pareto iteration. Although the L–2 norm was used to terminate the final automated parameter estimation process and guide termination of the pareto front analyses, final model fit is presented in terms of the calibration criteria defined in tables 9 and 10.

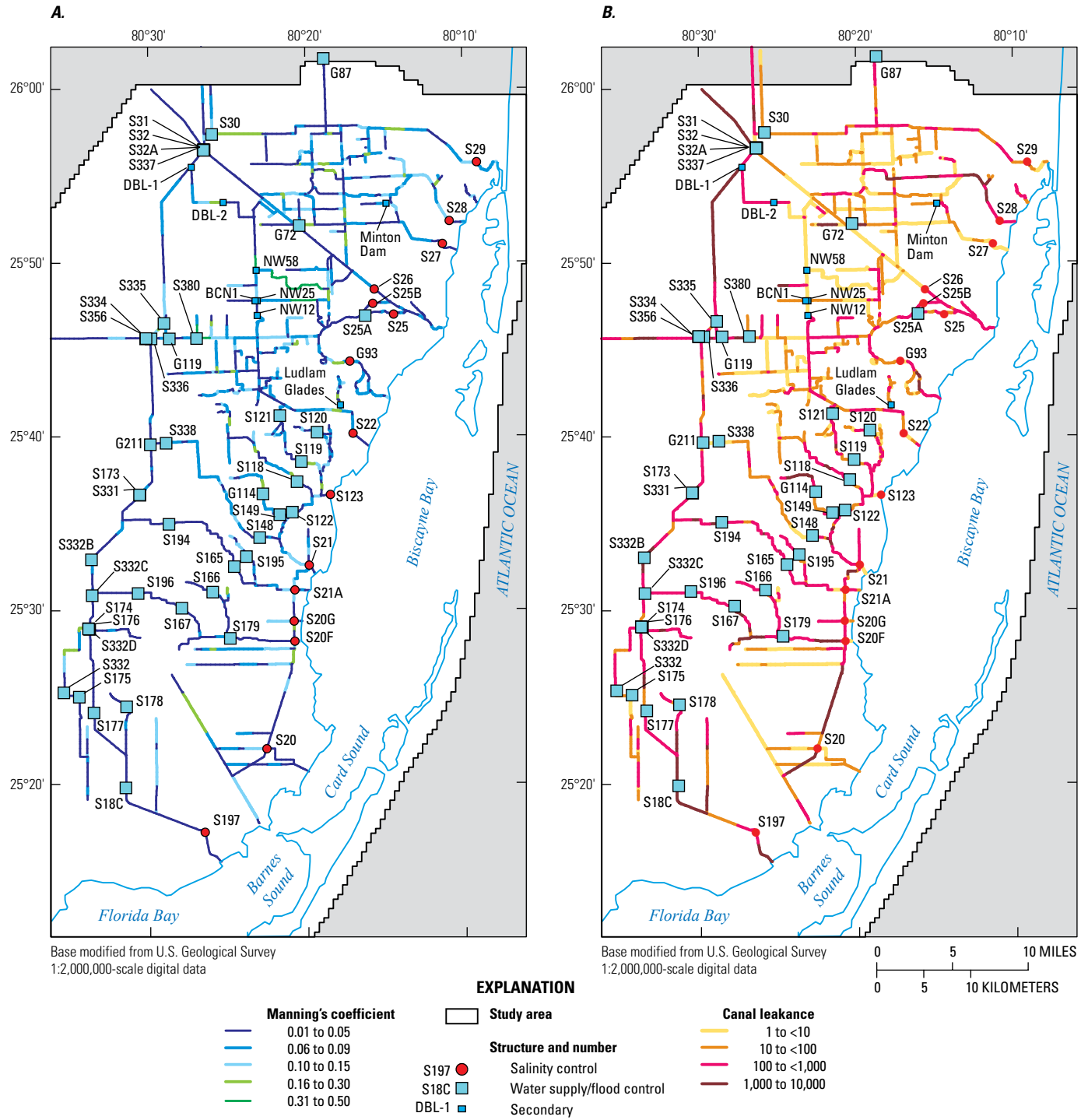


Figure 39. Calibrated, A, canal roughness and, B, bed leakage coefficients.

## Surface-Water Stage

Error statistics were calculated for 37,530 and 29,793 paired weekly average stage observations during the calibration and verification periods, respectively, at the 111 surface-water stage monitoring sites. During the calibration period, the overall model ME and RMSE were 0.10 and 0.42 ft, respectively, and ME and RMSE calibration targets (0.5 and 1 ft) were met at 95 and 99 percent of the surface-water stage monitoring sites, respectively. The small positive value for the overall ME indicates that the model is simulating surface-water stages that are, on average, higher than observed values.

Surface-water stage error statistics for individual stage-monitoring sites are summarized in table 6. The spatial distribution of ME during the calibration period indicates that simulation results met calibration targets at all but two observation locations in WCA3, at S-380 headwater and tailwater, and DBL2 tailwater (fig. 42A). Overall model performance for surface-water stage in the verification period was within defined stage ME and RMSE calibration criteria (table 6). Hydrographs of simulated and observed weekly average surface-water stage at the 111 surface-water stage monitoring sites for the warmup, calibration, and verification periods are included in appendix 2.

## Surface-Water Discharge

Error statistics were calculated for 17,139 and 13,144 paired weekly average discharge observations during the calibration and verification periods, respectively, at the 49 surface-water discharge monitoring sites. During the calibration period, the overall model NME, NRMSE, and E1 were 0.01, 0.08, and 0.61, respectively (table 14). NME, RMSE, and E1 calibration targets (0.1, 0.2, and 0.5) were met at 94, 94, and 83 percent of the surface-water discharge monitoring sites, respectively.

The spatial distribution of NME during the calibration period indicates that simulation results met calibration targets at all but two observation locations (fig. 42B). Overall model performance for surface-water discharge during the verification period was within defined stage ME, RMSE, and E1 calibration criteria (table 14). Hydrographs of simulated and observed surface-water weekly average discharge at the 49 surface-water discharge monitoring sites for the warmup, calibration, and verification periods are included in appendix 3.

## Net Surface-Water Subbasin Discharge

Error statistics were calculated for 2,843 and 2,108 paired monthly observations of average net surface-water canal

discharge for 31 surface-water subbasins during the calibration and verification periods, respectively. Each net surface-water subbasin discharge observation represents the difference between surface-water inflow and outflow for a basin. During the calibration period, the overall model NME, NRMSE, and E1 were 0.00, 0.12, and 0.48, respectively. NME and RMSE calibration targets (0.1 and 0.2) were met at 83 and 90 percent of the surface-water subbasins, respectively. The E1 calibration targets (0.5) were not satisfied because of poor model performance in subbasins associated with DBL2, L-31N at G211, L-31N at S331, C-102 at S165, C-102 at S21, Military Canal, C-103 at S167, L-31E at S20, and C-111E at S178. The net surface-water subbasin discharge in these subbasins is small relative to that in other basins, so poor performance is not expected to adversely affect model predictions.

Time-series graphs of simulated and observed net surface-water subbasin discharge for the primary basins in the urban area of the model domain are shown in figure 43; the C-2 to C-9 Basins have been combined because of uncontrolled interconnections between these basins. The NME net surface-water subbasin discharge criterion was met in the C-2 to C-9 Basins and 6 of the 7 other primary basins during the calibration period (fig. 44). Consistent with the subbasin results, the poorest model performance for net surface-water subbasin discharge occurred in the Homestead Subbasin (Military Canal). Model performance for net surface-water subbasin discharge was slightly poorer for the verification period but generally consistent with model performance for the calibration period (table 7). In general, model performance was better for the C-2 to C-9 Basins and the remaining 7 primary basins than it was for several individual subbasins. Time-series graphs of monthly simulated and observed net surface-water subbasin discharge for the 31 surface-water subbasins for the warmup, calibration, and verification periods are included in appendix 4.

## Groundwater Levels

Error statistics were calculated for 34,421 and 26,183 paired weekly average groundwater level observations during the calibration and verification periods, respectively, at the 112 groundwater monitoring sites. During the calibration period, the overall model ME and RMSE were 0.14 and 0.51 ft, respectively; ME and RMSE calibration targets of 0.5 and 1 ft, respectively, were met at 89 and 94 percent of the groundwater monitoring sites. The small positive value for the overall ME indicates that the model is simulating groundwater levels that are higher, on average, than observed values.

The spatial distribution of ME during the calibration period indicates that simulation results met calibration targets at all but 12 observation locations generally associated with

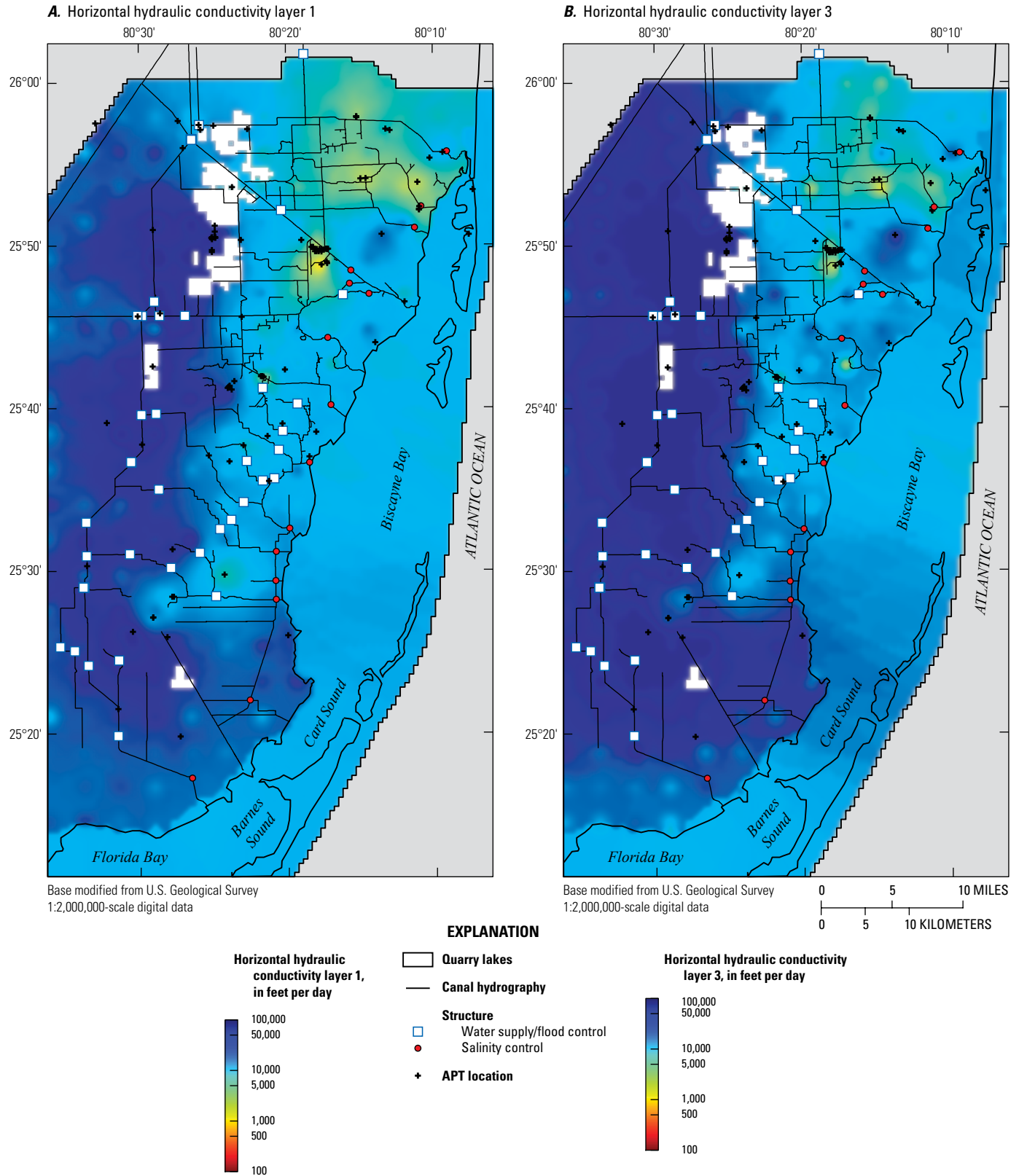


**Figure 40.** Calibrated horizontal hydraulic conductivity of permeable model layers, A, 1 and, B, 3. The calibrated horizontal conductivity of less permeable model layer 2 separating permeable model layers 1 and 3 is shown in C. The calibrated transmissivity of the Biscayne aquifer is shown in D. White areas in study area represent quarry lakes. [APT, aquifer performance test]

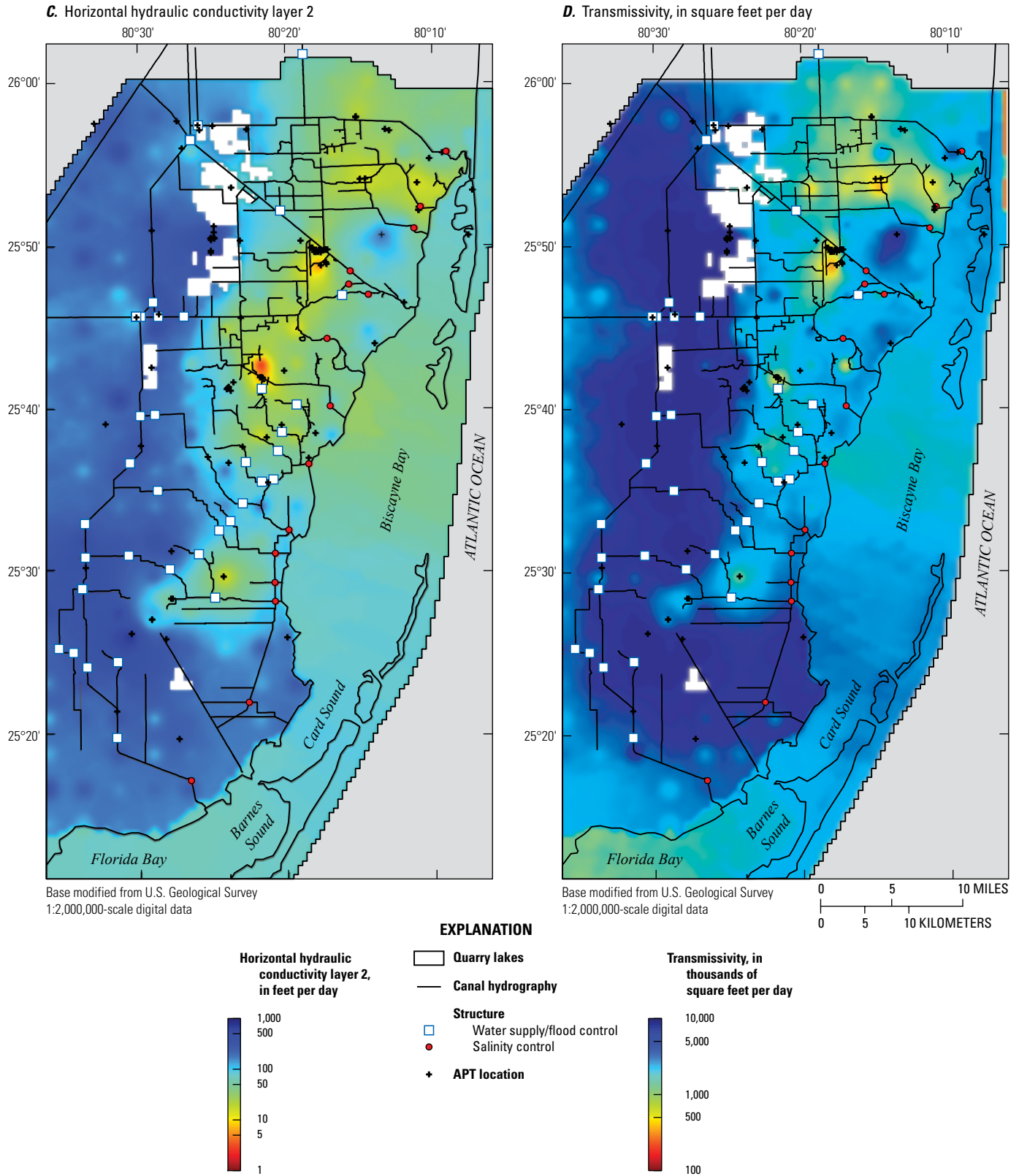


**Figure 40.** Calibrated horizontal hydraulic conductivity of permeable model layers, A, 1 and, B, 3. The calibrated horizontal conductivity of less permeable model layer 2 separating permeable model layers 1 and 3 is shown in C. The calibrated transmissivity of the Biscayne aquifer is shown in D. White areas in study area represent quarry lakes. [APT, aquifer performance test]—Continued

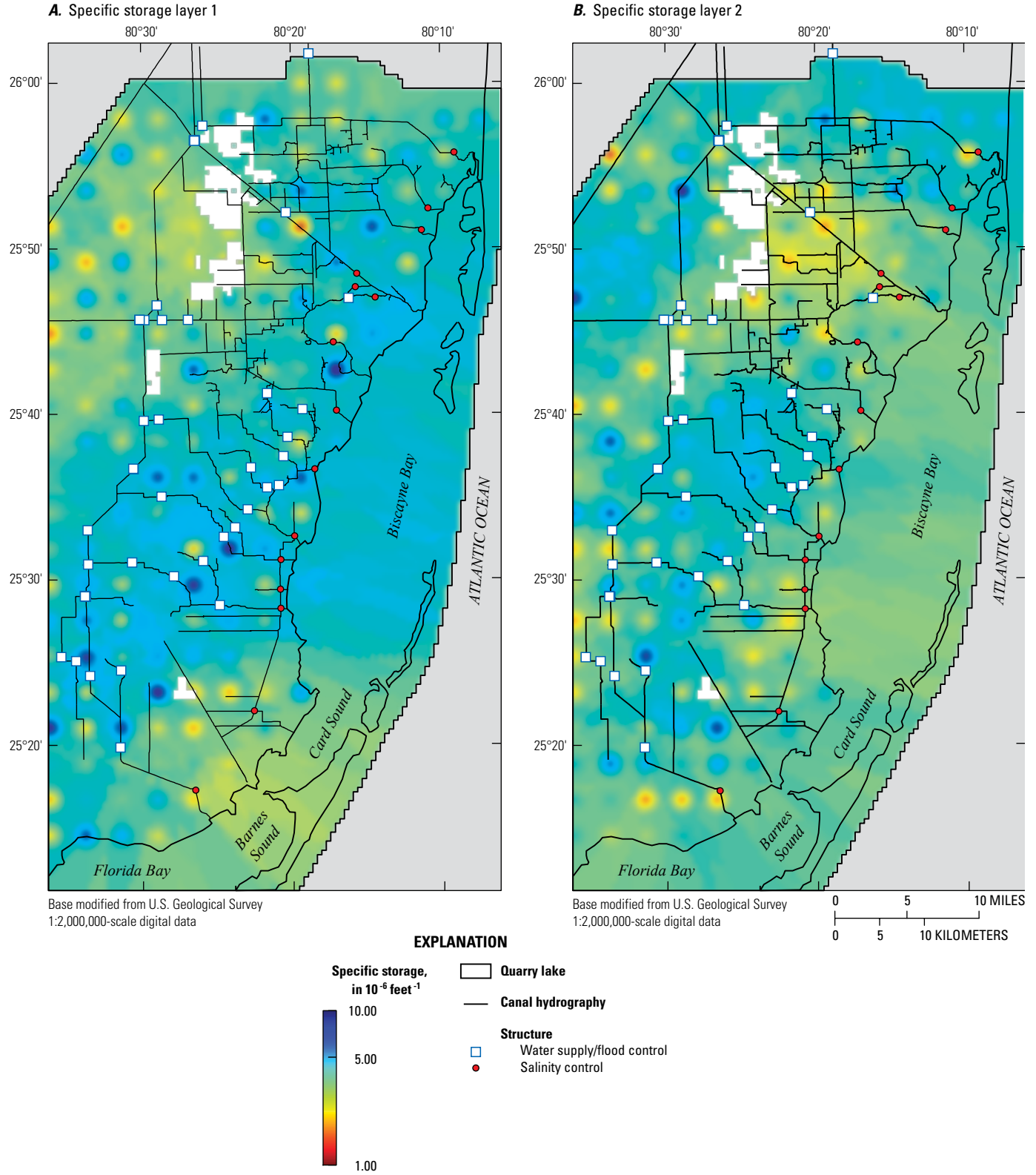
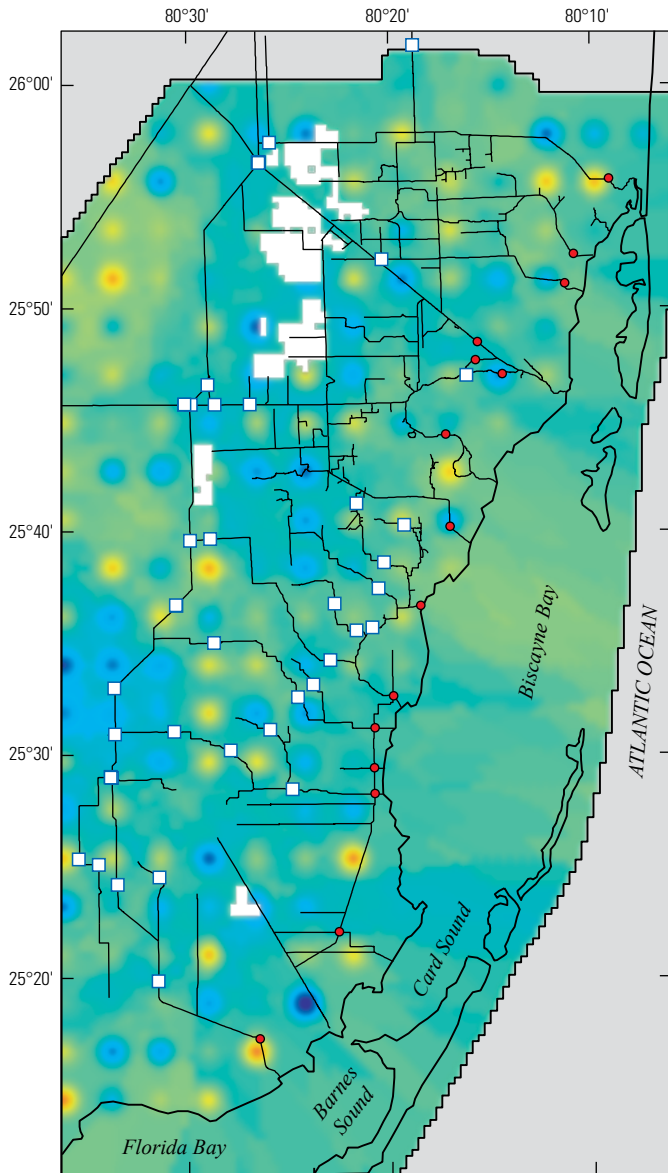


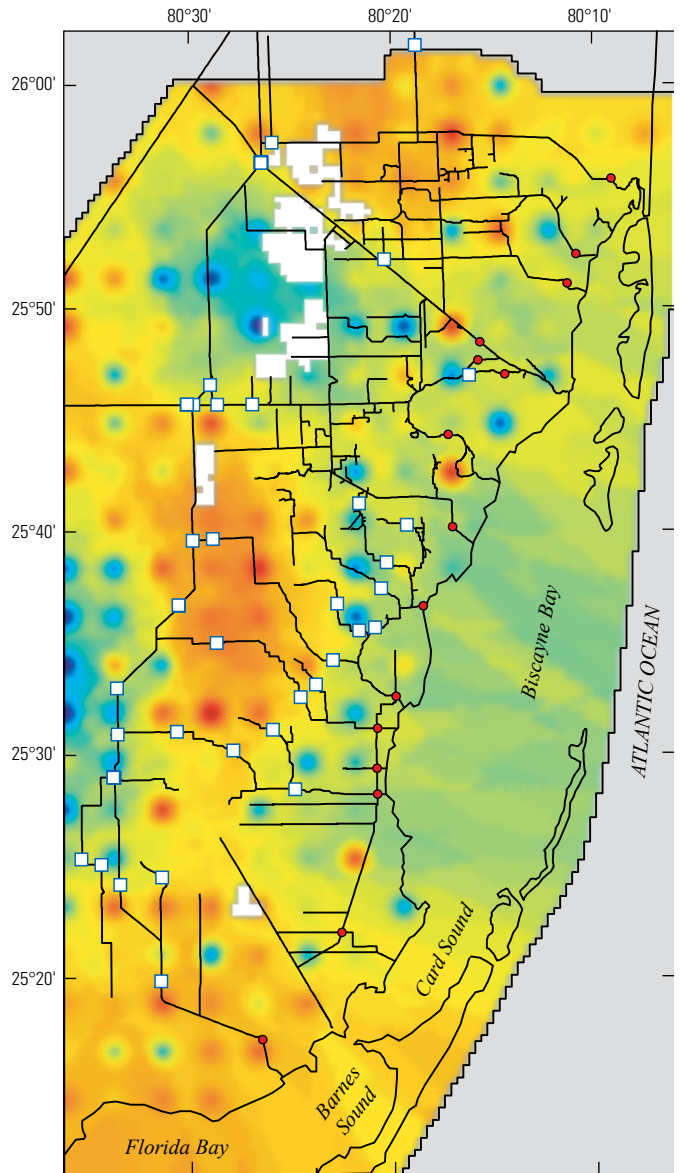
**Figure 41.** Calibrated specific storage coefficient for model layers, A, 1; B, 2; and C, 3; D, calibrated specific yield (model layer 1) of the Biscayne aquifer.

C. Specific storage layer 3

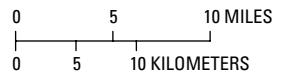


Base modified from U.S. Geological Survey  
1:2,000,000-scale digital data

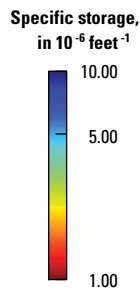
D. Specific yield layer 1



Base modified from U.S. Geological Survey  
1:2,000,000-scale digital data



EXPLANATION



- Quarry lake
- Canal hydrography
- Structure**
- Water supply/flood control
- Salinity control

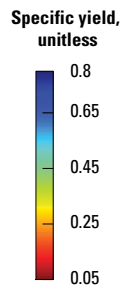


**Figure 41.** Calibrated specific storage coefficient for model layers, A, 1; B, 2; and C, 3; D, calibrated specific yield (model layer 1) of the Biscayne aquifer.—Continued

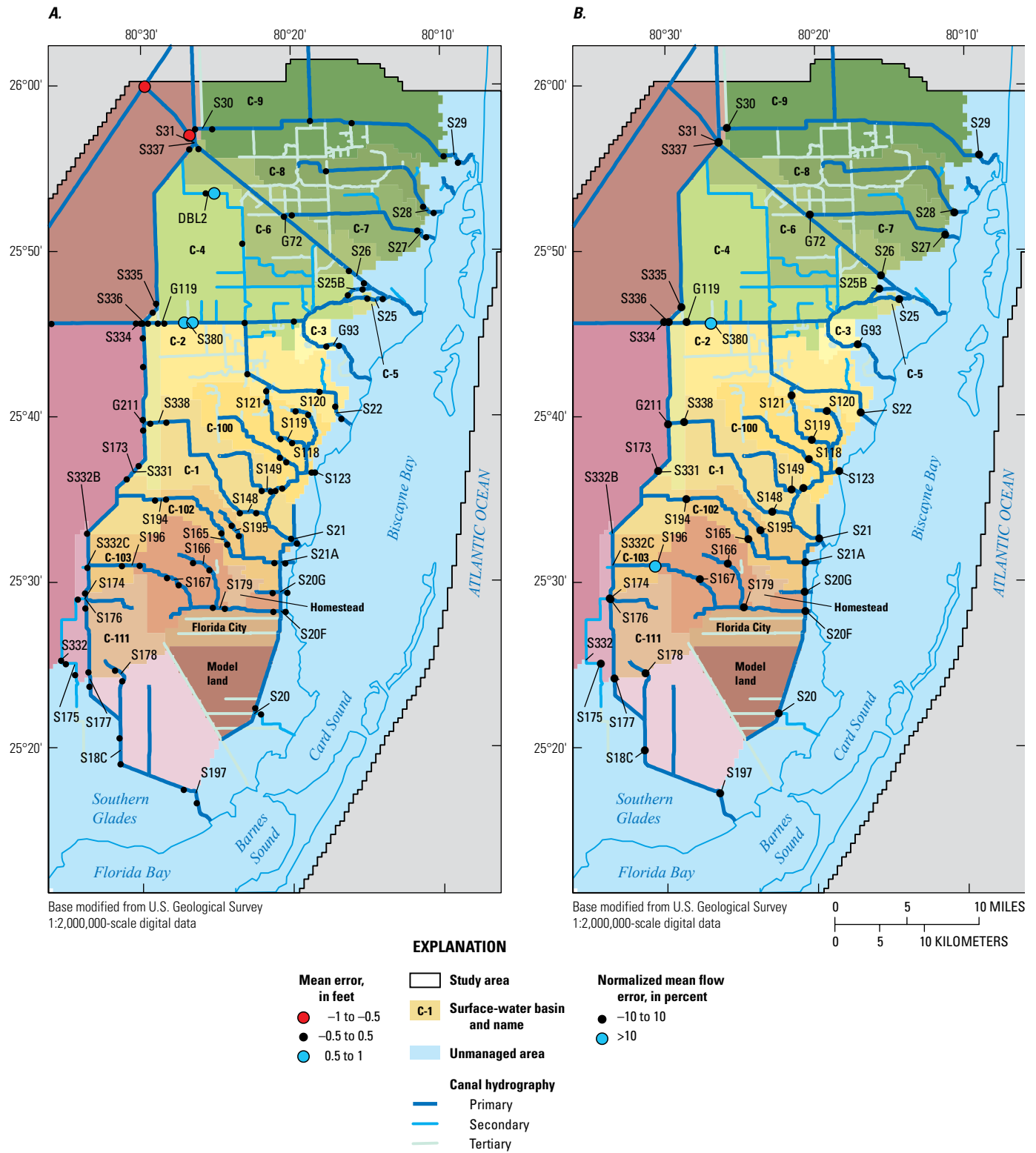


Figure 42. Mean surface-water stage differences, A, and normalized average surface-water discharge differences, B, between measured and model-simulated values, 1997–2004.

production well fields (fig. 45). Overall model performance for groundwater levels during the verification period was within defined water-level ME and RMSE calibration criteria (table 8). Hydrographs of weekly average simulated and observed groundwater levels for the 112 groundwater monitoring locations for the warmup, calibration, and verification periods are included in appendix 5.

There is more than a 1-ft difference in water-table elevations between the driest (1996) and wettest (2005) years throughout urban parts of the study area (figs. 46 and 47). Decreased water-table elevations near production well fields are more pronounced in the driest years of the simulation period (fig. 46). Furthermore, the effect of the canal system and surface-water control structures on water-table elevations is evident in both the driest and wettest years of the simulation period (figs. 46 and 47); in particular, the salinity control structures maintain water-table elevations at the coast during the dry season (figs. 46B and 47B).

## Groundwater Boundary Fluxes

Simulated net groundwater recharge (the sum of rainfall, agricultural water demand, recreational irrigation, septic return flow to the water table, and actual evapotranspiration) in onshore areas of the calibrated model averaged 27 in/yr (2,208 ft<sup>3</sup>/s) and 26 in/yr (2,122 ft<sup>3</sup>/s) during the calibration and verification periods, respectively (fig. 48). In the urban parts of the study area, simulated net groundwater recharge averaged 41 in/yr (1,672 ft<sup>3</sup>/s) and 42 in/yr (1,701 ft<sup>3</sup>/s) during the calibration and verification periods, respectively. Rainfall generally exceeds the sum of agricultural water use and evapotranspiration in urban areas of the study area, indicated by positive net groundwater recharge. In contrast, evapotranspiration exceeds rainfall in WCA3, parts of ENP, and the southern Glades, indicated by negative net groundwater recharge.

Simulated calibrated model boundary outflow, which is the sum of GHB and drain flow, in onshore areas exceeded inflow and averaged -1 in/yr (-87 ft<sup>3</sup>/s) and -8 in/yr (-666 ft<sup>3</sup>/s) during the calibration and verification periods, respectively. GHB flow exceeded drain flow by a factor of 1.8 and 13.6, respectively, during the calibration and verification periods. GHBs were a source of water in eastern parts of WCA3 adjacent to the L-30 Levee and L-30 Canal, near the L-29 Canal between WCA3 and ENP, and in northeastern parts of ENP adjacent to the L-31N Levee and Canal during the calibration and verification periods (fig. 49). General-head and drain boundaries discharge groundwater in Biscayne Bay, Florida Bay, and parts of the southern Glades near the southern end of the L-31W Canal during the calibration and verification periods (fig. 49).

## Water Budgets

Basin and subbasin water budget components were evaluated using model-derived surface-water and groundwater model flows. The simulation results quantified components of the water budget that have not been directly measured, focusing on the exchange between the canals and the Biscayne aquifer, groundwater seepage from WCA3 and ENP, and groundwater discharge to the coast. Simulated water budgets were calculated by accumulating surface-water and groundwater flow terms in the urban portion of the study area (fig. 50). The Model Land Basin was not included in the simulated water budgets. The C-111 Basin downstream of S177 and S178 was also excluded from the simulated water budgets.

Simulated surface-water budgets were calculated by accumulating rainfall, evaporation, and surface-water runoff terms for each reach group, which can include reaches in more than one groundwater cell, and canal seepage and leakage terms for each reach in the urban portion of the study area. Simulated groundwater budgets were calculated using ZONEBUDGET (Harbaugh, 1990) and a combination of cell-by-cell and individual boundary condition data. Because the surface-water and groundwater budget terms are accumulated differently, there are some differences between canal seepage and leakage terms in the two budgets.

The surface-water control volume was defined as the area between inflow and salinity surface-water control structures, and the groundwater control volume was defined as the area containing the surface-water control basins discretized using the groundwater model grid. Differences in the surface-water and groundwater control volumes also contribute to differences in calculated seepage and leakage terms between the two water budgets. The extent of the surface-water control volume is larger than the groundwater control volume and includes reach groups adjacent to WCA3, ENP, and salinity-control structures, which generally have high canal seepage and (or) leakage rates.

## Urban Area

The difference between canal seepage and canal leakage in the urban parts of the study area upstream from the salinity control structures exceeded surface-water inflow to the urban parts of the study area by a factor of 6.49 and 4.09 during the calibration and verification periods, respectively (fig. 51). In this instance, the urban area inflow refers to the flow into the C-1, C-4, C-6, C-9, C-102, C-103, and C-111 Basins through the S30, S31, G119, S338, S194, S196, and S176 structures. The predominance of canal-aquifer exchange indicates that most of the surface-water outflow discharging through the salinity control structures is derived from

**Table 14.** Surface-water discharge observation locations, data source, number of daily observations, and model-fit statistics.

[All data are from the South Florida Water Management District DBHYDRO database. SWR, surface-water routing; --, data not available; %, percent]

Station	Upstream		Downstream		Calibration period (1997–2004)				Verification period (2005–10)			
	SWR Process reach	SWR Process reach	SWR Process reach	SWR Process reach	Number of weekly observations	Normalized mean error	Normalized root mean square error	Nash-Sutcliffe model efficiency	Number of weekly observations	Normalized mean error	Normalized root mean square error	Nash-Sutcliffe model efficiency
S30	1964	1963			366	-0.01	0.05	0.86	272	-0.00	0.01	0.92
S29	2080	2081			366	-0.02	0.06	0.79	274	-0.01	0.05	0.84
S28	2150	2151			366	0.01	0.05	0.79	274	0.05	0.10	0.70
G72	261	260			365	0.00	0.01	0.80	267	0.00	0.00	0.00
S27	2179	2180			366	0.02	0.07	0.55	274	0.18	0.22	-0.28
S151	5	6			366	0.03	0.04	0.74	274	0.05	0.07	0.72
S31	24	25			366	-0.01	0.04	0.91	274	-0.02	0.05	0.88
S26	395	396			366	0.00	0.08	0.70	274	-0.02	0.09	0.78
S25	1735	1736			366	0.01	0.06	0.74	274	-0.00	0.06	0.74
S336	1177	1201			366	-0.04	0.18	0.20	274	0.01	0.09	0.23
G119	1206	1213			358	-0.01	0.04	0.88	256	-0.02	0.10	0.69
S380	1219	1220			24	0.23	0.43	0.08	274	-0.10	0.18	0.39
S25B	409	408			366	-0.00	0.05	0.77	274	0.01	0.05	0.84
G93	466	467			366	0.02	0.07	0.53	274	0.03	0.10	0.61
S22	1685	1686			364	0.02	0.06	0.83	274	0.02	0.05	0.86
S337	30	29			363	-0.03	0.08	0.82	274	-0.01	0.07	0.82
S335	1136	1135			366	-0.02	0.10	0.69	274	-0.09	0.13	0.55
S334	1180	1179			366	-0.03	0.10	0.76	274	-0.07	0.13	0.65
S338	1061	1062			366	-0.09	0.15	0.56	274	-0.11	0.16	0.63
S148	1104	795			366	-0.03	0.09	0.76	266	-0.02	0.06	0.87
S149	759	758			--	--	--	--	100	-0.03	0.11	0.64
S21	1545	1546			366	0.03	0.09	0.55	274	0.05	0.12	0.65
S121	675	676			366	-0.00	0.05	0.58	274	0.00	0.00	0.00
S120	724	723			366	-0.01	0.07	0.65	274	-0.03	0.10	0.62
S119	695	696			366	-0.01	0.05	0.74	270	-0.01	0.08	0.70
S118	1566	1565			366	-0.00	0.03	0.79	270	0.01	0.09	0.74
S122	752	753			366	0.00	0.00	0.00	274	0.00	0.00	0.00
S123	1627	1628			366	0.00	0.04	0.68	274	0.01	0.05	0.75
S194	964	965			366	0.08	0.16	0.43	274	0.04	0.12	0.71

**Table 14.** Surface-water discharge observation locations, data source, number of daily observations, and model-fit statistics.—Continued

[All data are from the South Florida Water Management District DBHYDRO database. SWR, surface-water routing; --, data not available; %, percent]

Station	Upstream		Downstream		Calibration period (1997–2004)				Verification period (2005–10)			
	SWR Process reach	SWR Process reach	SWR Process reach	SWR Process reach	Number of weekly observations	Normalized mean error	Normalized root mean square error	Nash-Sutcliffe model efficiency	Number of weekly observations	Normalized mean error	Normalized root mean square error	Nash-Sutcliffe model efficiency
S195	1024		1023		361	-0.02	0.07	0.70	274	-0.01	0.05	0.73
S165	990		991		366	0.01	0.05	0.79	269	0.01	0.05	0.81
S21A	1010		1011		366	0.01	0.04	0.69	274	0.03	0.06	0.52
S20G	1541		1542		366	0.00	0.05	0.77	274	0.01	0.04	0.69
S196	916		915		366	0.19	0.33	-0.19	274	0.12	0.31	0.23
S166	863		862		366	0.01	0.05	0.64	274	-0.01	0.10	0.66
S167	901		900		366	0.01	0.05	0.71	274	0.02	0.07	0.64
S179	846		845		366	0.01	0.07	0.74	274	0.00	0.03	0.83
S20F	1531		1532		366	0.03	0.08	0.59	274	0.04	0.07	0.60
S20	2324		2323		314	0.02	0.08	0.38	221	0.05	0.16	0.14
S174	1418		1419		366	-0.06	0.17	0.56	267	0.00	0.03	0.92
S175	1444		1445		366	0.00	0.03	0.84	274	-0.00	0.04	0.54
G211	1057		1056		366	-0.01	0.10	0.68	274	-0.07	0.20	0.33
S331 and S173	1043		1042		366	-0.01	0.02	0.93	274	-0.01	0.03	0.90
S176	1276		1277		366	0.00	0.04	0.75	274	0.01	0.07	0.74
S177	1311		1312		366	-0.00	0.03	0.87	274	0.01	0.04	0.83
S178	1342		1341		366	0.03	0.15	-0.76	274	0.23	0.47	-1.71
S18C	1357		1358		366	0.00	0.06	0.74	274	0.07	0.11	0.39
S197	1405		1406		366	0.00	0.03	0.78	274	0.01	0.04	0.71
DBL2	54		55		350	0.14	0.22	0.09	274	0.12	0.26	0.36
Global average						0.01	0.08	0.61		0.01	0.10	0.55
Percentage of observations satisfying calibration criteria						94%	94%	83%		90%	90%	76%

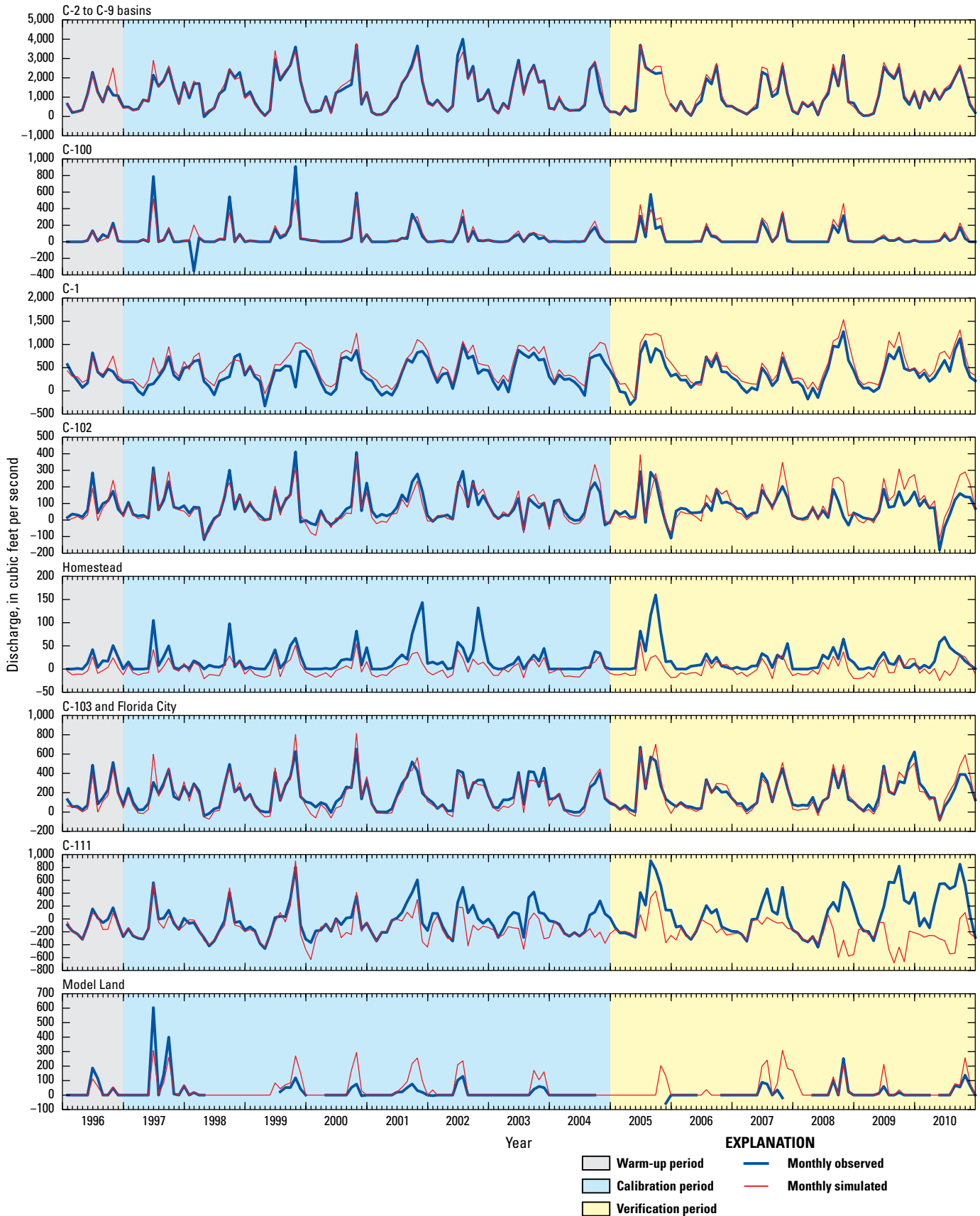


**Figure 43.** Net surface-water subbasin discharge differences between measured and model-simulated values for select surface-water basins in the urban area of the model domain, 1997–2004.

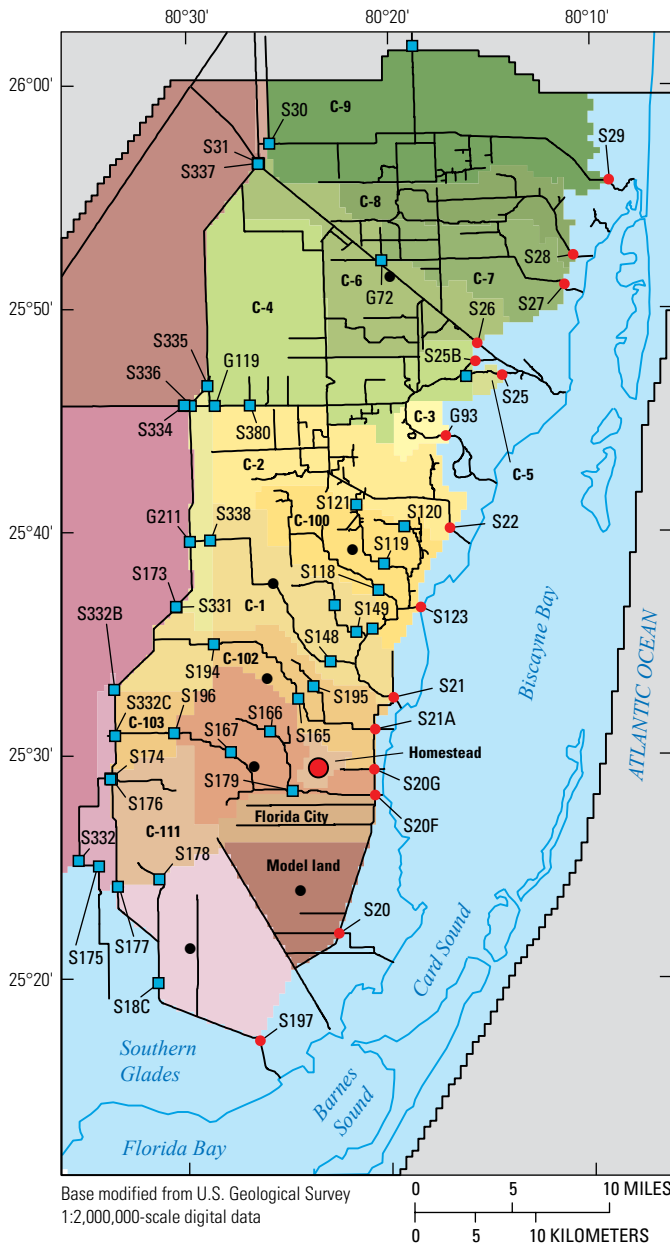


**Figure 44.** Normalized average net surface-water subbasin discharge differences between measured and model-simulated values results for select surface-water subbasins, 1997–2004.

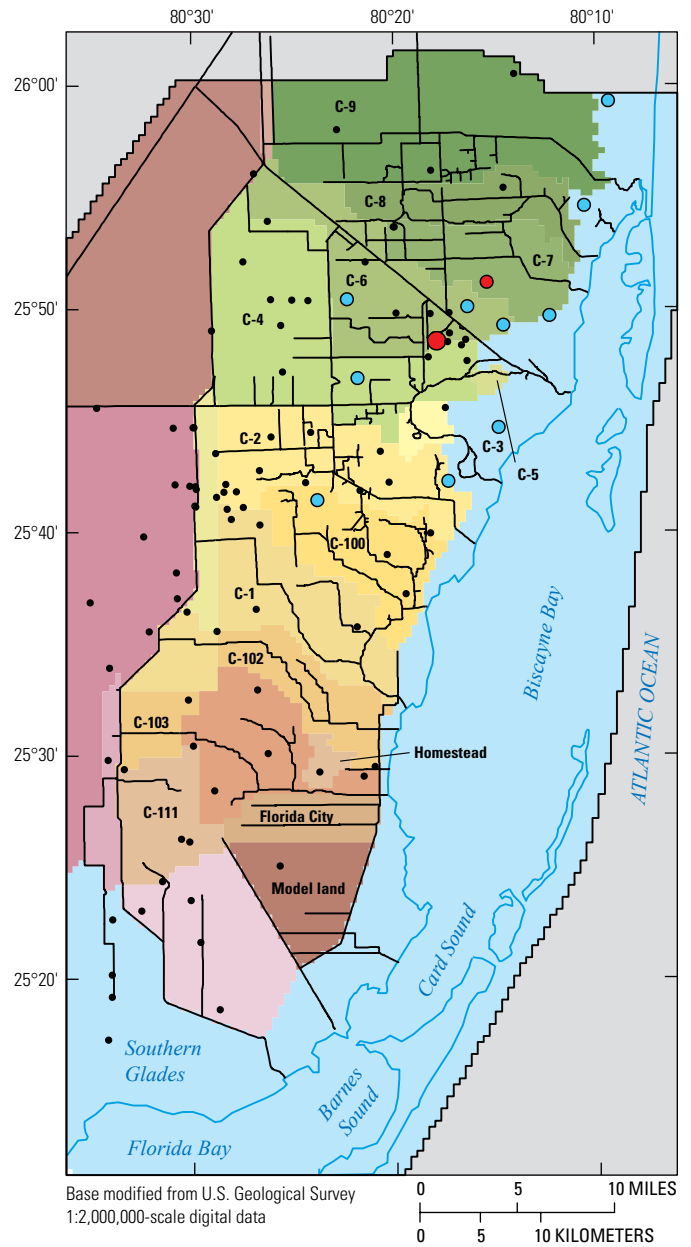


**Figure 45.** Mean differences between measured and model-simulated groundwater levels, 1997–2004.

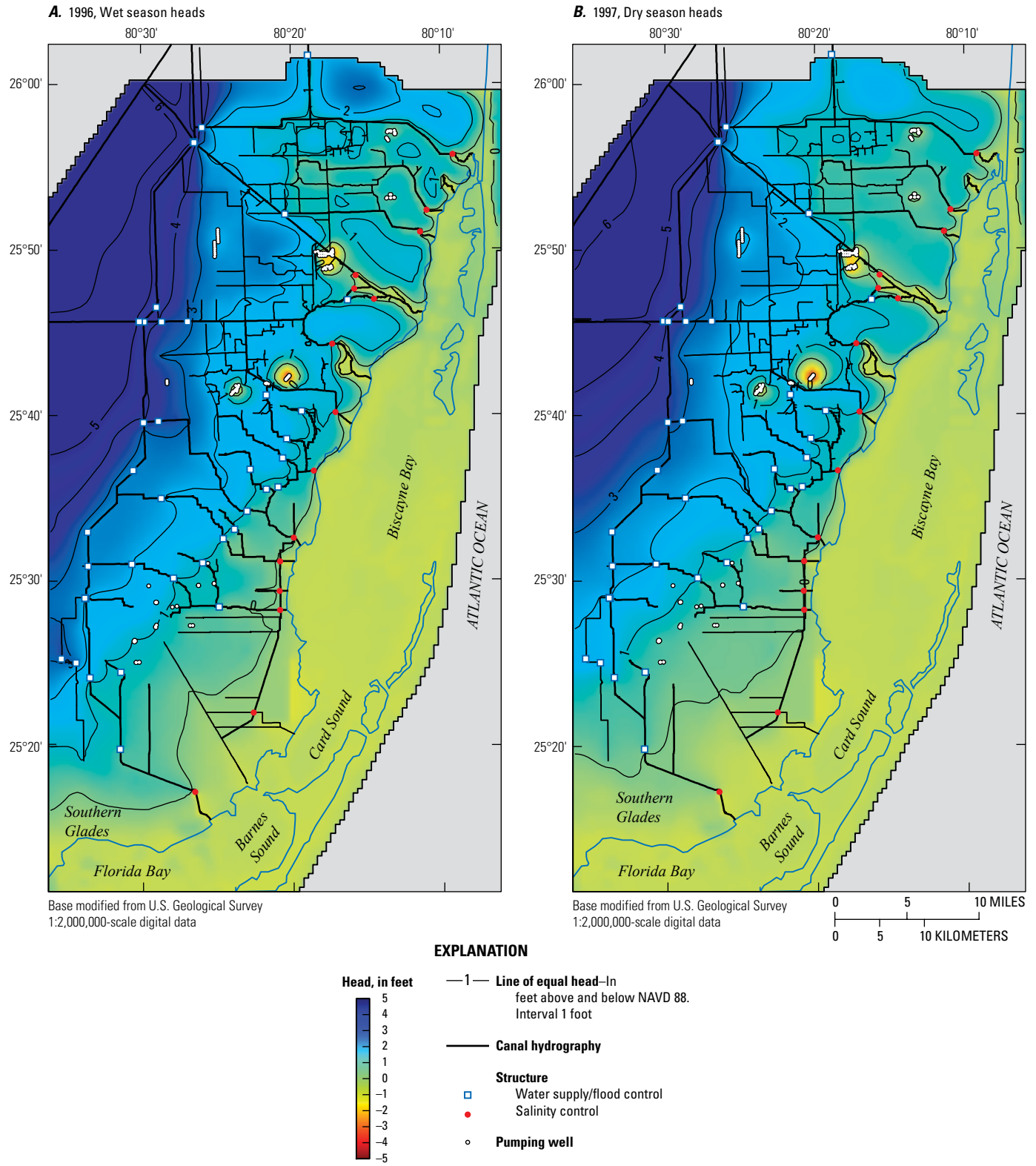


Figure 46. Simulated water-table elevation for, A, October 1996 and, B, May 1997.

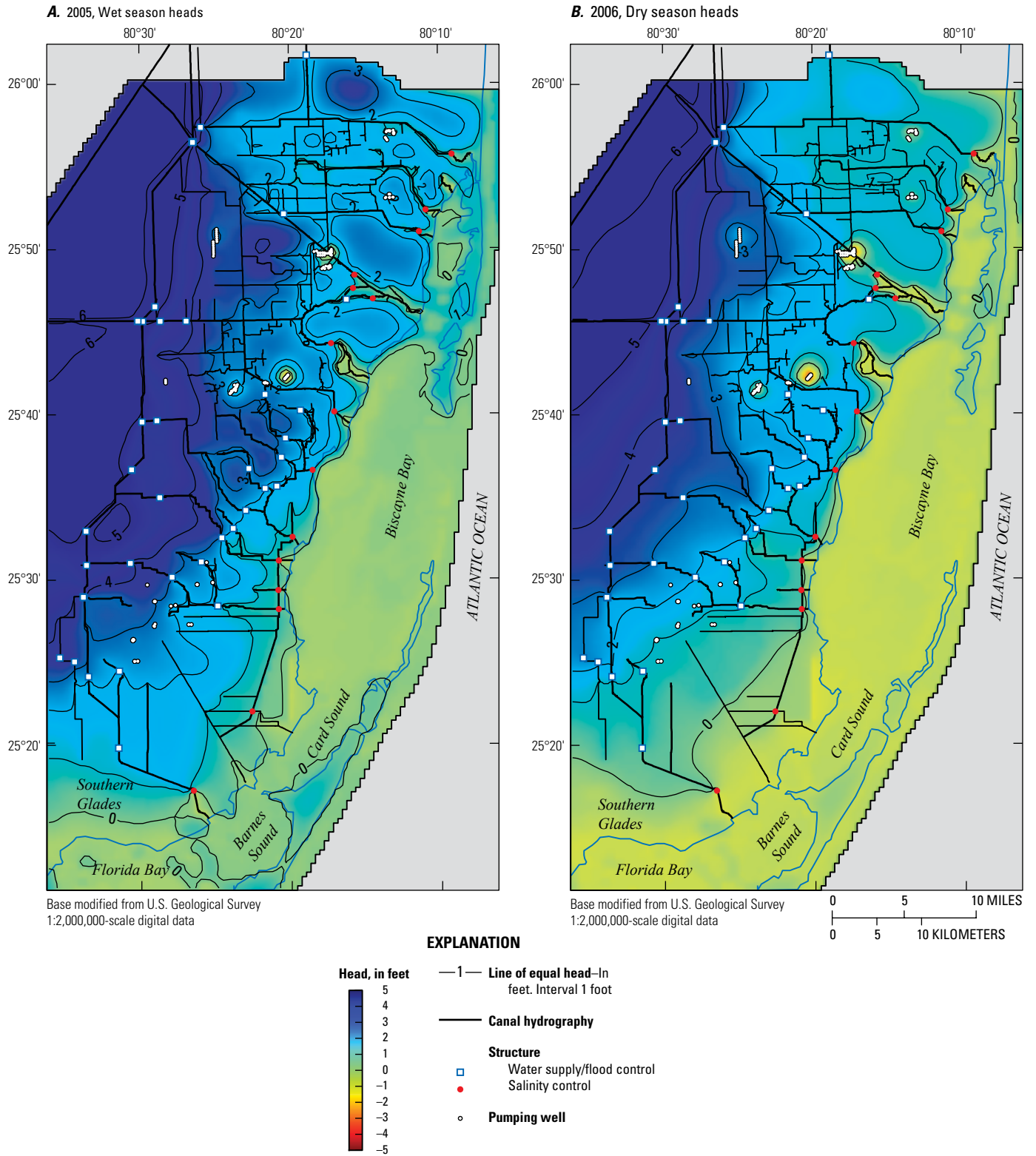


Figure 47. Simulated water-table elevation for, A, October 2005 and, B, May 2006.

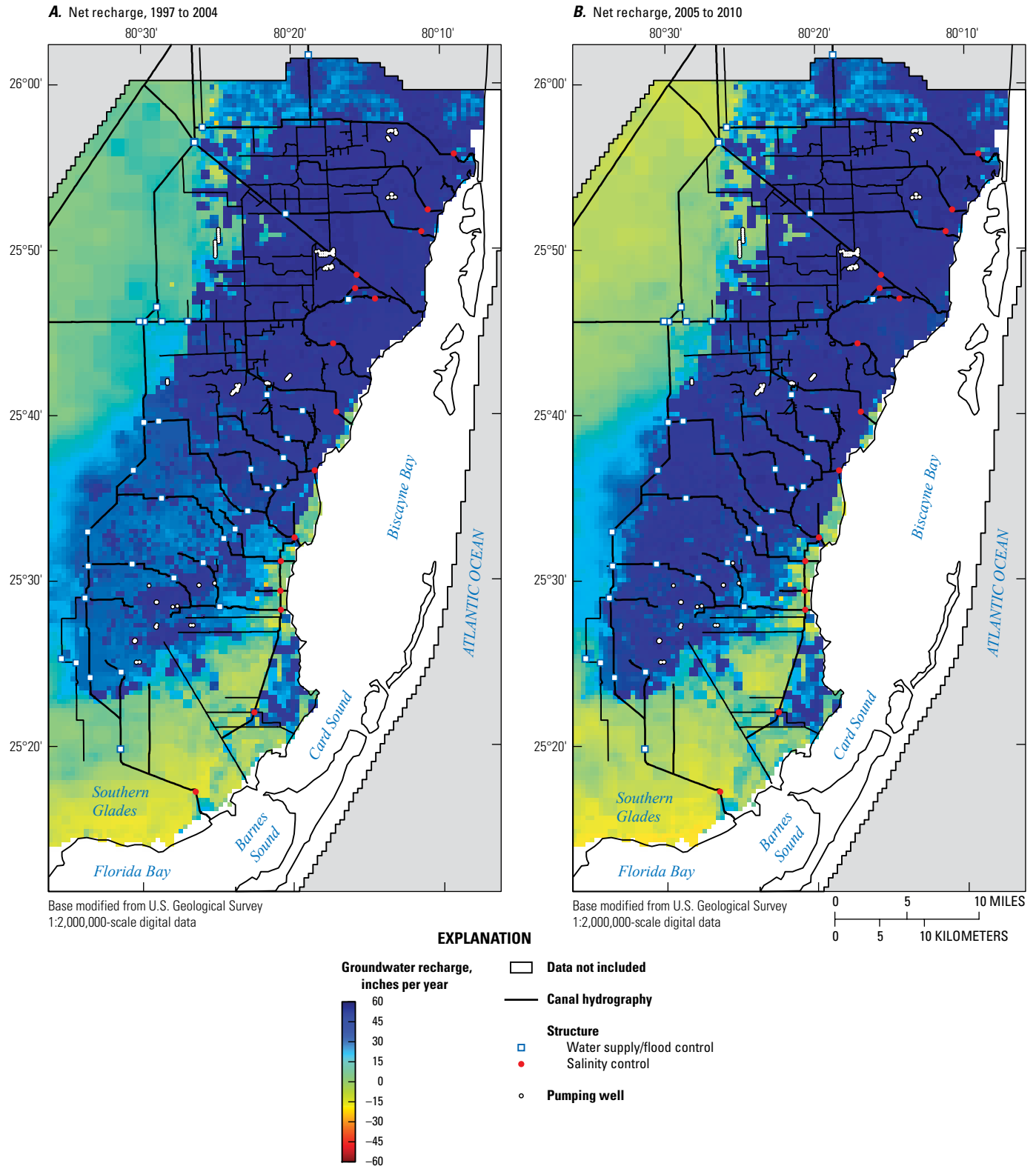
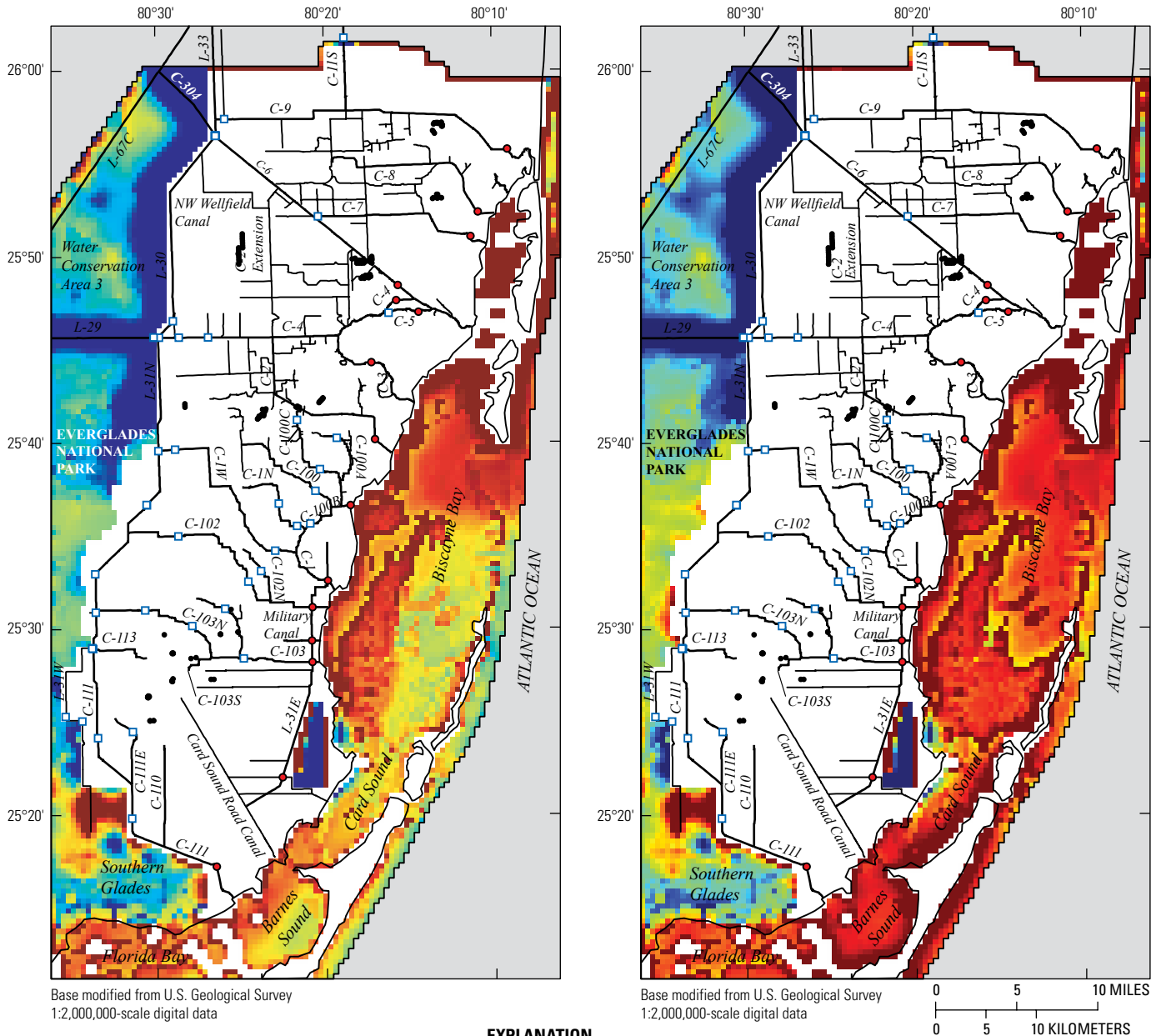


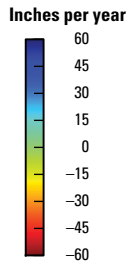
Figure 48. Simulated net groundwater recharge for the, A, calibration (1997–2004) and, B, verification (2005–2010) periods.

**A.** Net boundary flow, 1997 to 2004

**B.** Net boundary flow, 2005 to 2010



**EXPLANATION**



- Data not included
- Canal hydrography
- Structure**
  - Water supply/flood control
  - Salinity control
- Pumping well

**Figure 49.** Simulated net groundwater general head boundary and drain fluxes for the, *A*, calibration (1997–2004) and, *B*, verification (2005–2010) periods.

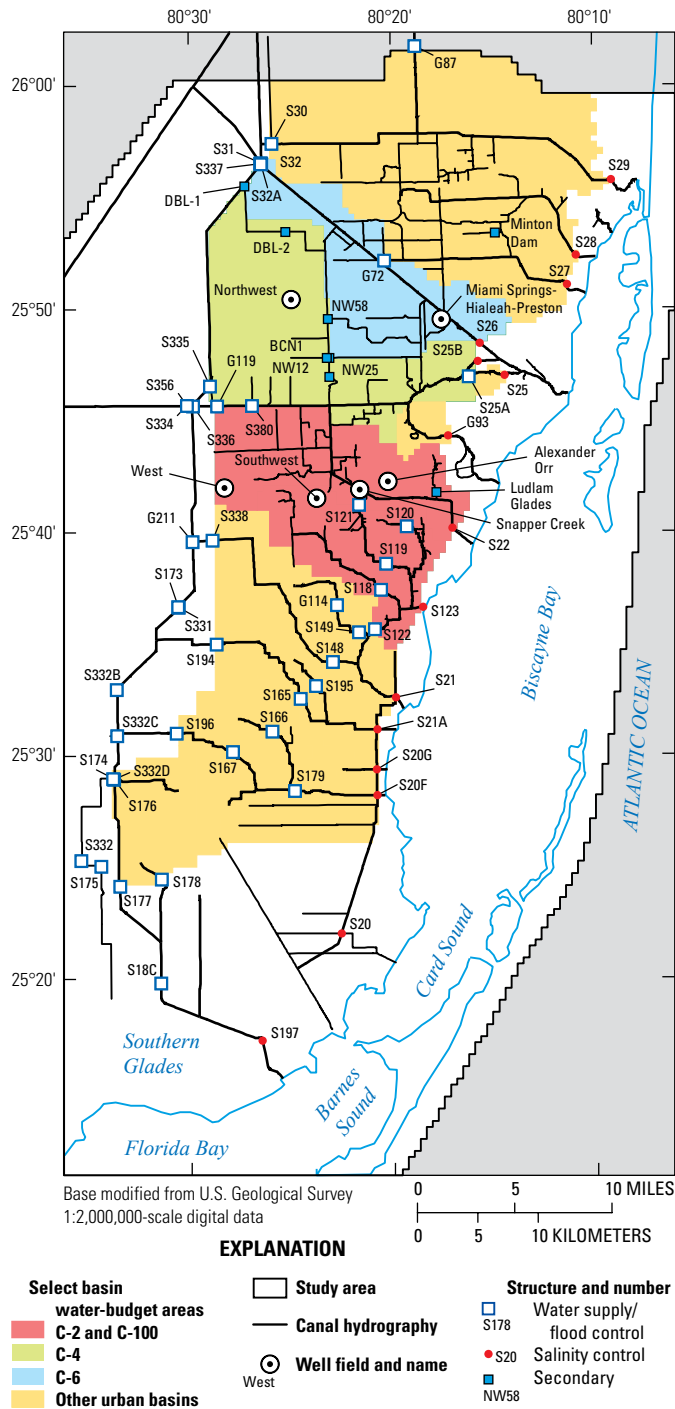


**Figure 50.** Urban surface-water and groundwater water budget area. Select water budget areas in the C-2 and C-100, C-4, and C-6 Basins are also shown.

urban parts of the study area and that, on average, the canals are draining the Biscayne aquifer. In this case, the difference between canal seepage and canal leakage represented 77 and 73 percent of the surface-water outflow through the salinity control structures during the calibration and verification periods, respectively.

Groundwater inflow to the urban area exceeded surface-water inflow to the urban area into the C-1, C-4, C-6, C-9, C-102, C-103, and C-111 Basins by factor of 2.49 (638 ft<sup>3</sup>/s / 256 ft<sup>3</sup>/s) and 1.58 (629 ft<sup>3</sup>/s / 397 ft<sup>3</sup>/s) during the calibration and verification periods, respectively (fig. 52). Although groundwater inflow to the urban area of the model domain exceeded surface-water inflow, the majority of surface-water outflow discharging through the salinity control structures was derived from local rainfall. The difference between net canal-aquifer exchange (the difference between canal seepage and canal leakage) for the Biscayne aquifer in the urban part of the study area and the net groundwater inflow and outflow from the urban area was about twice the net surface-water flow discharging through the salinity control structures. Specifically, net groundwater inflow and outflow equaled 50.45 and 50.41 percent of the net surface-water flow during the calibration and verification periods, respectively.

The net canal-aquifer exchange for the Biscayne aquifer was -1,427 and -1,409 ft<sup>3</sup>/s during the calibration and verification periods, respectively (fig. 52). Differences between canal and Biscayne aquifer water budgets represent the additional canal seepage and leakage occurring between the edges of the groundwater control volume and upstream and downstream surface-water control structures in the urban area of the model domain. The difference between net groundwater boundary flow and net canal-aquifer exchanges are opposite in sign but roughly equivalent in magnitude (fig. 52). In this instance, net groundwater boundary flow is the difference between groundwater boundary inflow and outflow. Groundwater boundary inflow includes rainfall, recreational irrigation, and septic return flow to the water table, whereas groundwater boundary outflow includes agricultural water demand, and actual evapotranspiration. Municipal groundwater pumpage was 23 and 25 percent of canal leakage and 92 and 96 percent of groundwater inflow to urban parts of the study area during the calibration and verification periods, respectively.

Groundwater outflow from the urban area ranged from 7.7 to 6.5 percent of the surface-water outflow from the salinity control structures during the calibration and verification periods, respectively. Most of the groundwater outflow from the urban area ultimately discharges to the coast, and it is nearly equal to the quantity of fresh groundwater discharge to Biscayne Bay. Langevin (2001) estimated fresh groundwater discharge to be approximately 6 percent of the total surface-water discharge to Biscayne Bay.

### Selected Surface-Water Basins

Groundwater budgets were calculated for the combined C-2 and C-100 Basins, the C-4 Basin, and the C-6 Basin because all of the major MDWASD well fields are within these basins (fig. 50). The Alexander Orr, Snapper Creek, Southwest, and West well fields are in the combined C-2 and C-100 Basins. The Northwest well field (NW58) is in the C-4 Basin and the Miami-Springs, Hialeah, and Preston well fields are in the C-6 Basin.

Canal seepage exceeded canal leakage in the combined C-2 and C-100 Basins, C-4 Basin, and C-6 Basin during the calibration and verification periods (tables 15 and 16). Canal seepage also exceeded canal leakage in the urban parts of the study area during the calibration and verification periods. In the C-2 and C-100 Basins, groundwater pumpage from the Alexander Orr, Snapper Creek, Southwest, and West well fields was 42 and 43 percent of the sum of local sources of inflow to the basins (net groundwater recharge and canal leakage) during the calibration and verification periods, respectively. In the C-4 and C-6 Basins, groundwater pumpage from MDWASD well fields was 13 and 14 percent and 26 and 27 percent of the sum of local sources of groundwater inflow to the basins during the calibration and verification periods, respectively. Differences between well-field pumpage and simulated groundwater inflows were less than values calculated in other studies (for example, Parker and others, 1955; Meyer, 1972; Miller, 1978; Sunderland and Krupa, 2007), but those studies did not evaluate the groundwater budget for the entire surface-water basin containing the well field of interest. Overall, groundwater pumpage represented 13 percent of the sum of local sources of inflow to the urban parts of the study area during the calibration and verification periods.

### Freshwater-Seawater Interface

Changes in the position of the freshwater-seawater interface at the base of the Biscayne aquifer were minor during the simulation period (fig. 53); such movement was consistent with the changes observed between 1984 and 1996.

Changes in the position of the freshwater-seawater interface at the bottom of model layers 1 and 2 during the simulation period were minor. In both model layers, the freshwater-seawater interface at the end of the dry season for 1997 (the driest year in the simulation) was landward of its position at the end dry season for 2006 (the wettest year in the simulation) (fig. 53).

The simulated position of the freshwater-seawater interface was at, or seaward of, the salinity control structure in model layer 1 at the end of the 1997 and 2006 dry seasons. In model layer 2 and at the base of the Biscayne aquifer (model layer 3), the simulated position of the freshwater-seawater interface was landward of the S29, S28, S27, S21, S21A, S20G, S20F, S20, and S197 salinity control structures at the end of the 1997 and 2006 dry seasons.

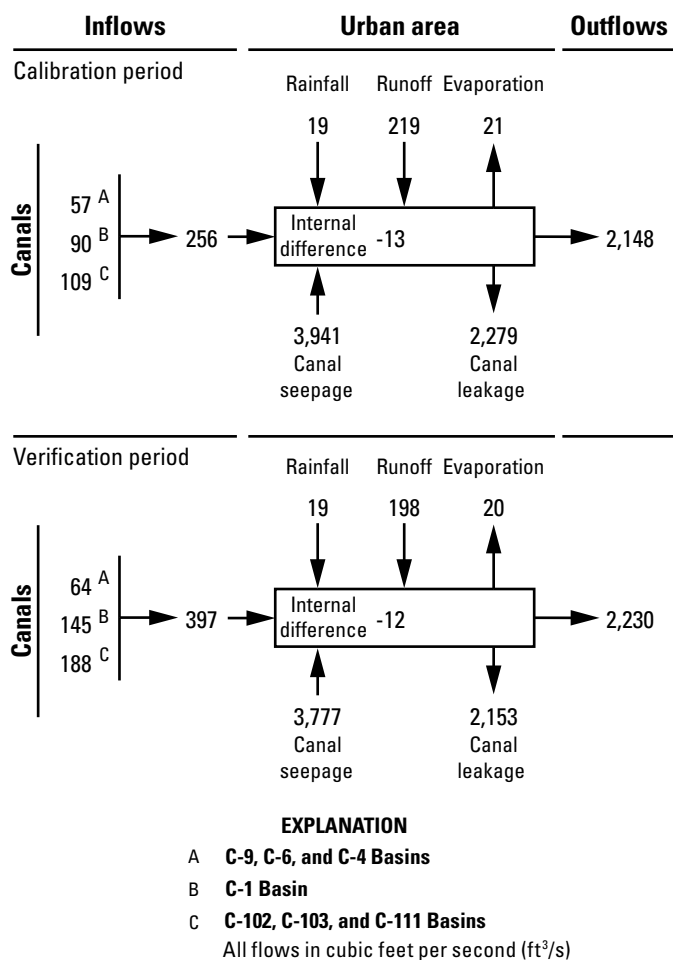


Figure 51. Simulated canal water budgets for urban area of the model domain.

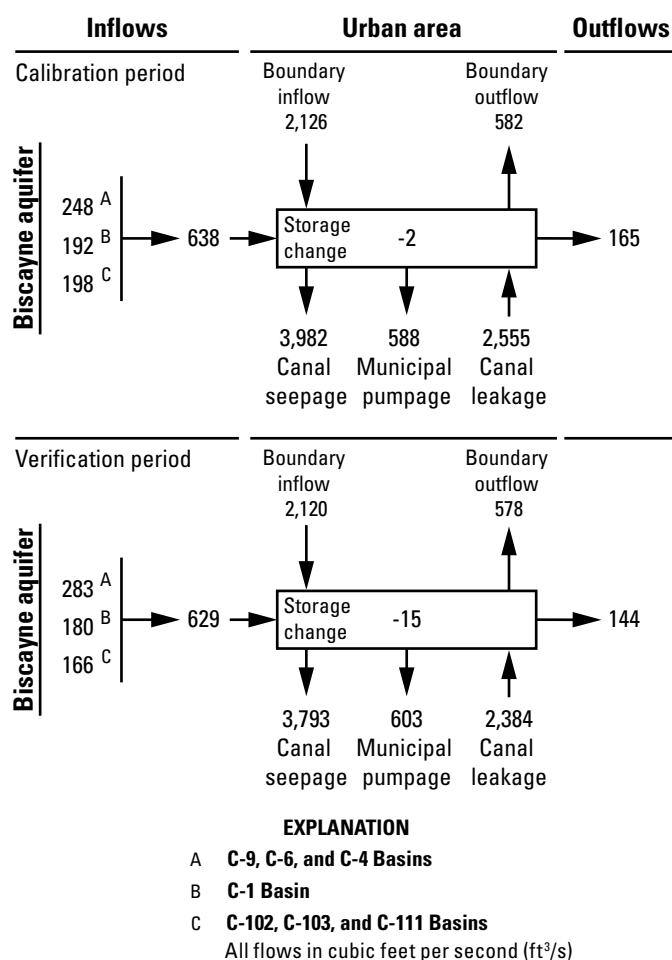


Figure 52. Simulated groundwater budgets for the urban area of the model domain.

## Response of the System to Increased Groundwater Pumpage and Sea Level

The response of the canal system and the underlying Biscayne aquifer in the Miami-Dade County urban area to increased groundwater pumpage, increased sea level, and a combination of both, were evaluated by simulations made using a version of the calibrated model that was modified to represent potential future conditions. A 30-year period of time was simulated. The base-case future climatic conditions were simulated by repeating the NEXRAD rainfall and reference evapotranspiration data from the calibrated model for 1996 through 2010 twice during the scenario simulation period. Land-use data from 2008 were used to develop direct surface-water runoff, agricultural water demand, recreational irrigation, and monthly crop coefficient values that were, in turn, used as input parameters in the base-case future scenarios. Estimated septic return flow data for 2010 were used for the entire base-case future scenario simulation period. Historical effective gate opening data were used during the base-case future scenario simulation period, and it was assumed that the structures would be operated identically under the same hydrologic conditions. NEXRAD rainfall, reference evapotranspiration, and historical effective gate opening data were used twice in a repeating pattern to define boundary-condition data for the entire 30-year base-case future scenario simulation period.

Base-case future scenarios of groundwater pumpage for MDWASD production well fields were based on current, permitted groundwater pumping rates (Virginia Walsh, Miami Dade Water and Sewer Department, written commun., 2013); base-case future groundwater pumping rates for MDWASD well fields exceeded actual annual groundwater use. The base-case groundwater pumping rate for each well field (table 17) was distributed equally to each production well in the well field. A constant pumping rate was used for each well during the base-case future scenario simulation period. Reported monthly pumping rates for 2010 were used for all other production wells in the model domain.

The coastal boundary condition for the scenarios was developed using average daily predicted tides for Virginia Key. The tide values were predicted from hourly data calculated using the NTP4 program developed by the National Ocean Service (Zetler, 1982) and harmonic constituents for the Virginia Key tidal gage.

Historical tidal data collected from 1913 to 2006 at Key West indicate that sea level has been increasing and global climate model simulation results indicate sea level may increase more rapidly in the future (Southeast Florida Regional Climate Change Compact Technical Ad hoc Work Group, 2011). The U.S. Army Corps of Engineers (2011) has developed the following equation for sea-level change, which accounts for linear and nonlinear components and has been applied by others in southern Florida (for example, Southeast Florida Regional Climate Change Compact Technical Ad hoc Work Group, 2011):

**Table 15.** Simulated groundwater budget for selected basins during the calibration period.

[All values are in cubic feet per second]

Basin	Lateral groundwater flow		External boundaries		Canal exchanges		Municipal pumpage	Storage change
	Inflow	Outflow	Inflow	Outflow	Seepage	Leakage		
C-2 and C-100	179	96	327	38	402	286	257	0
C-4	220	147	335	189	702	621	122	-16
C-6	176	89	218	41	377	230	116	-2
Urban area	738	265	2,126	582	3,982	2,555	588	-4

**Table 16.** Simulated groundwater budget for selected basins during the verification period.

[All values are in cubic feet per second]

Basin	Lateral groundwater flow		External boundaries		Canal exchanges		Municipal pumpage	Storage change
	Inflow	Outflow	Inflow	Outflow	Seepage	Leakage		
C-2 and C-100	186	95	323	36	410	297	266	-1
C-4	260	128	354	177	728	558	124	-15
C-6	162	96	227	40	366	243	127	-3
Urban area	734	248	2,119	578	3,793	2,384	603	-12

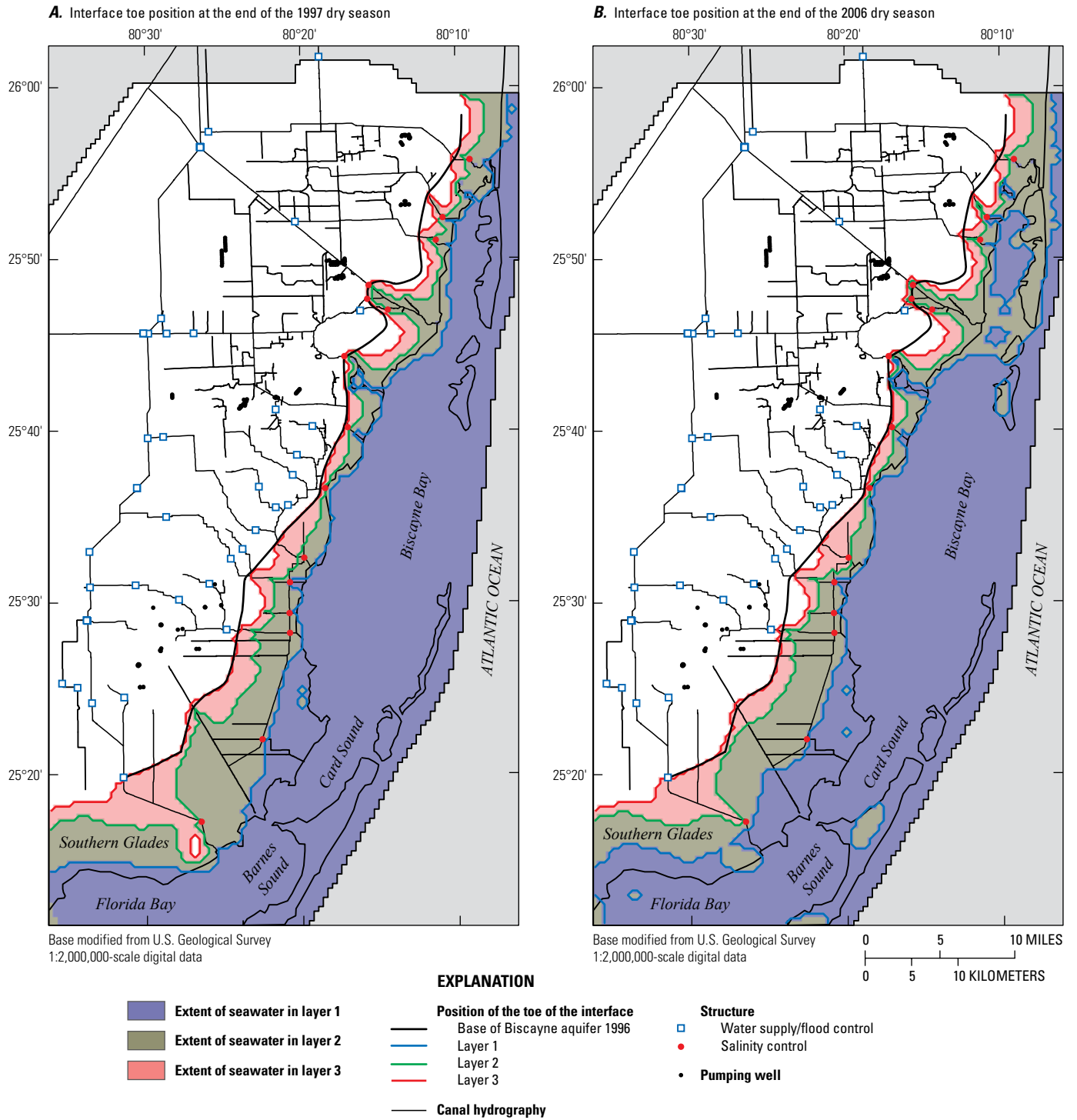


**Figure 53.** Simulated position of the freshwater-seawater interface in, *A*, May 1997 and, *B*, May 2006. The mapped position of the freshwater-seawater interface at the base of the Biscayne aquifer in 1996 (Sonenshein, 1997) is shown for reference.

$$\Delta s = SLR_L t + SLR_N t^2, \tag{27}$$

where

- $SLR_L$  is a linear sea-level rise rate constant [L/T],
- $t$  is number of years since 1992 [T], and
- $SLR_N$  is a nonlinear constant that depends on the National Research Council sea-level curve (National Research Council, 1987) [LT<sup>-2</sup>].

For southern Florida,  $SLR_L$  is equal to 0.0073 foot per year (ft/yr). For the future sea-level rise scenarios, the sea-level change applied to average daily predicted tides ( $\Delta s$ ) is calculated as

$$\Delta s(t - t_0) = \Delta s(t) - \Delta s(t_0) + \Delta w, \tag{28}$$

where

- $t_0$  is based on the starting year of the simulated scenarios (2011) and
- $\Delta w$  is the difference between predicted and observed average daily tides [L].

The historical difference between the predicted and observed average daily tide,  $\Delta w$ , for the 15-year period from 1996 through 2010 was added to equation 28 to account for meteorological forcing effects (such as wind forcing) on tides; calculated daily data for meteorological forcing effects were used twice in a repeating pattern to define meteorological forcing effects for the entire 30-year scenario simulation period. In the base-case future scenario, Virginia Key tidal stage was calculated using the current rate of sea-level rise, an  $SLR_N$  value equal to zero, and calculated daily meteorological forcing effects; sea level in the base-case future scenario increases from an annual average stage of -1.13 to -0.63 ft NAVD 88 (a 0.50-ft increase) during the 30-year scenario simulation period (fig. 54).

Land-surface elevations in a small southern part of the onshore study area are below the average observed stage at Virginia Key (-0.72 ft NAVD 88) during the calibration and verification periods (fig. 55A). A larger part of the onshore study area in the southern Glades, the Model Land Basin, and seaward of some salinity control structures is below the maximum observed stage at Virginia Key (0.64 ft NAVD 88) during the calibration and verification periods (fig. 55A). After 30 years, onshore areas below the average (-0.62 ft NAVD 88) and maximum (0.81 ft NAVD 88) calculated stage at Virginia Key are more extensive in the southernmost part of the study

**Table 17.** Base and increased Miami-Dade Water and Sewer Department future groundwater pumpage rates.

[All values are in millions of gallons per day]

Well field	Base rate	Increased groundwater pumpage rates			
		2016	2020	2025	2030
Hialeah	3.1	3.1	3.1	3.1	3.1
Preston	37.2	37.2	37.2	37.2	37.2
Miami Springs	29.7	29.7	29.7	29.7	29.7
Northwest	85.4	85.4	85.4	85.4	85.4
Alex Orr	40	40	40	40	40
Snapper Creek	21.9	21.9	21.9	21.9	21.9
Southwest	109.4	109.4	109.4	123.92	137.28
West	15	15	15	15	15
Leisure City	1.6	0	0	0	0
Naranja	0.1	0	0	0	0
Elevated Tank	1.3	0	0	0	0
Everglades Labor	2.2	2.2	2.2	0	0
Newton	2.6	2.6	2.6	0	0
South Miami Heights	0	3	3	3	3
Total	349.5	349.5	349.5	359.22	372.58

area, given the current rate of sea-level rise and calculated daily meteorological forcing effects (fig. 55B).

EDEN data were used in the scenarios to define GHB stages in WCA3 and ENP, except where the EDEN stage in a cell was less than the calculated Virginia Key stage with the current rate of sea-level rise and calculated daily meteorological forcing effects. EDEN stage data from 1996 through 2010 were repeated twice during the scenario simulation period. Use of the EDEN stage data assumes that sufficient water would be available from external sources to maintain historical stages in WCA3 and ENP. Delaunay triangulation (de Berg and others, 2008) was used to fill gaps in the southern Glades between the EDEN stage dataset and base-case sea-level data.

All of the scenarios evaluated used initial conditions extracted from the end of the verification period (December 31, 2010). Initial conditions extracted from the calibrated model include simulated groundwater levels in model layers 1 to 3, simulated SWR1 reach stages, and simulated freshwater-sea-water interface elevations in model layers 1 to 3.

Simulated groundwater budget items for the base-case future scenario in the combined C-2 and C-100 Basins, the C-4 Basin, the C-6 Basin, and urban parts of the study area (table 18) were within ±20 percent of groundwater budgets items calculated for the calibration (table 15) and verification periods (table 16). Allocated municipal pumpage in the urban parts of the study area was approximately 3 to 6 percent greater than reported groundwater pumpage during the calibration and verification periods. Differences in municipal pumpage have resulted in corresponding differences in lateral groundwater flow and canal seepage, when compared to groundwater budgets for the calibration and verification periods.

The surface-water inflow into urban areas of the study area through the S30, S31, G119, S338, S194, S196, and S176 structures and outflow through the salinity control structures were 338 and 2,280 ft<sup>3</sup>/s in the base-case future scenario, respectively. These flows represent a 1-ft<sup>3</sup>/s decrease and 51-ft<sup>3</sup>/s increase relative to the corresponding inflow and outflow, respectively, during the 1996 through 2010 simulation period. Both differences are partially a result of the following in the base-case future scenario: (1) linearly increasing sea-level elevations, which result in additional canal seepage, and

(2) the combined use of datasets derived from 2008 land-use data and allocated rather than observed groundwater pumping rates. The surface-water inflow and outflow from the urban areas in the base-case future scenario was less than 1 percent, and approximately 2 percent different, respectively, than during the 1996 through 2010 simulation period.

The water table was less than 0.5 ft below land surface in 5,565 onshore model cells (537.16 mi<sup>2</sup>) in the base-case future scenario during the 30th year of the simulation period. In flood-prone areas, the average water-table depth was less than 0.5 ft below land surface 75 percent of the year. The water table was less than 0.5 ft below land surface in the base-case future scenario more than 25 percent of the time in WCA3, ENP, the southern Glades, the Model Land Basin, and just west of WCA3 (fig. 56A).

### Increased Groundwater Pumpage (Scenario 1)

In scenario 1, Southwest well field pumpage was increased relative to the base-case future scenario in 2025 and 2030, the proposed South Miami Heights well field was brought online in 2016, and pumpage was reduced at the Naranja, Elevated Tank, Everglades, and Newton well fields (fig. 18, table 17). The extent of the proposed South Miami Heights well field includes two model grid cells; groundwater pumpage for the proposed well field was distributed equally between these two cells. The simulated total groundwater pumpage for MDWASD well fields was 349.5 Mgal/d until 2025 and 2030, when it was increased to 359.2 and 372.6 Mgal/d, respectively. No other changes were made to the base-case future scenario model for the increased groundwater pumpage scenario.

The water table was less than 0.5 ft below land surface in a total of 5,569 onshore model cells in the increased groundwater pumpage scenario during the 30th year of the simulation period and was comparable to the base-case future scenario (fig. 56B). The change in flood-prone areas resulting from increased groundwater pumpage was small (0.39 mi<sup>2</sup>) and flood-prone areas were inundated approximately the same percentage of the year in each case.

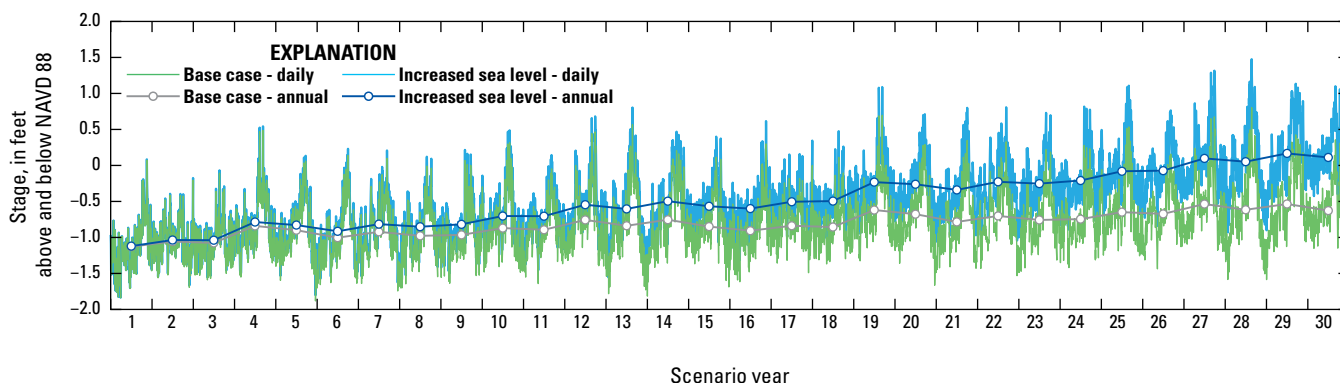


**Figure 54.** Calculated daily and annual-average Virginia Key tidal stage used in the 30-year base-case future and increased sea-level scenarios.

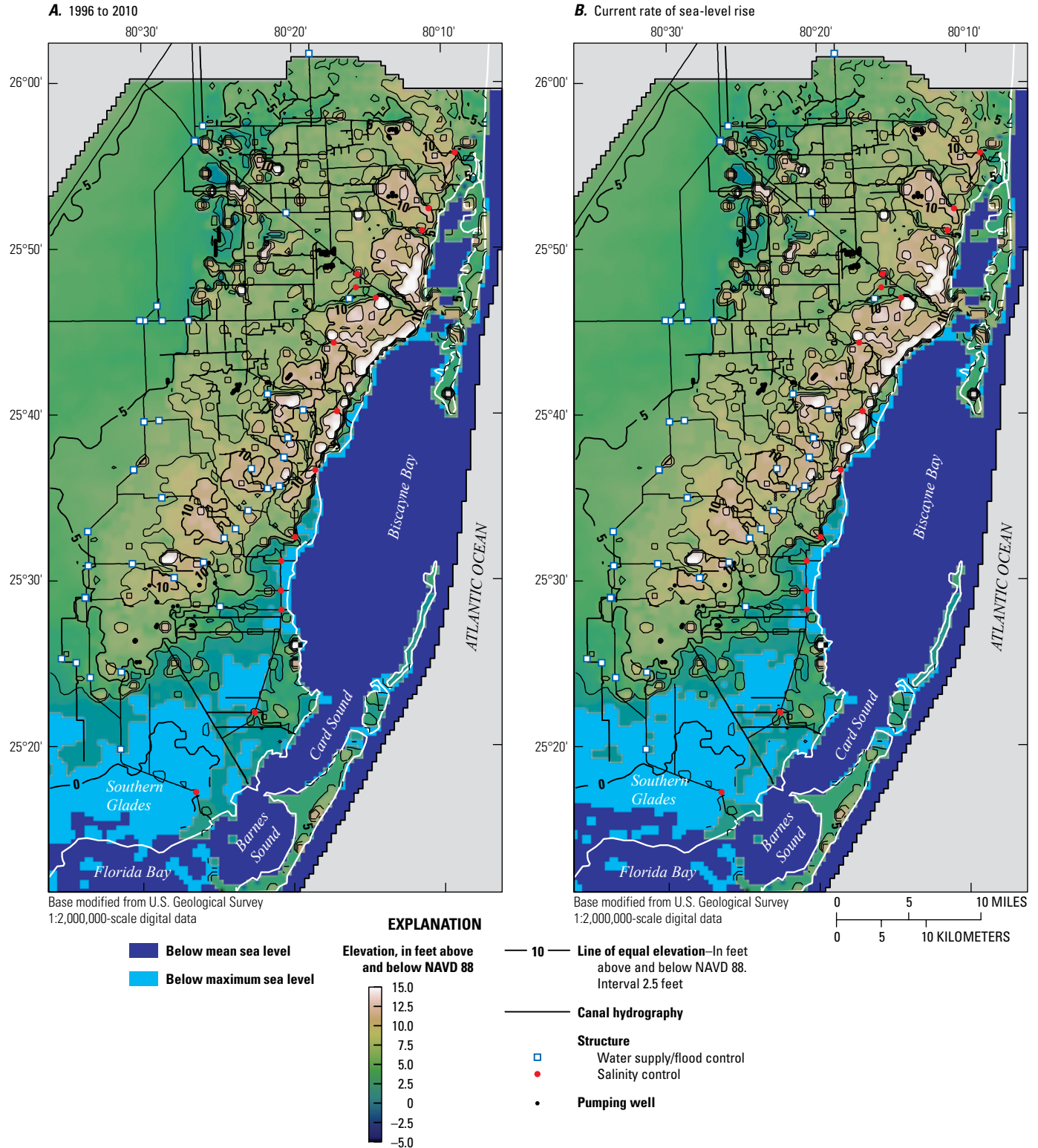


**Figure 55.** Areas with land-surface elevations, *A*, at or below the average and maximum stage at Virginia Key between 1996 and 2010, and areas with land-surface elevations at or below the average and maximum stage under, *B*, current and, *C*, high rates of sea-level rise after 30-years.

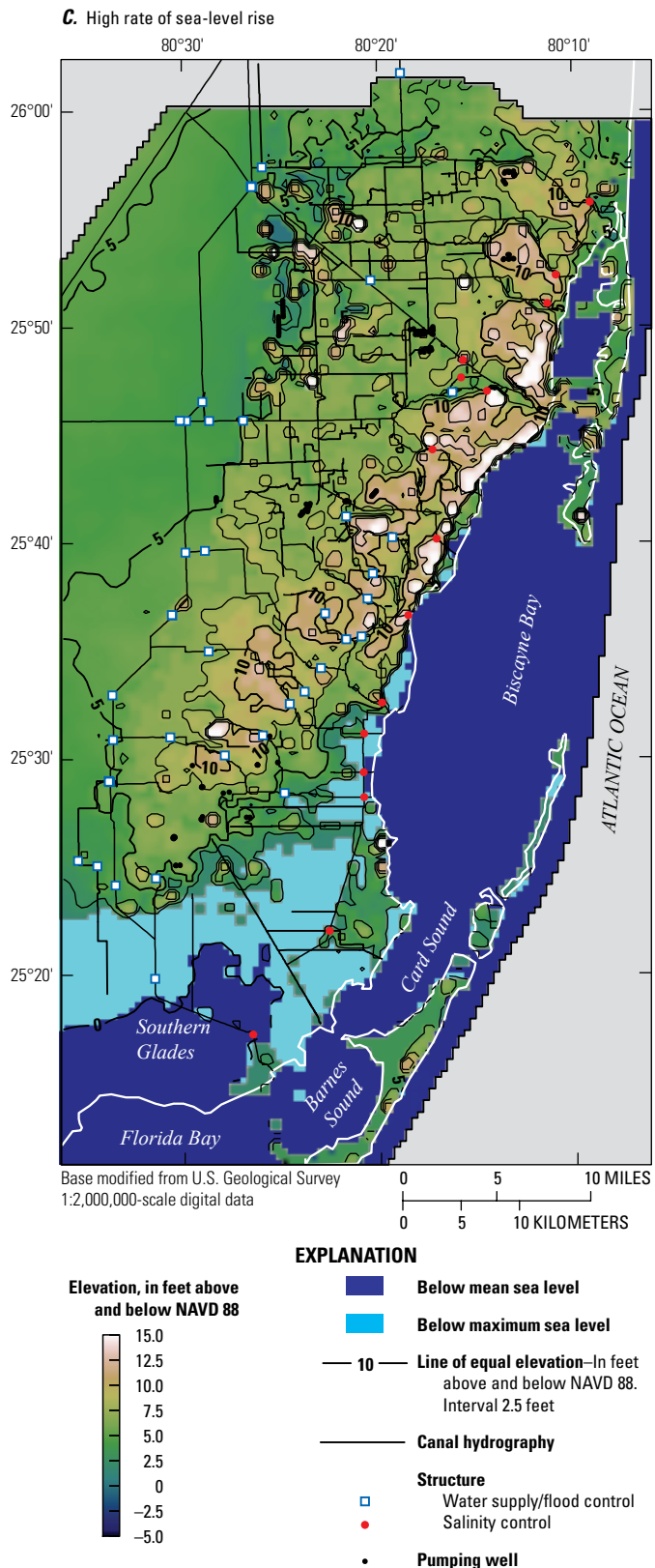


**Figure 55.** Areas with land-surface elevations, A, at or below the average and maximum stage at Virginia Key between 1996 and 2010, and areas with land-surface elevations at or below the average and maximum stage under, B, current and, C, high rates of sea-level rise after 30-years.—Continued

The simulated change in water-table elevations exceeding  $-0.5$  ft resulting from increased pumpage at the end of May in the last year of the scenario simulation period was restricted to the vicinity of the Southwest and South Miami Heights well fields (fig. 57A). Water-table elevation changes exceeding  $-0.1$  ft that resulted from increased pumpage at the Southwest well field extend over most of the C-2 and C-100 Basins and part of the C-4 Basin. At the South Miami Heights well field, water-table elevation changes did not extend much beyond the well field. Increased groundwater pumpage did not have a substantial effect on the position of the freshwater-seawater interface (fig. 58A). However, comparison of the position of the freshwater-seawater interface during the 1996 to 2010 simulation period (fig. 53) and at the end of May in the 30th year of the scenario simulation period for the base and increased groundwater pumpage cases (fig. 58A) indicate seawater intrusion may be an issue at the Miami-Springs well field if the Miami Springs, Hialeah, and Preston well fields are operated using current permitted groundwater pumping rates.

Notable simulated changes in groundwater budgets for the increased groundwater pumpage scenario relative to the base-case future scenario in the combined C-2 and C-100 Basins were increased lateral groundwater inflows, decreased lateral groundwater outflow, reduced canal seepage, and increased leakage (table 19). Additional groundwater inflow accounted for only 25 percent of the increased groundwater pumpage in the combined C-2 and C-100 Basins. Most of the increased groundwater pumpage in these basins (55 percent) is accounted for by local changes in canal exchanges. Changes in the groundwater budget relative to the base-case future scenario in the C-4 and C-6 Basins were small (table 19). Similar to the combined C-2 and C-100 Basins, lateral inflow increased, lateral outflow decreased, canal seepage decreased, and canal leakage increased in the urban part of the study area, but increased lateral groundwater inflow only accounted for a small percentage (19 percent) of the increased groundwater pumpage.

Increased groundwater pumpage resulted in a small (less than  $1 \text{ ft}^3/\text{s}$ ) increase in surface-water inflow through the S30, S31, G119, S338, S194, S196, and S176 structures into urban areas of the study area, relative to the base-case future scenario. Likewise, increased groundwater pumpage resulted in decreased surface-water outflow through the salinity control structures by  $6 \text{ ft}^3/\text{s}$  relative to the base-case future scenario. The reduction in outflow from the salinity control structures accounted for a small percentage (38 percent) of the  $16\text{-ft}^3/\text{s}$  increase in groundwater pumpage in urban parts of the study area (table 19).

### Increased Sea Level (Scenario 2)

In scenario 2, equation 28 and an  $SLR_N$  constant of 0.000113 were used to calculate daily coastal-boundary tidal data for increased sea level. The increased sea-level scenario is representative of a National Research Council curve III (NRC III) increase (National Research Council, 1987). The difference between the average annual sea level for current

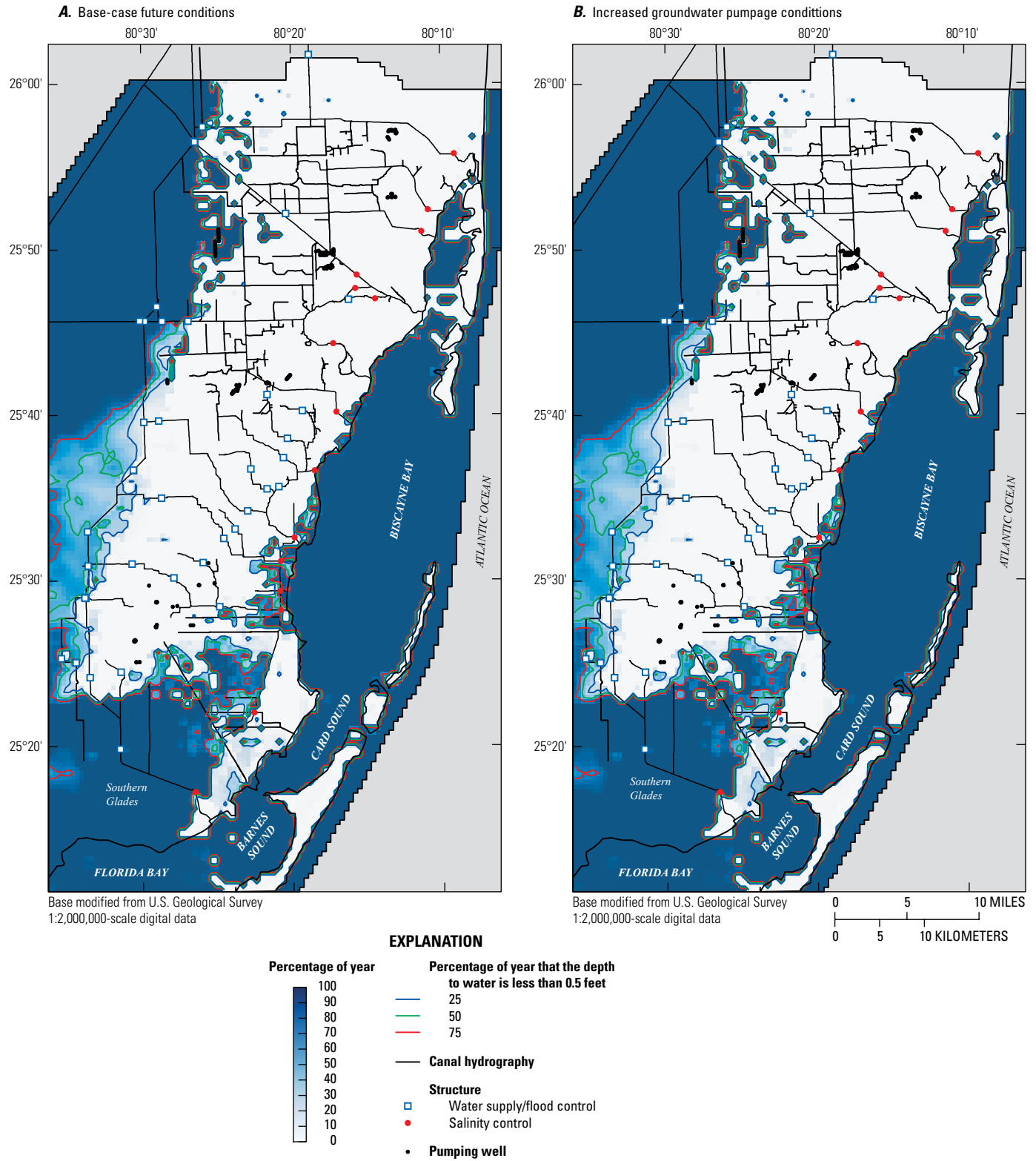


**Figure 56.** Percentage of time water-table elevations are less than 0.5 ft below land surface in the 30th year of the scenario simulation period for, *A*, base-case future, *B*, increased groundwater pumpage, *C*, increased sea level, and *D*, increased sea-level and groundwater pumpage conditions.

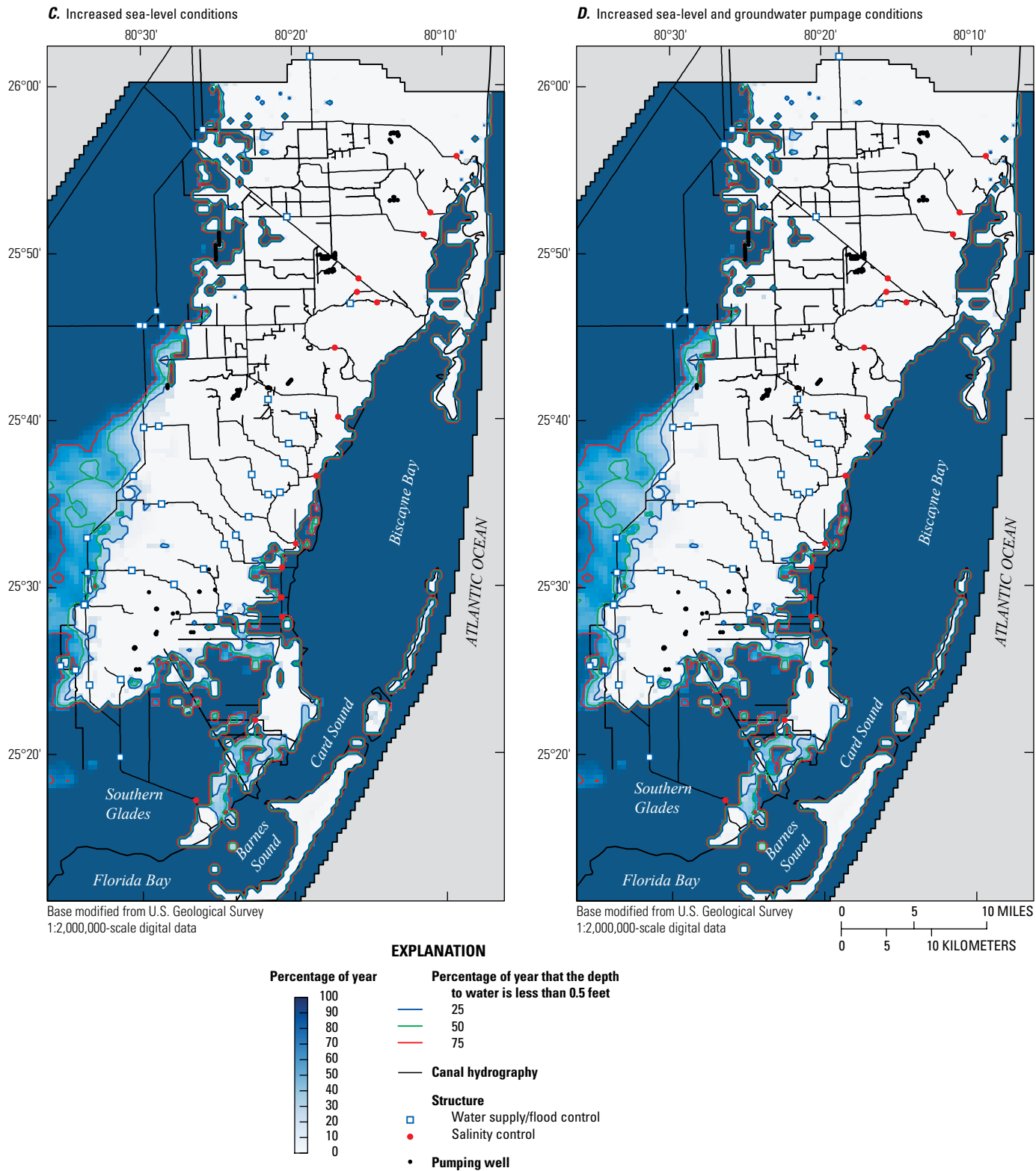


**Figure 56.** Percentage of time water-table elevations are less than 0.5 ft below land surface in the 30th year of the scenario simulation period for, *A*, base-case future, *B*, increased groundwater pumpage, *C*, increased sea level, and *D*, increased sea-level and groundwater pumpage conditions.—Continued

and high rates of sea-level rise is 0.73 ft after 30 years (fig. 54). After 30 years, onshore areas below the average (0.05 ft NAVD 88) and maximum (1.48 ft NAVD 88) calculated stage at Virginia Key are more extensive in the southernmost part of the study area, with the NRC III rate of sea-level rise and calculated daily meteorological forcing effects (fig. 55C).

Delaunay triangulation (de Berg and others, 2008) was used to fill gaps in the southern Glades between the EDEN stage dataset and increased sea-level data where EDEN stages were lower than sea level. No other changes were made to the base-case future scenario model for the increased sea-level scenario.

The water table was less than 0.5 ft below land surface in a total of 5,672 onshore model cells in the increased sea-level scenario during the 30th year of the scenario simulation period (fig. 56C). Increased sea level resulted in a 10.32-mi<sup>2</sup> increase in flood-prone areas and a 4-percent increase in the percentage of the time flood-prone areas have a water-table depth less than 0.5 ft below land surface.

The simulated change in water-table elevations for the increased sea-level scenario relative to the base-case future scenario exceeded 0.5 ft primarily in areas seaward of the salinity control structures (with a couple of notable exceptions), as measured at the end of the May in the last year of the scenario simulation period (fig. 57B). Water-table elevation changes ranged from approximately 0.5 ft along the coast to

0.1 ft in western parts of the urban area. Relative to the base-case future scenario, increased sea level caused the freshwater-seawater interface to move landward in southern parts of the onshore study area in all three model layers (fig. 58B). This movement was greatest in model layer 1 but was still substantial in model layers 2 and 3.

Increased sea level resulted in reduced groundwater inflow, groundwater outflow, and canal exchanges in the combined C-2 and C-100 Basins, C-4 Basin, C-6 Basin, and in urban parts of the study area (table 20). Increased water-table elevations (fig. 57B) resulted in increased evapotranspiration (increased external outflow). Furthermore, the combination of historical stages in WCA3 and ENP and increased sea level reduced water-table gradients throughout the system, which resulted in decreased groundwater flow (reduced lateral groundwater outflow) and, consequently, reduced canal exchanges.

Increased sea level resulted in a simulated 7-ft<sup>3</sup>/s decrease in surface-water inflow into urban areas of the study area relative to the base-case future scenario. Increased sea level also decreased the surface-water outflow through the salinity control structures by 48 ft<sup>3</sup>/s relative to the base-case future scenario. The reduction in outflow from the salinity control structures was notably greater than reductions resulting from increased groundwater pumpage.

**Table 18.** Simulated base-case future scenario groundwater budget for select basins.

[All values in cubic feet per second]

Basin	Lateral groundwater flow		External boundaries		Canal exchanges		Municipal pumpage	Storage change
	Inflow	Outflow	Inflow	Outflow	Seepage	Leakage		
C-2 and C-100	188	93	328	34	408	306	288	0
C-4	243	118	349	180	737	575	132	1
C-6	151	95	223	38	361	228	108	0
Urban area	730	268	2,140	481	4,006	2,504	622	1

**Table 19.** Simulated groundwater budget change from the base-case future scenario for select basins with increased groundwater pumpage.

[All values in cubic feet per second]

Basin	Lateral groundwater flow		External boundaries		Canal exchanges		Municipal pumpage	Storage change
	Inflow	Outflow	Inflow	Outflow	Seepage	Leakage		
C-2 and C-100	5	-3	0	-1	-3	8	20	0
C-4	1	-1	0	0	4	0	0	0
C-6	0	0	0	0	-1	-1	0	0
Urban area	3	-2	0	-2	-2	7	16	0

### Increased Groundwater Pumpage and Sea Level (Scenario 3)

The modifications to the base-case future scenario for the increased groundwater pumpage (scenario 1) and increased sea-level scenarios (scenario 2) were combined in scenario 3 to evaluate the combined effects of these changes. No other changes were made to the base-case future scenario model for scenario 3.

The water table was less than 0.5 ft below land surface in a total of 5,572 onshore model cells in scenario 3 during the 30th year of the scenario simulation period (fig. 56D). Increased sea level resulted in a 10.23-mi<sup>2</sup> increase in flood-prone areas and a 4-percent increase in the percentage of the time flood-prone areas have water-table elevation less than 0.5 ft below land surface. The extent of flood-prone areas in this scenario was comparable to those in the increased sea-level scenario.

The simulated change in water-table elevations exceeding 0.5 ft that resulted from the combined effect of increased groundwater pumpage and increased sea level at the end of the May in the last year of the scenario simulation period exceeding 0.5 ft was generally restricted to areas seaward of the salinity control structures, with a couple of notable exceptions (fig. 57C). Water-table elevation changes varied from approximately 0.5 ft along the coast to 0.1 ft in western parts of the urban area. Water-table elevation changes exceeding -0.5 ft were restricted to the area near the Southwest well field (fig. 57C). Water-table elevation changes exceeding -0.1 ft that resulted from increased groundwater pumpage at the Southwest well field extended over a limited part of the C-2 and C-100 Basins; decreased water levels did not extend into the C-4 Basin. Increased sea level effectively eliminated decreased water levels at the South Miami Heights well field observed in the increased groundwater pumpage scenario (fig. 57A). Landward movement of the freshwater-seawater interface was comparable to that in the increased sea-level scenario, indicating that sea-level increases are the predominant factor controlling movement of the freshwater-seawater interface (fig. 58C).

The combination of increased groundwater pumpage and increased sea level resulted in reduced groundwater inflow, groundwater outflow, and net canal exchanges in the

combined C-2 and C-100 Basins, C-4 Basin, C-6 Basin, and urban parts of the study area (table 21). Reductions in groundwater inflow, groundwater outflow, and canal exchanges, however, were less than or similar to reductions observed in the increased sea-level scenario (table 20). Increased water-table elevations (fig. 57C) caused increased evapotranspiration (increased external outflow), although less than in the increased sea-level scenario. Water budget changes resulting from increased sea level overwhelm the changes resulting from increased groundwater pumpage.

Relative to the base-case future scenario, the combination of increased sea level and increased groundwater pumpage decreased the surface-water inflow into urban parts of the study area through the S30, S31, G119, S338, S194, S196, and S176 structures and surface-water outflow through the salinity control structures by 6 and 54 ft<sup>3</sup>/s, respectively. The effects of increased sea level and increased groundwater pumpage on surface-water inflow and outflow are additive, although the effects of increased sea level exceed the effects of increased groundwater pumpage alone.

## Model Reliability

As with all models, the urban Miami-Dade surface-water/groundwater model is a mathematical simplification of the canal system and Biscayne aquifer in the study area. As such, it needs to be recognized that (1) the model has been developed for a specific purpose, (2) the model calibration process has been informed only by expert knowledge and available observation data, and as a result, (3) the model is limited in its ability to represent the response of the system to actual hydrologic conditions and to changes in those conditions.

## Model Sensitivity

Model calibration was completed with PEST and involved the use of highly parameterized inversion techniques. During the calibration process, the observation processing methodology was refined several times to increase parameter sensitivity and to improve the ability of the model to simulate the effect of groundwater withdrawals on canal leakage.

**Table 20.** Simulated groundwater budget change for select basins with increased sea level.

[All values in cubic feet per second]

Basin	Lateral groundwater flow		External Boundaries		Canal exchanges		Municipal pumpage	Storage change
	Inflow	Outflow	Inflow	Outflow	Seepage	Leakage		
C-2 and C-100	-6	-5	0	3	-13	-8	0	0
C-4	-5	-5	0	3	-16	-13	0	-1
C-6	-4	-3	0	2	-12	-9	0	0
Urban area	-19	-6	-2	27	-108	-62	0	-3

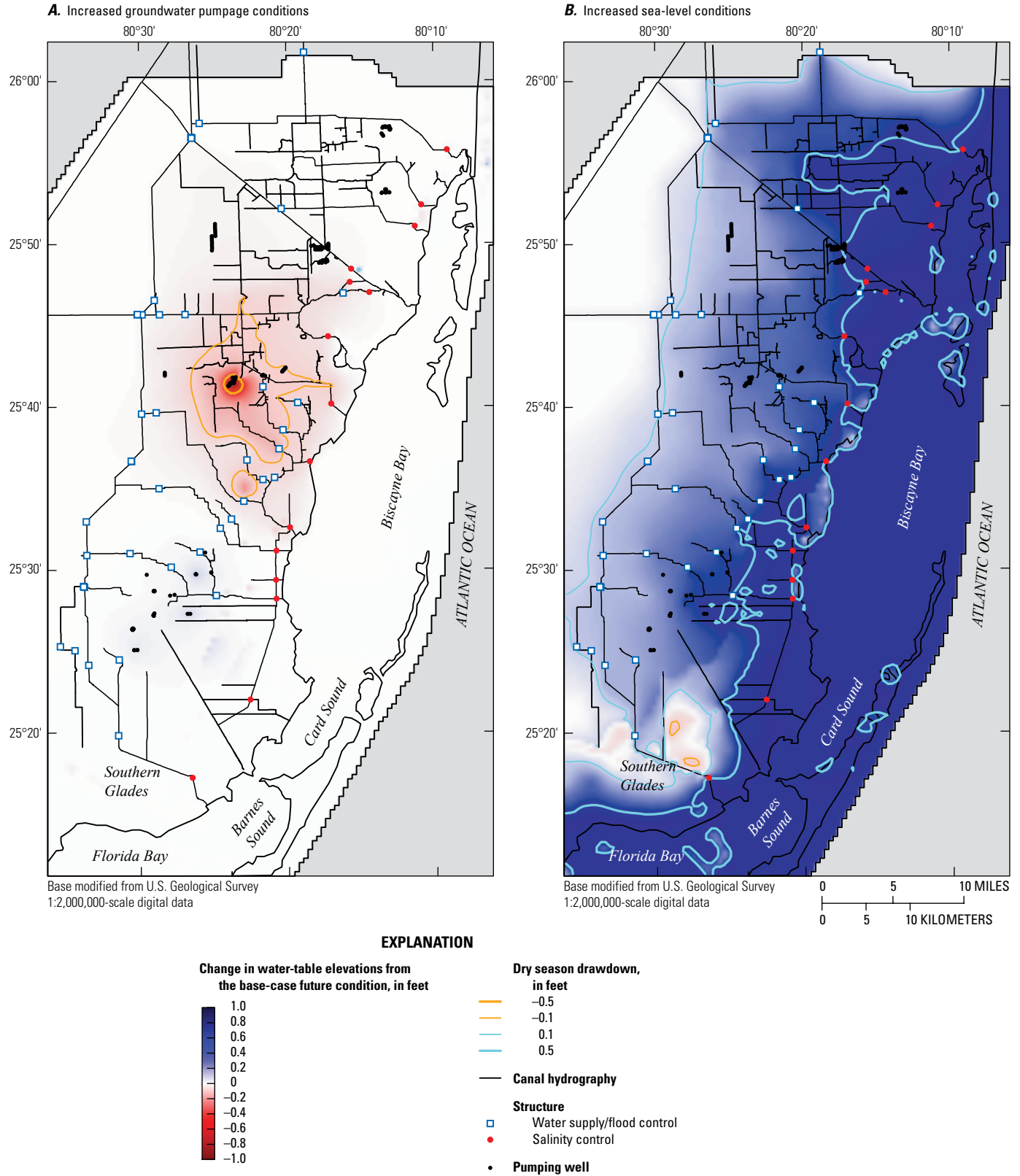


**Figure 57.** Simulated change in water-table elevations from the base-case future scenario for the, *A*, increased groundwater pumpage, *B*, increased sea level, and *C*, increased sea-level and groundwater pumpage scenarios at the end of May in the 30th year of the scenario simulation period.

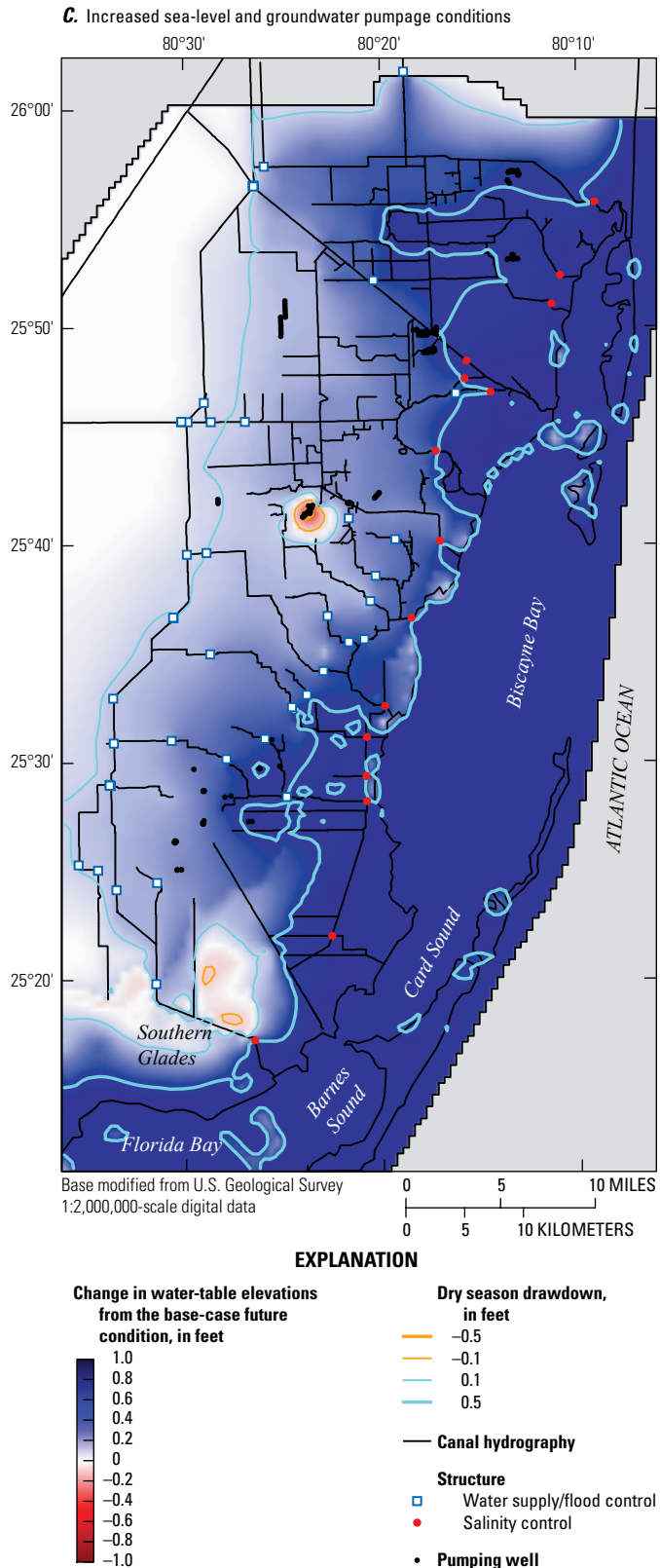


**Figure 57.** Simulated change in water-table elevations from the base-case future scenario for the, *A*, increased groundwater pumpage, *B*, increased sea level, and *C*, increased sea-level and groundwater pumpage scenarios at the end of May in the 30th year of the scenario simulation period.—Continued

Furthermore, insensitive parameters and observations that did not provide any information about parameter values were manually removed from the calibration process.

Composite parameter sensitivities, which are a measure of the information content of observations relative to a specific model parameter, are useful in identifying sensitive model parameters (Doherty, 2010). Furthermore, because composite parameter sensitivities are normalized, they can be used to compare the contribution of each parameter to minimizing the objective function during the automated parameter estimation process. The composite sensitivity of parameter, *i*, is calculated using the equation

$$s_i = \frac{(\mathbf{J}^T \mathbf{w}^2 \mathbf{J})_{ii}^{1/2}}{m}, \quad (29)$$

where

- J** is the Jacobian (sensitivity) matrix,
- T** is the matrix transpose operation,
- w** is the diagonal matrix of observation weights, and
- m** is the number of observations with nonzero weights.

Composite parameter sensitivities were calculated for the 3,668 parameters estimated during model calibration. Frequency analyses of calculated composite parameter sensitivities for parameters grouped by (1) parameter type (for example, hydraulic conductivity) and (2) model layer (where appropriate) indicated that most calculated composite parameter sensitivities in each group vary by an order of magnitude or less (between  $1 \times 10^{-3}$  and  $1 \times 10^{-2}$ ) and were generally clustered in one to two bins (fig. 59). Manning’s roughness coefficients and reach-aquifer leakance parameters varied by more than an order of magnitude (between  $1 \times 10^{-5}$  and  $1 \times 10^{-1}$ ), but most of the parameters were clustered in adjacent bins. The magnitude and distribution of calculated composite parameter sensitivities for unique parameter types indicate that refinements made to the observation processing methodology, parameters included in the calibration processing, and observation weighting were all effective. Furthermore, the use of highly parameterized techniques has effectively removed the artificial parameter hypersensitivity that commonly occurs with the use of piecewise constant parameter zonation calibration techniques.

Traditionally, sensitivity analyses have been used to quantify the uncertainty of a calibrated model resulting from uncertainty in estimated model parameters, stresses, and boundary conditions (Anderson and Woessner, 1992). The calculated composite parameter sensitivities demonstrate that the parameters included in the calibration process are informed by the processed observation dataset and that minimization of the objective function by PEST has resulted in parameters with maximum likelihood.

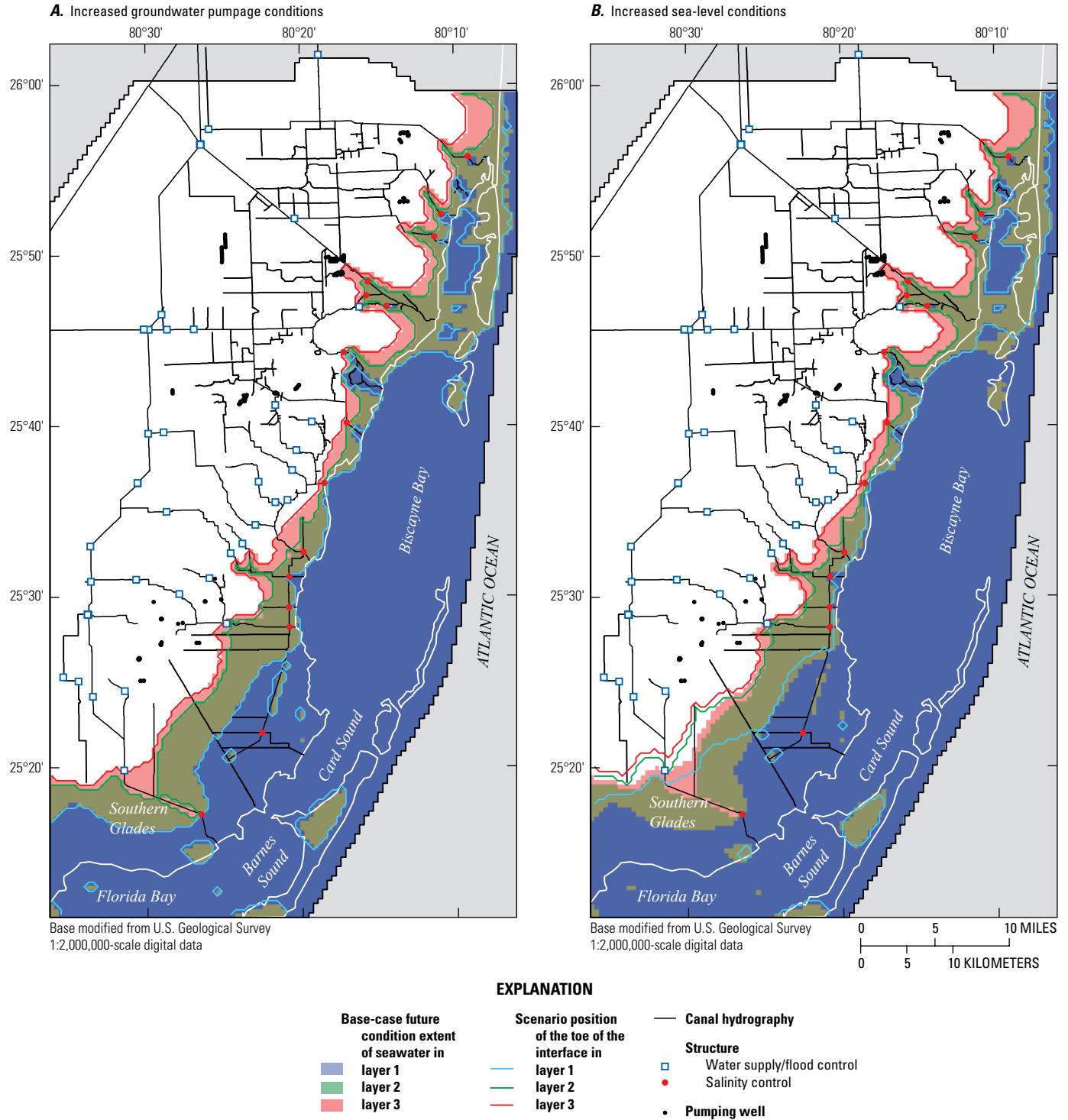


**Figure 58.** Simulated change in the position of the freshwater-seawater interface from the base-case future scenario for the, *A*, increased groundwater pumpage, *B*, increased sea level, and, *C*, increased sea-level and groundwater pumpage scenarios at the end of May in the 30th year of the scenario simulation period.

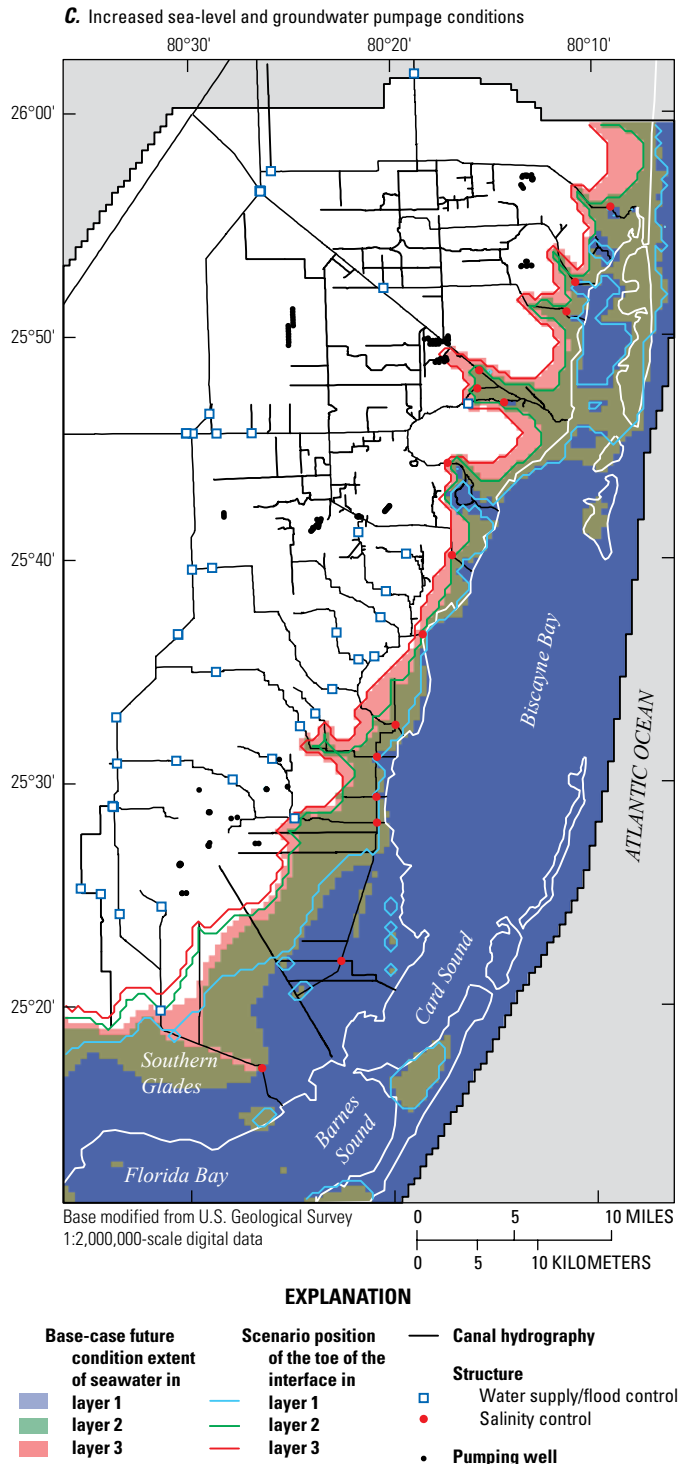


**Figure 58.** Simulated change in the position of the freshwater-seawater interface from the base-case future scenario for the, *A*, increased groundwater pumpage, *B*, increased sea level, and, *C*, increased sea-level and groundwater pumpage scenarios at the end of May in the 30th year of the scenario simulation period.—Continued

It is not uncommon to infer that the uncertainty of model predictions is reduced if model parameters are estimated as part of a maximum likelihood estimation process, such as the process implemented with PEST in this study. However, without consideration of prior probabilities in a Bayesian context and evaluation of specific model predictions, actual model uncertainty cannot be quantified (Doherty and others, 2010b; Fienen and others, 2010). Formal uncertainty quantification, using linear or nonlinear subspace methods or true Bayesian methods would be required to quantify the uncertainty of specific predictions made using the model developed in this study.

The uncertainty associated with the specific scenarios evaluated using the model developed in this study, and other similar scenarios, has not been formally quantified. Therefore, model projection uncertainties must be inferred from the calculated composite parameter sensitivities. Based on (1) calculated composite parameter sensitivities, (2) minimization of the objective function using PEST, and (3) verification-period model fit, it is expected that the model will be useful for evaluating surface-water stage and flow, groundwater levels, and canal-aquifer leakage, provided the model is applied at similar spatial and temporal scales under hydrologic conditions comparable to those observed during the calibration and verification periods.

### Model Limitations

The application and reliability of the model developed in this study are limited by the conceptual model of the hydrologic system, model construction (including physical properties used to describe the system and boundary conditions), and to some degree, observation measurement errors. Some of the model limitations are explicitly demonstrated in the fit of the model to the observed system, and others are more conceptual in nature. The following discussion of model limitations is not intended to dissuade use of the model for its intended or other comparable purposes or to highlight its flaws; rather, it is intended to acknowledge that its application, like that of all models, is limited in its ability to make predictions as a result of the assumptions, data, and methods used to develop and calibrate the model.

In the surface-water component of the model, all of the surface-water basins have been assumed to be disconnected, except where primary surface-water control structures connect adjacent basins. In fact, the C-4, C-6, C-7, C-8, and C-9 Basins are connected and inter-basin water transfers may be large during localized convective rainfall events, particularly during the wet season. Furthermore, although the canal geometry data of Giddings and others (2006) accurately define the general characteristics of canals in the study area, they are less detailed than canal geometry data typically used in event-based surface-water models. As a result, the model may not accurately simulate system responses during specific events or within short timeframes.

**Table 21.** Simulated groundwater budget change for select basins with increased sea level and increased groundwater pumpage.

[All values in cubic feet per second]

Basin	Lateral groundwater flow		External Boundaries		Canal exchanges		Municipal pumpage	Storage change
	Inflow	Outflow	Inflow	Outflow	Seepage	Leakage		
C-2 and C-100	-1	-7	0	2	-15	1	20	0
C-4	-3	-5	0	3	-13	-12	0	-1
C-6	-4	-3	0	1	-13	-10	0	0
Urban area	-16	-8	-2	25	-108	-54	16	-3

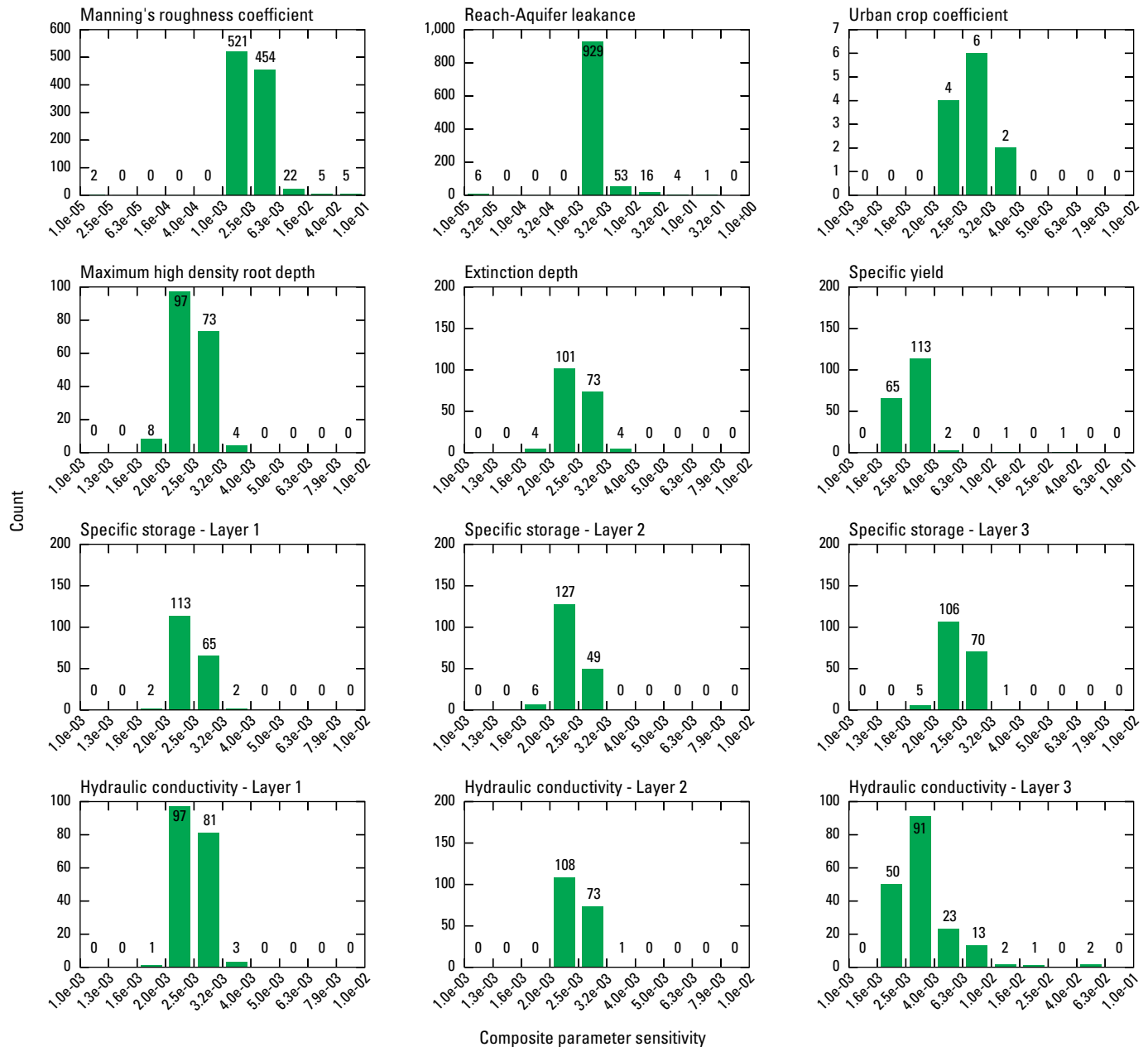


**Figure 59.** Composite parameter sensitivity of simulated surface-water stages, groundwater levels, and net surface-water subbasin discharge at calibration points to parameter changes. Composite parameter sensitivities are used here to show relative parameter sensitivity; the definition and derivation are described in Doherty (2010).

Canal seepage and leakage are controlled by a calibrated leakance parameter. Canal leakance values are difficult to measure in the field and have been parameterized by matching the sum of (1) direct rainfall on the canal system, (2) evaporation from the canal system, and (3) simulated canal leakage and seepage to calculated net surface-water subbasin discharge between primary surface-water structures. The accuracy of these calculated values is uncertain because of the abundance of un-gauged secondary and tertiary drainage features and canals that contribute flow into the canals simulated in the model. Furthermore, direct surface-water runoff, which may also directly or indirectly flow into canals and affect the estimated value of canal leakage and seepage, has been estimated but is highly uncertain because it has been quantified for only a few basins in the study area. Finally, because local canal discharge and (or) canal-aquifer exchange may be large within the canal system in a surface-water basin that is not expressed as discharge at a structure, the model was calibrated against calculated average monthly net surface-water subbasin discharge. Accordingly, the accuracy of simulated net surface-water subbasin discharge and canal-aquifer exchanges at submonthly time scales is unknown.

Simulations of net surface-water subbasin discharge for DBL2, L-31N at G211, L-31N at S331, C-102 at S165, C-102 at S21, Military Canal, C-103 at S167, L-31E at S20, and C-111E at S178 were relatively poor. As a result, specific predictions for these subbasins should be evaluated with caution. The total magnitude of discharge from these subbasins is small relative to that of other basins; therefore, model misfit in these subbasins should not adversely affect overall model predictions.

The groundwater component of the model is represented by variable hydraulic conductivity in the horizontal and vertical directions. This distribution has been informed by published data from field tests and observed surface-water stage and groundwater level data; however, observation data are sparse in some parts of the study area. As a result, the hydraulic conductivity data used in the model may not accurately represent hydraulic properties in areas where observation data did not inform the calibration process. Furthermore, nested groundwater monitoring wells are sparse in the study area. As a result, the hydraulic conductivity data may not accurately reflect the vertical heterogeneity within the Biscayne aquifer. There are also a limited number of groundwater monitoring wells cased in the lower production zone, and as a result, the hydraulic properties assigned in model layer 3 may be less accurate than those assigned in overlying layers.

In general, the largest groundwater level errors during the calibration and verification simulations occurred in the northern part of the modeled area. This is especially true in areas where observation sites are located in the same (or adjacent) model cells as those containing major well fields, particularly the Miami Springs, Hialeah, and Preston well fields. The discretization used in the groundwater component of the model may not be refined enough to resolve the groundwater flow field around major well fields or to represent the spatial variability of hydraulic properties.

Seawater intrusion was simulated using the SWI2 Package, which is designed to efficiently simulate three-dimensional, vertically integrated variable-density groundwater flow and seawater intrusion in large-scale MODFLOW models. The SWI2 Package can simulate horizontal and vertical movement of the freshwater-seawater interface in multi-layer coastal multi-aquifer systems at the regional scale. However, the SWI2 Package is not designed to simulate chloride concentrations in groundwater wells or changes in chloride concentrations in a groundwater well between different scenarios. A coupled groundwater flow and advective-dispersive transport code, such as SEAWAT (Langevin and others, 2007), would be required to make these types of predictions.

The density of water in the Turkey Point cooling canal is currently twice that of seawater (63.98 lb/ft<sup>3</sup>). Current cooling canal fluid densities were not represented in the equivalent freshwater heads specified for general head boundaries (GHBs) representing the cooling canals because the SWI2 Package is designed to simulate seawater intrusion rather than vertical brine movement in the subsurface (Bakker and others, 2013). Hughes and others (2010) demonstrated that landward movement of the 2-percent seawater isochlor is sensitive to the fluid density of surface water in the cooling canals. Therefore, the simulated position of the freshwater-seawater interface may underestimate its actual landward position westward of the Turkey Point cooling canals and should be used with caution. To more accurately represent the effects of the density contrast between freshwater in the aquifer, seawater in Biscayne Bay, and surface water in the cooling canals on seawater intrusion in southeastern Miami-Dade County, it may be necessary to use of a coupled groundwater flow and advective-dispersive transport code such as SEAWAT (Langevin and others, 2007).

In the three scenarios evaluated using a version of the calibrated model modified to represent future conditions, it was assumed that (1) the surface-water control structures would be operated as they were during the calibration and verification periods, and (2) sufficient water would be available to maintain stages observed during the calibration and verification periods in WCA3 and ENP. It is expected that the SFWMD would alter structure operations in response to increased sea level, even under identical hydrologic conditions, to maintain the current seasonal stages and corresponding water-table elevations (level of service) in the study area. Yet, it is unknown if it will be possible to maintain observed stages in WCA3 and ENP in the future. It is expected that lower stages in WCA3 and (or) ENP would reduce the water-table elevation in urban parts of the study area, increase drawdown resulting from municipal groundwater pumpage, and possibly cause additional landward movement of the freshwater-seawater interface.

Despite the limitations discussed, the model developed for the study area represents the best available tool to evaluate the relative effects of groundwater pumpage on canal leakage and regional groundwater flow at the scale represented in the model. In southern Florida, the groundwater and surface-water systems are closely coupled, and the model documented in this

report provides an approach that allows explicit representation of both systems and the tight coupling between them. A variety of data types were used to calibrate the model, and even though hydraulic properties of the canal system and Biscayne aquifer are known only at a select number of locations, the model is designed to simulate physically based surface-water and groundwater processes. Although the model simulates processes on a daily time scale, evaluation of model simulation results is probably most appropriate at longer time scales. As a corollary, although the model provides reasonable results at weekly to monthly time scales, its predictive capabilities for shorter time periods is unknown and thus should be used with caution.

## Summary

Previous studies in Miami-Dade County have determined that on a local scale, leakage from surface-water canals adjacent to well fields can supply 46 to 78 percent of the total groundwater pumpage. In addition to providing leakage to the Biscayne aquifer, canals in the urban areas also receive seepage from the Biscayne aquifer that is derived from a combination of local rainfall and lateral groundwater flow from Water Conservation Area 3 and Everglades National Park, located west of urban areas of Miami-Dade County. To evaluate the effects of groundwater pumpage on canal leakage and regional groundwater flow, the U.S. Geological Survey developed and calibrated a coupled surface-water/groundwater model of the urban areas of Miami-Dade County, Florida. The model is based on a number of previous groundwater flow and solute-transport models designed to (1) investigate groundwater flux into Biscayne Bay, (2) evaluate the factors contributing to hypersalinity events in Biscayne Bay, and (3) estimate time-based capture zones and drawdown contours for two well fields in Miami-Dade County. This study extends the scope and findings of previous studies by specifically simulating surface-water stage and discharge in the managed canal system and dynamic canal leakage to the Biscayne aquifer and canal seepage from the Biscayne aquifer.

The model was developed by using MODFLOW–NWT program, with the Surface-Water Routing (SWR1) Process, which is intended for solving unconfined groundwater-flow problems, and the Seawater Intrusion (SWI2) Package, which simulated movement of the freshwater-seawater interface. The SWR1 Process was developed specifically for this study to simulate stages, surface-water discharge, and surface-water/groundwater interactions in areas where surface-water gradients are small and (or) the surface-water system is managed using surface-water control structures. The SWI2 Package was developed to simulate variable-density flow in regional-scale models using a rigorous but simplified approach that requires fewer layers than required by variable-density groundwater flow models that solve the advective-dispersive transport equation. The model includes the urban area of Miami-Dade County and parts of Broward County that contribute

surface-water and groundwater to surface-water basins and the Biscayne aquifer in urban Miami-Dade County, respectively. Parts of Water Conservation Area 3 and Everglades National Park are included in the model so that surface-water deliveries and groundwater seepage from these areas can be simulated. The modeled area also includes Biscayne Bay, Card Sound, Barnes Sound, and parts of Florida Bay and the Atlantic Ocean to simulate the effects of offshore saline groundwater on groundwater discharge to the coast and the position of the freshwater-seawater interface.

The model grid consists of 101 columns and 189 rows of square model cells (1,640.4×1,640.4 ft). The surface-water hydrography was intersected with the model grid to develop the surface-water component. The surface-water component was discretized into 2,352 SWR1 reaches representing primary, secondary, and selected tertiary canals and having lengths ranging from 0.67 to 2,868 ft. The discretized SWR1 reaches were grouped into 637 SWR1 reach groups to reduce the numerical overhead associated with the SWR1 Process. The groundwater component is composed of three layers within the Biscayne aquifer. The model simulates surface-water discharge, groundwater flow, and surface-water/groundwater exchange between the canal system and the Biscayne aquifer. External stresses for the surface-water component included direct rainfall on the canal system, evaporation, and estimated direct surface-water runoff. External stresses for the groundwater component of the model included rainfall, evapotranspiration, agricultural water use, recreational irrigation, septic return flow to the water table, and groundwater pumpage.

The model was calibrated to weekly average observed surface-water stage, surface-water discharge, and groundwater levels for the period from January 1997 through December 2004. The model also was calibrated to match monthly average net surface-water subbasin discharge for the same period. Model parameters were calibrated using automated parameter estimation software (PEST) and used highly parameterized inversion techniques. Model parameters that were estimated include the hydraulic conductivity of model layers 1 to 3, the specific storage coefficient of model layers 2 and 3, the specific yield of the Biscayne aquifer, the evapotranspiration extinction depth, the depth of dense roots, monthly crop coefficients for urban land-use types, canal roughness coefficients (Manning's  $n$  values), and canal leakance coefficients. A total of 3,665 parameters were adjusted during calibration. Tikhonov regularization was used to produce parameter distributions that deviated from initial values only if parameter adjustments are necessary to fit observation data.

In general, the model met defined error-based calibration targets for surface-water stage, surface-water discharge, net surface-water subbasin discharge, and groundwater levels. The modified Nash-Sutcliffe model efficiency coefficient (E1) calibration target for net surface-water subbasin discharge was not satisfied in the C-4 at DBL2, L-31N at G211, L-31N at S331, C-102 at S165, C-102 at S21, Military Canal, C-103 at S167, L-31E at S20, and C-111E at S178 Subbasins as a result of

poor model performance. The net surface-water subbasin discharge in these subbasins is relatively small when compared to other basins, so poor performance is not expected to have an adverse effect on model predictions. The model also met defined error-based calibration targets (except for E1 calibration targets) during the 2005 through 2010 verification period.

Canal and Biscayne aquifer water budgets for urban areas of the model indicate that most of the water discharging through the salinity control structures is derived from within the urban parts of the study area and that, on average, the canals are draining the Biscayne aquifer. Groundwater discharge from the urban areas to the coast is approximately 7 percent of the total surface-water inflow to Biscayne Bay and is consistent with previous estimates of fresh groundwater discharge to Biscayne Bay.

Groundwater budgets for the combined C-2 and C-100 Basins, C-4 Basin, and C-6 Basin indicate that groundwater pumpage in these basins ranges from 13 to 27 percent of the sum of local sources of groundwater inflow to the basins. The largest percentage of groundwater pumpage to local sources of groundwater inflow was observed in the combined C-2 and C-100 Basins, which include the Alexander Orr, Snapper Creek, Southwest, and West well fields and have the highest groundwater pumping rates of the three basins evaluated (257 and 266 cubic feet per second in the calibration and verification periods, respectively). Calculated contributions of local sources of groundwater inflow to well field pumpage in selected basins are less than values calculated in previous studies, and reflect groundwater inflow estimates at larger (basin-level) scales than evaluated previously.

Changes in the position of the freshwater-seawater interface at the base of the Biscayne aquifer during the simulation period were minor, which is consistent with movement of the interface between 1984 and 2011. The position of the freshwater-seawater interface at the bottom of model layer 1 and 2 did change during the simulation period in response to annual rainfall amounts. Landward movement of the freshwater-seawater interface in model layers 1 and 2 was more prone to occur during relatively dry years.

The effects of increased groundwater pumpage and (or) increased sea level on canal leakage and the position of the freshwater-seawater interface were evaluated using a modified version of the calibrated model to determine how the system may respond to future conditions. Permitted groundwater pumping rates were used for Miami-Dade Water and Sewer Department (MDWASD) groundwater pumping wells in the base-case future scenario. In general, permitted MDWASD groundwater pumping rates exceed historical groundwater pumping rates. As a result, base-case future and increased pumping scenario results suggest seawater intrusion may be an issue at the Miami-Springs well field if the Miami Springs, Hialeah, and Preston well fields are operated using current permitted groundwater pumping rates. Simulations also show that, in general, the canal system limits the adverse effects of proposed groundwater pumpage increases in the combined C-2 and C-100 Basins and the C-1 Basin containing the

Southwest and South Miami Heights well fields, respectively. Proposed increases in groundwater pumpage did not have a notable effect on the position of the freshwater-seawater interface. Increased groundwater pumpage increased lateral groundwater inflow in the basins, but only 25 percent of the pumpage increases in the combined C-2 and C-100 Basins could be accounted for by increased groundwater inflows, whereas 55 percent of the pumpage increases could be accounted for by local changes in canal exchanges. Water-table elevations increased and water-table gradients decreased across the system with increased sea level; with increased sea level, the largest increases in water-table elevations occurred seaward of the salinity control structures. Increased sea level caused flood-prone areas in onshore parts of the study area to increase by 10.32 square miles and increased the percentage of time water-table elevations in flood-prone areas were less than 0.5 foot below land surface by 4 percent. Increased sea level also resulted in landward migration of the freshwater-seawater interface; the largest changes in the position of the freshwater-seawater interface occurred seaward of the salinity control structures, except in parts of the model area that were inundated by increased sea level. Groundwater inflow, groundwater outflow, canal exchanges, surface-water inflow, and surface-water outflow were reduced as a result of decreased water-table gradients across the system. Furthermore, increased water-table elevations resulted in increased evapotranspiration (increased external outflow). The effects of the combination of increased groundwater pumpage and increased sea level were comparable to those in the increased sea-level scenario. Similar to the results for the increased sea-level scenario, groundwater inflow, groundwater outflow, and canal exchanges in the scenario representing groundwater pumpage and increased sea level were reduced as a result of decreased water-table gradients across the system. Water-level reductions (drawdown) resulting from increased groundwater pumpage decreased with increased sea level. Furthermore, reductions in surface-water outflow from the salinity control structures were greatest for the combined increased sea level and increased groundwater pumpage scenario.

Model limitations should be considered when interpreting model simulation results. The model was designed specifically to evaluate the effect of groundwater pumpage on canal leakage and may not be appropriate for predictions based on observations not used in model calibration, at different spatial and temporal scales, and (or) for hydrologic conditions substantially different from those the calibration and verification periods. The reliability of the model is limited by the conceptual model of the surface-water and groundwater system, the spatial distribution of physical properties, the scale and discretization of the system, and specified boundary conditions. Some of the limitations of the model are manifested in model errors. Despite its limitations, the model represents the complexities of the hydrologic system that effect how the system responds to groundwater pumpage and other hydrologic stresses.

## References Cited

- ADA Engineering, 2012, City of South Miami stormwater management master plan—Technical memorandum #1, data collection and evaluation: Consultant report prepared for the City of South Miami accessed March 18, 2013, at [http://www.southmiamifl.gov/clientuploads/PDFs\\_PublicWorks/C218-0211-17%20-%20South%20Miami%20SWMMP%20-%20TM1%20-%20Data%20Collection%20-%20Final.pdf](http://www.southmiamifl.gov/clientuploads/PDFs_PublicWorks/C218-0211-17%20-%20South%20Miami%20SWMMP%20-%20TM1%20-%20Data%20Collection%20-%20Final.pdf).
- Allen, R.G., Pereira, L.S., Raes, D., and Smith, M., 1998, Crop evapotranspiration—Guidelines for computing crop water requirements: FAO Irrigation and Drainage Paper no. 56, Rome, Italy, 300 p.
- Anderson, M.P., and Woessner, W.W., 1992, Applied groundwater modeling, simulation of flow and advective transport: San Diego, Calif., Academic Press, Inc., 381 p.
- Appel, C.A., 1973, Electrical-analog model study of a hydrologic system in southeast Florida: U.S. Geological Survey Open-File Report FL-73004, 51 p.
- Aster, R.C., Borchers, B., and Thurber, C.H., 2005, Parameter estimation and inverse problems: Amsterdam, Elsevier Academic Press, 301 p.
- Bakker, Mark, Schaars, Frans, Hughes, J.D., Langevin, C.D., and Dausman, A.M., 2013, Documentation of the Seawater Intrusion (SWI2) Package for MODFLOW: U.S. Geological Survey Techniques and Methods, book 6, chap. A46, 47 p., <http://pubs.usgs.gov/tm/6a46/>.
- Bedient, P.B., and Huber, W.C., 1988, Hydrology and floodplain analysis: Reading, Mass., Addison-Wesley, 650 p.
- Bidlake, W.R., Woodham, W.M., and Lopez, M.A., 1996, Evapotranspiration from areas of native vegetation in west-central Florida: U.S. Geological Survey Water-Supply Paper 2430, 35 p.
- Brakefield, Linzy, Hughes, J.D., Langevin, C.D., and Chartier, Kevin, 2013, Estimation of capture zones and drawdown at the Northwest and West well fields, Miami-Dade County, Florida, using an unconstrained Monte Carlo analysis—Recent (2004) and proposed conditions: U.S. Geological Survey Open File Report 2013-1086, 124 p.
- Brown, R.H., and Parker, G.G., 1945, Salt water encroachment in limestone at Silver Bluff, Miami, Florida: Economic Geology, v. 60, no. 4, p. 235-262.
- Causaras, C.R., 1985, Geology of the surficial aquifer system, Broward County, Florida: U.S. Geological Survey Water-Resources Investigations Report 84-4068, 167 p, 2 sheets.
- Causaras, C.R., 1987, Geology of the surficial aquifer system, Dade County, Florida: U.S. Geological Survey Water-Resources Investigations Report 86-4126, 240 p, 3 sheets.
- CDM, 2003, Stormwater master plan C-100 Basin, Phase II—hydrologic and hydraulic modeling for existing and future conditions with and without control measures: Consultant report prepared for Miami-Dade Department of Environmental Resources Management.
- CDM, 2005, Stormwater master plan C-7 Basin, Phase II—hydrologic and hydraulic modeling for existing and future conditions with and without control measures: Consultant report prepared for Miami-Dade Department of Environmental Resources Management.
- CH2MHILL, 2003, Executive summary—Phase II Miami-Dade County stormwater master plan C-103, Florida City, and North Canal basins—executive summary: Consultant report prepared for Miami-Dade Department of Environmental Resources Management.
- CH2MHILL, 2006, South Miami-Dade watershed planning stormwater modeling component Phase II—C-2 Basin executive summary: Consultant report prepared for Miami-Dade Department of Environmental Resources Management.
- Chatfield, C., 1999, The analysis of time series, an introduction (5th ed.): Chapman and Hall.
- Chin, D.A., 1990, A method to estimate canal leakage to the Biscayne aquifer, Dade County, Florida: U.S. Geological Survey Water-Resources Investigations Report 90-4135, 32 p.
- Chin, D.A., 2004, An overview of urban stormwater-management practices in Miami-Dade County, Florida: U.S. Geological Survey Open-File Report 2004-1346, 17 p.
- Chin, D.A., and Patterson, R.D., 2005, Quantification of hydrologic processes and assessment of rainfall-runoff models in Miami-Dade County, Florida: U.S. Geological Survey Scientific Investigations Report 2004-5191.
- Chin, D.A., Iudicello, J.J., Kajder, K.C., Kelly, P.M., Porzilli, D.V., and Guha, Hillol, 2010, Lake effect in wellhead protection: Journal of Water Resources Planning and Management, v. 136, no. 3, p. 403-407.
- Cook, Amy, 2012, Development of an integrated surface and subsurface model of Everglades National Park: Miami, Fla., Florida International University, M.S. thesis, 84 p., 43 figs., accessed February 19, 2013, at <http://digitalcommons.fiu.edu/etd/634>.
- Cooper, H.H., 1959, A hypothesis concerning the dynamic balance of fresh water and salt water in a coastal aquifer: Journal of Geophysical Research, v. 64, no. 4, p. 461-467.
- Cooper, R.P., and Lane, J., 1987, An atlas of eastern Dade County surface water management basins: South Florida Water Management District Technical Memorandum.

- Cunningham, K.J., Bukry, David, Sato, Tokiyuki, Barron, J.A., Guertin, L.A., and Reese, R.S., 2001, Sequence stratigraphy of a South Florida carbonate ramp and bounding siliciclastics (Late Miocene-Pliocene), in Missimer, T.M., and Scott, T.M., eds., *Geology and hydrology of Lee County, Florida—Durward H. Boggess Memorial Symposium: Tallahassee, Florida Geological Survey Special Publication 49*, p. 35-66.
- Cunningham, K.J., Carlson, J.L., Wingard, G.L., Robinson, Edward, and Wacker, M.A., 2004, Characterization of aquifer heterogeneity using cyclostratigraphy and geophysical methods in the upper part of the karstic Biscayne aquifer, southeastern Florida: U.S. Geological Survey Water-Resources Investigations Report 03-4208, 66 p., 5 apps., 5 pl., 1 CD.
- Cunningham, K.J., Sukop, M.C., Huang, Haibo, Alvarez, P.F., Curran, H.A., Dixon, J.F., and Renken, R.A., 2009, Prominence of ichnologically-influenced macroporosity in the karst Biscayne aquifer—Stratiform “super-K” zones: *Geological Society of America Bulletin*, v. 121, no. 1-2, p. 164-235, <http://dx.doi.org/10.1130/B26392.1>.
- Cunningham, K.J., and Sukop, M.C., 2011, Multiple technologies applied to characterization of the porosity and permeability of the Biscayne aquifer, Florida: U.S. Geological Survey Open-File Report 2011-1037, 8 p.
- Cunningham, K.J., Wacker, M.A., Robinson, E., Dixon, J.F., and Wingard, G.L., 2006, A cyclostratigraphic and borehole-geophysical approach to development of a three-dimensional conceptual hydrogeologic model of the karstic Biscayne aquifer, southeastern Florida: U.S. Geological Survey Scientific Investigations Report 2005-5235, 69 p., plus CD.
- Cunningham, K.J., Wacker, M.A., Robinson, E., Gefvert, C.J., and Krupa S.L., 2004, Hydrogeology and ground-water flow at Levee 31N, Miami-Dade County, Florida, July 2003 to May 2004: U.S. Geological Survey Scientific Investigations Map I-2846, 1 sheet.
- de Berg, Mark, Cheong, Otfried, van Kreveld, Marc, and Overmars, Mark, 2008, *Computational geometry—Algorithms and applications*: Berlin Heidelberg, Springer-Verlag, 398 p.
- Doherty, J.E., 2010, *PEST, Model-independent parameter estimation—User manual (5th ed.)*: Brisbane Australia, Watermark Numerical Computing.
- Doherty, J.E., and Hunt, R.J., 2010, Approaches to highly parameterized inversion—A guide to using PEST for groundwater model calibration: U.S. Geological Survey Scientific Investigations Report 2010-5169, 59 p.
- Doherty, J.E., Fioren, M.F., and Hunt, R.J., 2010a, Approaches to highly parameterized inversion—Pilot point theory, guidelines and research directions: U.S. Geological Survey Scientific Investigations Report 2010-5168, 36 p.
- Doherty, J.E., Hunt, R.J., and Tonkin, M.J., 2010b, Approaches to highly parameterized inversion—A guide to using PEST for model-parameter and predictive-uncertainty analysis: U.S. Geological Survey Scientific Investigations Report 2010-5211, 71 p.
- Doherty, J.E., and Welter, D.E., 2010, A short exploration of structural noise: *Water Resources Research*, v. 46, W05525
- Deutsch, C.V., and Journel, A.G., 1998, *GSLIB: Geostatistical software library*: Oxford University Press, 384 p.
- Earth Tech, 2003, Stormwater management master plan C-1 Basin—Executive summary: Consultant report prepared for Miami-Dade Department of Environmental Resources Management.
- Earth Tech, 2006, Stormwater management master plan C-6 Basin: control measures evaluation—Executive summary: Consultant report prepared for Miami-Dade Department of Environmental Resources Management.
- Federal Register Notice, 1979, Biscayne aquifer; notice of determination: Notice FRL 1264-3, v. 44, no. 198, p. 58797-58798.
- Florida Department of Transportation, 1999, Florida land use, cover and forms classification system: Florida Department of Transportation, Surveying and Mapping, Geographic Mapping Section, 93 p., accessed March 13, 2013, at <http://www.dot.state.fl.us/surveyingandmapping/documentsandpubs/fluccmanual1999.pdf>.
- Fish, J.E., 1988, Hydrogeology, aquifer characteristics, and ground-water flow of the surficial aquifer system, Broward County, Florida: U.S. Geological Survey Water-Resources Investigations Report 87-4034, 92 p.
- Fioren, M.N., Doherty, J.E., Hunt, R.J., and Reeves, H.W., 2010, Using prediction uncertainty analysis to design hydrologic monitoring networks—Example applications from the Great Lakes water availability pilot project: U.S. Geological Survey Scientific Investigations Report 2010-5159, 44 p.
- Fish, J.E., and Stewart, M.T., 1991, Hydrogeology of the surficial aquifer system, Dade County, Florida: U.S. Geological Survey Water-Resources Investigations Report 90-4108, 50 p.
- German, E.R., 2000, Regional evaluation of evapotranspiration in the Everglades: U.S. Geological Survey Water-Resources Investigations Report 00-4217, 48 p.

- Ghyben, W.B., 1889, Nota in verband met de voorgenomen putboring nabij Amsterdam: Tijdschrift van het Koninklijk Instituut van Ingenieurs, p. 8–22.
- Giddings, J.B., 1999, Deposition and chronostratigraphic subdivision of the Quaternary sediments, Broward County, Florida: Unpublished Master's Thesis, Florida Atlantic University, Boca Raton, Fla., 155 p.
- Giddings, J.B., Kuebler, L.L., Restrepo, J.I., Rodberg, K.A., Montoya, A.M., and Radin, H.A., 2006, Draft report of Lower East Coast subRegional (LECsR) MODFLOW Model documentation: South Florida Water Management District, 294 p.
- Guha, H., 2008, A stochastic modeling approach to address hydrogeologic uncertainties in modeling wellhead protection boundaries in karst aquifers: *Journal of the American Water Resources Association*, v. 44, no. 3, p. 654–662, <http://dx.doi.org/10.1111/j.1752-1688.2008.00191.x>.
- Guha, H., and Panday, Sorab, 2012, Impact of sea level rise on groundwater salinity in a coastal community of South Florida: *Journal of the American Water Resources Association*, v. 48, no. 3, p. 510–529, <http://dx.doi.org/10.1111/j.1752-1688.2011.00630.x>.
- Hall, Pamela, and Clancy, S.J., 2009, Statewide inventory of onsite sewage treatment and disposal systems in Florida—Final report: Consultant report prepared for the State of Florida Department of Health, Division of Environmental Health, Bureau of Onsite Sewage Programs, 157 p., accessed July 15, 2014, at [http://www.floridahealth.gov/healthy-environments/onsite-sewage/research/\\_documents/research-reports/\\_documents/statewide\\_inventory\\_ostds.pdf](http://www.floridahealth.gov/healthy-environments/onsite-sewage/research/_documents/research-reports/_documents/statewide_inventory_ostds.pdf).
- Harbaugh, A.W., 1990, A computer program for calculating subregional water budgets using results from the U.S. Geological Survey modular three-dimensional ground-water flow model: U.S. Geological Survey Open-File Report 90-392, 46 p.
- Harbaugh, A.W., 2005, MODFLOW-2005, the U.S. Geological Survey modular ground-water model—The Ground-Water Flow Process: U.S. Geological Survey Techniques and Methods, book 6, chap. A16, variously paged.
- Harvey, J.W., Krupa, S.L., Gefvert, C.G., Mooney, R.H., Choi, J., King, S.A., and Giddings, J.B., 2002, Interactions between surface water and ground water and effects on mercury transport in the north-central Everglades: U.S. Geological Survey Water-Resources Investigations Report 02-4050, 82 p.
- Harvey, J.W., Krupa, S.L., and Krest, J.M., 2004, Ground water recharge and discharge in the central Everglades: *Ground Water*, v. 42, p. 1090–1102, <http://dx.doi.org/10.1111/j.1745-6584.2004.tb02646.x>.
- Henry, H.R., 1964, Effects of dispersion on salt encroachment in coastal aquifers: U.S. Geological Survey Water-Supply Paper 1613-C, p. C71-C84.
- Herzberg, A., 1901, Die Wasserversorgung einiger Nordseebäder: *Journal für Gasbeleuchtung und Wasserversorgung*, v. 44, p. 815–819.
- Hickey, T.D., Hine, A.C., Shinn, E.A., Kruse, S.E., and Poore, R.Z., 2010, Pleistocene carbonate stratigraphy of South Florida—Evidence for high-frequency sea-level cyclicity: *Journal of Coastal Research*: v. 26, p. 605–614.
- Hughes, J.D., Langevin, C.D., Chartier, K.L., and White, J.T., 2012, Documentation of the Surface-Water Routing (SWR1) Process for modeling surface-water flow with the U.S. Geological Survey Modular Ground-Water Model (MODFLOW-2005): U.S. Geological Survey Techniques and Methods, book 6, chap. A40 (Version 1.0), 113 p.
- Hughes, J.D., Langevin, C.D., and Brakefield-Goswami, Linzy, 2010, Effect of hypersaline cooling canals on aquifer salinization: *Hydrogeology Journal*, <http://dx.doi.org/10.1007/s10040-009-0502-7>.
- Hughes, J.D., and White, J.T., 2016, MODFLOW-NWT model used to evaluate the potential effect of ground-water pumpage and increased sea level on canal leakage and regional groundwater flow in Miami-Dade County, Florida: U.S. Geological Survey data release, <http://dx.doi.org/10.5066/F79P2ZRH>.
- Hull, J.E., and Meyer, F.W., 1973, Salinity studies in East Glades agricultural area, southeastern Dade County, Florida: Florida Bureau of Geology Report of Investigation, no. 66, 39 p.
- Isaaks, E. H., and Srivastava, R. M., 1989, An introduction to applied geostatistics: New York, Oxford University Press, 561 p.
- Jacobs J.M., Mecikalski, J.R., and Paech, S.J., 2008, Satellite-based solar radiation, net radiation, and potential and reference evapotranspiration estimates over Florida: Report prepared for the U.S. Geological Survey, 138 p., accessed March 12, 2013, at [http://fl.water.usgs.gov/et/publications/GOES\\_FinalReport.pdf](http://fl.water.usgs.gov/et/publications/GOES_FinalReport.pdf).
- Keith and Schnars, 2004, South Miami-Dade watershed study and plan—Sub-task 1.5: Consultant report prepared for the South Florida Regional Planning Council, Miami-Dade County, and the South Florida Water Management District, accessed March 18, 2013, at <http://southmiamidadewatershed.net/WorkProducts/SMDWM-Webfiles/Sub-task%201.5%20Water%20Resources.pdf>.
- Kerans and Tinker, 1997, Sequence stratigraphy and characterization of carbonate reservoirs: SEPM Short course notes, v. 40, 130 p.

- Klein, Howard, 1957, Salt-water encroachment in Dade County, Florida: Florida Geological Survey Information Circular 9, 5 p.
- Klein, Howard, and Waller, B.G., 1985, Synopsis of saltwater intrusion in Dade County, Florida, through 1984: U.S. Geological Survey Water-Resources Investigations Report 85-4101, 1 sheet.
- Klein, Howard, and Ratzlaff, K.W., 1989, Changes in salt-water intrusion in the Biscayne aquifer, Hialeah-Miami Springs area, Dade County, Florida: U.S. Geological Survey Water-Resources Investigations Report 87-4249, 1 sheet.
- Klein, Howard, Armbruster, J.T., McPherson, B.F., and Freiburger, H.J., 1975, Water and the South Florida environment: U.S. Geological Survey Water-Resources Investigations Report 24-75, 165 p.
- Kohout, F.A., 1960a, Cyclic flow of saltwater in the Biscayne aquifer of southeastern Florida: *Journal of Geophysical Research*, v. 65, no. 7, p. 2133-2141.
- Kohout, F.A., 1960b, Flow pattern of fresh water and salt water in the Biscayne aquifer of the Miami area, Florida: *International Association of Scientific Hydrology, Commission of Subterranean Waters*, p. 440-448.
- Kohout, F.A., 1961a, Fluctuations of ground-water levels caused by dispersion of salts: *Journal of Geophysical Research*, v. 66, no. 8, p. 2429-2434.
- Kohout, F.A., 1961b, Case history of salt water encroachment caused by a storm sewer in Miami: *Journal of the American Water Works Association*, v. 53, no. 11, p. 1406-1416.
- Kohout, F.A., 1964, The flow of fresh water and salt water in the Biscayne aquifer of the Miami area, Florida, in *Sea water in coastal aquifers*: U.S. Geological Survey Water-Supply Paper 1613-C, p. 12-32.
- Kohout, F.A., and Hoy, N.D., 1963, Some aspects of sampling salty ground water in coastal aquifers: *Ground Water*, v. 1, no. 1, p. 28-32.
- Kohout, F.A., and Klein, Howard, 1967, Effect of pulse recharge on the zone of diffusion in the Biscayne aquifer: *International Association of Scientific Hydrology, Publication no. 70*, p. 252-270.
- Kohout, F.A., and Kolipinski, M.C., 1967, Biological zonation related to groundwater discharge along the shore of Biscayne Bay, Miami, Florida: *Estuaries*, v. 83, p. 488-499.
- Kohout, F.A., and Leach, S.D., 1964, Salt-water movement caused by control-dam operation in the Snake Creek Canal, Miami, Florida: Florida Geological Survey Report of Investigations 24, part 4, 49 p.
- Krause, Peter, Boyle, D.P., and Bäse, Frank, 2005, Comparison of different efficiency criteria for hydrological model assessment: *Advances in Geosciences*, v. 5, p.89-97, <http://dx.doi.org/10.5194/adgeo-5-89-2005>.
- Langevin, C.D., 2001, Simulation of ground-water discharge to Biscayne Bay, Southeastern Florida: U.S. Geological Survey Water-Resources Investigations Report 00-4251, 127 p.
- Langevin, C.D., Swain, E.D., and Wolfert, M.A., 2005, Simulation of integrated surface-water/ground-water flow and salinity for a coastal wetland and adjacent estuary: *Journal of Hydrology*, v. 314, p. 212-234.
- Langevin, C.D., Thorne, D.T., Jr., Dausman, A.M., Sukop, M.C., and Guo, W., 2007, SEAWAT Version 4—A computer program for simulation of multi-species solute and heat transport: U.S. Geological Survey Techniques and Methods, book 6, chap. A22, 39 p.
- Leach, S.D., and Grantham, R.G., 1966, Salt-water study of the Miami River and its tributaries, Dade County, Florida: Florida Geological Survey Report of Investigations 45, 36 p.
- Leach, S.D., Klein, Howard, and Hampton, E.R., 1972, Hydrologic effects of water control and management of southeastern Florida: Florida Bureau of Geology Report of Investigations 60, 115 p.
- Leach, S.D., and Sherwood, C.B., 1963, Hydrologic studies in the Snake Creek Canal area, Dade County, Florida: Florida Geological Survey Report of Investigations 24, part 3, 33 p.
- Legates, D.R., and McCabe, G.J., Jr., 1999, Evaluating the use of “goodness-of-fit” measures in hydrologic and hydroclimatic model validation: *Water Resources Research*, v. 35, no. 1, p. 233-241, <http://dx.doi.org/10.1029/1998WR900018>.
- Lin, H.C., Talbot, C.A., Richards, D.R., Edris, E.V., Jones, N.L., Yeh, G.T., and Cheng, H.P., 2000, Development of a multidimensional modeling system for simulating canal, overland, and groundwater flow in South Florida: Waterways Experiment Station, Vicksburg, Miss., U.S. Army Corps of Engineers report.
- Lirman, Diego, Orlando, Beth, Maciá, Silvia, Manzello, Derek, Kaufman, Louis, Biber, Patrick, and Jones, Tahzay, 2003, Coral communities of Biscayne Bay, Florida and adjacent offshore areas—Diversity, abundance, distribution, and environmental correlates: *Aquatic Conservation Marine and Freshwater Ecosystems*, v. 13, no. 2, p. 121-135, <http://dx.doi.org/10.1002/aqc.552>.

- Lohmann, M.A., Swain, E.D., Wang, J.D., and Dixon, Joann, 2012, Evaluation of effects of changes in canal management and precipitation patterns on salinity in Biscayne Bay, Florida, using an integrated surface-water/groundwater model: U.S. Geological Survey Scientific Investigations Report 2010-5099, 94 p.
- MacVicar, T.K., VanLent, Thomas, and Castro, Alvin, 1984, South Florida Water Management Model documentation report: South Florida Water Management District Technical Publication 84-3, 123 p.
- Marella, R.L., 1999, Water withdrawals, use, discharge, and trends in Florida, 1995: U.S. Geological Survey Water-Resources Investigations Report 99-4002, 90 p.
- Marella, R.L., 2004, Water withdrawals, use, discharge, and trends in Florida, 2000: U.S. Geological Survey Scientific Investigations Report 2004-5151, 136 p.
- Marella, R.L., 2009, Water withdrawals, use, and trends in Florida, 2005: U.S. Geological Survey Scientific Investigations Report 2009-5125, 49 p.
- Marquardt, Donald, 1963, An algorithm for least-squares estimation of nonlinear parameters: *SIAM Journal on Applied Mathematics*, v. 11, no. 2, p. 431-441.
- McPherson, B.F., and Halley, R.B., 1996, The South Florida environment—A region under stress: U.S. Geological Survey Circular 1134, 61 p.
- Mecikalski, J.R., Sumner, D.M., Jacobs, J.M., Pathak, C.S., Paech, S.J., and Douglas, E.M., 2011, Use of visible geostationary operational meteorological satellite imagery in mapping reference and potential evapotranspiration over Florida, in Labedzki, Leszek, ed., *Evapotranspiration: InTech*, p. 229-254, <http://dx.doi.org/10.5772/14478>.
- Merritt, M.L., 1996a, Assessment of saltwater intrusion in southern coastal Broward County, Florida: U.S. Geological Survey Water-Resources Investigations Report 96-4221, 133 p.
- Merritt, M.L., 1996b, Numerical simulation of a plume of brackish water in the Biscayne aquifer originating from a flowing artesian well, Dade County, Florida: U.S. Geological Survey Water-Supply Paper 2464, 74 p.
- Merritt, M.L., 1997, Simulation of the water-table altitude in the Biscayne aquifer, southern Dade County, Florida, Water Years 1945-89: U.S. Geological Survey Water-Supply Paper 2458, 148 p., 9 pls.
- Meyer, F.W., 1972, Preliminary evaluation of infiltration from the Miami Canal to well fields in the Miami Springs-Hialeah area, Dade County, Florida: U.S. Geological Survey Open-File Report FL-72027, 84 p.
- Miami-Dade Department of Environmental Resources Management, 2000, Hydrologic/hydraulic modeling of the C-103, Florida City, North, C-102, and C-1 Canals and tributary secondary canals in Miami-Dade County.
- Miller, W.L., 1978, Effects of bottom sediments on infiltration from the Miami and tributary canals to the Biscayne aquifer, Dade County, Florida: U.S. Geological Survey Water-Resources Investigations 78-36, 63 p.
- Moore, C.A., and Doherty, J.E., 2005, The role of the calibration process in reducing model predictive error: *Water Resources Research*, v. 41, no. 5, W05020.
- Nash, J.E., and Sutcliffe, J.V., 1970, River flow forecasting through conceptual models part I—A discussion of principles: *Journal of Hydrology*, v. 10, no. 3, p. 282-290.
- Nathan, R.J., and McMahon, T.A., 1990, Evaluation of automated techniques for base flow and recession analyses: *Water Resources Research*, v. 26, no. 7, 1465-1473.
- National Oceanic and Atmospheric Administration, 2006, National Geophysical Data Center (NGDC) Coastal Relief Model: National Oceanic and Atmospheric Administration database, accessed June 1, 2006, at <http://www.ngdc.noaa.gov/mgg/coastal/crm.html>.
- National Oceanic and Atmospheric Administration, 2013, Tides and currents—8723214 Virginia Key, FL: National Oceanic and Atmospheric Administration, accessed January 1, 2013, at <http://tidesandcurrents.noaa.gov/waterlevels.html?id=8723214>.
- National Oceanic and Atmospheric Administration, 2014, Comparative climatic data for the United States through 2012: National Oceanic and Atmospheric Administration, accessed February 25, 2014, at <http://www1.ncdc.noaa.gov/pub/data/ccd-data/CCD-2012.pdf>.
- National Research Council, 1987, Responding to changes in sea level—Engineering implications: National Academy Press, Washington, D.C., 169 p.
- Neary, V.S., Habib, E.H., and Fleming, M.J., 2004, Hydrologic modeling with NEXRAD precipitation in middle Tennessee: *Journal of Hydrologic Engineering*, v. 9, no. 5, p. 339-349, [http://dx.doi.org/10.1061/\(ASCE\)1084-0699\(2004\)9:5\(339\)](http://dx.doi.org/10.1061/(ASCE)1084-0699(2004)9:5(339)).
- Nemeth, M.S., Wilcox, W.M., and Solo-Gabriele, H.M., 2000, Evaluation of the use of reach transmissivity to quantify leakage beneath Levee 31N, Miami-Dade County, Florida: U.S. Geological Survey Water-Resources Investigations Report 00-4066, 80 p.
- Nemeth, M.S., and Solo-Gabriele, H.M., 2003, Evaluation of the use of reach transmissivity to quantify exchange between groundwater and surface water: *Journal of Hydrology*, v. 274, no. 1-4, p. 145-159, [http://dx.doi.org/10.1016/S0022-1694\(02\)00419-5](http://dx.doi.org/10.1016/S0022-1694(02)00419-5).

- Niswonger, R.G., Panday, Sorab, and Ibaraki, Motomu, 2011, MODFLOW-NWT, A Newton formulation for MODFLOW-2005: U.S. Geological Survey Techniques and Methods, book 6, chap. A37, 44 p.
- Oliver, D.S., Reynolds, A.C., and Liu, Ning, 2008, Inverse theory for petroleum reservoir characterization and history matching: Cambridge University Press.
- Parker, G.G., 1945, Salt water encroachment in southern Florida: *Journal of the American Water Works Association*, v. 37, no. 6, p. 526-542.
- Parker, G.G., 1951, Geologic and hydrologic factors in the perennial yield of the Biscayne aquifer, Miami area, Florida: *Journal American Water Works Association*, v. 43, no. 10, p. 817-835.
- Parker, G.G., Ferguson, G.E., Love, S.K., and others, 1955, Water resources of southeastern Florida: Geological Survey Water-Supply Paper 1255, 965 p.
- PBS&J, 2004, Stormwater master plan C-4 Basin, Phase II—Hydrologic and hydraulic modeling for existing and future conditions with and without control measures: Consultant report prepared for Miami-Dade Department of Environmental Resources Management.
- PBS&J, 2006, North Miami-Dade County watershed planning—C-9 Basin Project, Phase II: Consultant report prepared for Miami-Dade Department of Environmental Resources Management.
- Pearlstine, Leonard, Higer, Aaron, Palaseanu, Monica, Fujisaki, Ikuko, and Mazzotti, Frank, 2007, Spatially continuous interpolation of water stage and water depths using the Everglades Depth Estimation Network (EDEN): Gainesville, Fla., Institute of Food and Agriculture, University of Florida, CIR 1521, 18 p., 2 apps., accessed June 17, 2013, at <http://edis.ifas.ufl.edu/pdf/files/UW/UW27800.pdf>.
- Peel, M.C., Finlayson, B.L., and McMahon, T.A., 2007, Updated world map of the Köppen-Geiger climate classification: *Hydrology and Earth System Sciences*, v. 11, p. 1633-1644, <http://dx.doi.org/10.5194/hess-11-1633-2007>.
- Perkins, R.D., 1977, Depositional framework of Pleistocene rocks in South Florida, in Enos, Paul, and Perkins, R.D., eds., *Quaternary sedimentation in South Florida*: Geological Society of America Memoir 147, p. 131-198.
- Prager, E.J., and Halley, R.B., 1997, Florida Bay bottom types: U.S. Geological Survey Open-File Report 97-526, 1 oversize sheet.
- Press, W.H., Teukolsky, S.A., Vetterling, W.T., and Flannery, B.P., 1990, *Numerical recipes in C*: New York, Cambridge University Press, 994 p.
- Prinos, S.T., Wacker, M.A., Cunningham, K.J., and Fitterman, D.V., 2014, Origins and delineation of saltwater intrusion in the Biscayne aquifer and changes in the distribution of saltwater in Miami-Dade County, Florida: U.S. Geological Survey Scientific Investigations Report 2014-5025, 101 p., <http://dx.doi.org/10.3133/sir20145025>.
- Reese, R.S., and Cunningham, K.J., 2000, Hydrogeology of the gray limestone aquifer in Southern Florida: U.S. Geological Survey Water-Resources Investigations Report 99-4213, 244 p.
- Remy, Nicolas, Boucher, Alexandre, and Wu, Jianbing, 2009, *Applied geostatistics with SGeMS—A user's guide*: Cambridge University Press, 286 p.
- Renken, R.A., Dixon, Joann, Koehmstedt, John, Lietz, A.C., Marella, R.L., Telis, Pamela, Rodgers, Jeff, and Memberg, Steven, 2005a, Impact of anthropogenic development on coastal ground-water hydrology in southeastern Florida, 1900-2000: Reston, Va., U.S. Geological Survey Circular 1275, 77 p.
- Renken, R.A., Cunningham, K.J., Shapiro, A.M., Harvey, R.W., Zygnerski, M.R., Metge, D.W., and Wacker, M.A., 2008, Pathogen and chemical transport in the karst limestone of the Biscayne aquifer—1. Revised conceptualization of groundwater flow: *Water Resources Research*, v. 44, W08429, <http://dx.doi.org/10.1029/2007WR006058>.
- Renken, R.A., Shapiro, A.M., Cunningham, K.J., Harvey, R.W., Metge, D.W., Zygnerski, M.R., Osborn, C.L., Wacker, M.A., and Ryan, J.N., 2005b, Assessing the vulnerability of a municipal well field to contamination in a karst aquifer: *Environmental and Engineering Geoscience*, v. 11, no. 4, p. 319-331.
- Schroeder, M.C., Klein, Howard, and Hoy, N.D., 1958, Biscayne aquifer of Dade and Broward Counties, Florida: Florida Geological Survey Report of Investigations 17, 56 p.
- Shapiro, A.M., Renken, R.A., Harvey, R.W., Zygnerski, M.R., and Metge, D.W., 2008, Pathogen and chemical transport in the karst limestone of the Biscayne aquifer—2. Chemical retention from diffusion and slow advection: *Water Resources Research*, v. 44, W08430, <http://dx.doi.org/10.1029/2007WR006059>.
- Sherwood, C.B., and Leach, S.D., 1962, Hydrologic studies in the Snapper Creek Canal area, Dade County, Florida: Florida Geological Survey Report of Investigations 24, part 2, 32 p.
- Shoemaker, W.B., and Lopez, C.D., and Duever, Michael, 2011, Evapotranspiration over spatially extensive plant communities in the Big Cypress National Preserve, southern Florida, 2007-2010: U.S. Geological Survey Scientific Investigations Report 2011-5212, 46 p.

- Skinner, Courtney, Bloetscher, Fredrick, and Pathak, C.S., 2009, Comparison of NEXRAD and rain gauge precipitation measurements in South Florida: *Journal of Hydrologic Engineering*, v. 14, no. 3, p. 248–260, [http://dx.doi.org/10.1061/\(ASCE\)1084-0699\(2009\)14:3\(248\)](http://dx.doi.org/10.1061/(ASCE)1084-0699(2009)14:3(248)).
- Sonenshein, R.S., 1997, Delineation and extent of saltwater intrusion in the Biscayne aquifer, Eastern Dade County, Florida, 1995: U.S. Geological Survey Water Resources Investigations Report 96-4285, 1 sheet.
- Sonenshein, R.S., 2001, Methods to quantify seepage beneath Levee 30, Miami-Dade County, Florida: U.S. Geological Survey Water-Resources Investigations Report 01-4074, 36 p.
- Sonenshein, R.S., and Koszalka, E.J., 1996, Trends in water-table altitude (1984-93) and saltwater intrusion (1974-93) in the Biscayne aquifer, Dade County, Florida: U.S. Geological Survey Open-File Report 95-705, 2 sheets.
- Southeast Florida Regional Climate Change Compact Technical Ad hoc Work Group, 2011, A unified sea level rise projection for southeast Florida: Southeast Florida Regional Climate Change Compact Steering Committee, 27 p., accessed July 24, 2013, at <http://southeastfloridaclimatecompact.org/pdf/Sea%20Level%20Rise.pdf>.
- South Florida Water Management District, 1995, Land cover land use 1995: South Florida Water Management District, West Palm Beach, Fla., accessed March 8, 2013, at [http://my.sfwmd.gov/gisapps/sfwmdxwebdc/dataview.asp?query=unq\\_id=297](http://my.sfwmd.gov/gisapps/sfwmdxwebdc/dataview.asp?query=unq_id=297).
- South Florida Water Management District, 2002, Composite land use for the South Florida Water Management Model 2000: South Florida Water Management District, West Palm Beach, Fla., accessed March 8, 2013, at [http://my.sfwmd.gov/gisapps/sfwmdxwebdc/dataview.asp?query=unq\\_id=1175](http://my.sfwmd.gov/gisapps/sfwmdxwebdc/dataview.asp?query=unq_id=1175).
- South Florida Water Management District, 2005, Documentation of the South Florida Water Management Model—Version 5.5: South Florida Water Management District, 305 p., accessed March 13, 2013, at [http://www.sfwmd.gov/portal/page/portal/xrepository/sfwmd\\_repository\\_pdf/sfwmm\\_final\\_121605.pdf](http://www.sfwmd.gov/portal/page/portal/xrepository/sfwmd_repository_pdf/sfwmm_final_121605.pdf).
- South Florida Water Management District, 2008, Water conservation—A comprehensive program for South Florida: South Florida Water Management District, 27 p., accessed February 11, 2013, at [http://www.sfwmd.gov/portal/page/portal/xrepository/sfwmd\\_repository\\_pdf/waterconservationplan.pdf](http://www.sfwmd.gov/portal/page/portal/xrepository/sfwmd_repository_pdf/waterconservationplan.pdf).
- South Florida Water Management District, 2009a, 2007-08 Miami-Dade 50-ft DEM in NAVD 1988, release version 1: South Florida Water Management District, accessed June 1, 2012, at <http://my.sfwmd.gov/gisapps/sfwmdxwebdc/dataview.asp>.
- South Florida Water Management District, 2009b, 2007 Broward 50-ft DEM in NAVD 1988, release version 1: South Florida Water Management District, accessed June 1, 2012, at <http://my.sfwmd.gov/gisapps/sfwmdxwebdc/dataview.asp>.
- South Florida Water Management District, 2010, Wet season, dry season—Managing every drop: South Florida Water Management District, accessed February 27, 2014, at <http://www.sfwmd.gov/portal/pls/portal/docs/15617306.PDF>.
- South Florida Water Management District, 2011a, Land cover land use 2004: South Florida Water Management District, West Palm Beach, Fla., accessed March 8, 2013, at [http://my.sfwmd.gov/gisapps/sfwmdxwebdc/dataview.asp?query=unq\\_id=1813](http://my.sfwmd.gov/gisapps/sfwmdxwebdc/dataview.asp?query=unq_id=1813).
- South Florida Water Management District, 2011b, Land cover land use 2008: South Florida Water Management District, West Palm Beach, Fla., accessed March 8, 2013, at [http://my.sfwmd.gov/gisapps/sfwmdxwebdc/dataview.asp?query=unq\\_id=2184](http://my.sfwmd.gov/gisapps/sfwmdxwebdc/dataview.asp?query=unq_id=2184).
- South Florida Water Management District, 2011c, DBHYDRO database: Accessed May 29, 2011, at <http://www.sfwmd.gov/portal/page/portal/xweb%20environmental%20monitoring/dbhydro%20application>.
- Sukop, M.C., Huang, Haibo, Alvarez, P.F., Variano, E.A., and Cunningham, K.J., 2013, Evaluation of permeability and non-Darcy flow in vuggy macroporous limestone aquifer samples with lattice Boltzmann methods: *Water Resources Research*, v. 49, no. 1, p. 216-230, <http://dx.doi.org/10.1029/2011WR011788>.
- Sumner, D.M., 1997, Evapotranspiration from successional vegetation in a deforested area of the Lake Wales Ridge, Florida: U.S. Geological Survey Water-Resources Investigations Report 96-4244, 38 p.
- Sumner, D.M., 2001, Evapotranspiration from a cypress and pine forest subjected to natural fires in Volusia County, Florida, 1998-99: U.S. Geological Survey Water-Resources Investigations Report 01-4245, 55 p.
- Sunderland, R.S.A., and Krupa, S.L., 2007, Groundwater – surface water interaction along the C-2 Canal, Miami-Dade County, Florida: South Florida Water Management District Technical Publication WS-22, 48 p., plus apps.

- Swain, E.D., Howie, Barbara, and Dixon, Joann, 1996, Description and field analysis of a coupled groundwater/surface-water flow model (MODFLOW/BRANCH) with modifications for structures and wetlands in southern Dade County, Florida: U.S. Geological Survey Water-Resources Investigations Report 96-4118, 67 p.
- Swancar, A., Lee, T.M., and O'Hare, T.M., 2000, Hydrogeologic setting, water budget, and preliminary analysis of ground-water exchange at Lake Starr, a seepage lake in Polk County, Florida: U.S. Geological Survey Water-Resources Investigations Report 00-4030, 72 p.
- Telis, P.A., 2006, The Everglades Depth Estimation Network (EDEN) for support of ecological and biological assessments: U.S. Geological Survey Fact Sheet 2006-3087, 4 p.
- Tikhonov, A.N., and Arsenin, V.Y., 1977, Solutions of ill-posed problems: New York, Halstead Press-Wiley, 258p.
- Tonkin, M.J., and Doherty, J.E., 2005, A hybrid regularized inversion methodology for highly parameterized models: *Water Resources Research*, v. 29, <http://dx.doi.org/10.1029/2005WR003995>.
- U.S. Army Corps of Engineers, 2011, Sea-level change considerations for civil works programs: United States Army Corps of Engineers Circular No. 1165-2-212, 32 p., accessed July 24, 2013, at [http://publications.usace.army.mil/publications/eng-circulars/EC\\_1165-2-212.pdf](http://publications.usace.army.mil/publications/eng-circulars/EC_1165-2-212.pdf).
- U.S. Geological Survey, 2012, Everglades Depth Estimation Network (EDEN) database: U.S. Geological Survey, accessed June 1, 2012, at <http://sofia.usgs.gov/eden/models/groundelevmod.php>.
- URS, 2003, C-102 and Goulds Drainage Basin volume 1—Hydrologic and hydraulic modeling: Consultant report prepared for Miami-Dade Department of Environmental Resources Management.
- URS, 2005, C-3 and C-5 Basins stormwater master plan: Consultant report prepared for Miami-Dade Department of Environmental Resources Management.
- Vogel, C.R., 2002, Computational methods for inverse problems: *Frontiers in Applied Mathematics*, SIAM.
- Wang, J.D., Swain, E.D., Wolfert, M.A., Langevin, C.D., James, D.E., and Telis, P.A., 2007a, Application of FTLO-ADDS to simulate flow, salinity, and surface-water stage in the southern Everglades, Florida: U.S. Geological Survey Scientific Investigations Report 2007-5010, 112 p.
- Wang, Xianwei, Xie, Hongjie, Sharif, Hatim, and Zeitler, Jon, 2007b, Validating NEXRAD MPE and Stage III precipitation products for uniform rainfall on the Upper Guadalupe River Basin of the Texas Hill Country: *Journal of Hydrology*, v. 348, no. 1-2, p. 73-86, <http://dx.doi.org/10.1016/j.jhydrol.2007.09.057>.
- Watkins, D.W., Li, Hebi, and Cowden, J.R., 2007, Adjustment of radar-based precipitation estimates for Great Lakes hydrologic modeling: *Journal of Hydrologic Engineering*, v. 12, no. 3, p. 298-305, [http://dx.doi.org/10.1061/\(ASCE\)1084-0699\(2007\)12:3\(298\)](http://dx.doi.org/10.1061/(ASCE)1084-0699(2007)12:3(298)).
- Westenbroek, S.M., Doherty, J.E., Walker, J.F., Kelson, V.A., Hunt, R.J., and Cera, T.B., 2012, Approaches in highly parameterized inversion—TSPROC, a general time-series processor to assist in model calibration and result summation: U.S. Geological Survey Techniques and Methods, book 7, chap. C7, 79 p., 3 apps.
- White, W.A., 1970, The geomorphology of the Florida peninsula: Florida Bureau of Geology Bulletin no. 51, 164 p., 4 pl.
- Zetler, B.S., 1982, Computer applications to tides in the National Ocean Survey: National Oceanic and Atmospheric Administration, National Ocean Survey, Supplement to Manual of Harmonic Analysis and Prediction of Tides: Special Publication no. 98, 85 p.

## Appendix 1. Documentation for the General Flux Boundary (GFB) Package for MODFLOW

The General Flux Boundary (GFB) Package for MODFLOW was used to apply NEXRAD rainfall and septic return flow in the urban Miami-Dade County model. The GFB package was developed from the standard MODFLOW recharge (RCH) and well (WEL) Packages (Harbaugh, 2005) and allows combinations of individual specified fluxes and two-dimensional arrays containing different specified fluxes to be applied to the MODFLOW model in each stress period. Two-dimensional multiplier arrays can be specified for each specified flux term and, similar to the RCH Package, specified fluxes can be applied to (1) the top layer, (2) a specified layer, or (3) the upper most active cell in each row and column location; each specified flux can use a different vertical distribution option. Individual specified fluxes are reported separately to the global MODFLOW budget and to cell-by-cell flow files. MODFLOW parameters are not supported in the GFB Package.

### Input Instructions

The use of the GFB is similar to the RCH and WEL Packages, and it is assumed that users are familiar with the use of MODFLOW and the input files required for MODFLOW as documented in Harbaugh (2005); thus, this appendix only describes input files required by GFB.

### MODFLOW Name (NAM) File

Use of the GFB Package is activated by including a record in the MODFLOW name file using the file type (Ftype) "GFB" to indicate that relevant calculations are to be made in the model and to specify the related input data file.

### GFB Data Input Instructions

The GFB file contains package options and data values for the different flux items. Optional variables are indicated in [brackets].

FOR EACH SIMULATION

1. Data: NGFBITEMS IGFCB [OPTIONS]  
Module: URWORD

FOR EACH NGFBITEM

2. Data: NAME NTYPE [MXGFBF] [NOPT] [NMULT]  
Module: URWORD

Item 2 must be repeated NGFBITEM times.

FOR EACH STRESS PERIOD

3. Data: INGFB  
Module: URWORD

IF INGFB > 0

FOR EACH ITEM IN NGFBITEM

IF NTYPE (ITEM) = 1

- 4a. Data: ITMP  
Module: URWORD

IF ITMP > 0

- 4b. Data: Layer Row Column Q  
Module: URWORD

Item 4b must be repeated ITMP times.

```

IF NTYPE (ITEM) = 2
5a.  Data:  INRATE [INLAY] [INMULT]
      Module:  URWORD

      IF INRATE > 0
5b.  Data:  RATE2D (NCOL, NROW)
      Module:  U2DREL

      IF INLAY > 0 AND NOPT (ITEM) = 2
5c.  Data:  LAYER2D (NCOL, NROW)
      Module:  U2DINT

      IF INMULT > 0 AND NMULT (ITEM) > 0
5d.  Data:  MULTIPLIER2D (NCOL, NROW)
      Module:  U2DREL
    
```

Explanation of variables read by the GFB Package

NGFBITEMS—Number of GFB flux items.

IGFBCB—Flag and a unit number for BUDGET output. When this option is selected, corrections to the cell by cell flows computed by MODFLOW will be written to the same or different file (depending on the unit number). GFB flux items are given the NAME specified in dataset 2.

If IGFBCB > 0, unit number for BUDGET  
 If IGFBCB ≤ 0, BUDGET will not be recorded for GFB flux items.

OPTIONS—Is an optional list of character values

“NOPRINT” — suppresses printing of GFB Package input data in the MODFLOW listing file.

NAME—is the name of the GFB Package flux item. This name is written to BUDGET output and the global budget printed to the MODFLOW listing file. The text string is limited to 20 alphanumeric characters. If the name of the well includes spaces, then enclose the name in quotes.

NTYPE—Integer flag that defines if this GHB flux item is point or two-dimensional data.

If NTYPE = 1, point data  
 If NTYPE = 2, two-dimensional data.

MXGFB—Integer flag that defines the maximum number of point data that will be specified for this GFB flux item. MXGFB is only specified if NTYPE = 1.

NOPT—Integer flag that layer option code for this GFB flux item. NOPT is only specified if NTYPE = 2.

If NOPT = 1, Two-dimensional GFB flux is only applied to the top grid layer.  
 If NOPT = 2, Vertical distribution of two-dimensional GFB flux is specified in GFB LAYER variable.  
 If NOPT = 3, Two-dimensional GFB flux is applied to the highest active cell in each vertical column. A constant-head node intercepts the specified GFB flux and prevents deeper application.

NMULT—Integer flag that defines the specified two-dimension GFB flux will be multiplied by a multiplier array. MXGFB is only specified if NTYPE = 2.

If NMULT ≤ 0, Two-dimensional GFB multiplier data will not be read.  
 If NMULT > 0, Two-dimensional GFB multiplier data will be read.

INGFB—Integer flag that defines whether GFB data will be read for this stress period.

If  $INGFB \leq 0$ , GFB data from the preceding stress period are used.

If  $INGFB > 0$ , GFB data will be read for this stress period.

ITMP—Integer flag and counter that defines point GFB data will be read for this stress period for the GFB item.

If  $ITMP < 0$ , GFB data from the preceding stress period are used for this GFB item.

If  $ITMP \geq 0$ , ITMP will be the number of point GFB data that will be read for this GFB item.

LAYER—Integer variable that defines the layer number of the model cell that contains the specified GFB flux.

ROW—Integer variable that defines the row number of the model cell that contains the specified GFB flux.

COLUMN—Integer variable that defines the column number of the model cell that contains the specified GFB flux.

Q—Real variable that defines the volumetric rate for the specified GFB flux. A positive value indicates recharge and a negative value indicates discharge

INRATE—Integer flag that defines two-dimensional GFB rate data will be read for this stress period for the GFB item.

If  $INRATE \leq 0$ , GFB rate data from the preceding stress period are used for this GFB item.

If  $INRATE > 0$ , GFB rate data that will be read for this GFB item.

INLAY—Integer flag that defines two-dimensional GFB layer data will be read for this stress period for the GFB item. INLAY is only read if NOPT for this GFB flux item is equal to 2.

If  $INLAY \leq 0$ , GFB layer data from the preceding stress period are used for this GFB item.

If  $INLAY > 0$ , GFB layer data that will be read for this GFB item.

INMULT—Integer flag that defines two-dimensional GFB multiplier data will be read for this stress period for the GFB item.

INMULT is only read if NMULT for this GFB flux item is greater than 0.

If  $INLAY \leq 0$ , GFB layer data from the preceding stress period are used for this GFB item.

If  $INLAY > 0$ , GFB layer data that will be read for this GFB item.

RATE2D—Real array that defines the two-dimensional specified flux ( $LT^{-1}$ ) for this GFB flux item. Read only if INRATE for this GFB flux item is greater than 0.

LAYER2D—Integer array that defines the layer number in each vertical column where the two-dimensional specified flux ( $LT^{-1}$ ) for this GFB flux item is applied. Read only if INLAYER for this GFB flux item is greater than 0.

MULTIPLIER2D—Real array that defines the two-dimensional multiplier to apply to the specified flux ( $LT^{-1}$ ) for this GFB flux item. Read only if INMULT for this GFB flux item is greater than 0.

## Example GFB Data Input File

An example GFB input file that includes FORTRAN source code for the GFB package for MODFLOW is listed below.

```
#Example GFB Input file
#NGFBITEMS      IGFBCB
      3          30

#NAME           NTYPE  MXGFBF  NOPT  NMULT
'RECHARGE DATA'      2          3      0
'WELL 1'              1          1
'WELL 2'              1          1
#      INGFB
```

```

1 #STRESS PERIOD 00001
# RECHARGE DATA STRESS PERIOD 1
# INRATE INLAY INMULT
1 0 0 #RECHARGE DATA
CONSTANT .0040
# WELL 1 STRESS PERIOD 1
# ITMP
0
# WELL 2 STRESS PERIOD 1
# ITMP
0
# INGFB
1 #STRESS PERIOD 00002
# INRATE INLAY INMULT
-1 0 0 #RECHARGE DATA
# WELL 1 STRESS PERIOD 2
# ITMP
1
2 8 4 -35000.
# WELL 2 STRESS PERIOD 2
# ITMP
1
2 3 4 -35000.

```

## FORTRAN Source Code

FORTRAN source code for the GFB Package for MODFLOW is listed below.

```

MODULE GWFGFBMODULE

TYPE GFB_DATAITEM
CHARACTER (LEN=16) :: TEXT
INTEGER :: NTYPE
INTEGER :: MXACTF
INTEGER :: NFLUX
INTEGER :: NFLUXVL
INTEGER :: N2DOP
INTEGER :: N2DMULT
INTEGER :: NAUX
CHARACTER (LEN=16), DIMENSION(:), ALLOCATABLE :: FLUXAUX
REAL, DIMENSION(:, :), ALLOCATABLE :: FLUX
REAL, DIMENSION(:, :), ALLOCATABLE :: MULTIPLIER
REAL, DIMENSION(:, :), ALLOCATABLE :: RATE
INTEGER, DIMENSION(:, :), ALLOCATABLE :: LAYER
END TYPE GFB_DATAITEM

C
INTEGER, SAVE, POINTER :: NGFBITEMS
INTEGER, SAVE, POINTER :: IGFBBCB
INTEGER, SAVE, POINTER :: IGFBPR
TYPE(GFB_DATAITEM), SAVE, DIMENSION(:), POINTER :: GFB_DATA
TYPE GWFGFBTYPE
INTEGER, POINTER :: NGFBITEMS
INTEGER, POINTER :: IGFBBCB
INTEGER, POINTER :: IGFBPR
TYPE(GFB_DATAITEM), DIMENSION(:), POINTER :: GFB_DATA
END TYPE GWFGFBTYPE
TYPE(GWFGFBTYPE), SAVE :: GWFGFBDAT(10)
END MODULE GWFGFBMODULE

```

```

SUBROUTINE GWF2GFB7AR(IN, IGRID)
C *****
C ALLOCATE ARRAY STORAGE FOR GFB
C *****
C
C SPECIFICATIONS:
C -----
C USE GLOBAL, ONLY:IOUT,NCOL,NROW,IFREFM
C USE GWF2GFBMODULE,ONLY:NGFBITEMS,IGFBCB,IGFBPR,GFB_DATA
C
C IMPLICIT NONE
C
C DUMMY VARIABLES
C INTEGER, INTENT(IN) :: IN
C INTEGER, INTENT(IN) :: IGRID
C
C LOCAL VARIABLES
C CHARACTER*200 LINE
C CHARACTER (LEN=16) :: TEXT
C
C INTEGER :: LLOC
C INTEGER :: ISTART
C INTEGER :: ISTOP
C INTEGER :: IC, IR
C INTEGER :: I, K, N
C INTEGER :: MXACTF
C INTEGER :: NAUX
C INTEGER :: NFLUXVL
C
C REAL :: R
C
C-----FORMATS
2000 FORMAT(1X,'CELL-BY-CELL FLOWS WILL BE SAVED ON UNIT ',I4)
2005 FORMAT(1X,'LISTS OF GFB FLUXES WILL NOT BE PRINTED')
2010 FORMAT(1X,'GFB ITEM ',A16,' WITH NTYPE = ',I5)
2020 FORMAT(1X,'ILLEGAL GFB OPTION CODE (NTYPE = ',I5,
& ' ) -- SIMULATION ABORTING')
2030 FORMAT(1X,'OPTION 1 -- RATE APPLIED TO TOP LAYER')
2040 FORMAT(1X,'OPTION 2 -- RATE APPLIED TO ONE SPECIFIED NODE IN',
1 ' EACH VERTICAL COLUMN')
2050 FORMAT(1X,'OPTION 3 -- RATE APPLIED TO HIGHEST ACTIVE NODE IN',
1 ' EACH VERTICAL COLUMN')
2060 FORMAT(1X,'MULTIPLIERS WILL BE APPLIED TO RATE FOR GFB ITEM',
! I5, '( ', A16, ' )')
C
C -----
C
C-----ALLOCATE SCALAR VARIABLES.
ALLOCATE(NGFBITEMS,IGFBCB,IGFBPR)
C
C-----IDENTIFY PACKAGE.
WRITE(IOUT,1) IN
00001 FORMAT(1X,/1X,'GFB -- GENERAL FLUX BOUNDARY PACKAGE, VERSION 1, ',
& '02/19/2013',/1X,'INPUT READ FROM UNIT ',I4)
C
C-----READ NGFBITEMS AND IGFBCB.
CALL URDCOM(IN,IOUT,LINE)
LLOC=1
CALL URWORD(LINE,LLOC,ISTART,ISTOP,2,NGFBITEMS,R,IOUT,IN)
CALL URWORD(LINE,LLOC,ISTART,ISTOP,2,IGFBCB,R,IOUT,IN)

```

```

C
CC-----IF CELL-BY-CELL FLOWS ARE TO BE SAVED, THEN PRINT UNIT NUMBER.
      IF(IGFBCB.GT.0) WRITE(IOUT,2000) IGFBCB
C
CC-----READ AUXILIARY VARIABLES AND PRINT FLAG.
      IGFBCB = 1
      10 CALL URWORD(LINE,LLOC,ISTART,ISTOP,1,N,R,IOUT,IN)
      IF(LINE(ISTART:ISTOP).EQ.'NOPRINT') THEN
          WRITE(IOUT,2005)
          IGFBCB = 0
          GO TO 10
      END IF
C
CC-----ALLOCATE SPACE FOR EACH ITEM
      ALLOCATE(GFB_DATA(NGFBITEMS))
C
CC-----READ DATA FOR EACH ITEM
      DO K = 1, NGFBITEMS
          CALL URDCOM(IN,IOUT,LINE)
          LLOC=1
          CALL URWORD(LINE,LLOC,ISTART,ISTOP,1,I,R,IOUT,IN)
          TEXT = LINE(ISTART:ISTOP)
          GFB_DATA(K)%TEXT = ADJUSTR(TEXT)
          CALL URWORD(LINE,LLOC,ISTART,ISTOP,2,I,R,IOUT,IN)
          GFB_DATA(K)%NTYPE = I
          WRITE(IOUT,2010) GFB_DATA(K)%TEXT, GFB_DATA(K)%NTYPE
          SELECT CASE (GFB_DATA(K)%NTYPE)
C
              POINTS
              CASE (1)
                  CALL URWORD(LINE,LLOC,ISTART,ISTOP,2,MXACTF,R,IOUT,IN)
                  NAUX = 0
                  NFLUXVL = 4 + NAUX
                  GFB_DATA(K)%NFLUXVL = NFLUXVL
                  GFB_DATA(K)%NAUX = NAUX
                  GFB_DATA(K)%MXACTF = MXACTF
                  ALLOCATE(GFB_DATA(K)%FLUXAUX(20))
                  ALLOCATE(GFB_DATA(K)%FLUX(NFLUXVL, MXACTF))
                  DO N = 1, MXACTF
                      DO I = 1, NFLUXVL
                          GFB_DATA(K)%FLUX(I,N) = 0.0
                      END DO
                  END DO
C
              ARRAYS
              CASE (2)
                  CALL URWORD(LINE,LLOC,ISTART,ISTOP,2,I,R,IOUT,IN)
                  GFB_DATA(K)%N2DOP = I
C
                  CHECK TO SEE THAT OPTIONS ARE LEGAL
                  IF(GFB_DATA(K)%N2DOP.LT.1.OR.GFB_DATA(K)%N2DOP.GT.3) THEN
                      WRITE(IOUT,2020) GFB_DATA(K)%N2DOP
                      CALL USTOP(` `)
                  END IF
                  CALL URWORD(LINE,LLOC,ISTART,ISTOP,2,I,R,IOUT,IN)
                  GFB_DATA(K)%N2DMULT = I
C
                  ALLOCATE MEMORY FOR ITEM
                  ALLOCATE(GFB_DATA(K)%RATE(NCOL,NROW))
                  ALLOCATE(GFB_DATA(K)%MULTIPLIER(NCOL,NROW))
                  DO IR=1,NROW
                      DO IC=1,NCOL
                          GFB_DATA(K)%RATE(IC,IR)=0.0
                          GFB_DATA(K)%MULTIPLIER(IC,IR)=1.0
                      END DO

```

```

        END DO
        IF ( GFB_DATA(K) %N2DOP.EQ.2.OR.GFB_DATA(K) %N2DOP.EQ.3) THEN
            ALLOCATE (GFB_DATA(K) %LAYER (NCOL,NROW) )
        END IF
C      WRITE SUMMARY INFORMATION
        IF (GFB_DATA(K) %N2DOP.EQ.1)    WRITE (IOUT,2030)
        IF (GFB_DATA(K) %N2DOP.EQ.2)    WRITE (IOUT,2040)
        IF (GFB_DATA(K) %N2DOP.EQ.3)    WRITE (IOUT,2050)
        IF (GFB_DATA(K) %N2DMULT.NE.0)  WRITE (IOUT,2060)
    END SELECT
END DO

C
C-----SAVE POINTERS
    CALL SGWF2GFB7PSV (IGRID)
C
C-----RETURN
    RETURN
END SUBROUTINE GWF2GFB7AR

SUBROUTINE GWF2GFB7RP (IN, IGRID)
C *****
C READ RECHARGE DATA FOR STRESS PERIOD
C *****
C
C   SPECIFICATIONS:
C   -----
C   USE GLOBAL,          ONLY:IOUT
C   USE GWF2GFBMODULE, ONLY:NGFBITEMS,GFB_DATA

    IMPLICIT NONE

C
C   DUMMY VARIABLES
    INTEGER, INTENT (IN) :: IN
    INTEGER, INTENT (IN) :: IGRID

C
C   LOCAL VARIABLES
    CHARACTER (LEN=200) :: LINE

    INTEGER :: LLOC
    INTEGER :: ISTART
    INTEGER :: ISTOP
    INTEGER :: INGFB
    INTEGER :: K

    REAL :: R
C   -----
C
C-----FORMATS
    2000  FORMAT(1X,/1X,'REUSING GFB FROM LAST STRESS PERIOD')
C
CC-----SET POINTERS FOR THE CURRENT GRID.
    CALL SGWF2GFB7PNT (IGRID)
C
CC-----READ FLAG SHOWING WHETHER DATA IS TO BE REUSED.
    CALL URDCOM (IN, IOUT, LINE)
    LLOC=1
    CALL URWORD (LINE, LLOC, ISTART, ISTOP, 2, INGFB, R, IOUT, IN)
C
CC-----TEST INGFB TO SEE HOW TO DEFINE RECH.
    IF (INGFB.LT.1) THEN
C
CC-----INGFB<1, SO REUSE GFB ARRAYS FROM LAST STRESS PERIOD.

```

```

        WRITE(IOUT,2000)
C
C-----CYCLE THROUGH ITEMS
      ELSE
        DO K = 1, NGFBITEMS
          SELECT CASE (GFB_DATA(K)%NTYPE)
            CASE (1)
              CALL GFB1DITEMREAD(IN,GFB_DATA(K))
            CASE (2)
              CALL GFB2DITEMREAD(IN,GFB_DATA(K))
          END SELECT
        END DO
      END IF
C
C6-----RETURN
      RETURN
    END SUBROUTINE GWF2GFB7RP

    SUBROUTINE GWF2GFB7FM(IGRID)
C *****
C SUBTRACT RECHARGE FROM RHS
C *****
C
C   SPECIFICATIONS:
C   -----
C   USE GLOBAL,          ONLY:NCOL,NROW,NLAY,IBOUND,RHS
C   USE GWF2GFBMODULE, ONLY:NGFBITEMS,GFB_DATA
C
C   IMPLICIT NONE
C
C   DUMMY VARIABLES
C   INTEGER, INTENT(IN) :: IGRID
C
C   LOCAL VARIABLES
C   INTEGER :: K
C   -----
C
C-----SET POINTERS FOR THE CURRENT GRID.
      CALL SGWF2GFB7PNT(IGRID)
C
C-----CYCLE THROUGH EACH ITEM
      DO K = 1, NGFBITEMS
        SELECT CASE (GFB_DATA(K)%NTYPE)
          CASE (1)
            CALL GFB1DITEMFORMULATE(GFB_DATA(K))
          CASE (2)
            CALL GFB2DITEMFORMULATE(GFB_DATA(K))
        END SELECT
      END DO
C
C-----RETURN
      RETURN
    END SUBROUTINE GWF2GFB7FM

    SUBROUTINE GWF2GFB7BD(KSTP,KPER,IGRID)
C *****
C CALCULATE VOLUMETRIC BUDGET FOR RECHARGE
C *****
C
C   SPECIFICATIONS:

```

```

C -----
C   USE GLOBAL,          ONLY:IOUT,NCOL,NROW,NLAY,IBOUND,BUFF
C   USE GWFBASMODULE, ONLY:MSUM,VBVL,VBNM,ICBCFL,DELT,PERTIM,TOTIM
C   USE GWFGFBMODULE, ONLY:NGFBITEMS,GFB_DATA

C   IMPLICIT NONE

C
C   DUMMY VARIABLES
C   INTEGER, INTENT(IN) :: KSTP
C   INTEGER, INTENT(IN) :: KPER
C   INTEGER, INTENT(IN) :: IGRID

C
C   LOCAL VARIABLES
C   INTEGER :: K
C -----

C1-----SET POINTERS FOR THE CURRENT GRID.
C   CALL SGWF2GFB7PNT(IGRID)

C
C-----CYCLE THROUGH ITEMS
C   DO K = 1, NGFBITEMS
C     SELECT CASE (GFB_DATA(K)%NTYPE)
C       CASE (1)
C         CALL GFB1DITEMBUDGET(KSTP,KPER,GFB_DATA(K))
C       CASE (2)
C         CALL GFB2DITEMBUDGET(KSTP,KPER,GFB_DATA(K))
C     END SELECT
C   END DO

C
C13-----RETURN
C   RETURN
C   END SUBROUTINE GWF2GFB7BD

C   SUBROUTINE GWF2GFB7DA(IGRID)
C   Deallocate GFB DATA
C   USE GWFGFBMODULE

C
C   DEALLOCATE(GWFGFBDAT(IGRID)%NGFBITEMS)
C   DEALLOCATE(GWFGFBDAT(IGRID)%IGFBCB)
C   DEALLOCATE(GWFGFBDAT(IGRID)%IGFBPR)
C   DEALLOCATE(GWFGFBDAT(IGRID)%GFB_DATA)

C
C   RETURN
C   END SUBROUTINE GWF2GFB7DA

C   SUBROUTINE SGWF2GFB7PNT(IGRID)
C   Set GFB pointers for grid.
C   USE GWFGFBMODULE

C
C   NGFBITEMS=>GWFGFBDAT(IGRID)%NGFBITEMS
C   IGFBCB=>GWFGFBDAT(IGRID)%IGFBCB
C   IGFBPR=>GWFGFBDAT(IGRID)%IGFBPR
C   GFB_DATA=>GWFGFBDAT(IGRID)%GFB_DATA

C
C   RETURN
C   END SUBROUTINE SGWF2GFB7PNT

C   SUBROUTINE SGWF2GFB7PSV(IGRID)
C   Save GFB pointers for grid.
C   USE GWFGFBMODULE

```

```

C
      GWFGFBDAT (IGRID) %NGFBITEMS=>NGFBITEMS
      GWFGFBDAT (IGRID) %IGFBCB=>IGFBCB
      GWFGFBDAT (IGRID) %IGFBPR=>IGFBPR
      GWFGFBDAT (IGRID) %GFB_DATA=>GFB_DATA
C
      RETURN
      END SUBROUTINE SGWF2GFB7PSV

      SUBROUTINE GFB1DITEMREAD (IN, DATAITEM)
C
      *****
C
      READ WELL DATA FOR A STRESS PERIOD
C
      *****
C
      SPECIFICATIONS:
C
      -----
      USE GLOBAL,          ONLY:IOUT,NCOL,NROW,NLAY,IFREFM
      USE GWFGFBMODULE, ONLY:IGFBPR, GFB_DATAITEM
C
      IMPLICIT NONE
C
      DUMMY VARIABLES
      INTEGER, INTENT (IN) :: IN
      TYPE (GFB_DATAITEM), INTENT (INOUT) :: DATAITEM
C
      LOCAL VARIABLES
      CHARACTER*200 :: LINE
      CHARACTER*24  :: ANAME(1)
      CHARACTER*11  :: CFLUX
      INTEGER :: LLOC
      INTEGER :: ISTART, ISTOP
      INTEGER :: ITMP
      INTEGER :: LDIM
      INTEGER :: I, N

      REAL :: R

C
      DATA ANAME(1) /'          SPECIFIED FLUX' /
C
C-----FORMATS
      2000  FORMAT(1X,/1X,'REUSING ',A,1X,A,1X,
      2          'DATA FROM LAST STRESS PERIOD')
      2010  FORMAT(1X,/1X,'THE NUMBER OF ACTIVE FLUX ITEMS (',I6,
      1          ') IS GREATER THAN MXACTF(',I6,')')
      2020  FORMAT(1X,/1X,I6,A)
C
      -----
C
C-----READ FLAGS SHOWING WHETHER DATA FOR DATA ITEM IS TO BE REUSED.
      CALL URDCOM (IN, IOUT, LINE)
      LLOC=1
      CALL URWORD (LINE, LLOC, ISTART, ISTOP, 2, ITMP, R, IOUT, IN)
      IF (ITMP.LT.0) THEN
          WRITE (IOUT, 2000) DATAITEM%TEXT, ANAME(1)
      END IF
C
C-----IF THERE ARE NEW FLUX ITEMS, READ THEM.
      IF (ITMP.GT.0) THEN
          IF (ITMP.GT.DATAITEM%MXACTF) THEN
              WRITE (IOUT, 2010) ITMP, DATAITEM%MXACTF
              CALL USTOP (' ')
          END IF
          LDIM = DATAITEM%NFLUXVL

```

```

      CALL ULSTRD(ITMP,DATAITEM%FLUX,1,LDIM,DATAITEM%MXACTF,0,
2      IN,IOUT,'FLUX NO. LAYER ROW COL STRESS RATE',
3      DATAITEM%FLUXAUX,20,DATAITEM%NAUX,IFREFM,
4      NCOL,NROW,NLAY,4,4,IGFBPR)
      END IF
      DATAITEM%NFLUX = ITMP
C
C3-----PRINT NUMBER OF WELLS IN CURRENT STRESS PERIOD.
      CFLUX=' FLUX ITEMS'
      IF(DATAITEM%NFLUX.EQ.1) CFLUX = ' FLUX ITEM '
      WRITE(IOUT,2020) DATAITEM%NFLUX, CFLUX
C
C6-----RETURN
      RETURN
      END SUBROUTINE GFB1DITEMREAD

      SUBROUTINE GFB2DITEMREAD(IN,DATAITEM)
C      *****
C      READ TWO DIMENSIONAL DATA FOR STRESS PERIOD
C      *****
C      SPECIFICATIONS:
C      -----
      USE GLOBAL, ONLY:IOUT,NCOL,NROW,NLAY,DELR,DELCL
      USE GWFGFBMODULE,ONLY:GFB_DATAITEM

      IMPLICIT NONE

C      INTEGER, INTENT(IN) :: IN
      TYPE (GFB_DATAITEM), INTENT(INOUT) :: DATAITEM

C      LOCAL VARIABLES
      CHARACTER*200 LINE
      CHARACTER*24 ANAME(3)

      INTEGER :: INRATE
      INTEGER :: INLAY
      INTEGER :: INMULT
      INTEGER :: LLOC
      INTEGER :: ISTART
      INTEGER :: ISTOP
      INTEGER :: IR, IC, IL

      REAL :: R

C      DATA ANAME(1) /' RATE' /
      DATA ANAME(2) /' LAYER INDEX' /
      DATA ANAME(3) /' RATE MULTIPLIER' /
C      -----
C
C-----FORMATS
2000  FORMAT(1X,/1X,'REUSING ',A,1X,A,1X,
2      'DATA FROM LAST STRESS PERIOD')
2010  FORMAT(1X,/1X,'INVALID LAYER NUMBER IN IRCH FOR COLUMN',I4,
1      ' ROW',I4,' ',I4)
C
C-----INITIALIZE FLAGS
      INRATE = 0
      INLAY = 0
      INMULT = 0

```

```

C
C-----READ FLAGS SHOWING WHETHER DATA FOR DATA ITEM IS TO BE REUSED.
  CALL URDCOM(IN, IOUT, LINE)
  LLOC=1
  CALL URWORD(LINE, LLOC, ISTART, ISTOP, 2, INRATE, R, IOUT, IN)
  IF (INRATE.LT.1) THEN
    WRITE(IOUT, 2000) DATAITEM%TEXT, ANAME(1)
  END IF
  IF (DATAITEM%N2DOP.EQ.2) THEN
    CALL URWORD(LINE, LLOC, ISTART, ISTOP, 2, INLAY, R, IOUT, IN)
    IF (INLAY.LT.1) THEN
      WRITE(IOUT, 2000) DATAITEM%TEXT, ANAME(2)
    END IF
  END IF
  IF (DATAITEM%N2DMULT.GT.0) THEN
    CALL URWORD(LINE, LLOC, ISTART, ISTOP, 2, INMULT, R, IOUT, IN)
    IF (INMULT.LT.1) THEN
      WRITE(IOUT, 2000) DATAITEM%TEXT, ANAME(3)
    END IF
  END IF
C-----READ DATA
  IF (INRATE.GT.0) THEN
    CALL U2DREL(DATAITEM%RATE, ANAME(1), NROW, NCOL, 0, IN, IOUT)
C-----MULTIPLY RATE BY CELL AREA TO GET VOLUMETRIC RATE.
    DO IR=1, NROW
      DO IC=1, NCOL
        DATAITEM%RATE(IC, IR)=DATAITEM%RATE(IC, IR)*DELR(IC)*DELC(IR)
      END DO
    END DO
  END IF
  IF (INLAY.GT.0) THEN
    CALL U2DINT(DATAITEM%LAYER, ANAME(2), NROW, NCOL, 0, IN, IOUT)
    DO IR=1, NROW
      DO IC=1, NCOL
        IL = DATAITEM%LAYER(IC, IR)
        IF (IL.LT.1 .OR. IL.GT.NLAY) THEN
          WRITE(IOUT, 2010) IC, IR, IL
          CALL USTOP(' ')
        END IF
      END DO
    END DO
  END IF
  IF (INMULT.GT.0) THEN
    CALL U2DREL(DATAITEM%MULTIPLIER, ANAME(3), NROW, NCOL, 0, IN, IOUT)
  END IF
C
C-----RETURN
  RETURN
  END SUBROUTINE GFB2DITEMREAD

  SUBROUTINE GFB1DITEMFORMULATE(DATAITEM)
C *****
C SUBTRACT Q FROM RHS
C *****
C
C SPECIFICATIONS:
C -----
  USE GLOBAL, ONLY: IBOUND, RHS, HCOF, LBOTM, BOTM, HNEW, IOUT
  USE GWFGFBMODULE, ONLY: GFB_DATAITEM

  IMPLICIT NONE

```

```

C
C      DUMMY VARIABLES
C      TYPE (GFB_DATAITEM), INTENT(INOUT) :: DATAITEM
C
C      LOCAL VARIABLES
C      INTEGER :: L
C      INTEGER :: IR, IC, IL
C      REAL :: Q
C      -----
C
C1-----IF NUMBER OF WELLS <= 0 THEN RETURN.
C      IF(DATAITEM%NFLUX.LE.0) RETURN
C
C-----PROCESS EACH WELL IN THE FLUX LIST.
C      LFLUX: DO L = 1, DATAITEM%NFLUX
C          IR = DATAITEM%FLUX(2,L)
C          IC = DATAITEM%FLUX(3,L)
C          IL = DATAITEM%FLUX(1,L)
C          Q  = DATAITEM%FLUX(4,L)
C
C-----IF THE CELL IS INACTIVE THEN BYPASS PROCESSING.
C      IF(IBOUND(IC,IR,IL).LE.0) CYCLE LFLUX
C
C-----IF THE CELL IS VARIABLE HEAD THEN SUBTRACT Q FROM
C      THE RHS ACCUMULATOR.
C          RHS(IC,IR,IL) = RHS(IC,IR,IL) - Q
C      END DO LFLUX
C
C3-----RETURN
C      RETURN
C      END SUBROUTINE GFB1DITEMFORMULATE

SUBROUTINE GFB2DITEMFORMULATE(DATAITEM)
C      *****
C      SUBTRACT TWO DIMENSIONAL DATA FROM RHS
C      *****
C
C      SPECIFICATIONS:
C      -----
C      USE GLOBAL,          ONLY:NCOL,NROW,NLAY,IBOUND,RHS
C      USE GWFGFBMODULE,ONLY:GFB_DATAITEM

C      IMPLICIT NONE
C
C      DUMMY VARIABLES
C      TYPE (GFB_DATAITEM), INTENT(IN) :: DATAITEM
C
C      LOCAL VARIABLES
C      INTEGER :: IR, IC, IL
C      -----
C
C-----DETERMINE WHICH RECHARGE OPTION.
C      IF(DATAITEM%N2DOP.EQ.1) THEN
C
C-----NRCHOP IS 1, SO RATE IS APPLIED TO THE TOP LAYER. LAYER INDEX IS 1.
C          DO IR = 1, NROW
C              DO IC = 1, NCOL
C-----IF CELL IS VARIABLE HEAD, SUBTRACT RECHARGE RATE FROM
C-----RIGHT-HAND-SIDE.
C          IF(IBOUND(IC,IR,1).GT.0) THEN
C              RHS(IC,IR,1)=RHS(IC,IR,1)-

```

```

2          DATAITEM%RATE(IC,IR)*DATAITEM%MULTIPLIER(IC,IR)
          END IF
          END DO
          END DO
          ELSE IF(DATAITEM%N2DOP.EQ.2) THEN
C
C-----NRCHOP IS 2, SO RECHARGE IS INTO LAYER IN INDICATOR ARRAY
          DO IR = 1, NROW
            DO IC = 1, NCOL
              IL=DATAITEM%LAYER(IC,IR)
C-----IF THE CELL IS VARIABLE HEAD, SUBTRACT RECHARGE FROM
C-----RIGHT-HAND-SIDE.
              IF(IL.EQ.0) CYCLE
              IF(IBOUND(IC,IR,IL).GT.0) THEN
                RHS(IC,IR,IL)=RHS(IC,IR,IL)-
2          DATAITEM%RATE(IC,IR)*DATAITEM%MULTIPLIER(IC,IR)
                END IF
              END DO
            END DO
          ELSE
C
C-----NRCHOP IS 3, RECHARGE IS INTO HIGHEST VARIABLE-HEAD CELL, EXCEPT
C-----CANNOT PASS THROUGH CONSTANT HEAD NODE
          LROW: DO IR = 1, NROW
            LCOL: DO IC = 1, NCOL
              HLAY: DO IL = 1, NLAY
C
C-----IF CELL IS CONSTANT HEAD MOVE ON TO NEXT HORIZONTAL LOCATION.
              IF(IBOUND(IC,IR,IL).LT.0) EXIT HLAY
C
C-----IF THE CELL IS VARIABLE HEAD, SUBTRACT RECHARGE FROM
C-----RIGHT-HAND-SIDE AND MOVE TO NEXT HORIZONTAL LOCATION.
              IF(IBOUND(IC,IR,IL).GT.0) THEN
                RHS(IC,IR,IL)=RHS(IC,IR,IL)-
2          DATAITEM%RATE(IC,IR)*DATAITEM%MULTIPLIER(IC,IR)
                EXIT HLAY
              END IF
            END DO HLAY
          END DO LCOL
        END DO LROW
      END IF
    END IF
  END IF
C
C-----RETURN
  RETURN
END SUBROUTINE GFB2DITEMFORMULATE

SUBROUTINE GFB1DITEMBUDGET(KSTP,KPER,DATAITEM)
C *****
C CALCULATE VOLUMETRIC BUDGET FOR SPECIFIED FLUX DATA
C *****
C
C SPECIFICATIONS:
C -----
C USE GLOBAL,          ONLY:IOUT,NCOL,NROW,NLAY,IBOUND,BUFF
C USE GWFBASMODULE,ONLY:MSUM,ICBCFL,IAUXSV,DELT,PERTIM,TOTIM,
1          VBVL,VBNM
C USE GWFGFBMODULE,ONLY:GFB_DATAITEM,IGFBCB

C
C IMPLICIT NONE
C
C DUMMY VARIABLES
C INTEGER, INTENT(IN) :: KSTP, KPER

```

132 Hydrologic Conditions and Effect of Pumpage and Sea Level on Canal Leakage and Regional Groundwater Flow

```

TYPE (GFB_DATAITEM), INTENT(INOUT) :: DATAITEM
C
C LOCAL VARIABLES
CHARACTER*16 TEXT

INTEGER :: IBD, IBDLBL
INTEGER :: NFLUX, NAUX
INTEGER :: IC, IR, IL
INTEGER :: L

REAL :: ZERO
REAL :: RIN, ROUT, Q

DOUBLEPRECISION RATIN , RATOUT, QQ
C
C FORMAT STATEMENTS
02000 FORMAT(1X,/1X,A,' PERIOD ',I4,' STEP ',I3)
02010 FORMAT(1X,'FLUX ',I6,' LAYER ',I3,' ROW ',I5,' COL ',I5,
2 ' RATE ',1PG15.6)
C
C -----
C
C-----CLEAR RATIN AND RATOUT ACCUMULATORS, AND SET CELL-BY-CELL
C-----BUDGET FLAG.
ZERO = 0.
RATIN = ZERO
RATOUT = ZERO
IBD = 0
IF(IGFBCB.LT.0 .AND. ICBCFL.NE.0) IBD = -1
IF(IGFBCB.GT.0) IBD=ICBCFL
IBDLBL=0

NFLUX = DATAITEM%NFLUX
NAUX = DATAITEM%NAUX
TEXT = DATAITEM%TEXT
C
C-----IF CELL-BY-CELL FLOWS WILL BE SAVED AS A LIST, WRITE HEADER.
IF(IBD.EQ.2) THEN
IF (IAUXSV.EQ.0) NAUX = 0
CALL UBDSV4(KSTP,KPER,TEXT,NAUX,DATAITEM%FLUXAUX,IGFBCB,
2 NCOL,NROW,NLAY,
3 NFLUX,IOUT,DELT,PERTIM,TOTIM,IBOUND)
END IF
C
C-----CLEAR THE BUFFER.
DO IL=1,NLAY
DO IR=1,NROW
DO IC=1,NCOL
BUFF(IC,IR,IL)=ZERO
END DO
END DO
END DO
C
C-----IF THERE ARE NO FLUX ITEMS, DO NOT ACCUMULATE FLOW.
IF(NFLUX.EQ.0) GO TO 200
C
C-----LOOP THROUGH EACH WELL CALCULATING FLOW.
LCALCQ: DO L = 1, NFLUX
C
C-----GET LAYER, ROW & COLUMN OF CELL CONTAINING WELL.
IR = DATAITEM%FLUX(2,L)
IC = DATAITEM%FLUX(3,L)
IL = DATAITEM%FLUX(1,L)

```

```

      Q = ZERO
C
C-----IF THE CELL IS NO-FLOW OR CONSTANT_HEAD, IGNORE IT.
      IF (IBOUND(IC,IR,IL).LE.0) GO TO 99
C
C-----GET FLOW RATE FROM WELL LIST.
      Q = DATAITEM%FLUX(4,L)
      QQ = Q
C
C-----PRINT FLOW RATE IF REQUESTED.
      IF (IBD.LT.0) THEN
        IF (IBDLBL.EQ.0) WRITE (IOUT,2000) TEXT,KPER,KSTP
        WRITE (IOUT,2010) L,IL,IR,IC,Q
        IBDLBL=1
      END IF
C
C-----ADD FLOW RATE TO BUFFER.
      BUFF(IC,IR,IL) = BUFF(IC,IR,IL) + Q
C
C-----SEE IF FLOW IS POSITIVE OR NEGATIVE.
      IF (Q.GE.ZERO) THEN
C-----FLOW RATE IS POSITIVE (RECHARGE). ADD IT TO RATIN.
        RATIN = RATIN + QQ
      ELSE
C-----FLOW RATE IS NEGATIVE (DISCHARGE). ADD IT TO RATOUT.
        RATOUT = RATOUT - QQ
      END IF
C
C-----IF SAVING CELL-BY-CELL FLOWS IN A LIST, WRITE FLOW. ALSO
C-----COPY FLOW TO WELL LIST.
      99 IF (IBD.EQ.2) CALL UBDSVB (IGFBCB,NCOL,NROW,IC,IR,IL,Q,
        2 DATAITEM%FLUX (:,L),
        3 DATAITEM%NFLUXVL,DATAITEM%NAUX,4,IBOUND,NLAY)
      END DO LCALLCQ
C
C-----IF CELL-BY-CELL FLOWS WILL BE SAVED AS A 3-D ARRAY,
C-----CALL UBUDSV TO SAVE THEM.
      IF (IBD.EQ.1) CALL UBUDSV (KSTP,KPER,TEXT,IGFBCB,BUFF,NCOL,NROW,
        2 NLAY,IOUT)
C
C-----MOVE RATES, VOLUMES & LABELS INTO ARRAYS FOR PRINTING.
      200 RIN = RATIN
      ROUT = RATOUT
      VBVL(3,MSUM) = RIN
      VBVL(4,MSUM) = ROUT
      VBVL(1,MSUM) = VBVL(1,MSUM) + RIN*DELT
      VBVL(2,MSUM) = VBVL(2,MSUM) + ROUT*DELT
      VBNM(MSUM) = TEXT
C
C-----INCREMENT BUDGET TERM COUNTER(MSUM).
      MSUM=MSUM+1
C
C-----RETURN
      RETURN
      END SUBROUTINE GFB1DITEMBUDGET

      SUBROUTINE GFB2DITEMBUDGET(KSTP,KPER,DATAITEM)
C *****
C CALCULATE VOLUMETRIC BUDGET FOR TWO DIMENSIONAL DATA

```

134 Hydrologic Conditions and Effect of Pumpage and Sea Level on Canal Leakage and Regional Groundwater Flow

```

C *****
C
C SPECIFICATIONS:
C -----
C USE GLOBAL, ONLY:IOUT,NCOL,NROW,NLAY,IBOUND,BUFF
C USE GWF BASMODULE, ONLY:MSUM,VBVL,VBNM,ICBCFL,DELT,PERTIM,TOTIM
C USE GWF GFBMODULE, ONLY:GFB_DATAITEM,IGFBCB
C
C IMPLICIT NONE
C
C DUMMY VARIABLES
C INTEGER, INTENT(IN) :: KSTP, KPER
C TYPE (GFB_DATAITEM), INTENT(INOUT) :: DATAITEM
C
C LOCAL VARIABLES
C CHARACTER*16 TEXT
C
C INTEGER :: IBD
C INTEGER :: IC, IR, IL
C
C REAL :: ZERO
C REAL :: RIN, ROUT, Q
C REAL QMULT
C
C DOUBLEPRECISION RATIN, RATOUT, QQ
C -----
C
C-----CLEAR THE RATE ACCUMULATORS.
C ZERO=0.
C RATIN=ZERO
C RATOUT=ZERO
C
C-----CLEAR THE BUFFER & SET FLAG FOR SAVING CELL-BY-CELL FLOW TERMS.
C DO IL=1,NLAY
C DO IR=1,NROW
C DO IC=1,NCOL
C BUFF(IC,IR,IL)=ZERO
C END DO
C END DO
C END DO
C
C IBD = 0
C IF(IGFBCB.GT.0) IBD = ICBCFL
C
C TEXT = DATAITEM%TEXT
C
C-----DETERMINE THE RECHARGE OPTION.
C IF (DATAITEM%N2DOP.EQ.1) THEN
C
C-----NRCHOP=1, SO RECH GOES INTO LAYER 1. PROCESS EACH HORIZONTAL
C-----CELL LOCATION.
C DO IR = 1, NROW
C DO IC = 1, NCOL
C
C-----IF CELL IS VARIABLE HEAD, THEN DO BUDGET FOR IT.
C IF (IBOUND(IC,IR,1).GT.0) THEN
C
C Q=DATAITEM%RATE(IC,IR)*DATAITEM%MULTIPLIER(IC,IR)
C QQ=Q
C
C-----ADD RECH TO BUFF.

```

```

                BUFF(IC,IR,1)=Q
C
C-----IF RECH POSITIVE ADD IT TO RATIN, ELSE ADD IT TO RATOUT.
                IF(Q.GE.ZERO) THEN
                    RATIN=RATIN+QQ
                ELSE
                    RATOUT=RATOUT-QQ
                END IF
            END IF
        END DO
    END DO
ELSE IF(DATAITEM%N2DOP.EQ.2) THEN
C
C-----NRCHOP=2, RECH IS IN LAYER SPECIFIED IN INDICATOR ARRAY(IRCH).
C-----PROCESS EACH HORIZONTAL CELL LOCATION.
        DO IR = 1, NROW
            DO IC = 1, NCOL
C
C-----GET LAYER INDEX FROM INDICATOR ARRAY(IRCH).
                IL=DATAITEM%LAYER(IC,IR)
C
C-----IF CELL IS VARIABLE HEAD, THEN DO BUDGET FOR IT.
                IF(IL.EQ.0) CYCLE
                IF(IBOUND(IC,IR,IL).GT.0) THEN

                    Q = DATAITEM%RATE(IC,IR)*DATAITEM%MULTIPLIER(IC,IR)
                    QQ = Q
C
C-----ADD RECHARGE TO BUFF.
                    BUFF(IC,IR,IL) = Q
C
C-----IF RECHARGE IS POSITIVE ADD TO RATIN, ELSE ADD IT TO RATOUT.
                    IF (Q.GE.ZERO) THEN
                        RATIN = RATIN + QQ
                    ELSE
                        RATOUT = RATOUT - QQ
                    END IF
                END IF
            END DO
        END DO
    ELSE
C
C-----NRCHOP=3; RECHARGE IS INTO HIGHEST CELL IN A VERTICAL COLUMN
C-----THAT IS NOT NO FLOW. PROCESS EACH HORIZONTAL CELL LOCATION.
        LROW: DO IR=1,NROW
            LCOL: DO IC=1,NCOL
C
C-----INITIALIZE IRCH TO 1, AND LOOP THROUGH CELLS IN A VERTICAL
C-----COLUMN TO FIND WHERE TO PLACE RECHARGE.
                DATAITEM%LAYER(IC,IR)=1
                LLAY: DO IL = 1, NLAY
C
C-----IF CELL IS CONSTANT HEAD, MOVE ON TO NEXT HORIZONTAL LOCATION.
                IF(IBOUND(IC,IR,IL).LT.0) CYCLE LCOL
C
C-----IF CELL IS VARIABLE HEAD, THEN DO BUDGET FOR IT.
                IF (IBOUND(IC,IR,IL).GT.0) THEN

                    Q = DATAITEM%RATE(IC,IR)*DATAITEM%MULTIPLIER(IC,IR)
                    QQ = Q

```

```

C
C-----ADD RECHARGE TO BUFFER, AND STORE LAYER NUMBER IN DATAITEM%LAYER(IC,IR) .
      BUFF(IC,IR,IL) = Q
      DATAITEM%LAYER(IC,IR) = IL
C
C-----IF RECH IS POSITIVE ADD IT TO RATIN, ELSE ADD IT TO RATOUT.
      IF (Q.GE.ZERO) THEN
        RATIN = RATIN + QQ
      ELSE
        RATOUT = RATOUT - QQ
      END IF
      CYCLE LCOL
    END IF
  END DO LLAY
  END DO LCOL
  END DO LROW
C
  END IF
C
C-----IF CELL-BY-CELL FLOW TERMS SHOULD BE SAVED, CALL APPROPRIATE
C-----UTILITY MODULE TO WRITE THEM.
100  IF (IBD.EQ.1) CALL UBDSV (KSTP,KPER,TEXT,IGFBCB,BUFF,NCOL,NROW,
      2              NLAY,IOUT)
      IF (IBD.EQ.2) CALL UBDSV3 (KSTP,KPER,TEXT,IGFBCB,BUFF,
      2              DATAITEM%LAYER,DATAITEM%N2DOP,
      3              NCOL,NROW,NLAY,IOUT,DELT,PERTIM,TOTIM,IBOUND)
C
C-----MOVE TOTAL RECHARGE RATE INTO VBVL FOR PRINTING BY BAS1OT.
      ROUT = RATOUT
      RIN = RATIN
      VBVL(4,MSUM) = ROUT
      VBVL(3,MSUM) = RIN
C
C-----ADD RECHARGE FOR TIME STEP TO RECHARGE ACCUMULATOR IN VBVL.
      VBVL(2,MSUM) = VBVL(2,MSUM) + ROUT*DELT
      VBVL(1,MSUM) = VBVL(1,MSUM) + RIN*DELT
C
C-----MOVE BUDGET TERM LABELS TO VBNM FOR PRINT BY MODULE BAS_OT.
      VBNM(MSUM) = TEXT
C
C-----INCREMENT BUDGET TERM COUNTER.
      MSUM = MSUM + 1
C
C-----RETURN
      RETURN
      END SUBROUTINE GFB2DITEMBUDGET

```

## Appendix 2. Observed and Simulated Canal Stages

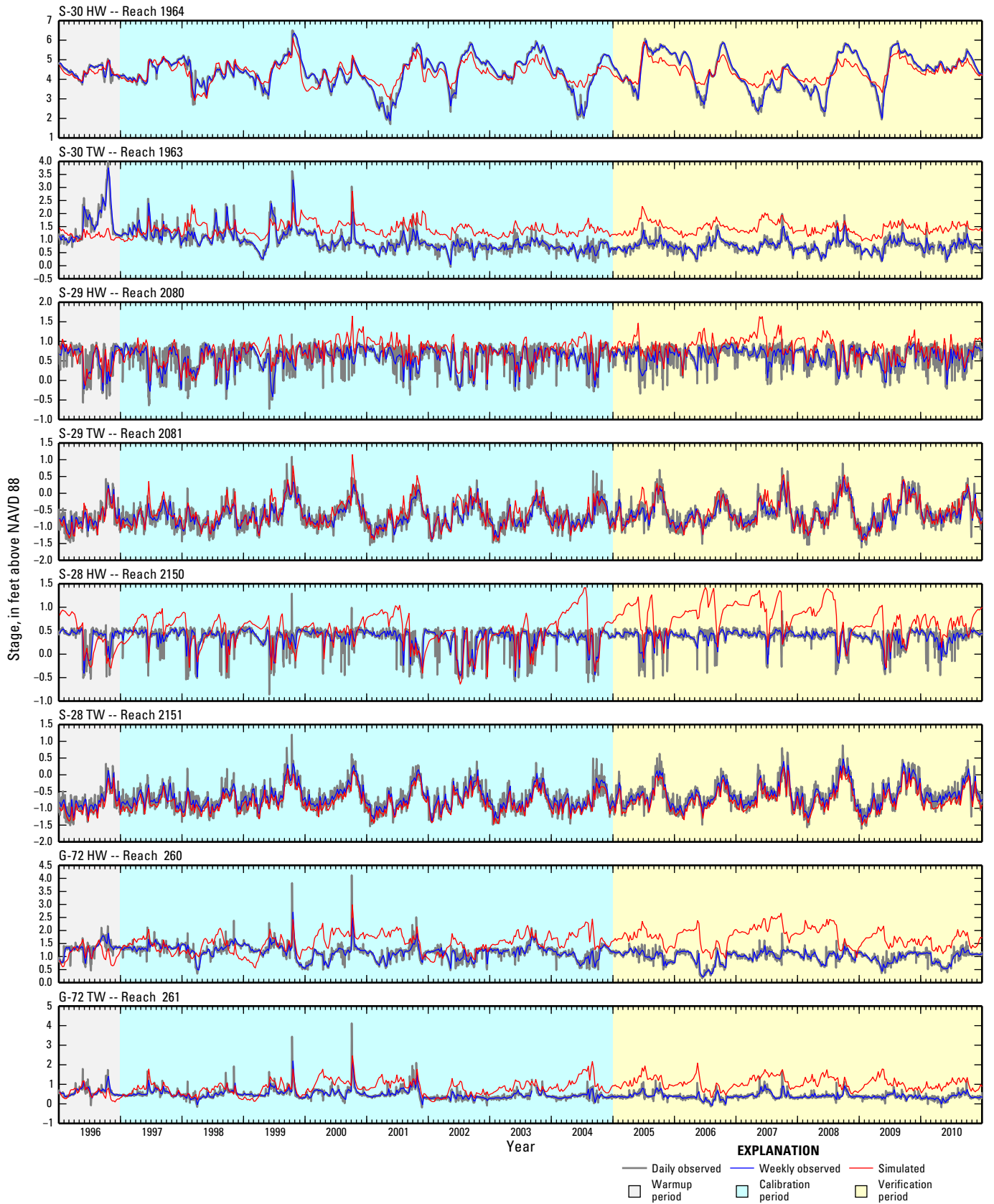


Figure 2-1. Observed and simulated stage at surface-water gages in the study area.

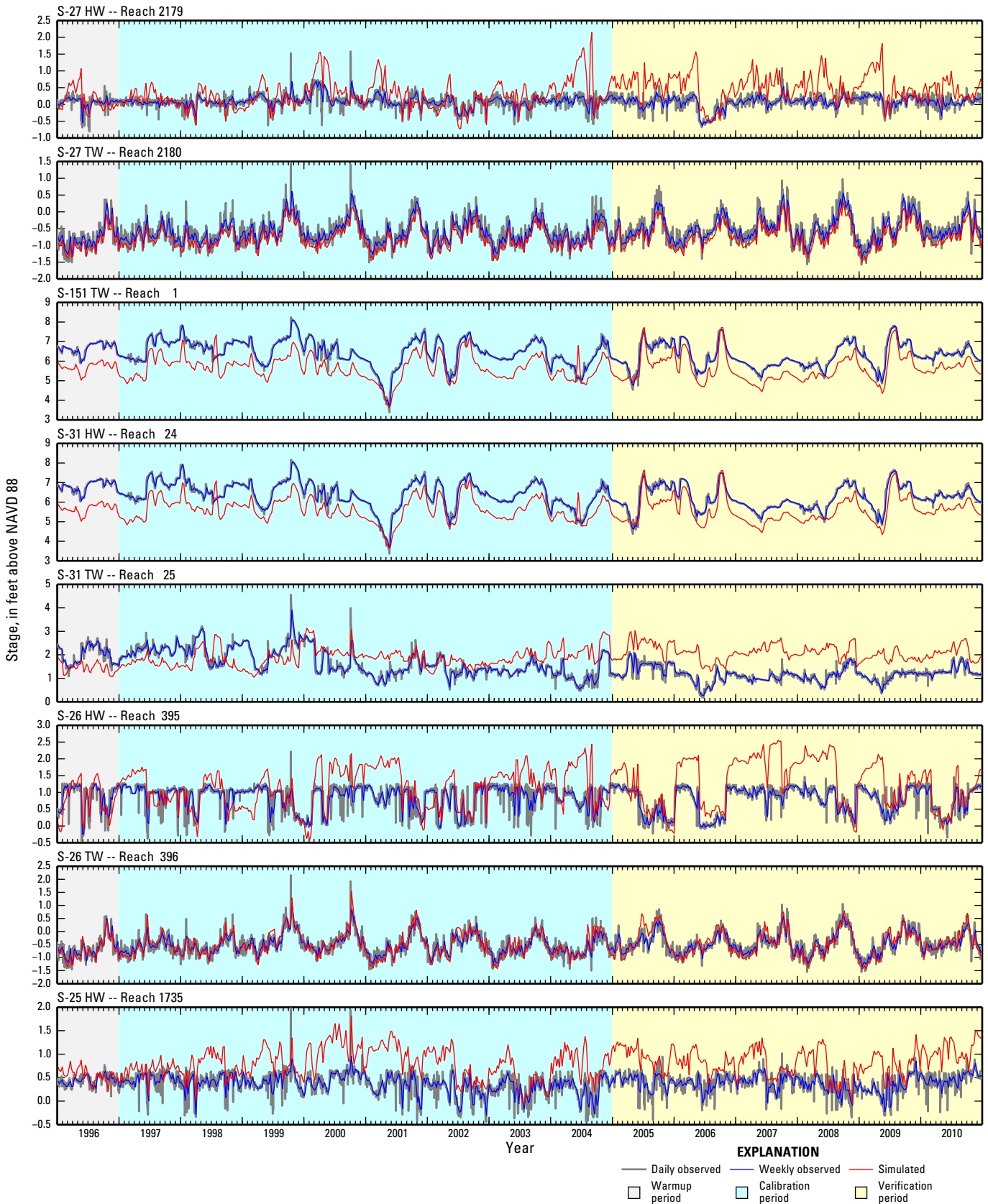


Figure 2-2. Observed and simulated stage at surface-water gages in the study area.

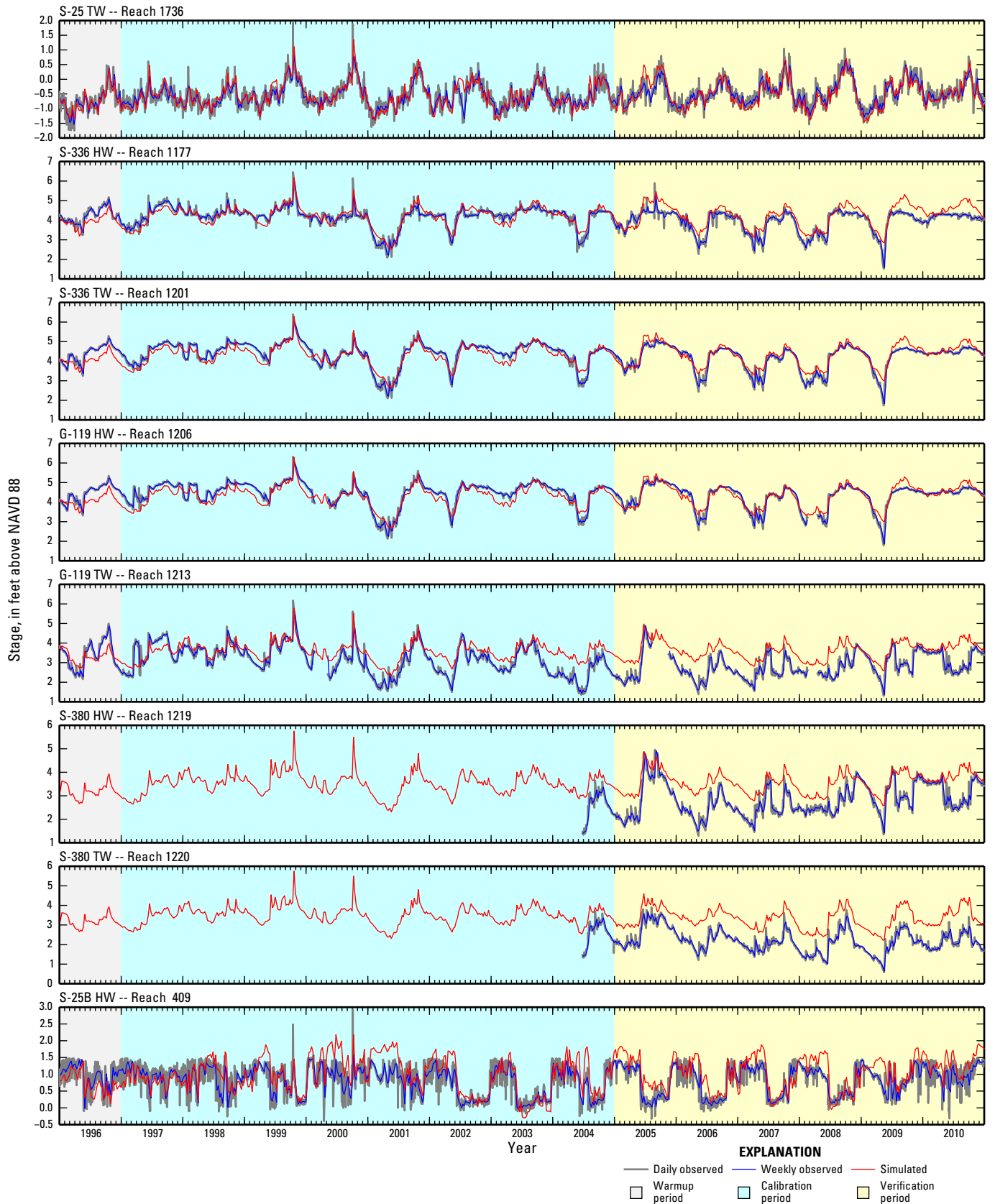


Figure 2-3. Observed and simulated stage at surface-water gages in the study area.

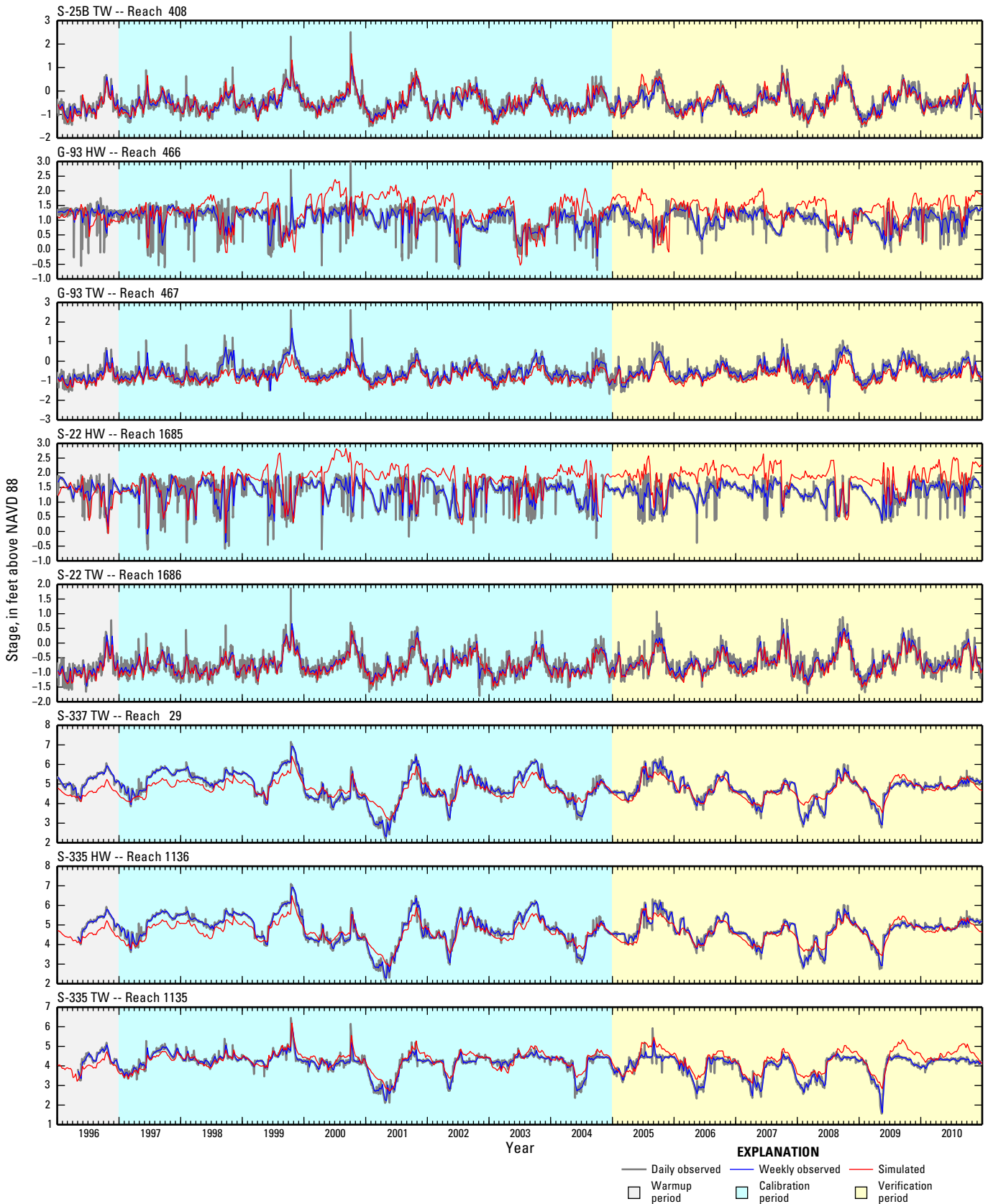


Figure 2-4. Observed and simulated stage at surface-water gages in the study area.

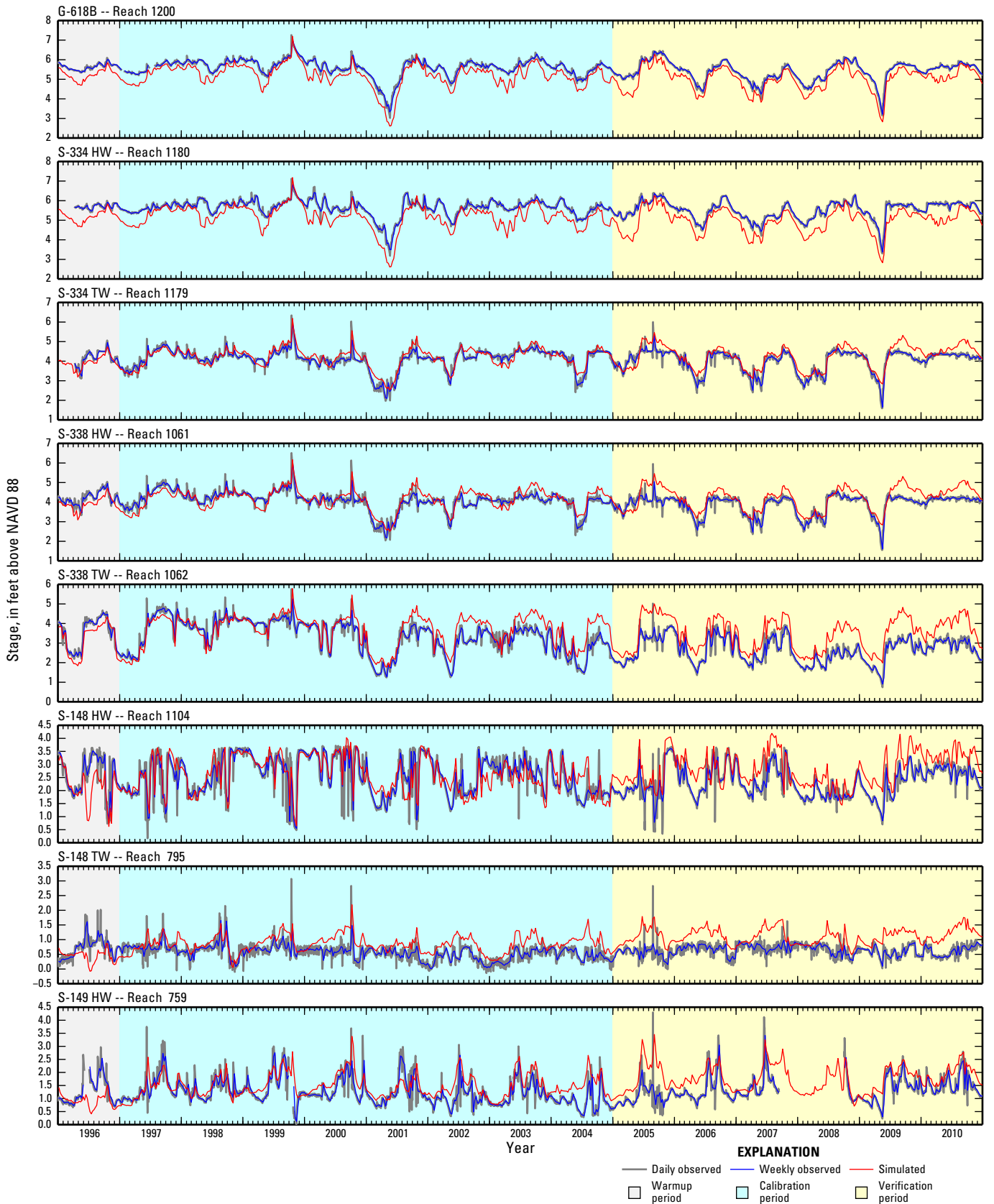


Figure 2-5. Observed and simulated stage at surface-water gages in the study area.

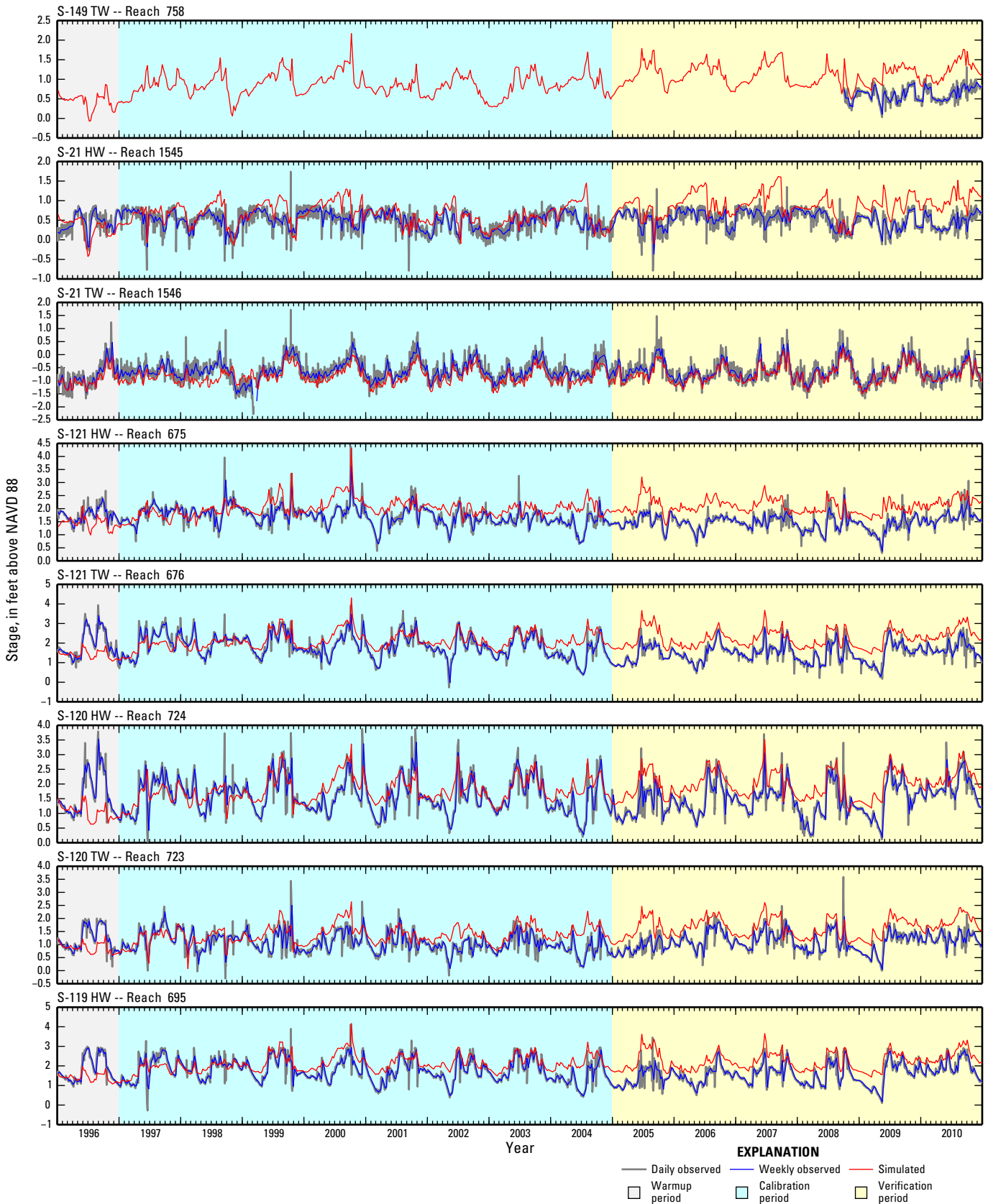


Figure 2-6. Observed and simulated stage at surface-water gages in the study area.

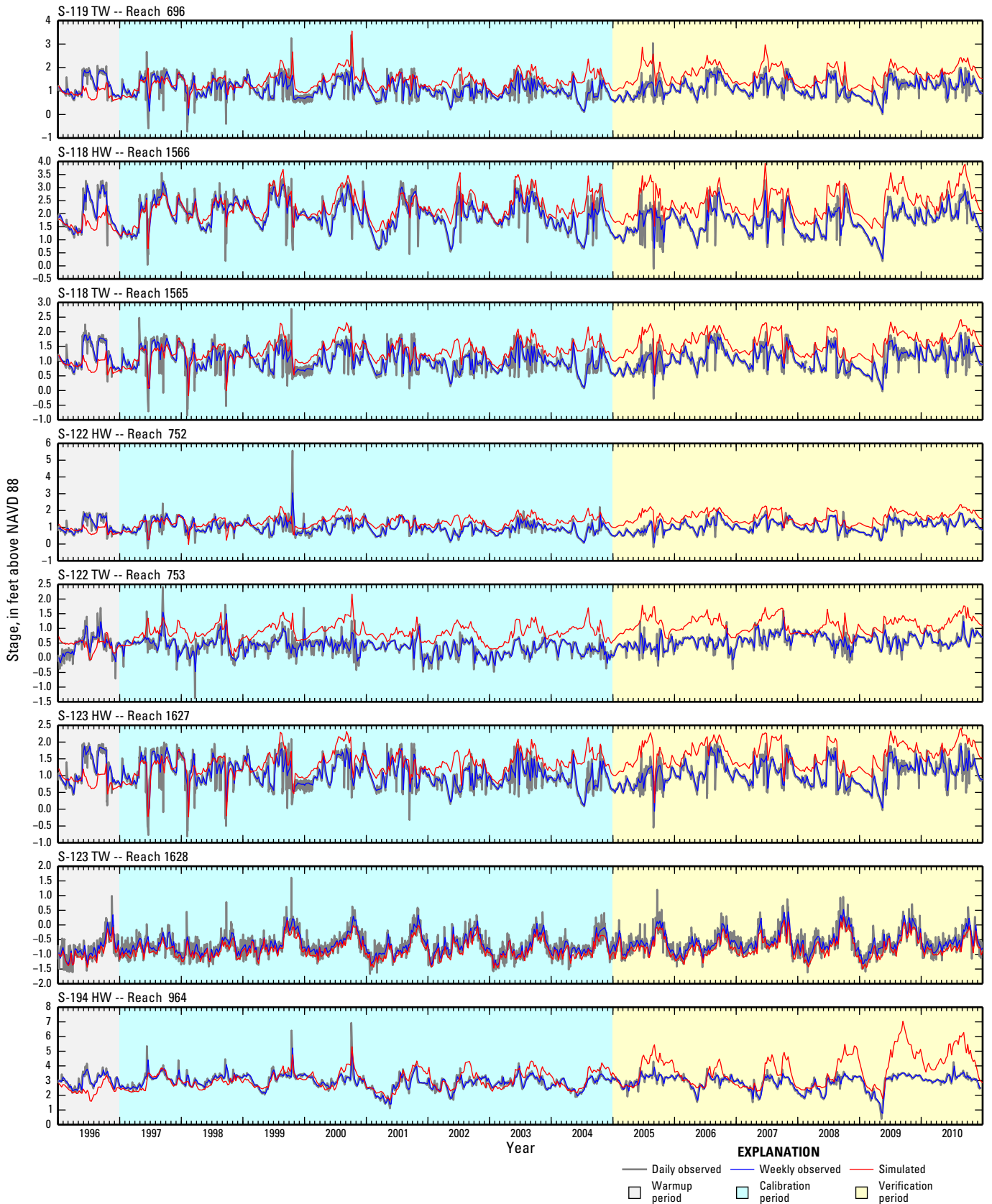


Figure 2-7. Observed and simulated stage at surface-water gages in the study area.

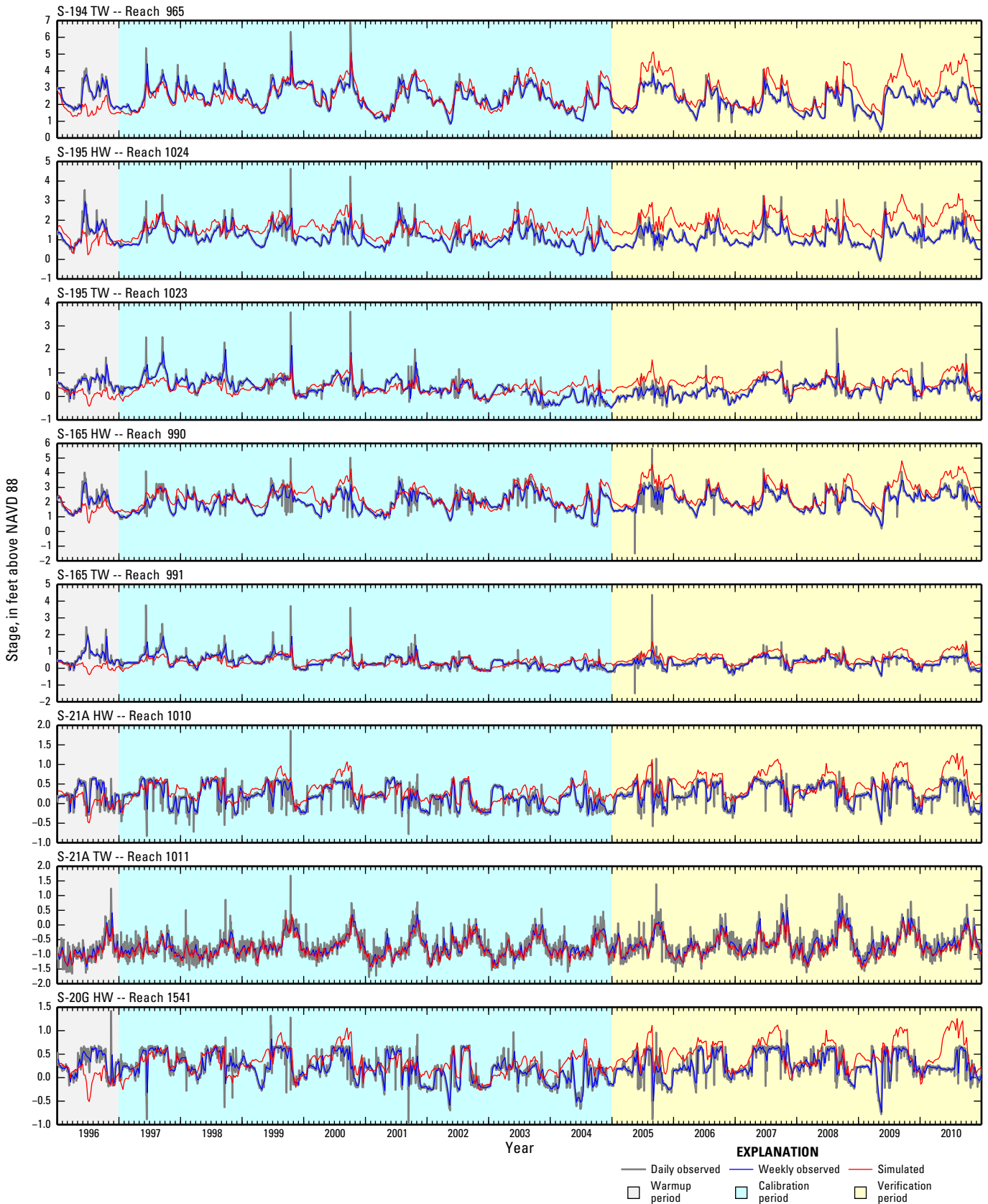


Figure 2-8. Observed and simulated stage at surface-water gages in the study area.

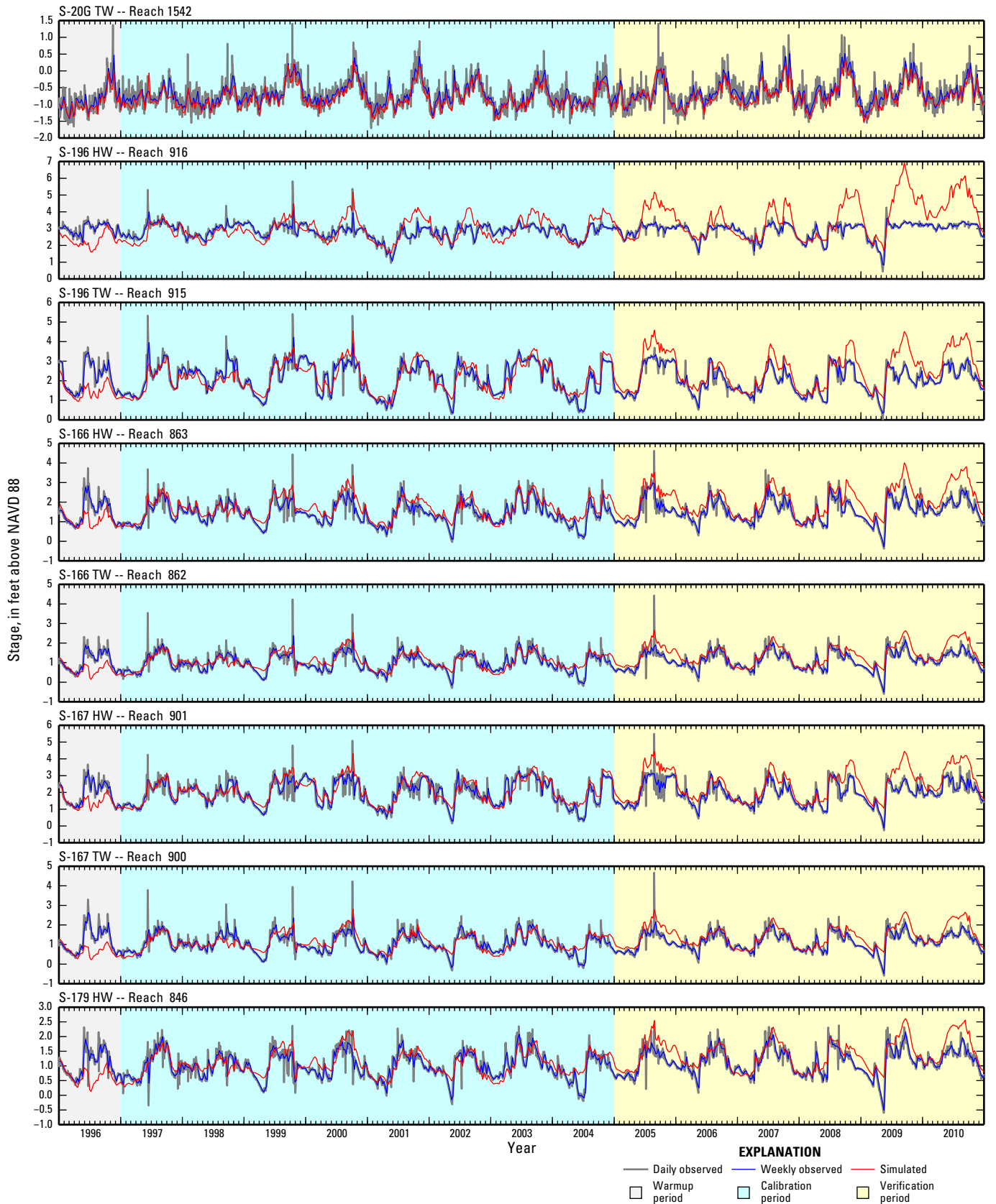


Figure 2-9. Observed and simulated stage at surface-water gages in the study area.

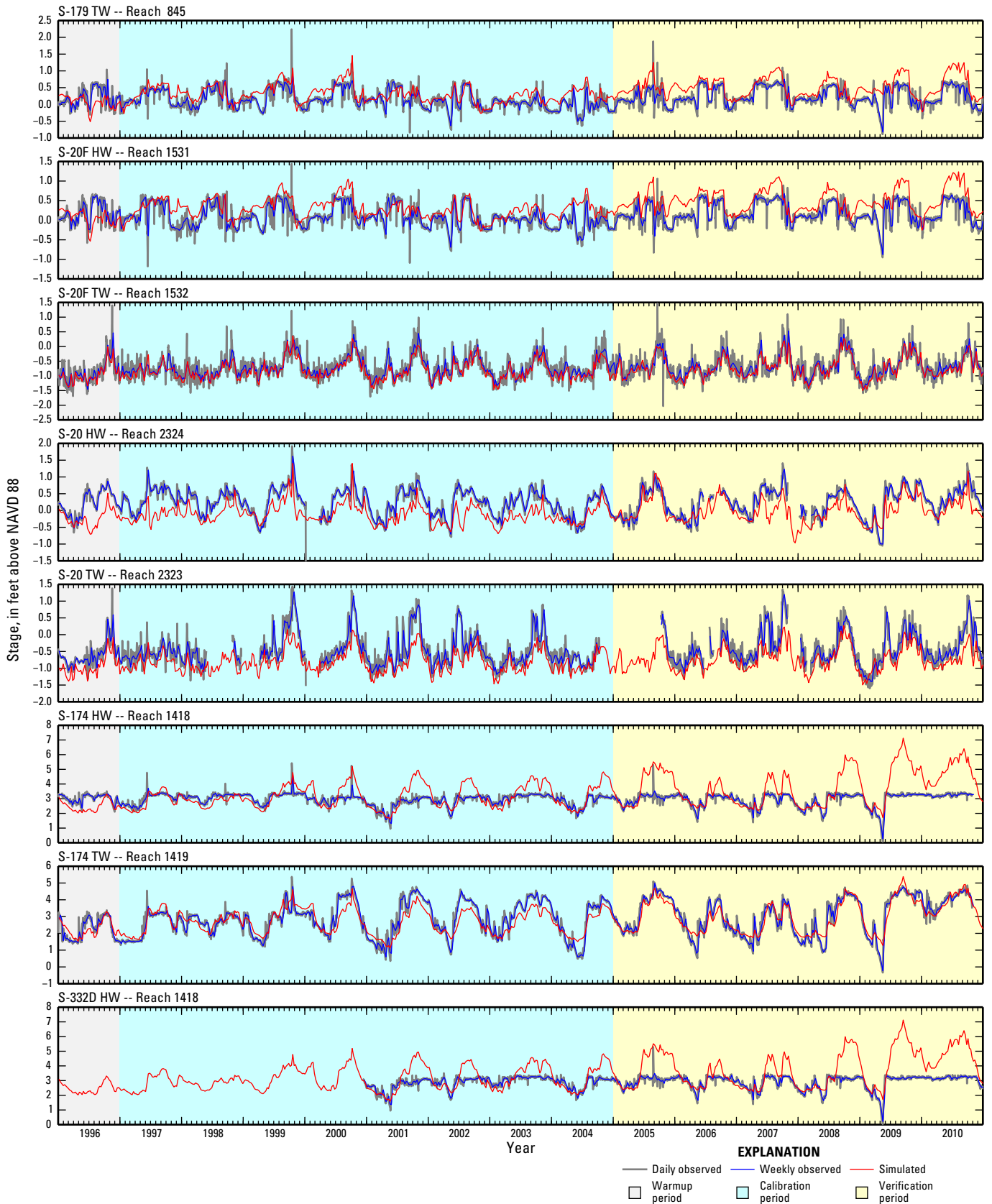


Figure 2-10. Observed and simulated stage at surface-water gages in the study area.

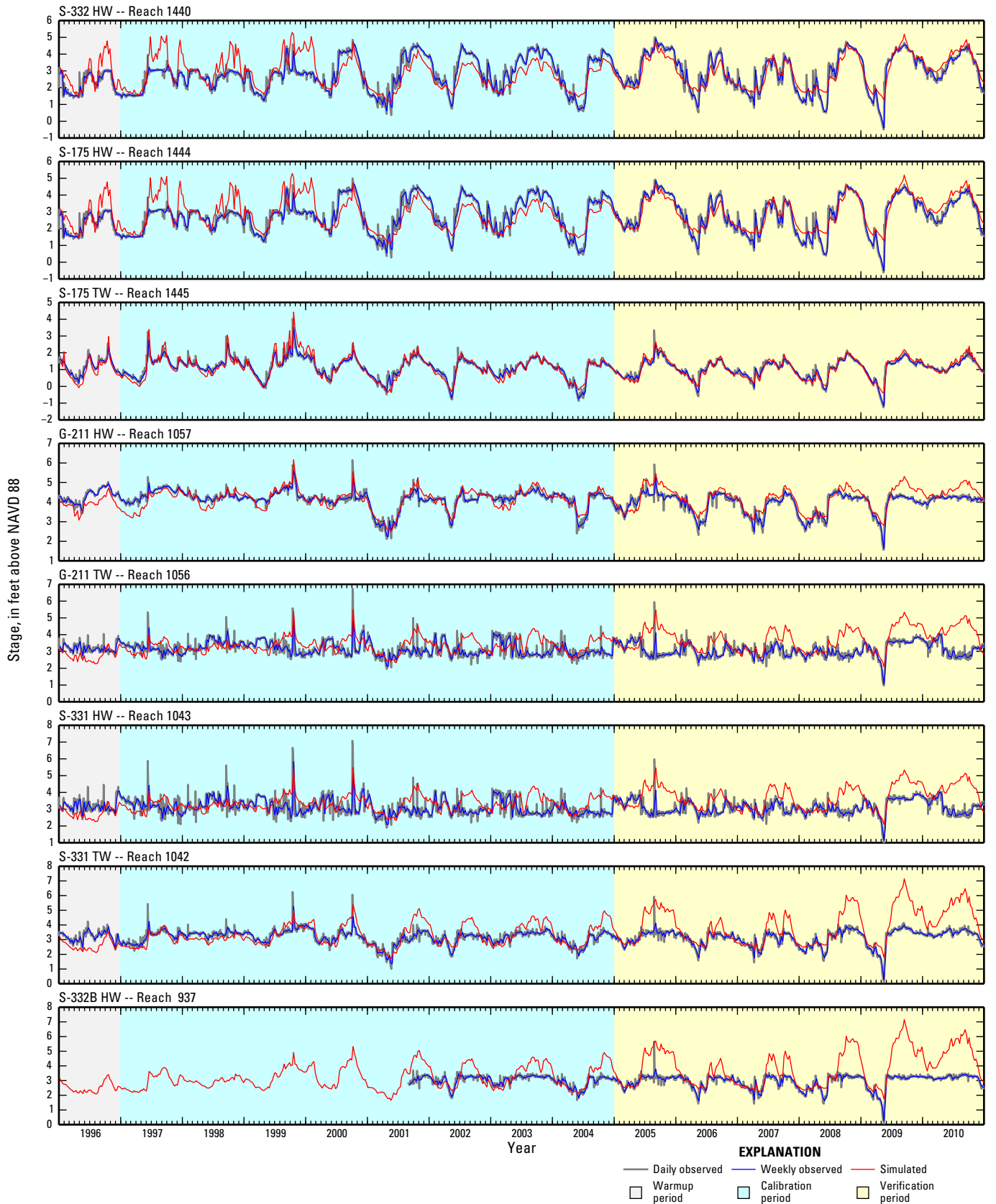


Figure 2-11. Observed and simulated stage at surface-water gages in the study area.

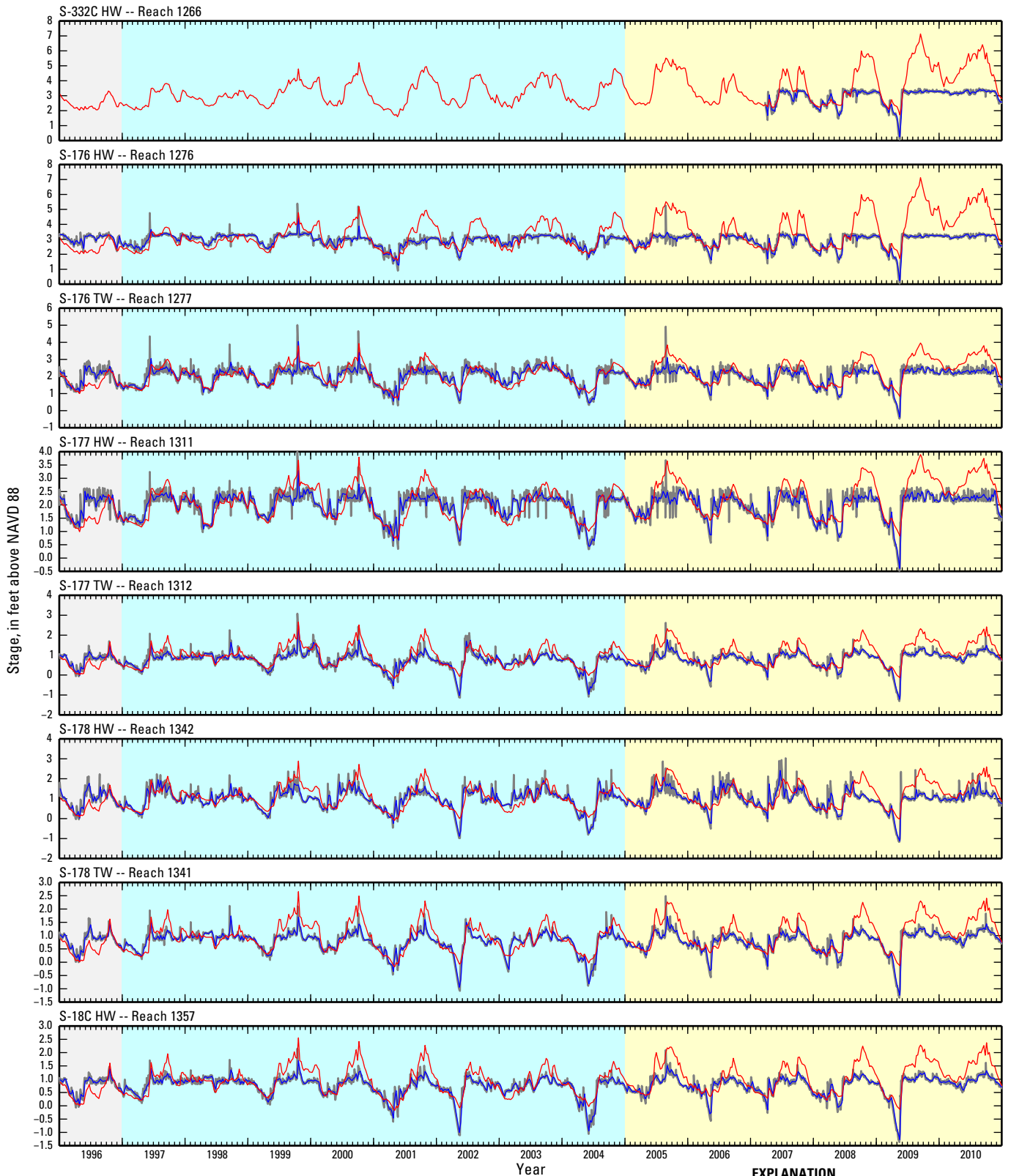


Figure 2-12. Observed and simulated stage at surface-water gages in the study area.

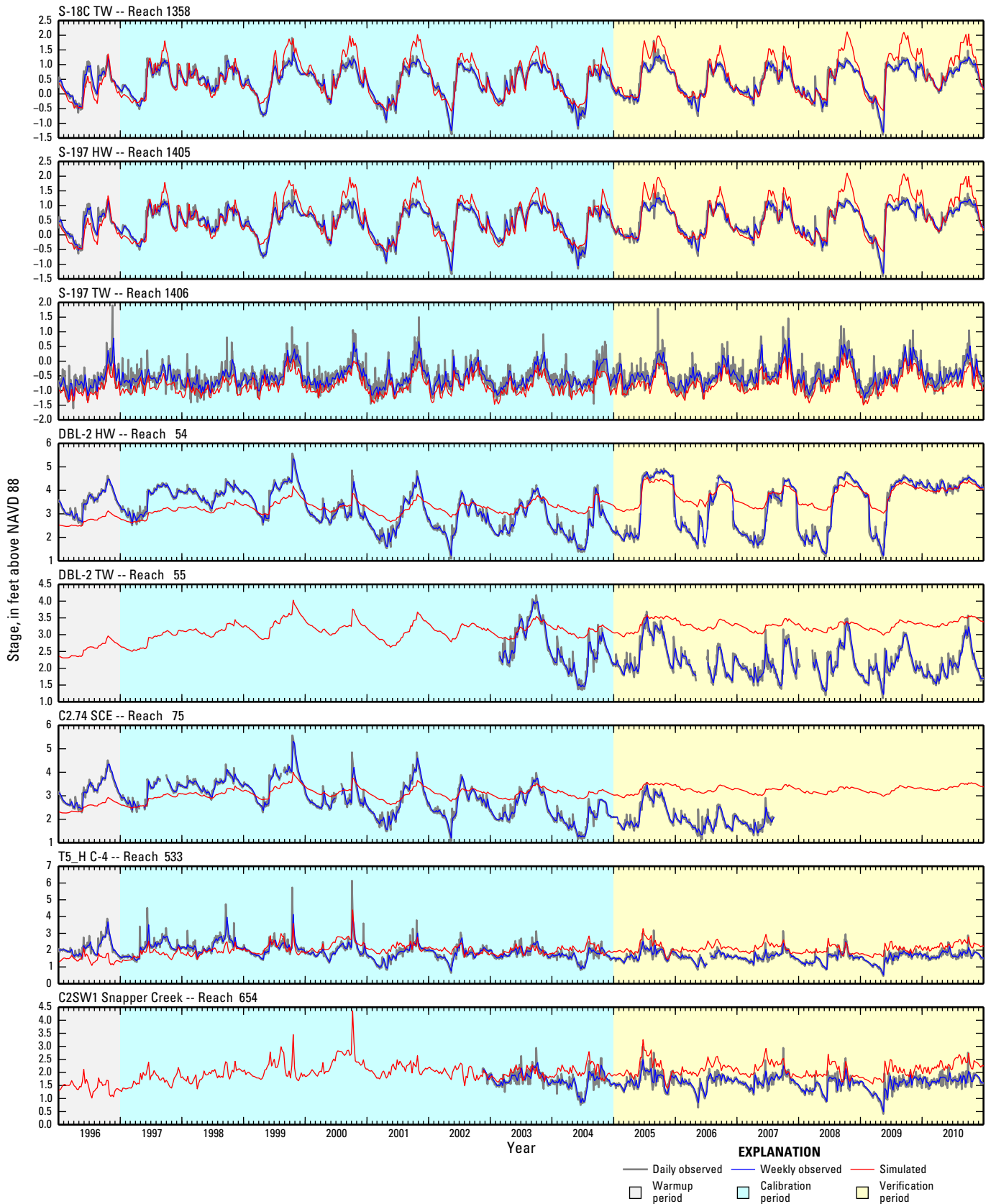


Figure 2-13. Observed and simulated stage at surface-water gages in the study area.

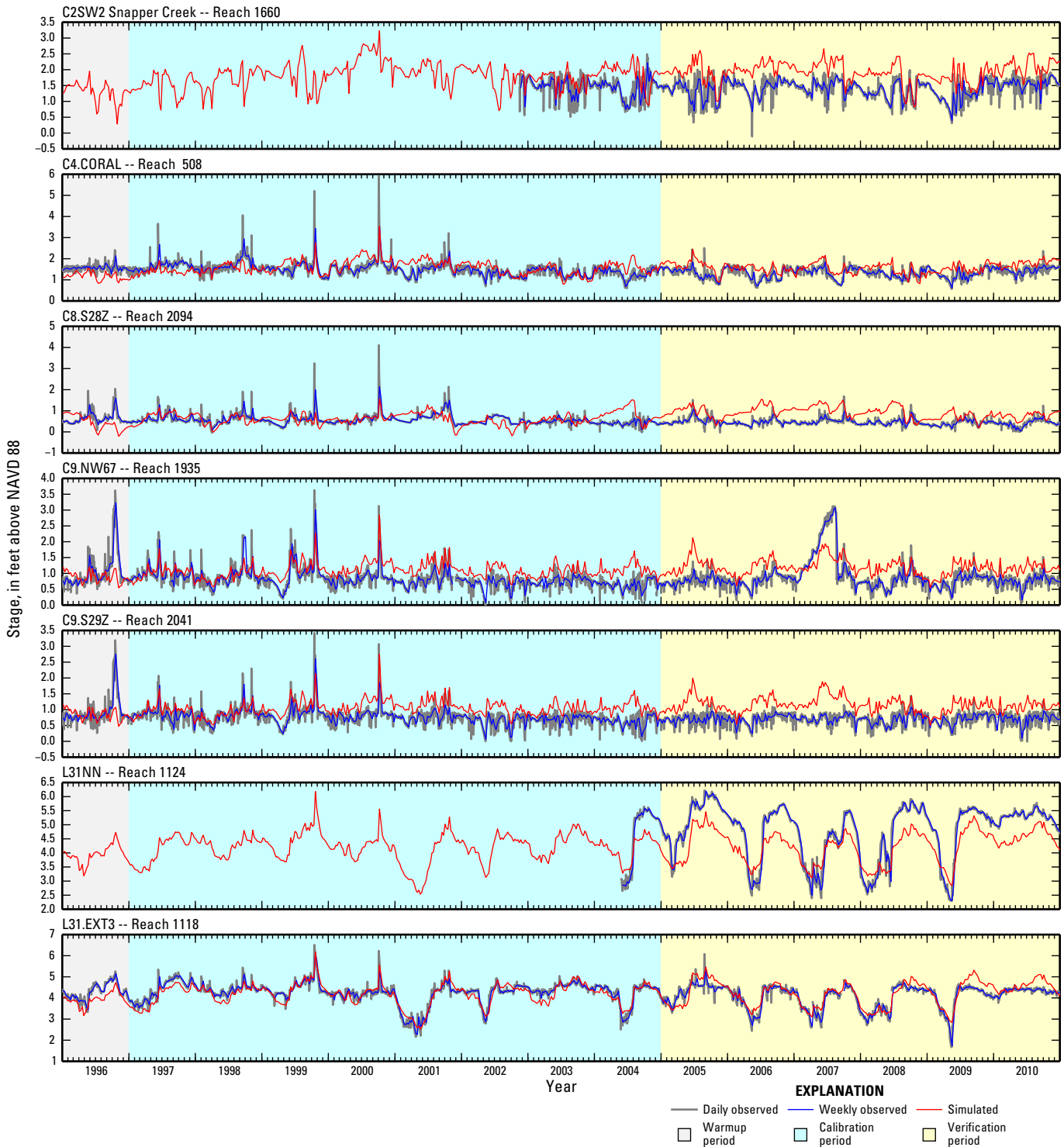


Figure 2-14. Observed and simulated stage at surface-water gages in the study area.

### Appendix 3. Observed and Simulated Canal Discharge

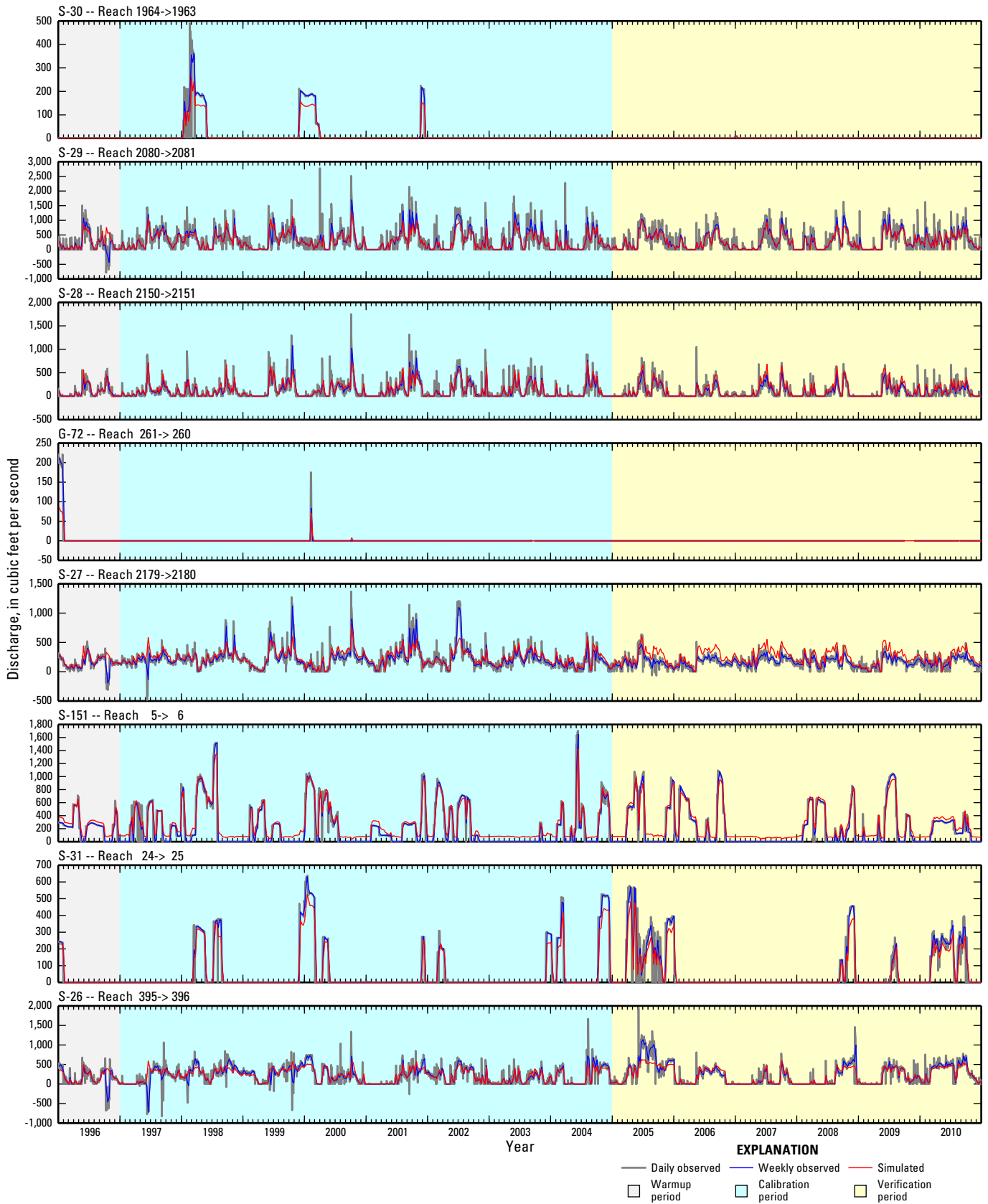


Figure 3-1. Observed and simulated discharge at surface-water structures in the study area.

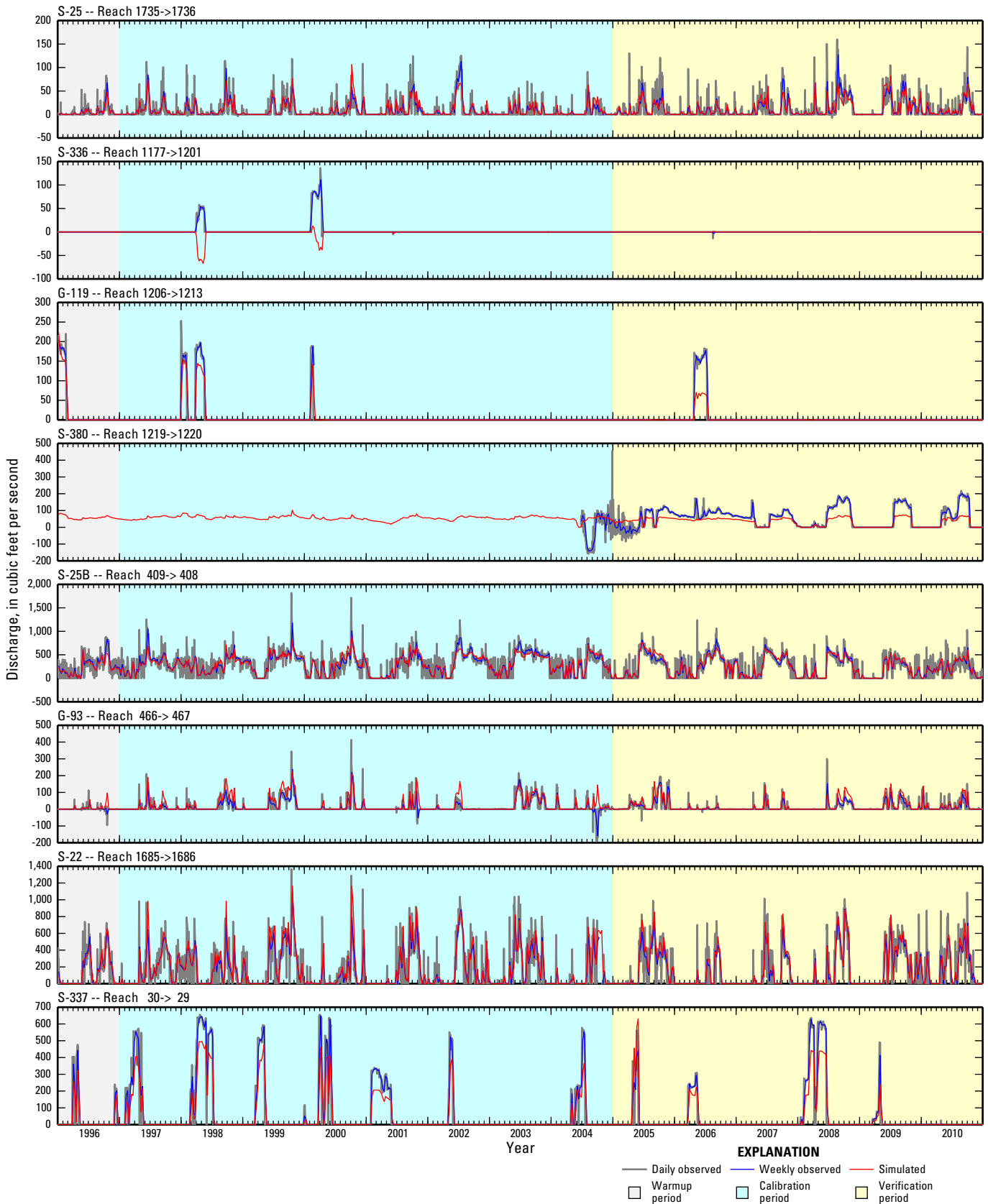


Figure 3-2. Observed and simulated discharge at surface-water structures in the study area.

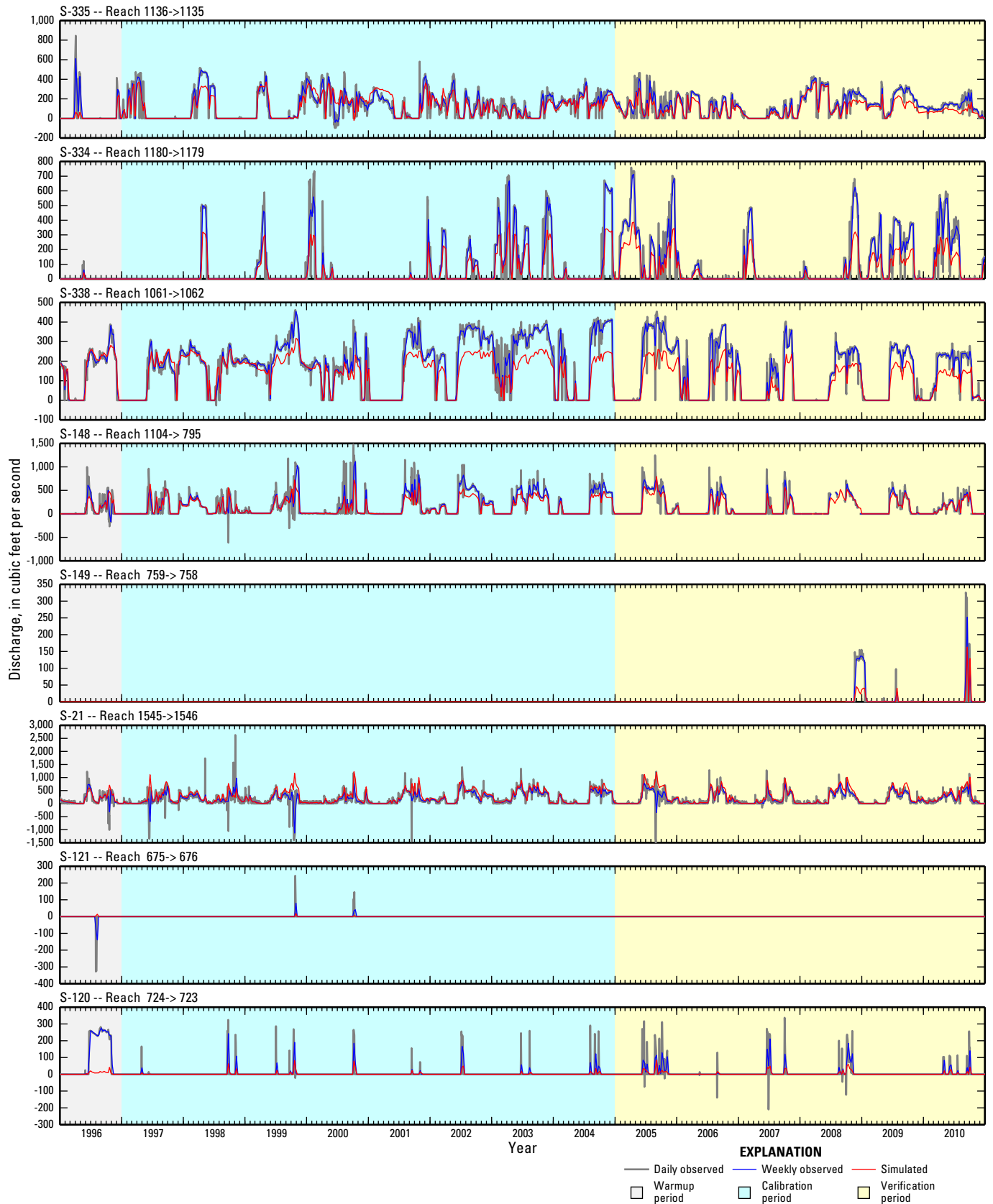


Figure 3-3. Observed and simulated discharge at surface-water structures in the study area.

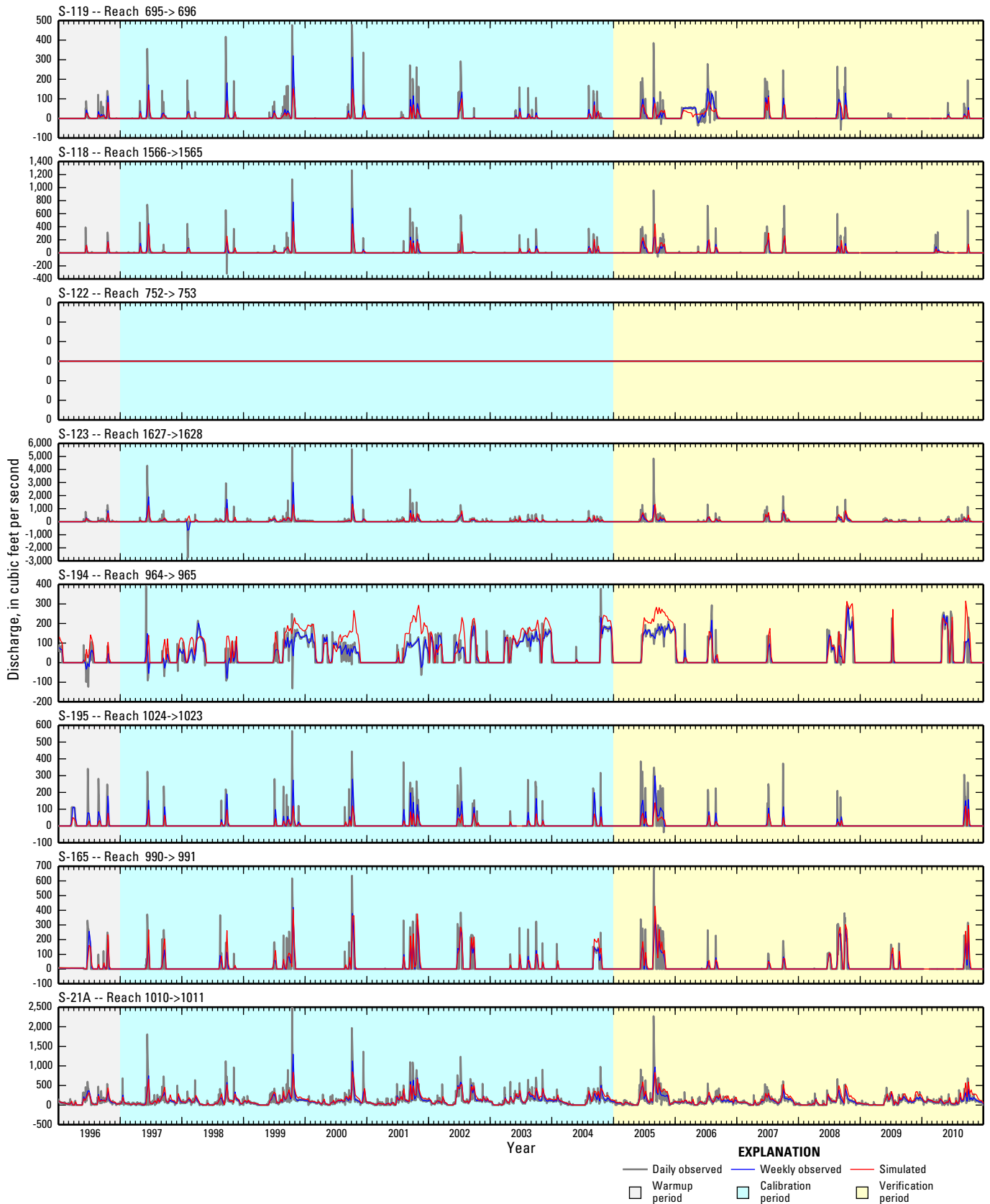
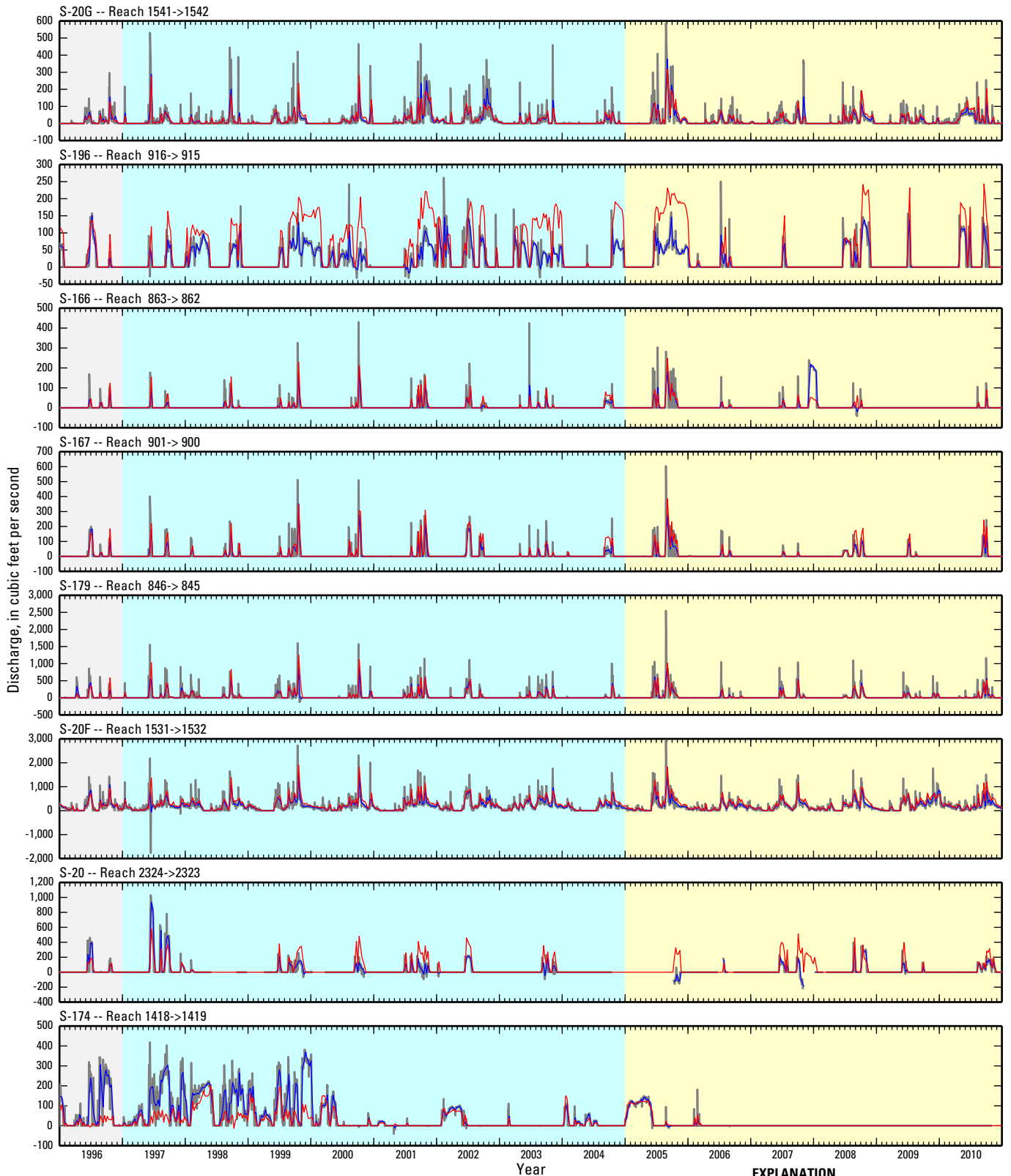


Figure 3-4. Observed and simulated discharge at surface-water structures in the study area.



**EXPLANATION**

- Daily observed
- Weekly observed
- Simulated
- Warmup period
- Calibration period
- Verification period

Figure 3-5. Observed and simulated discharge at surface-water structures in the study area.

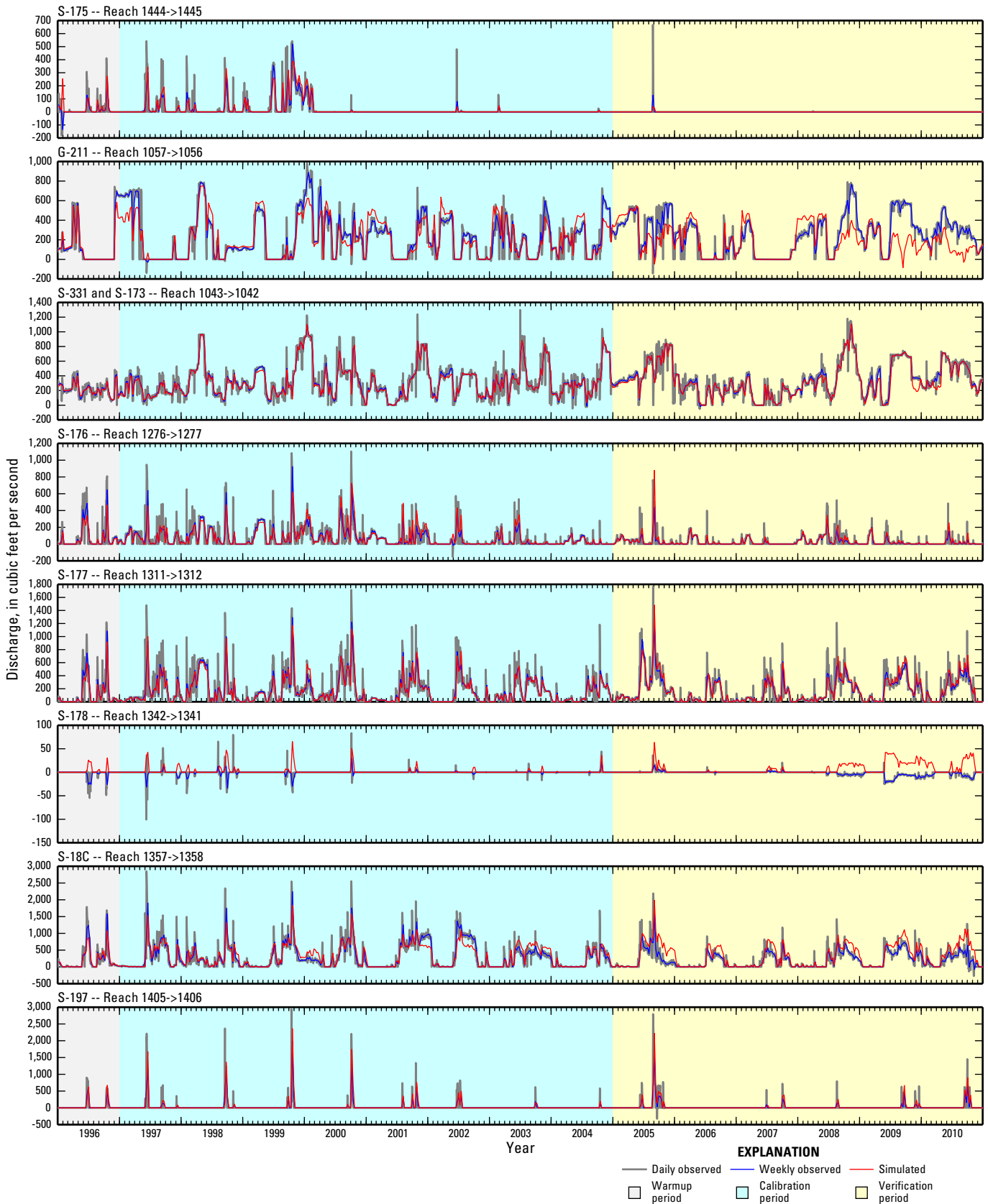


Figure 3-6. Observed and simulated discharge at surface-water structures in the study area.

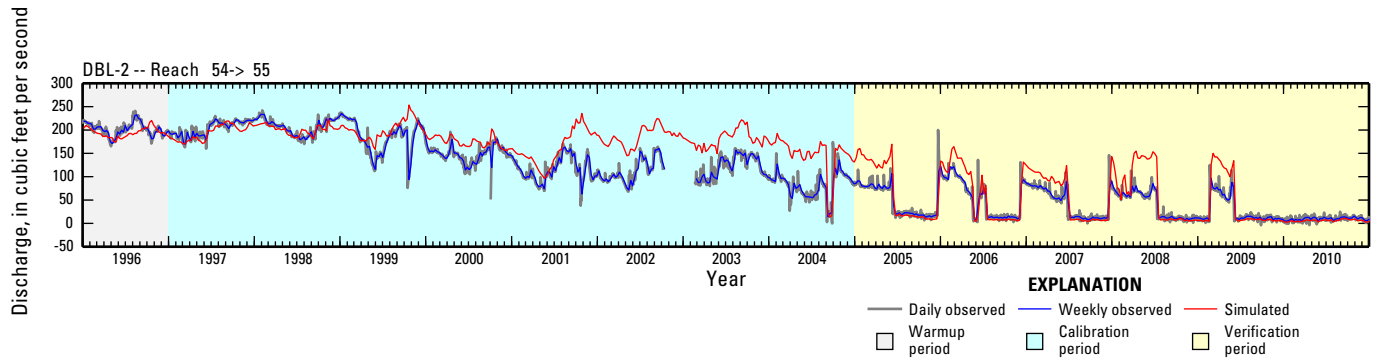


Figure 3-7. Observed and simulated discharge at surface-water structures in the study area.

## Appendix 4. Observed and Simulated Net Canal Discharge

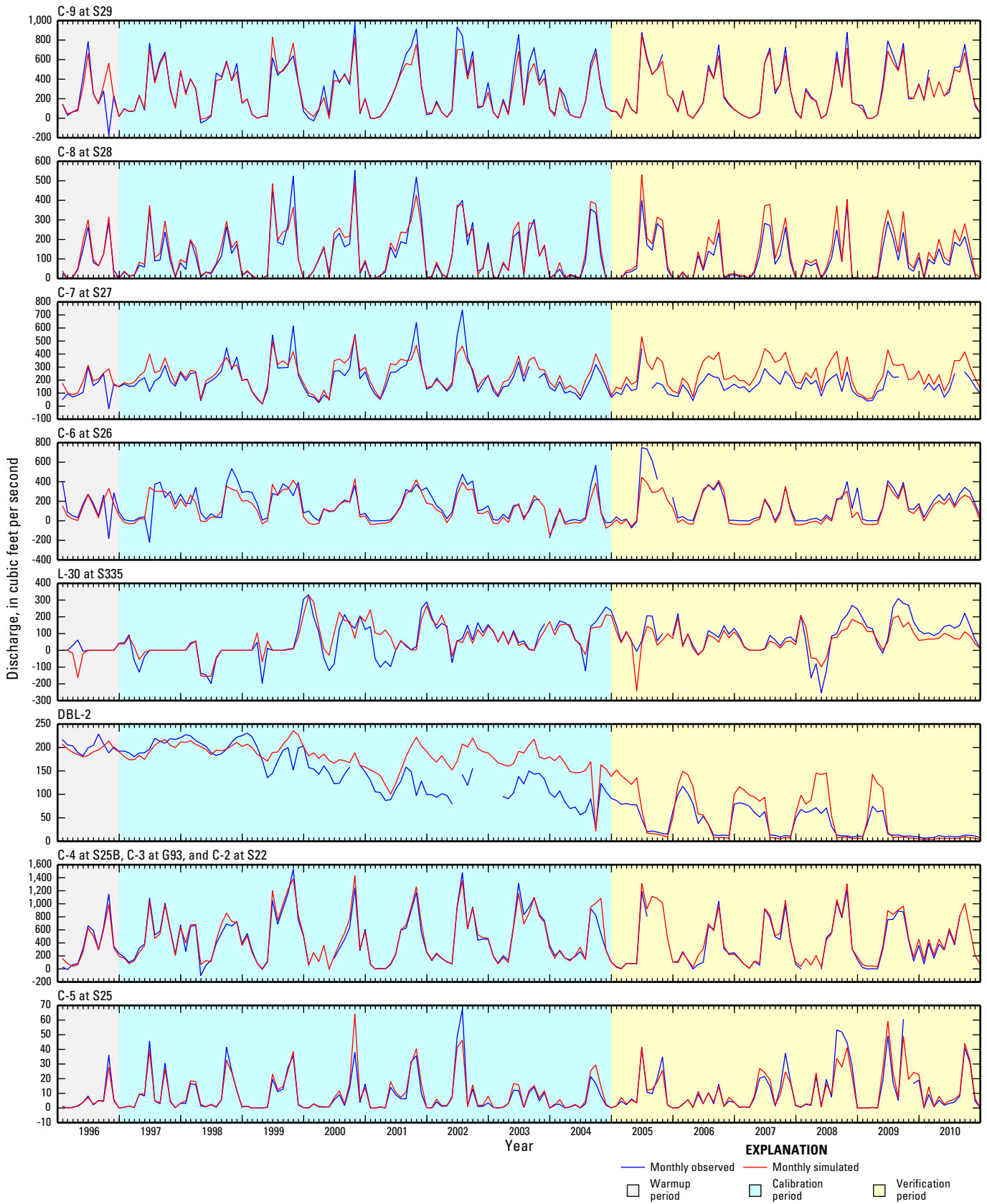


Figure 4-1. Observed and simulated net discharge from surface-water basins in the study area.

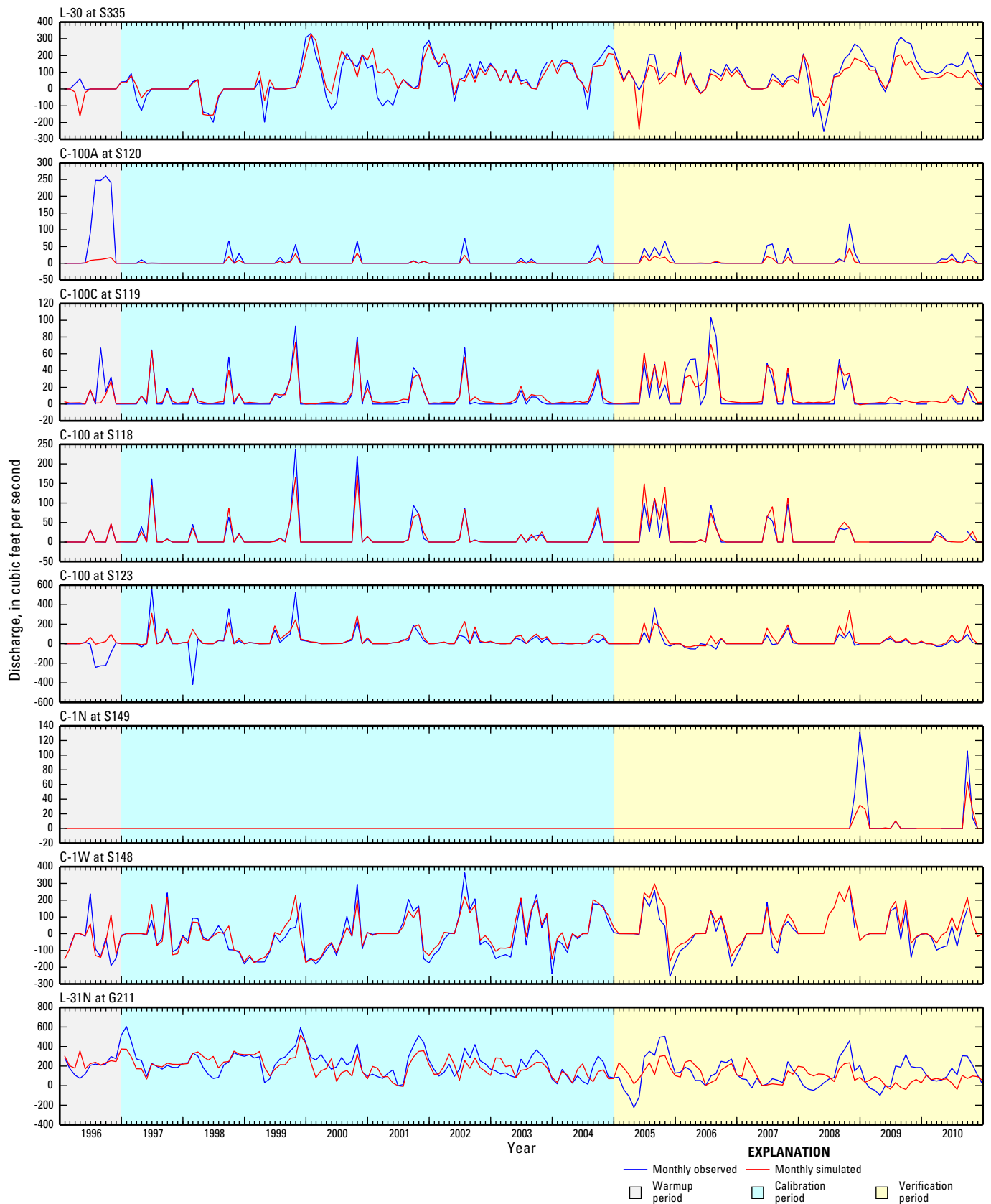


Figure 4-2. Observed and simulated net discharge from surface-water basins in the study area.



Figure 4-3. Observed and simulated net discharge from surface-water basins in the study area.

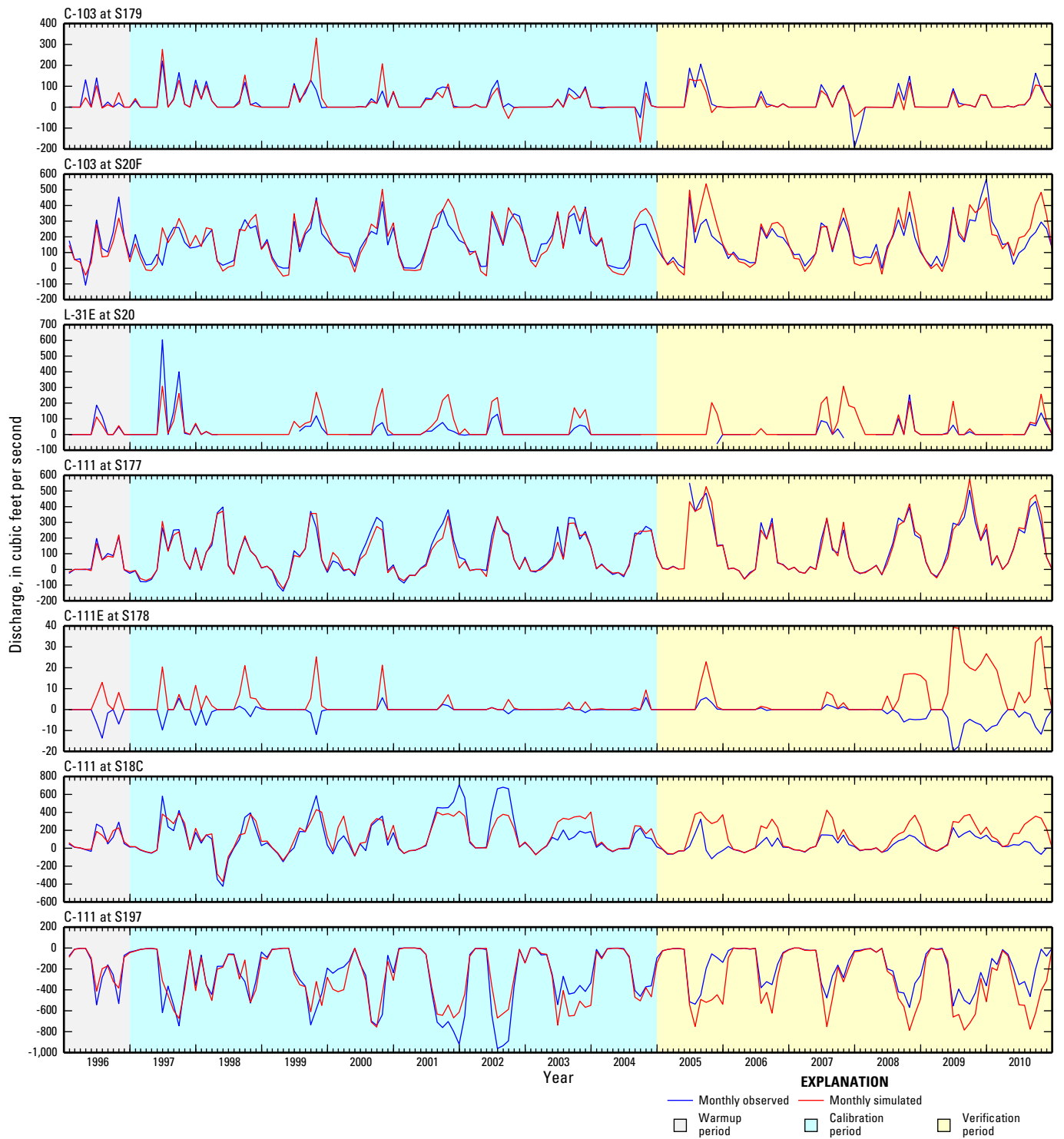


Figure 4-4. Observed and simulated net discharge from surface-water basins in the study area.

## Appendix 5. Observed and Simulated Groundwater Levels

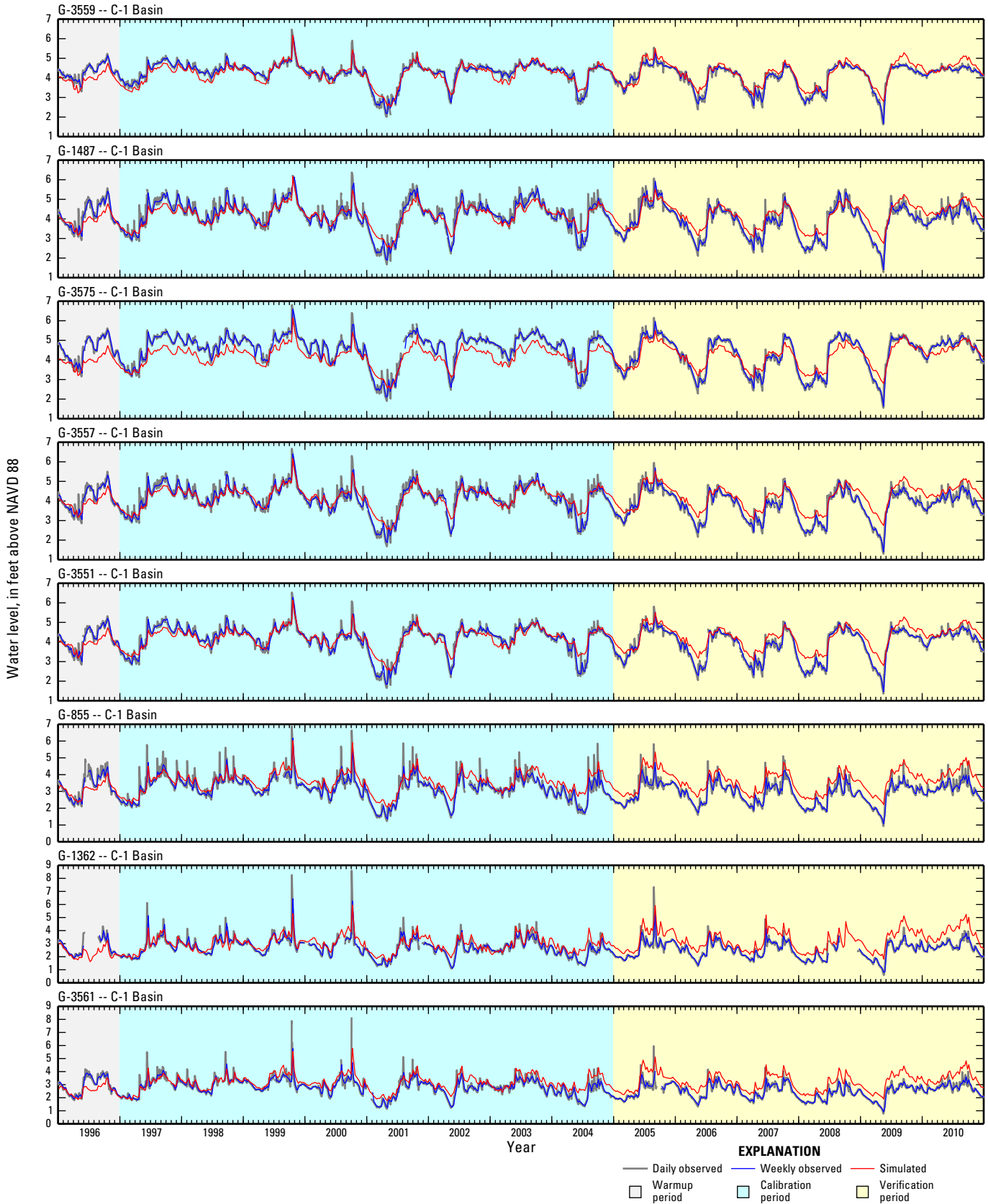


Figure 5-1. Observed and simulated water levels for monitoring wells in the study area.

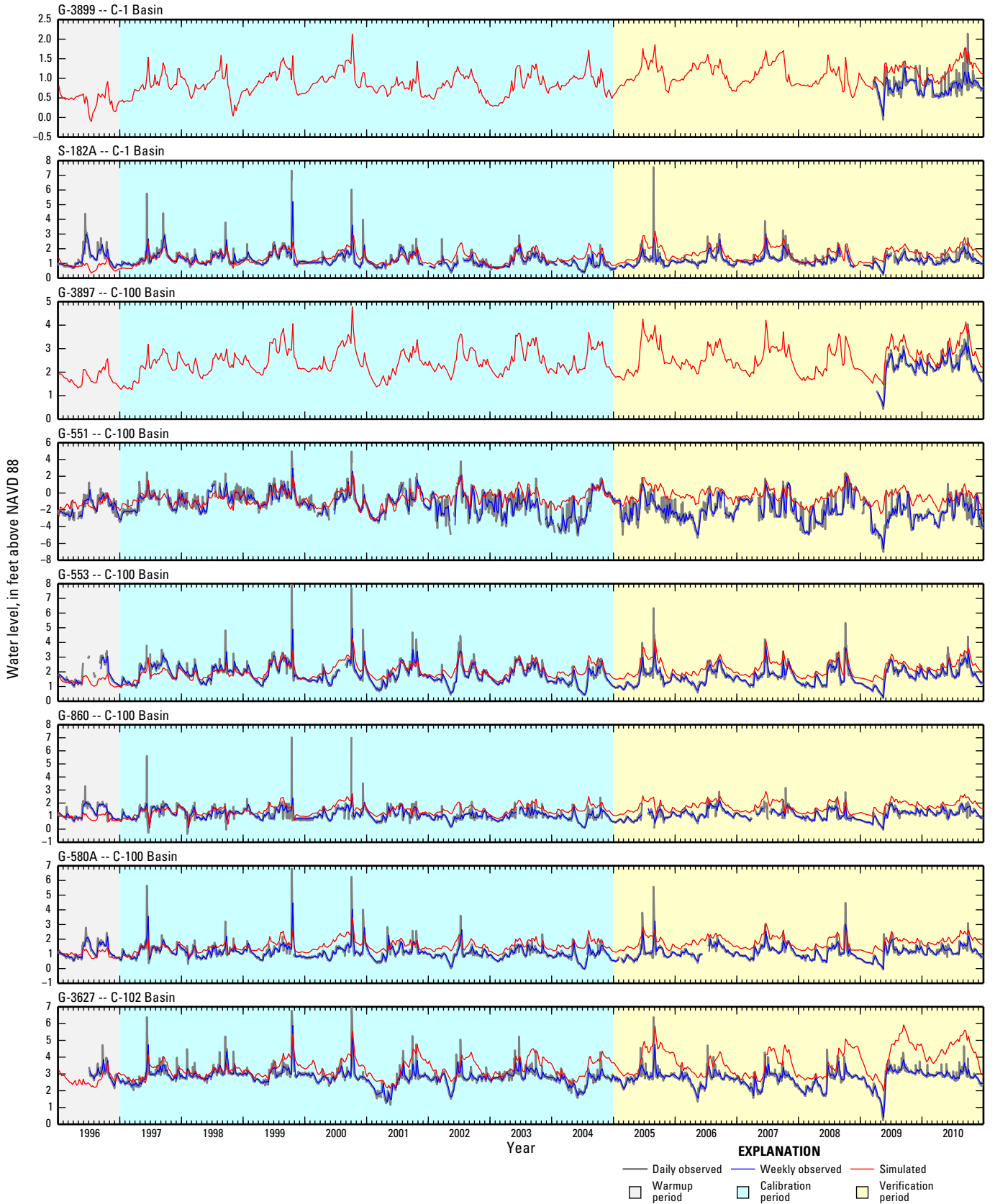


Figure 5-2. Observed and simulated water levels for monitoring wells in the study area.

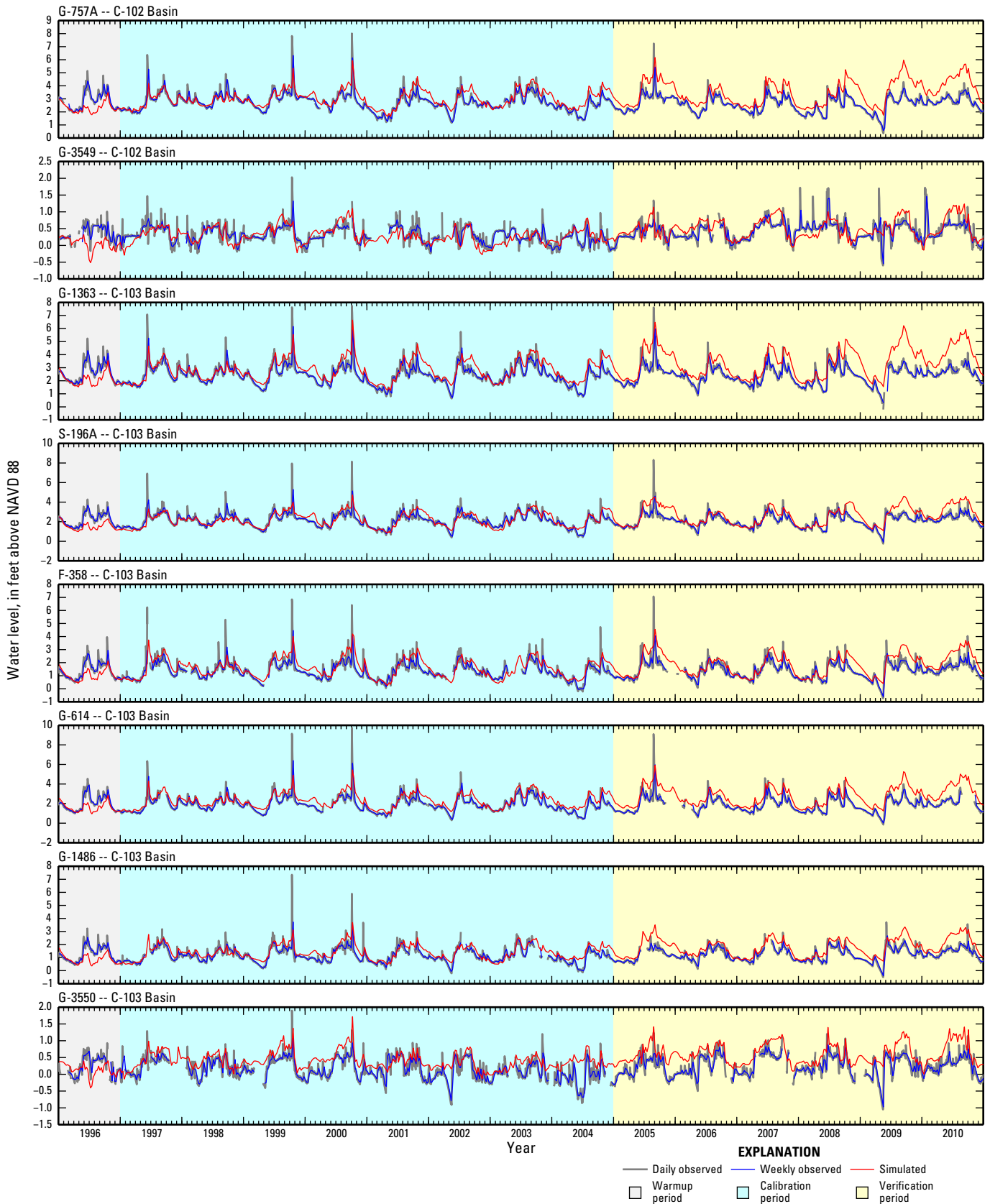


Figure 5-3. Observed and simulated water levels for monitoring wells in the study area.

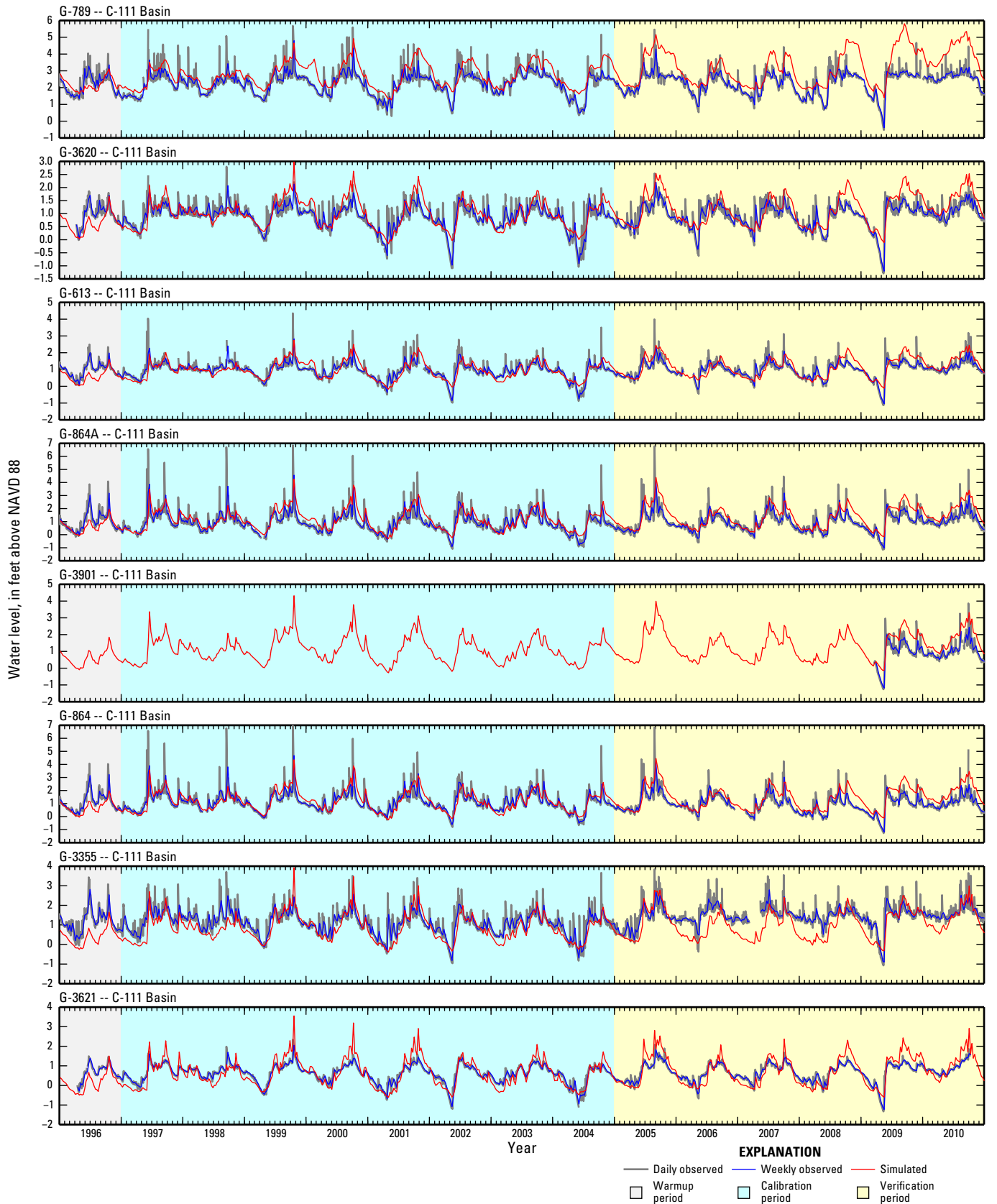


Figure 5-4. Observed and simulated water levels for monitoring wells in the study area.

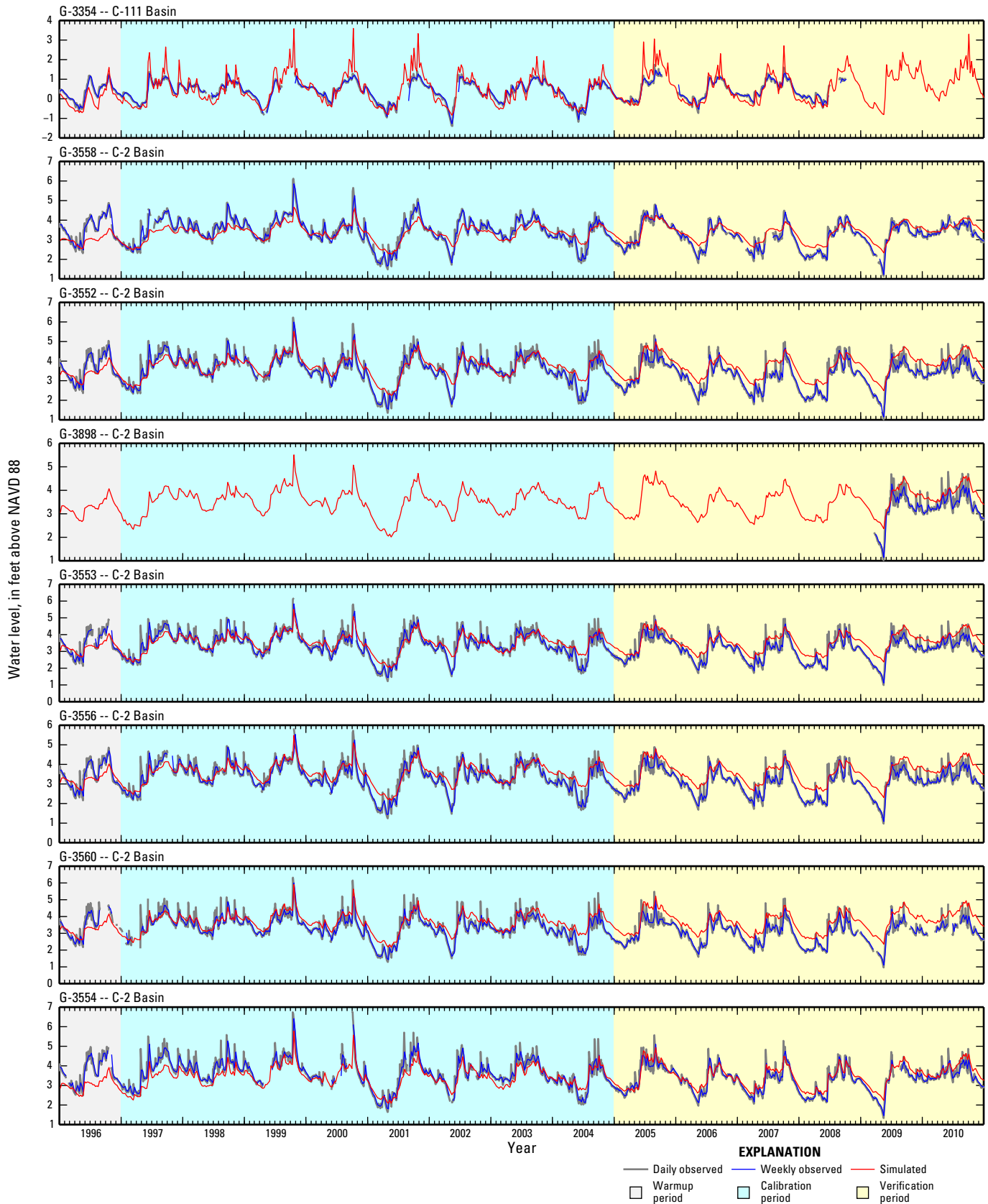


Figure 5-5. Observed and simulated water levels for monitoring wells in the study area.

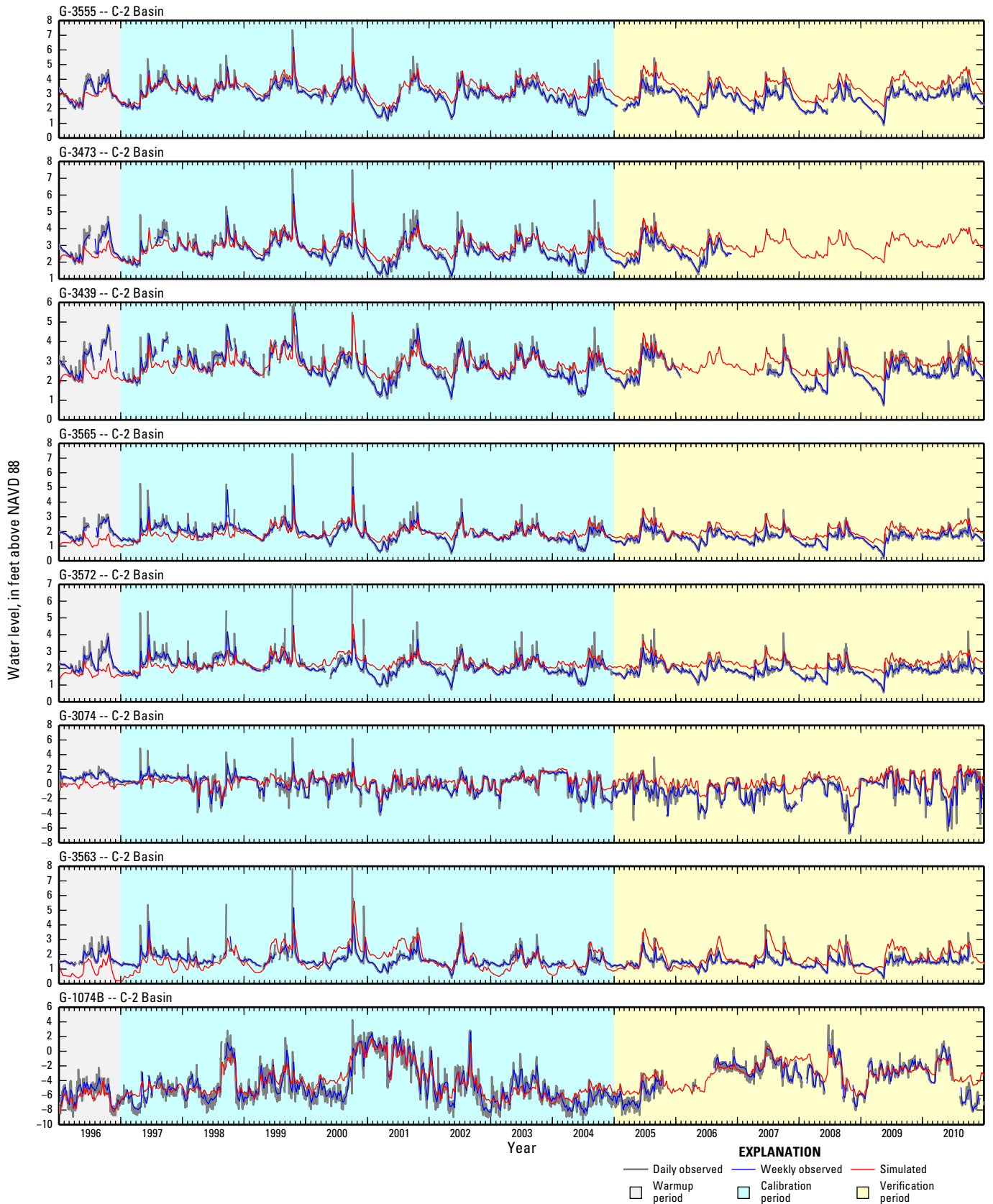


Figure 5-6. Observed and simulated water levels for monitoring wells in the study area.

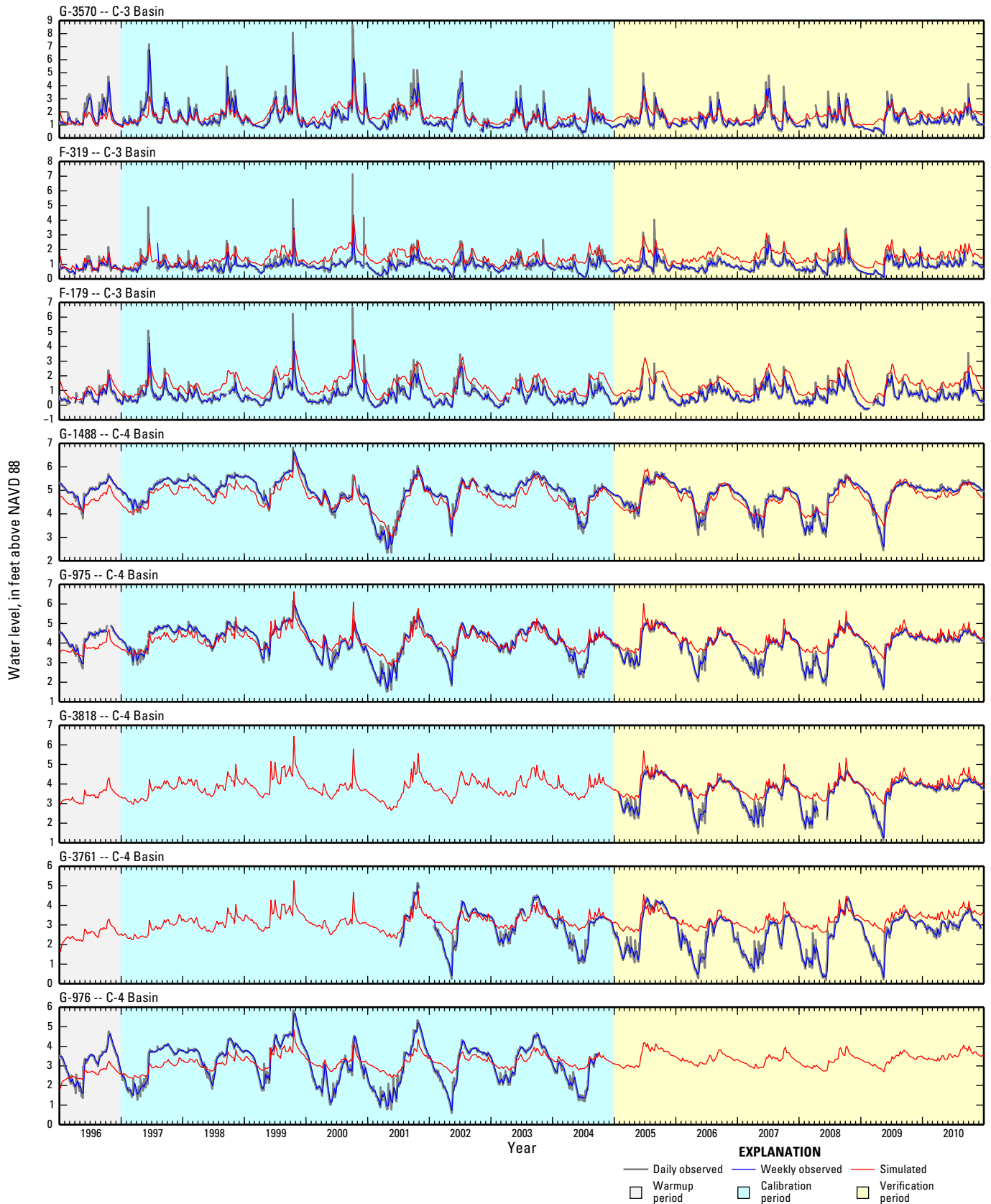


Figure 5-7. Observed and simulated water levels for monitoring wells in the study area.

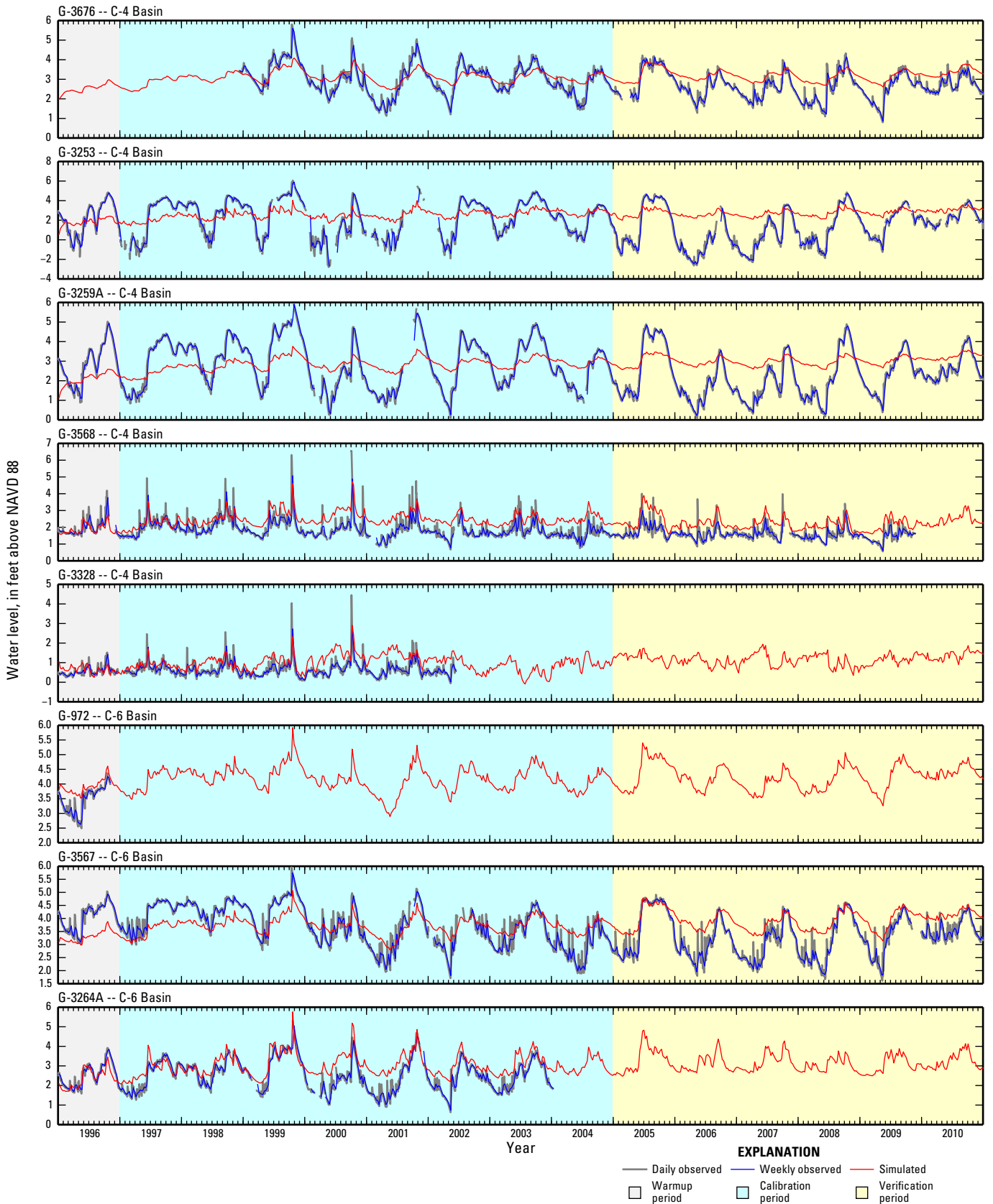


Figure 5-8. Observed and simulated water levels for monitoring wells in the study area.

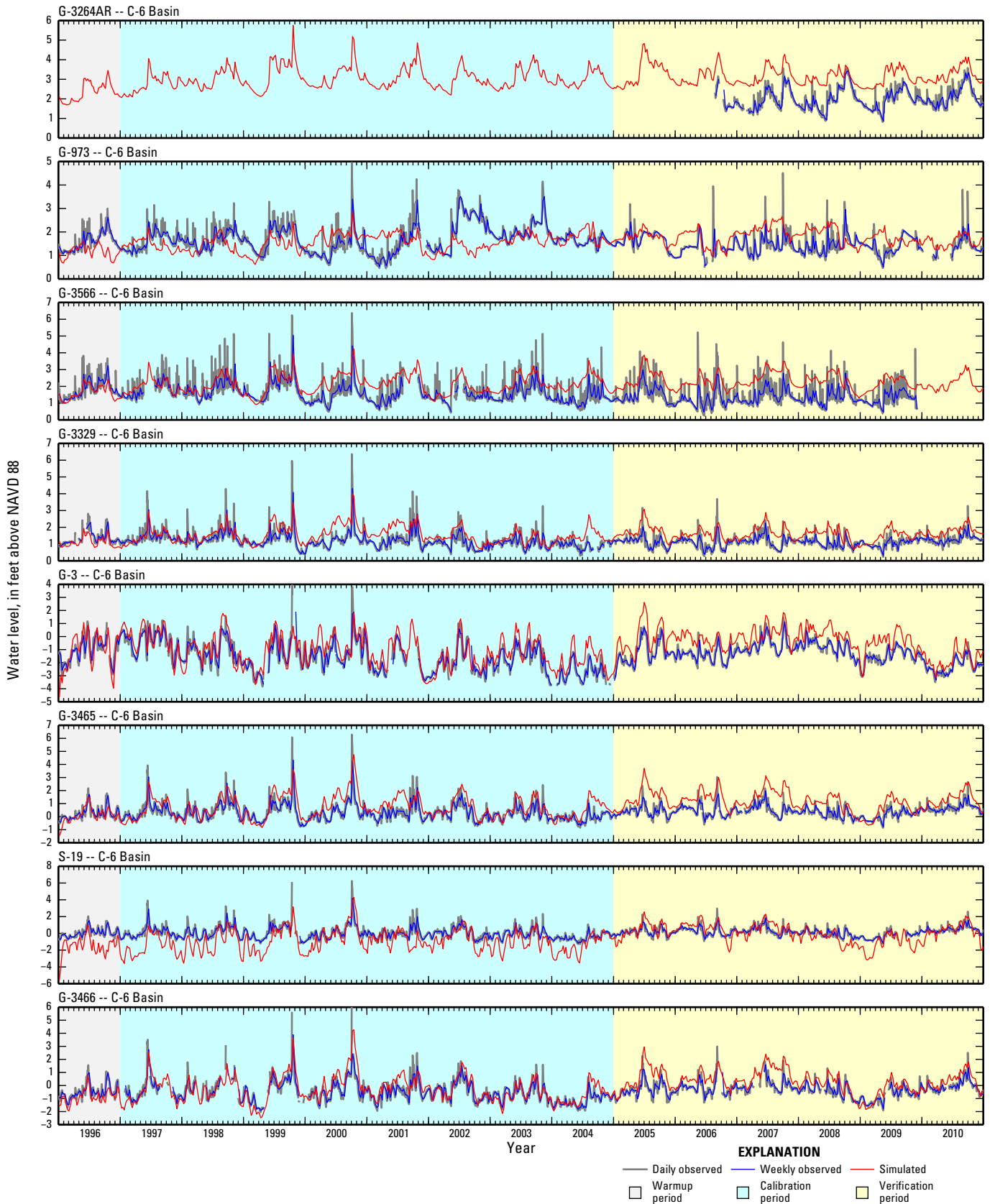


Figure 5-9. Observed and simulated water levels for monitoring wells in the study area.

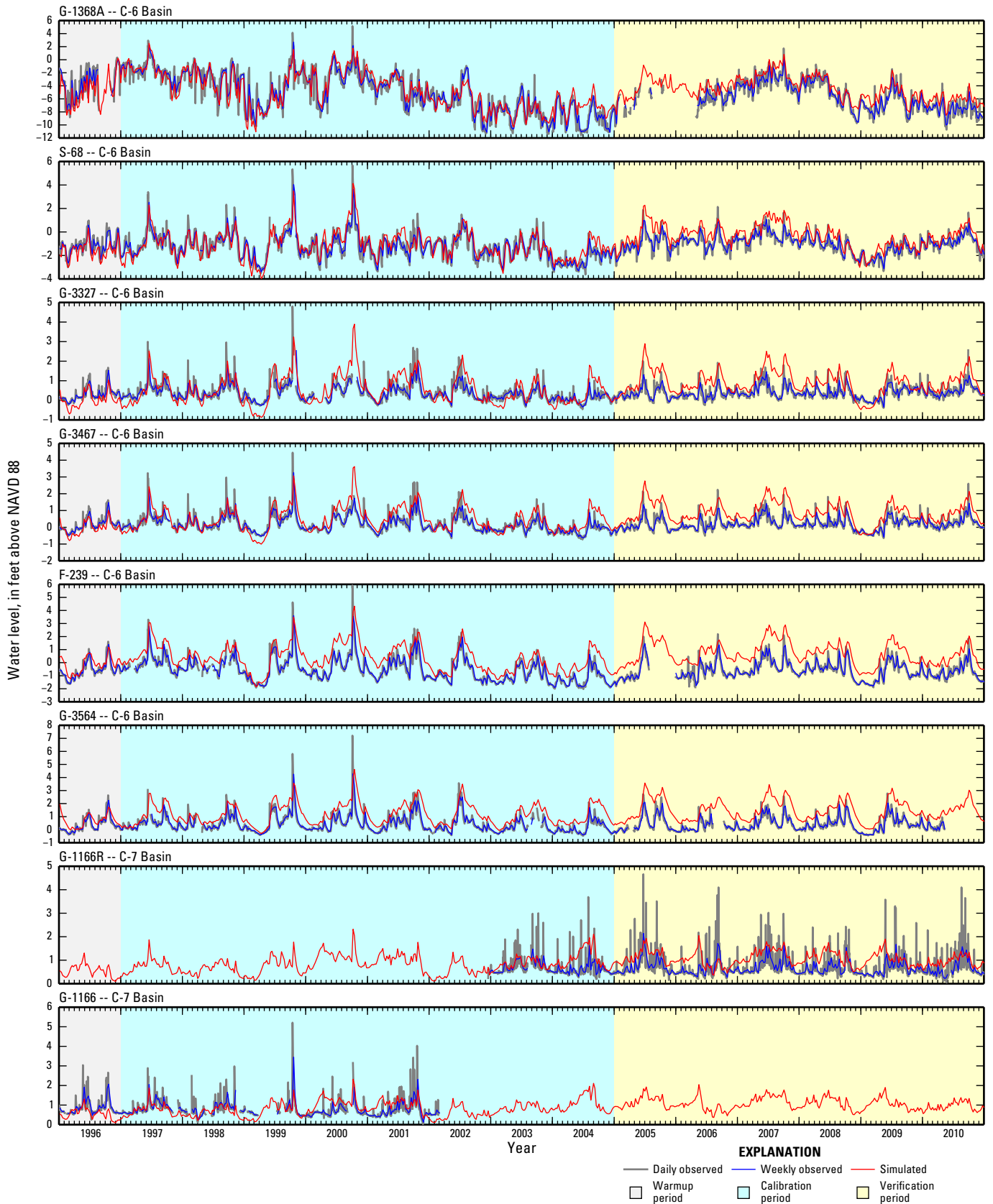


Figure 5-10. Observed and simulated water levels for monitoring wells in the study area.

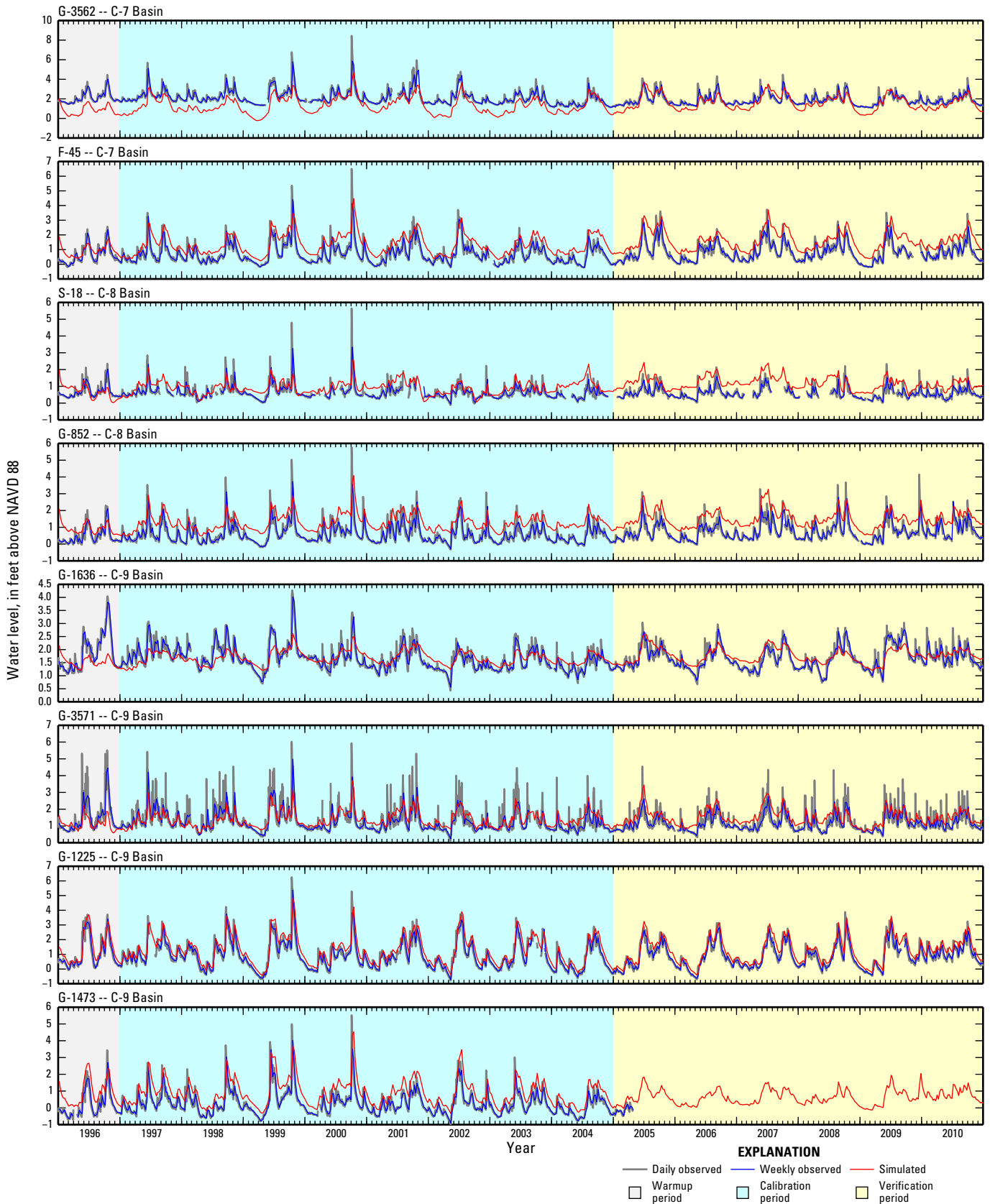


Figure 5-11. Observed and simulated water levels for monitoring wells in the study area.

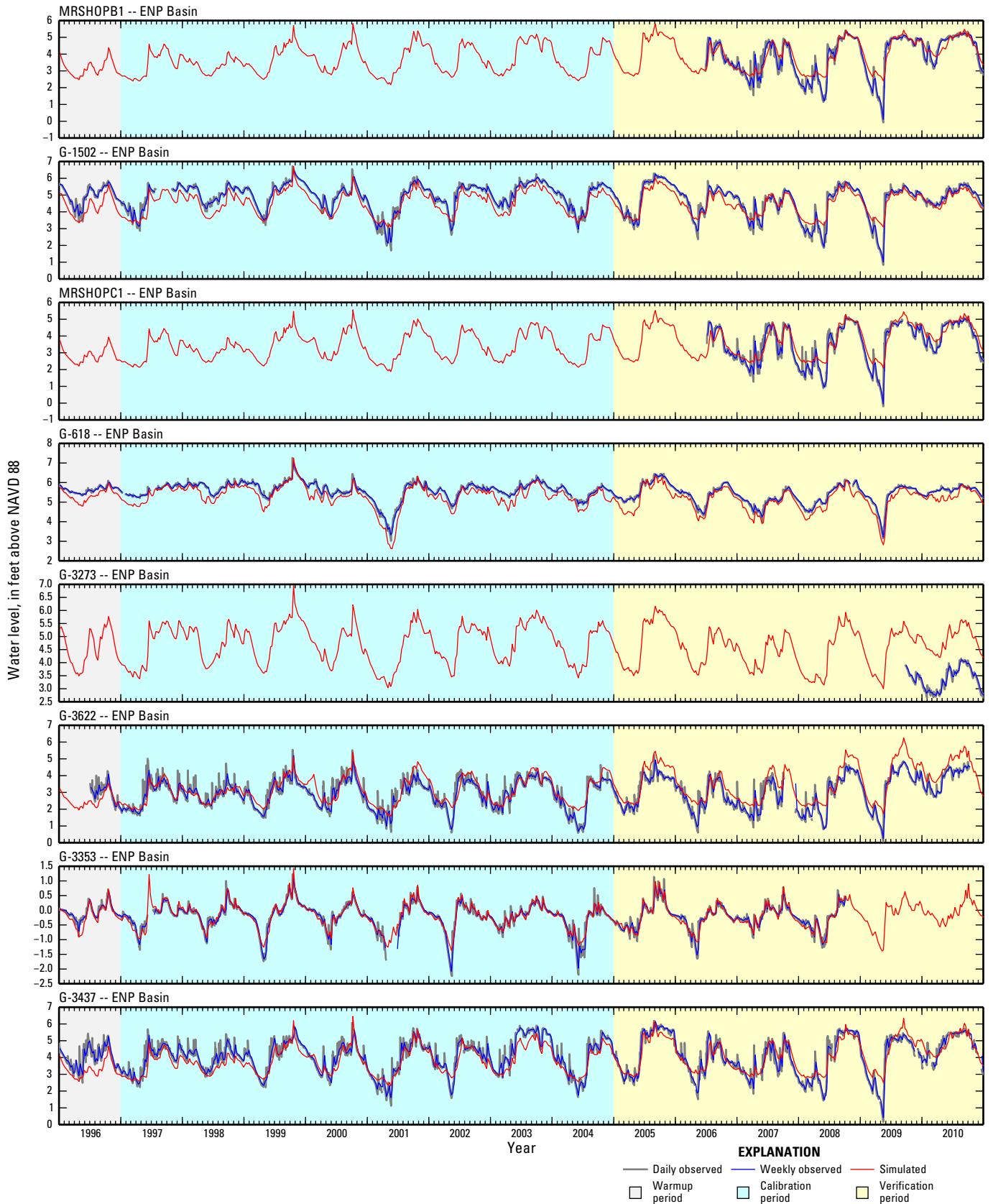


Figure 5-12. Observed and simulated water levels for monitoring wells in the study area.

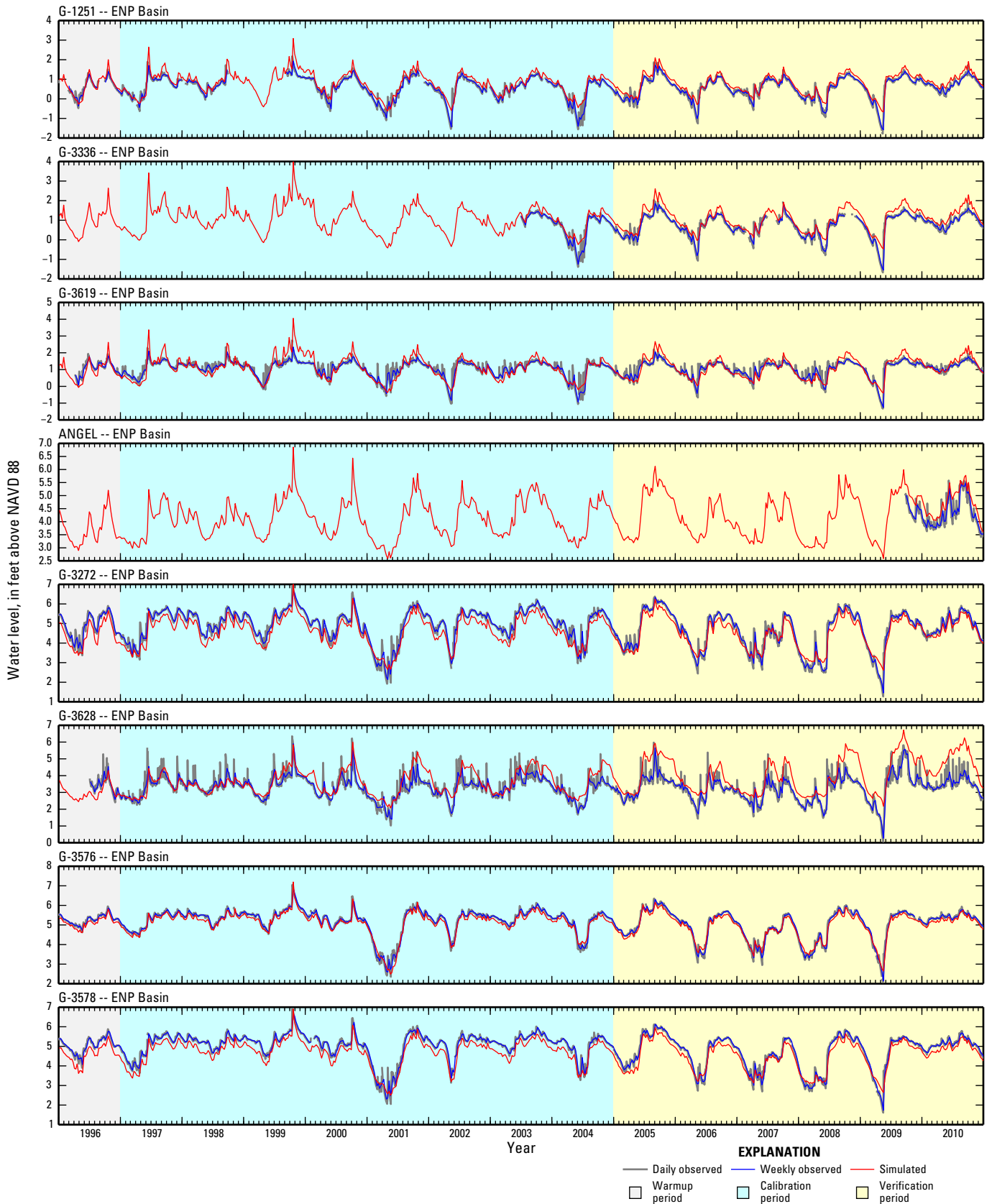


Figure 5-13. Observed and simulated water levels for monitoring wells in the study area.

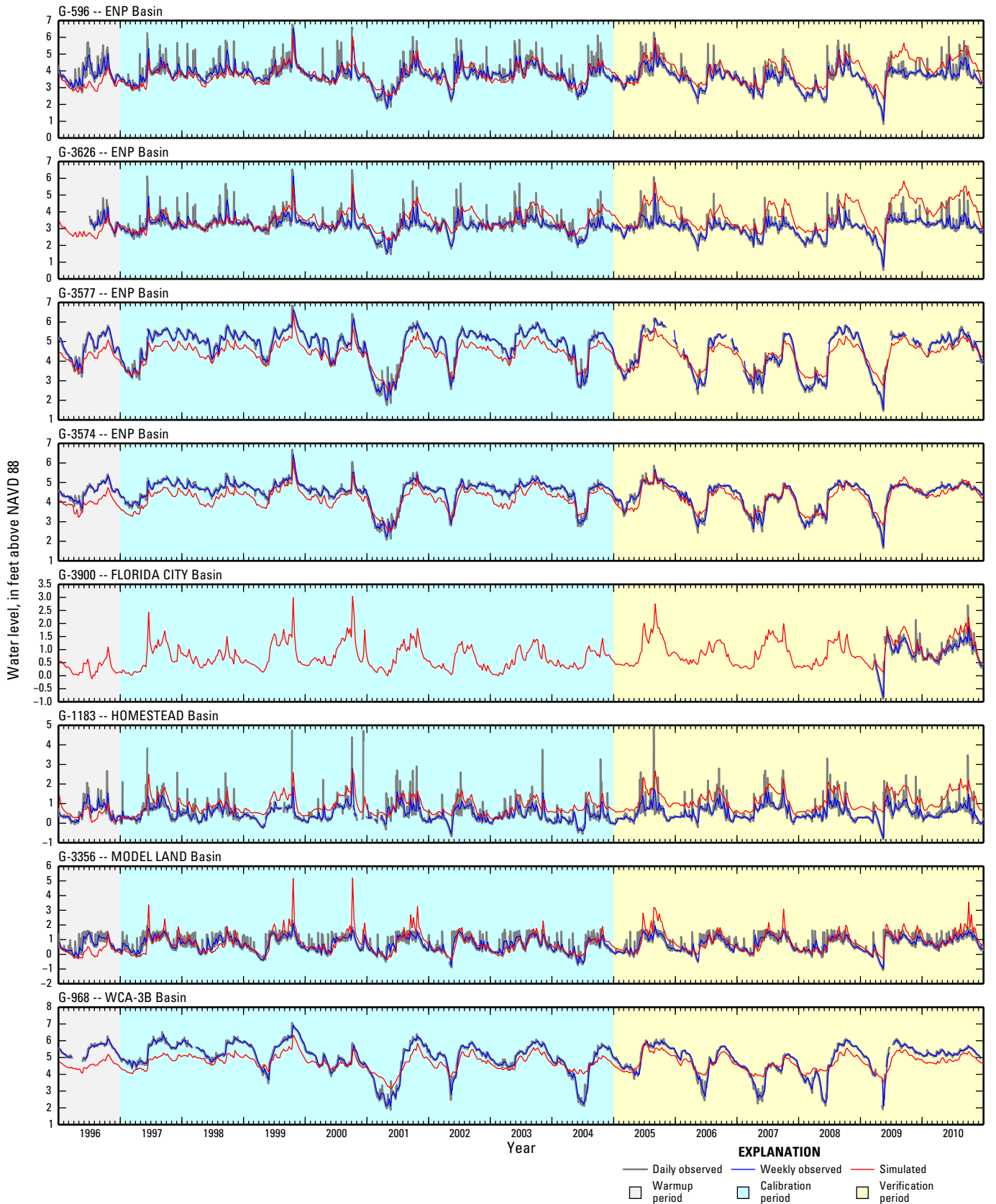


Figure 5-14. Observed and simulated water levels for monitoring wells in the study area.

Approved for publication on August 14, 2014

Prepared by:

USGS Science Publishing Network  
Raleigh Publishing Service Center  
3916 Sunset Ridge Road  
Raleigh, NC 27607

For additional information about this publication, contact:

Studies Section Supervisor  
USGS Caribbean-Florida Water Science Center  
4446 Pet Lane, Suite 108  
Lutz, FL 33559  
1-813-498-5000  
dmsumner@usgs.gov

Or visit the Caribbean-Florida Water Science Center Web site:

<http://fl.water.usgs.gov>



